

**Numerical and Experimental Investigation of Unreinforced
Masonry Wall Retrofitted with Timber Panels**

Jamiu Adetayo Dauda

Submitted in accordance with the requirements for the degree of
Doctor of Philosophy

The University of Leeds
School of Civil Engineering

January 2020

The candidate confirms that the work submitted is his own, except where work which has formed part of jointly authored publications. The candidate confirms that appropriate credit has been given within the thesis where reference has been made to other works.

Articles have been prepared and published as listed below. The candidate carried out all works in the publications and prepared all manuscripts with the co-authors providing guidance and editorial input.

Dauda J.A, Iuorio O and Lourenço P. B (2020). *Numerical Analysis and Experimental Characterization of Brick Masonry*. International Journal of Masonry Research and Innovation, Vol. 5 Issue: 3, pp.321–347, <https://doi.org/10.1504/IJMRI.2020.10028163>.

Dauda J.A, Lourenço P.B and Iuorio O (2020). *Out-of-Plane Testing of Masonry Walls Retrofitted with Oriented Strand Board (OSB) Timber Panels*. Institution of Civil Engineers – Structures and Buildings Journal <https://doi.org/10.1680/jstbu.19.00095>.

Iuorio O, **Dauda J.A**, and Lourenço P. B. (2020). *Experimental Evaluation of Out-of-Plane Strength of Masonry Wall Retrofitted with Oriented Strand Board*. Accepted for Publication in Construction and Building Material Journal, ISSN: 0950-0618.

Dauda J.A, Iuorio O., Silva L.C, and Lourenço P.B. (in press). *Numerical Evaluation of Out-of-Plane Strength of Masonry Wall Retrofitted with Oriented Strand Board*. Submitted to Engineering Structures Journal, ISSN: 0141-0296

Dauda J.A, Iuorio O, and Lourenço P.B (2018). *Characterisation of Brick Masonry: Study towards Retrofitting Masonry using Timber panel*. In Proceedings of 10th International Masonry Conference (10IMC), Milan, Italy 09-11 July 2018.

Dauda J.A, Iuorio O, and Lourenço P.B (2019). *Experimental Study of Out-of-Plane Behavior of Timber Retrofitted Masonry Prisms*. In Proceedings of the 13th North American Masonry Conference (13NAMC), Salt Lake City, Utah 16-19 June 2019.

Dauda J.A, and Iuorio O. (2019). *Timber-Masonry Composite Systems for Retrofit of Unreinforced Masonry Wall*. In Proceedings of 2019 Society for Earthquake and Civil Engineering Dynamics Conference, London September 2019.

Dauda J.A, Silva L.C, Lourenço P.B and Iuorio O (2020). *Numerical Study of Masonry Wall Retrofitted with Oriented Strand Board under Out-of-plane Loading*. Accepted in 2020 International Conf. of the Engineering Mechanics Institute.

Dauda J.A, Silva L.C, Iuorio O, and Lourenço P.B (2020). *Numerical Study of Out-of-Plane Behaviour of Timber Retrofitted Masonry Prisms*. Accepted in 12th Int. Conference on Structural Analysis of Historical Constructions.

Iuorio O, **Dauda J.A**, and Lourenço P.B (2020). *Flexural Resistance of Masonry Wall Retrofitted with Timber Panel under Out-Of-Plane Loading*. Accepted in 12th Int. Conference on Structural Analysis of Historical Constructions.

This copy has been supplied on the understanding that it is copyright material and that no quotation from the thesis may be published without proper acknowledgement.

Acknowledgements

My sincere appreciation goes to Almighty Allah, who in His infinite mercy has blessed me with the power to believe in my passion and pursue my dreams. I realised how true this gift of intellect is for me.

My respect and deepest appreciations go to my parents, my dear wife, and my children for been there for me throughout this program. Special thanks to everybody who has made achieving this feat possible.

I also would like to express my special appreciation and thanks to my supervisors, Dr Ornella Iuorio and Prof. Phil Purnell. You have been a tremendous mentor for me. I appreciate you for supervising and inspiring me. Your advice on both research and my career has been priceless. I also thank Prof. Paulo Lourenco and Dr Luis Silva of ISISE, Uminho for their collaboration on this project.

Abstract

Retrofit of unreinforced masonry (URM) buildings is continually attracting the interest of masonry professionals. This is because there are enormous URM building stocks in different parts of the world that have shown vulnerability to damage against out-of-plane actions due to having limited flexural strength and deformation resistance. As such, there is a global trend of promoting the development of different retrofit techniques for URM wall. Thus, this study proposed an experimental and numerical investigation into the possibility of retrofitting URM wall using oriented strand board (OSB) timber-panel. The aim is to estimate the improvements in the out-of-plane capacity of URM wall retrofitted with OSB panel. The study focuses on investigating out-of-plane behaviour because out-of-plane failure mode has been identified as the most critical failure mode of URM walls.

The proposed retrofitting approach is by securing an OSB/ type 3 timber-panel behind URM wall using threaded anchor rods together with an option of plastic plug or injection mortar. The methodologies adopted to deliver the overall aim and objectives of this study, as identified in this thesis were experimental tests and numerical analyses.

Flexural strength in the form of four-point bending tests has been obtained on nine small-scale masonry prisms (615 x 215 x 102.5mm) and six larger-scale masonry walls (1115 x 1115 x 225mm). The effectiveness of the proposed OSB-panel retrofit technique has been assessed in term of flexural strength, absorbed energy (toughness), out-of-plane load capacity and displacement. The test results show that OSB type 3 can considerably increase the load and flexure capacity of retrofitted masonry walls by (1.4 & 1.8), limiting toughness by (1.6 & 2.4) and overall toughness by (16 & 10) times that of plain wall subjected to out-of-plane loading for retrofit application on single (i.e tensile side only) and double-sides of the wall respectively. It can be concluded that the application of the proposed OSB retrofit technique greatly influenced the out-of-plane performance of the retrofitted wall and also prevents its quasi-brittle collapse.

Numerical analysis using commercial finite element software, ABAQUS was also performed and validated against the experimental data. The observed damage

pattern and load-displacement plots compared with the experimental observations are in good agreement (within 5% difference). The calibrated model was then extended to parametric analysis to assess the model capability to simulate URM walls retrofitted with different OSB panel thickness, different connection spacing and different retrofit application position. The parametric analysis reveals that the thickness of the OSB timber is directly proportional to the out-of-plane load and displacement resistance of the system. It also shows that there is not enough composite action between the masonry and the OSB timber when the connection spacing is greater than 500mm. The parametric analyses revealed that the application of the retrofit on only the compression side does not improve the load capacity of the retrofitted walls significantly. Hence it is recommended that the application should be applied on the tensile sides of the wall or both sides where desirable.

Interestingly, the cost of applying this proposed OSB technique on a square meter of a masonry wall (materials and labour) is estimated to be £47 as against £152 estimated for typical fibre-based retrofit applications on 1m² masonry wall using the market prices in England. The proposed retrofit technique in comparison with the other existing fibre-based retrofit techniques performed well in terms of increased capacity and it is cheaper and easy to apply.

Keywords: Experiment, Finite Element (FE) Analysis, Flexural Strength, Masonry, Out-of-Plane, OSB Timber-Panel, Retrofitting, URM Wall.

2.4.2.2.1	Base isolations	33
2.4.2.2.2	Energy- dissipation devices	34
2.4.2.2.3	Cam system	35
2.5	Evaluation of Different Retrofit Techniques	37
2.6	Previous Experimental Studies on Out-of-Plane Behaviour of URM Walls.....	42
2.7	Numerical Modelling of Masonry Structures	55
2.8	Summary of Review Carried Out.....	57
CHAPTER THREE- METHODOLOGY		63
3.0	Introduction	63
3.1	Experimental Program.....	63
3.2	Materials.....	69
3.3	Numerical Analysis Program.....	70
3.4	Summary	73
CHAPTER FOUR – RETROFIT OF URM WALL WITH TIMBER PANEL: EXPERIMENTAL STUDY		74
4.0	Introduction	74
4.1	Material Characterisation	74
4.1.1	Characterisation of Brick Units.....	74
4.1.1.1	Dimension of Brick Units	74
4.1.1.2	Dry Density of Brick Units.....	75
4.1.1.3	Water Absorption of Brick Units	76
4.1.1.4	Compressive Strength of Brick Units.....	77
4.1.1.5	Modulus of Elasticity and Poisson’s Ratio of Brick Units.....	78
4.1.1.6	Mechanical Properties of Brick Units	80
4.1.2	Characterisation of Mortar	82
4.1.2.1	Consistency of Fresh Mortar (Dropping ball test)	83
4.1.2.2	Consistency of Fresh Mortar (Flow table test)	84
4.1.2.3	Compressive strength test of hardened mortar	85
4.1.2.1	Mechanical Properties of Mortar.....	86
4.1.3	Characterisation of Masonry Cubic Specimen	87
4.1.3.1	Compressive Strength of MC Specimens: Experimental.....	87
4.1.3.2	Characteristic Compressive Strength of MC Specimen.....	89

4.1.4 Failure Mode of Masonry Units and Masonry Cubic Specimens	91
4.2 Small-Scale Test: Flexural Bond Strength of Masonry Prism.....	93
4.2.1 Test Specimen Characteristics	93
4.2.1.1 Materials	93
4.2.1.2 Test Specimen Construction	95
4.2.2 Test Program/Matrix.....	97
4.2.3 Test setup and Procedures	97
4.2.4 Test Results	100
4.2.4.1 Out-of-plane Displacement.....	100
4.2.4.2 Flexural Strength	101
4.2.5 Observed Failure Pattern	103
4.2.5.1 Failure Pattern of Plain MPs.....	103
4.2.5.2 Failure Pattern of Timber Retrofitted MPs.....	104
4.2.6 Evaluation of Performance of the Proposed Technique.....	106
4.3 Larger-Scale Test: Flexural strength of masonry wall.....	109
4.3.1 Test Specimen Characteristics	110
4.3.1.1 Materials	110
4.3.1.2 Test specimen construction	110
4.3.2 Test Program/Matrix.....	112
4.3.3 Test setup and Procedures	113
4.3.3.1 Loading Procedure.....	116
4.3.3.2 Instrumentation.....	117
4.3.4 Test Results	118
4.3.4.1 Out-of-plane Displacement.....	118
4.3.4.2 Behaviour of Plain Masonry Wall	119
4.3.4.3 Behaviour of Retrofitted Masonry Wall.....	122
4.3.5 Evaluation of Performance of the Proposed Technique.....	125
4.4 Summary of Findings.....	127
CHAPTER FIVE – RETROFIT OF URM WALL WITH TIMBER PANEL: NUMERICAL STUDY.....	132
5.0 Introduction	132
5.1 Adopted Numerical Modelling Techniques.....	132
5.2 Numerical Simulation of Compression Test on MC Specimen	133
5.2.1 Description of FE model	133
5.2.2 Properties of Brick unit and Mortar.....	135

5.2.3	General Parameter for CDP of Brick and Mortar	140
5.2.4	Properties of Brick-Mortar Interface.....	141
5.2.5	Input Parameter for Numerical Model.....	143
5.2.6	Calibration of the numerical model.....	145
5.2.7	Results and discussion	146
5.3	Numerical Simulation of the Small-Scale Test: Flexural Bond Strength Test on Masonry Prism	150
5.3.1	Description of FE model	151
5.3.1.1	Plain Masonry Prism Model (MP00-NM)	151
5.3.1.2	Retrofitted Masonry Prism Model (MPOSB-NM).....	152
5.3.2	Interaction and Constraint Conditions in FE Model	153
5.3.3	Boundary Condition and Loading.....	155
5.3.3	Analysis Method.....	156
5.3.4	Input Parameter for MP Model	156
5.3.5	Results and Discussion.....	159
5.3.5.1	MP00-NM compared with MP00 Test Results	159
5.3.5.2	MPOSB-NM compared with MPOSB-C1 Test Results	161
5.4	Numerical Simulation of Larger-Scale Test: Flexural Strength of Masonry Walls.....	164
5.4.1	Results and Discussion.....	166
5.4.1.1	PW1115-NM compared with PW1115 Test Results	166
5.4.1.2	1SRW1115-NM compared with 1SRW1115 Test Results.....	168
5.4.1.3	2SRW1115-NM compared with 2SRW1115 Test Results.....	170
5.5	Parametric Study.....	172
5.5.1	Influence of the application position of the retrofit	173
5.5.2	Influence of the thickness of OSB.....	175
5.5.3	Influence of number of connections	177
5.6	Cost Evaluation of the Proposed Retrofit Technique	179
5.7	Summary of Findings.....	180
CHAPTER SIX – CONCLUSION AND RECOMMENDATION FOR FUTURE WORKS		182
6.0	Overview	182
6.1	Experimental Study.....	183
6.2	Numerical Analyses.....	186
6.3	Contribution.....	188

6.4 Recommendation for future works.....	189
References	191
Appendix	206

List of Tables

- Table 2.1: Out-of-plane failure mechanism by FaMIVE
- Table 2.2: Summary of retrofit techniques
- Table 2.3: Summary of Previous Out-of-plane Testing of URM wall
- Table 3.1: Full Experimental Program
- Table 4.1: Dimension and dry density of brick units
- Table 4.2: Water absorption of bricks
- Table 4.3: Compressive strength of bricks
- Table 4.4: Modulus of elasticity and Poisson ratio of bricks
- Table 4.5: Mechanical properties of brick units
- Table 4.6: Dropping test value of fresh mortar
- Table 4.7: Flow test value of the adopted mix
- Table 4.8: Compressive strength of mortar
- Table 4.9: Compressive strength of masonry cubic specimen
- Table 4.10: Test program specimen identification
- Table 4.11: Summary of flexural bond strength test results
- Table 4.12: Test program for larger-scale test
- Table 4.13: Summary of out-of-plane bending test results
- Table 5.1: Mechanical properties of the brick unit
- Table 5.2: Mechanical properties of mortar
- Table 5.3: General parameter for damage-plasticity of brick unit and mortar
- Table 5.4: Interfacial properties [contact behaviour of joints]
- Table 5.5: Mesh sensitivity results
- Table 5.6: Mechanical properties of the mortar used for MP
- Table 5.7: Mechanical properties of Anchor Connector used for MP
- Table 5.8: Mechanical properties of OSB panel
- Table 5.9: Comparison of model and test average results
- Table 5.10: Comparison of model and test average results
- Table 5.11: Comparison of model and test average results (PW)

Table 5.12: Comparison of model and test average results (1SRW)

Table 5.13: Comparison of model and test average results (2SRW)

Table 5.14: Parametric study Model Identification

Table 5.15: Cost evaluation for different OSB thicknesses with 16 anchors

Table 5.15: Cost evaluation for different quantity of anchors

List of Figures

- Figure 2.1. Type of URM wall bond
- Figure 2.2. Type of URM walls
- Figure 2.3. Failure mechanism modes.
- Figure 2.4. In-plane failure modes of URM walls
- Figure 2.5. Out-of-plane failure modes of URM walls
- Figure 2.6. URM wall failure plane
- Figure 2. 7. Classification of retrofit techniques
- Figure 2. 8. Joint treatment of URM walls
- Figure 2.9. Surface treatment of URM wall
- Figure 2.10. Externally strengthen wall with supplemental steel
- Figure 2.11. Steel column and plate behind the wall
- Figure 2.12. Internal RC concrete skin
- Figure 2.13. FRP strengthening approach on masonry wall
- Figure 2.14. Post-tensioning of URM wall
- Figure 2.15. St. Giorgio bell tower retrofitted with SMA
- Figure 2.16. Reticulatus system showing the reinforcement idea and pattern
- Figure 2.17. Floor/Roof diaphragm strengthening intervention
- Figure 2.18. RC column confinement in a masonry wall
- Figure 2.19. Performance of RC confined masonry in 2007 Pisco earthquake
- Figure 2.20. Base isolator in the building
- Figure 2.21. Seismic energy dissipation in building
- Figure 2.22. CAM arrangement in URM wall
- Figure 2.24. Guidelines for choosing the level of FE modelling
- Figure 2.23. Masonry modelling techniques
- Figure 2.25. Timber confinement of URM
- Figure 2.26. Proposed Timber panel retrofit
- Figure 3.1. Full numerical analysis program
- Figure 4.1. Brick unit samples

- Figure 4.2. Brick samples immersed in water
- Figure 4.3. Compression test
- Figure 4.4. Strain gauges on the brick
- Figure 4.5. Lateral vs longitudinal strain for brick
- Figure 4.6. Summary of mechanical properties of brick units
- Figure 4.7. Test setup for dropping ball test
- Figure 4.8. Test setup for flow table test
- Figure 4.9. Compressive strength test of hardened mortar
- Figure 4.10. Consistency of fresh mortar
- Figure 4.11. Compressive strength of mortar
- Figure 4.12. Masonry cubic specimens
- Figure 4.13. Masonry cubic specimens with LVDTs attached
- Figure 4.14a. Failure modes of brick units
- Figure 4.14b. Failure of masonry cubic specimens
- Figure 4.15. Material (a) OSB timber, (b) Adhesive anchor, (c) Mechanical anchor
- Figure 4.16. Plain masonry prism specimen
- Figure 4.17. Retrofitted masonry prism specimen
- Figure 4.18. Small-scale test setup (drawing)
- Figure 4.19. Test setup. (as built)
- Figure 4.20. Instrumentation
- Figure 4.21. Typical load-displacement curve
- Figure 4.22a. Dimension on the prism
- Figure 4.22b. Equivalent section for the retrofitted prism
- Figure 4.23. Failure pattern of (a) MP00-1 (b) MP00-2 (c) MP00-3
- Figure 4.24. Load displacement curve for plain specimens
- Figure 4.25. Failure pattern of (a) MPOSBC1-2 (b) MPOSBC1-2* (c) MPOSBC1-3
- Figure 4.26. Failure pattern of (a) MPOSBC2-1 (b) MPOSBC2-2 (c) MPOSBC2-3
- Figure 4.27. Load displacement curve for plain and retrofitted specimens
- Figure 4.28. Performance in term of (a) Load Capacity (b) Displacement

- Figure 4.29. Wall specimen bonding pattern (plan drawing)
- Figure 4.30. Wall specimen bonding pattern (image during construction)
- Figure 4.31. Typical connection layout for retrofitted wall specimens
- Figure 4.32. Masonry wall specimens (as built)
- Figure 4.33. Larger-scale test arrangement (drawing scheme)
- Figure 4.34. Larger-scale test arrangement (as built)
- Figure 4.35. Applied out-of-plane load history
- Figure 4.36. Position of LVDTs on wall specimen
- Figure 4.37. Load vs Displacement curve for plain specimens
- Figure 4.38. Failure pattern of PW1115-1
- Figure 4.39. Failure pattern of PW1115-2
- Figure 4.40. Load vs Displacement curve for plain specimens
- Figure 4.41. Failure pattern of retrofitted masonry wall
- Figure 4.42. Performance at the occurrence of the first crack
- Figure 4.43. Performance at the failure
- Figure 5.1. Masonry modelling techniques
- Figure 5.2. Micro modelling of masonry cube
- Figure 5.3. Masonry unit behaviour under uniaxial compression
- Figure 5.4. Masonry unit behaviour under uniaxial tension
- Figure 5.5. Mortar behaviour under uniaxial compression
- Figure 5.6. Mortar behaviour under uniaxial tension
- Figure 5.7. Friction behaviour
- Figure 5.8. Tensile behaviour of present model vs experimental results
- Figure 5.9. Mesh seed global size control
- Figure 5.10. Influence of mesh density on the numerical model
- Figure 5.11. Model `output for masonry cubic model
- Figure 5.12. Stress-strain curve of masonry cubic model
- Figure 5.13. MP model comprising brick and mortar
- Figure 5.14. MP model comprising anchor rod and OSB timber

Figure. 5.15. Constraint and interaction surfaces in MP model

Figure. 5.16. General view of masonry prism model.

Figure. 5.17. Boundary condition and load application.

Figure. 5.18. Observed failure of MP00-NM

Figure. 5.19. Load displacement curve for plain MP (Experimental vs Numerical)

Figure. 5.20. Observed failure of MPOSB-NM n

Figure. 5.21. Load displacement curve for retrofitted MP (Exp. vs Numerical)

Figure. 5.22 Observed failure of MPOSB-NM vs MPOSBC1

Figure. 5.23. Boundary condition and load application on PW1115-NM

Figure. 5.24. Boundary condition and load application on 1SRW1115-NM

Figure. 5.25. Boundary condition and load application on 2SRW1115-NM

Figure. 5.26. Observed failure of PW1115-NM

Figure. 5.27. Load displacement curve for Plain Wall (Exp. vs Numerical)

Figure. 5.28. Observed failure of 1SRW1115-NM

Figure. 5.29. Load displacement curve for 1SRW1115 (Exp. vs Numerical)

Figure. 5.30. Observed failure of 2SRW1115-NM

Figure. 5.31. Load displacement curve for 2SRW1115 (Exp. vs Numerical)

Figure. 5.32. Damage plot for different application of the proposed technique

Figure. 5.33. Load vs Displacement curve and Load capacity of the application

Figure. 5.34. Damage plot for different thickness of OSB

Figure. 5.35. Load vs Displacement and Load capacity of different OSB thickness

Figure. 5.36. Damage plot for different number of anchor connections

Figure. 5.37. Load vs Displacement and Load capacity of different number of anchors

List of Notations

G_f^I	: interface mode I fracture energy
f_{bo}/f_{co}	: bi and unidirectional compressive strength ratio
μ_b	: Poisson ratio of the brick unit
σ_t	: tensile stress
E_b	: modulus of elasticity of brick unit
$E_{c,m}$: modulus of elasticity of mortar
$E_{i,b}$: modulus of elasticity of brick unit @ 30% $f_{c,b}$
$G_{f,c}$: compressive fracture energy
$G_{f,t}$: tensile fracture energy
M_{du}	: dry weight of brick unit
M_{wu}	: wet weight of brick unit
P_{max}	: maximum load
V_u	: volume of brick unit
W_u	: water absorption of brick unit
d_c	: coefficient of compressive damage
d_t	: coefficient of tensile damage
$d_{u,c}$: ductility index in compression
$d_{u,t}$: ductility index in tension
f_b	: compressive strength of the brick units
$f_{c,b}$: compressive strength of masonry unit
$f_{c,m}$: compressive strength of mortar
f_k	: characteristic compressive strength of masonry specimen.
f_m	: compressive strength of the mortar
f_{mc}	: compressive strength of the masonry cube
$f_{t,b}$: tensile strength of masonry unit
$f_{t,m}$: tensile strength of mortar
f_x	: flexural strength of the masonry prism
α_a	: parameter for ascending branch of the compression curve
α_d	: parameter for descending branch of the compression curve
α_t	: parameter for descending branch of the tensile curve
γ_{du}	: dry density of brick unit
$\varepsilon_{60\%}$: equivalent strain at 60% maximum load

ε_c	: compressive strain
ε_{c1}	: compressive strain at the peak stress
ε_{cr}	: tensile strain at cracking
ε_t	: tensile strain
$\sigma_{60\%}$: stress at 60% maximum load
σ_c	: compressive stress
σ_{max}	: maximum stress n brick unit
μ	: coefficient of friction
d	: displacement in the masonry specimen
e	: eccentricity parameter
h	: height of brick unit
K	: is a constant, function of the type of units and mortar
k	: stress ratio in tensile meridian
$K_{n,s,t}$: traction-separation stiffness coefficient
γ	: mass density
Ψ	: dilation angle
A	: loaded area
b	: breadth of the brick unit
l	: length of the brick unit
α, β	: constants based on mortar used for finding masonry compressive strength

CHAPTER ONE - INTRODUCTION

1.0 Background

Masonry is a configuration of brick units bonded together with mortar often categorised as a homogenous brittle composite material (Lourenco, 1996). Before the emergence of more recent building materials such as concrete and steel, masonry was the predominant building material. Masonry materials are relatively available at low cost and were used according to the common practice, mostly derived on empiric rules of proportion based on experience (Ingrid, 2016). These make masonry construction to be popular as one of the earliest building categories.

A large number of unreinforced masonry (URM) structures were built all over the world in the past, and now they constitute a unique historical value for civilisation, besides the evident housing and infrastructural value. Old URM structures were often designed and built using construction techniques with no conformity to any construction codes but rather to building's "rules of art" (Menon and Magenes, 2008). As a result, old URM structures perform worse than recent structures when subjected to excessive loading which may result in catastrophic failure (Ramos and Lourenco, 2004; Vasconcelos and Lourenco, 2009; Pena et al., 2010). Therefore, retrofit of old URM structures to increase their structural capacity and ductility is highly encouraged to avert substantial damages and loss of lives when subjected to excessive loading or in the case of disastrous events.

The failure of URM walls can be in out-of-plane (bending) or in-plane (shear), but the out-of-plane collapse is the predominant mode of failure of URM walls (Costa et al., 2011; Lin et al., 2016; Lourenço et al., 2017; Abrams et al., 2017). The out-of-plane failure is predominant in URM walls because of connection failures between perpendicular walls or between walls and diaphragms. Also, URM walls are vulnerable when subjected to out-of-plane loading (face-load) due to lack of tensile resisting elements in the out-of-plane direction (Hamoush et al., 2001; Derakhshan et al., 2009; Lourenço et al., 2017; Abrams et al., 2017). Under severe out-of-plane loading, the failure of a masonry wall is likely to be sudden and

severe, producing devastating damages, injuries and/or death of occupants and passers-by (Derakhshan et al., 2009; Costa et al., 2011; Lin et al., 2016; Lourenço et al., 2017; Abrams et al., 2017). Walls collapsing in out-of-plane direction cause the most significant amount of damages compared to in-plane failure. Out-of-plane loading can be due to overpressure from blast effect induced by an explosion, overpressure induced by impacts from a snow-avalanche for mountain area habitation. It can also be due to the effect of extreme wind, earthquake, and generally wall subjected to out-of-plane pressure (Zeiny and Larralde, 2010).

The response of URM walls to out-of-plane excitation is a complex and ill-understood research area (Priestley, 1985). However, recently, considerable efforts have been made by several researchers to understand the behaviour of URM walls subjected to out-of-plane loading both experimentally and numerically. This development is because there is a unanimity of researchers' opinion that out-of-plane failure is the most dangerous failure of URM walls (UMINHO, 2006). Subsequently, structural retrofits of URM buildings have been developed to increase their load capacity to meet the current load demand and prevent this dangerous out-of-plane failure of old URM structures.

Retrofitting is continually becoming an important issue across the urban infrastructure. Most retrofits are driven by a combination of improving energy efficiency as well as enhancing structural capacity to damaged or vulnerable structures. In the case of historical URM structure, retrofitting is aimed at making the building safer and less prone to major structural damage during an excessive loading to preserve their culture and heritage significances (Wang et al., 2018). This desire to retain historical buildings that have cultural and heritage value are the impetus for research on how to develop sustainable retrofit techniques for historical URM structures. Retrofitting is quite different from the commonly used terms, repair and rehabilitation. Retrofit is about making the structure more resistant to damages. On the other hand, repairing of structure is a process of fixing damaged structure to good working condition while rehabilitation is the process that entails restoring the integrity of structure to its original state.

Retrofit of historical URM structure has been the subject of multiple earlier studies. As such, many retrofit technologies have evolved. For instance, grout and epoxy injection, reinforced plaster and shotcretes, steel column and plate as

external reinforcement, elastomeric spray, internal concrete skin, post-tensioning and confining URM using reinforced concrete tie columns and masonry piers have all been reviewed as alternatives retrofit techniques by (ElGawady et al., 2004) and (Oliveira et al., 2012). These techniques were investigated to make existing masonry stronger and more capable of resisting the effects of out-of-plane loads safely. Most of the techniques are traditional retrofitting approaches requiring a considerable amount of time for implementation. They are also at a disadvantage because they can disrupt the historical and aesthetical form of the existing structures and sometimes encroaches the functional spaces.

Meanwhile, retrofit of historic structures should be such that it neither disrupts their custom nor alter their structural behaviour harshly. It should also be reversible (Chrysostomou et al., 2015). This claim by Chrysostomou et al. (2015) led to the emergent of innovative protection systems like base isolation and energy-dissipation devices, such as viscous dampers and shape memory alloys to enhance the seismic resilience of cultural heritage against the effects of earthquakes and excessive out-of-plane loading. These methods would mitigate the rocking response of block-like elements during earthquakes (Chrysostomou et al., 2015). However, the number of technical details and resources required for these techniques make them complex methods to be adopted. Also, the heavy non-structural objects like dampers, which are placed on top or inside the old URM buildings in these approaches, present a serious hazard for both human lives and cultural heritage in the event of structural failure (Chiozzi et al., 2015).

The application of composite materials such as epoxy and fibre reinforced polymer (FRP) mostly based on carbon, glass, and aramid fibre offers promising retrofitting possibilities for masonry buildings (Corradi et al., 2015; Ismail and Ingham, 2016). They present several well-known advantages over existing conventional techniques. They do not alter the configuration of the building on which they were applied. Most studies have highlighted that FRP application compared to the conventional techniques, make less ingress into functional space to achieve a reasonable increase in structural capacity (Nanni and Tumialan, 2003; Saadatmanesh, 2014; Corradi, et al., 2015). This is because FRP has quite higher strength and stiffness to thickness ratio. FRP composites have then arisen to be one of the most promising construction materials for retrofit of historic

structures (Alkhrdaji, 2013). Some of the drawbacks of FRP applications are the relatively high cost of the material, the technical requirement for the installation, and limited knowledge about the ageing properties of the material.

Moreover, some experimental tests showed that FRP is less so compatible with masonry due to the differences between stiffness, strengths, and thermal coefficients (Gattesco and Boem, 2017). Also, masonry surfaces showed a weak bond to the FRP (Alkhrdaji, 2013; Gattesco and Boem, 2017). The weak bond is due to the type of substrate material and irregularity of the masonry surface, which may induce debonding, and thus reduce the proclaimed effectiveness of FRP in retrofitting URM structures (Gattesco and Boem, 2017).

A different approach is the retrofit of adobe masonry building using canes (Varum et al., 2013) and rammed earth using timber posts (Silva et al., 2013) as external reinforcement. The applied timber post prevents the sudden failure of the earthen material, which is due to the low tensile strength of the earth material (Silva et al., 2013). The timber has high tensile strength and displaces gradually in the out-of-plane direction without brittle failure taking up the additional lateral load. This improvement recorded in the tensile strength of rammed earth retrofitted by fixing of timber posts behind the wall spurred the interest in aiming to propose retrofit of URM wall using timber panel. Therefore, the current study proposes to adopt an oriented strand board (OSB) timber panel to retrofit URM walls to improve out-of-plane performances. This study considered timber-based techniques because timber material is economical and can be easily sourced around the globe.

Indeed, timber-panels are currently being used as wall insulation for energy retrofit of old URM buildings (Pelenur, 2013; Giongo et al., 2017), but their application for structural retrofitting of URM wall is still not been thoroughly studied. To the researcher's knowledge, an experimental study by (Sustersic and Dujic, 2014) was the first study on the application of timber panels as strengthening system for existing buildings against seismic force. The in-plane behaviour of URM wall retrofitted with Cross Laminated Timber (CLT) panel was studied, the results showed that there is a considerable increase in strength and ductility of the retrofitted URM wall. This increase in ductility is because of an increase in the displacement capacity and resistance of the retrofitted wall.

Sustersic and Dujic (2014) reported a 100% increase in ductility when the CLT panel was connected to URM walls with a specially developed steel connection at top and bottom of the wall. However, the availability of these special connections in the open market is a concern limiting the acceptability of the techniques. Moreover, the difficulty in introducing heavy and stiff CLT panel in old URM buildings make this solution questionable. Here, in contrast, OSB panel connected to the URM walls by threaded dry rod connections and injectable chemical adhesive anchor readily available in the European market were investigated.

In this study, a four-point bending test on 615 x 215 x 102.5mm small-scale masonry prism and 1115 x 1115 x 215mm larger-scale masonry wall are presented to evaluate the flexural performance (out-of-plane load capacity and deflection), toughness (energy absorption capacity) of URM walls retrofitted with OSB timber panel. The experimental works involved subjecting both plain and timber retrofitted URM walls to out-of-plane loading using quasi-static (monotonic) loading scheme. The reasons for selecting the quasi-static loading scheme is that the test will be able to replicate the behaviour of URM wall when subjected to cycles of loadings through a hydraulic actuator. This quasi-static testing method is, of course, a simple test method to approximate the loading that a URM wall is subjected to during a seismic event but not to capture the entire dynamic nature of the earthquake (Beyer et al., 2014). Quasi-static loading has been widely accepted and implemented in previous studies in the absence of shaking table facilities (Lourenco, 1998; UMINHO, 2006; Beyer et al., 2014). Meanwhile, this research is not exclusively applicable to earthquakes but to generate knowledge and understanding of whether timber panels can improve the out-of-plane capacity of URM walls against excessive out-of-plane loading in general.

This research entails experimental and numerical investigation on the use of oriented stranded board (OSB/type 3) timber-panel in retrofitting unreinforced masonry wall. The significance of this study is to promote the use of oriented strand board (OSB) timber panels, which is cheaper, easily available and can be considered as a sustainable material in retrofitting URM walls. The introduction of this retrofit approach using OSB timber panel will add to the existing masonry retrofit techniques and also provide practitioners with the opportunity to choose

an appropriate retrofit technique for URM walls from the available pool. The research output will ultimately serve as aids in decision making when planning and during any retrofit of historic masonry structures.

1.1 Research Question and Hypotheses

To what extent the application of oriented stranded board (OSB/type 3) timber panel in retrofitting URM walls can improve the out-of-plane capacity of URM walls?

The research question is based on the following hypotheses:

- ❖ **Hypothesis 1:** URM walls that have been previously retrofitted will perform better than unretrofitted URM walls when subjected to similar loading scenario.
- ❖ **Hypothesis 2:** Retrofit of old URM walls will avert substantial damages and loss of lives when subjected to excessive loading or in the case of disastrous events.
- ❖ **Hypothesis 3:** URM walls failing in out-of-plane direction will be more likely devastating than the in-plane failure.
- ❖ **Hypothesis 4:** Adding a material such as OSB type 3, with improved tensile capacity will likely improve the out-of-plane capacity of URM walls.

1.2 Aim

- ❖ This research aims to develop and evaluate the performance of a new timber-based retrofit technique for URM walls. This research aim was achieved through the enabling objectives identified in section 1.3.

1.3 Objectives and Scope of the Study

- ❖ **Objective 1:** To review and analyse available experimental results to understand the structural behaviour and failure mechanism of masonry walls, and to understand the contribution of different retrofit technique in countering the out-of-plane failure of masonry walls (Section 2).

- ❖ **Objective 2:** To plan the experimental and numerical investigation exhaustively to study the efficiency of the proposed timber-based retrofit technique (Section 3).
- ❖ **Objective 3:** Experimental investigations (Section 4)
 - **Objective 3.1:** To experimentally characterise the mechanical properties of masonry brick units and mortar used in building the masonry specimens tested in this study (Section 4.1).
 - **Objective 3.2:** To perform flexural bond strength test on 615 x 215 x 102.5mm small-scale plain and retrofitted masonry prism to understand the behaviour of masonry prism specimens and the connection between masonry and timber panel (Section 4.2).
 - **Objective 3.3:** To perform out-of-plane flexural strength test on 1115 x 1115x 215mm larger-scale masonry walls (i.e. plain URM wall and URM walls retrofitted with timber-based panel) (Section 4.3).
- ❖ **Objective 4:** To develop finite element models (FEM) to perform numerical analysis on out-of-plane behaviour of URM walls (i.e. both plain URM wall and URM walls retrofitted with wood-based panel) (Section 5.1 – 5.4).
- ❖ **Objective 5:** To validate the finite element models against the experimental data and carry out a parametric study (Section 5.5).

The scope of this research is limited to a single leaf, double wythes solid wall panel without returning walls at the corners. This research is limited to investigating only the out-of-plane behaviour of masonry wall. Only quasi-static load will be considered in this study. In-plane behaviour and wall subject to a real earthquake (dynamic loads) are not treated.

1.4 Thesis Outlines

In addition to this introductory chapter, the thesis contains five other chapters as follow:

- ❖ **Chapter 2:** provides a concise review of literature about masonry structures, structural behaviour of URM walls, and failure modes of URM walls. After that, a review of existing retrofit techniques for countering the failure of URM wall is presented. Also, in this chapter is a review of the experimental tests to study

out-of-plane failure of URM wall. At the end of the review, then a brief introduction of the proposed timber-based retrofit technique, the objectives, scope, and the limitation of this research are presented.

- ❖ **Chapter 3:** presents the overall study program for investigating the proposed techniques. The full experimental and numerical program is presented here.
- ❖ **Chapter 4:** contains the details of the experimental campaign including material characterisation, small-scale test on 665 x 215 x 102.5mm masonry prisms, and larger-scale test on 1115 x 1115 x 215mm masonry walls.
- ❖ **Chapter 5:** discusses the details of the numerical analysis and validation, including material characterisation, small-scale and larger-scale numerical model. Parametric study on larger-scale model is also presented here.
- ❖ **Chapter 6:** presents the important conclusion from this research and recommendation for future works.

CHAPTER TWO - MASONRY BEHAVIOUR AND STRUCTURAL RETROFIT TECHNIQUES

2.0 Masonry

Masonry can be described as the configuration of masonry units bonded together with mortar. There are various materials of masonry construction such as building stones (e.g. granite, marble and limestone), clay tiles, glass block, concrete block and brick. The most used of these are bricks and concrete blocks. Masonry materials are relatively available at low cost and can be easily built. These make masonry to be popular as one of the earliest building categories. Masonries have proven history of durability and resistance to weathering. They behave fairly well under normal gravity loading. However, in the event of an extreme loading like earthquakes and excessive out-of-plane loads, they attain partial to total collapse, which results in large-scale loss of lives (Drysdale et al., 1993).

According to the British Standard Institution (BSI, 1996), masonry can be classified as unreinforced, reinforced, confined, and prestressed depending on the level of engineering details involved in the construction. Reinforced masonry is masonry construction in which bars or mesh are embedded in mortar or concrete so that all the materials act together in resisting action effects. Prestressed masonry is the one in which internal compressive stresses have been intentionally induced by tensioned reinforcement (BSI, 1996). Confined masonry is provided with reinforced concrete or reinforced masonry confining elements in the vertical and horizontal direction. Meanwhile, unreinforced masonry is a category of masonry construction with no or insufficient reinforcement to be considered as reinforced masonry (BSI, 1996).

However, the most common type in traditional and historical structures are unreinforced masonry which is particularly susceptible to damages from out-of-plane loads (Ingham and Griffith, 2011). Hence, this study focuses on unreinforced masonry walls.

2.1 Unreinforced Masonry (URM) Wall

URM walls are typically arranged masonry units bonded together by mortar without sufficient reinforcement or mostly no reinforcement at all. The arrangements are such that the units are in a regular pattern called bonds such as Stretcher, Flemish, and English bond etc. (Fig. 2.1). Typically, URM walls in masonry building are primarily structural walls. Their primary functions are to support their self-weight, dead loads from floors and roof, and live loads due to the usage. They can be single-leaf, double-leaves, cavity and grouted cavity walls (BSI, 1996).

Single-leaf wall: This is a solid wall without cavity or continuous vertical joint in its plane (Fig 2.2a). This also includes double wythe single leaf wall (Fig. 2.2b).

Double-leaves wall: This comprises of two parallel wall leaves with the longitudinal joint between the leaves filled solidly with mortar (collar joint). The leaves are securely tied together with wall ties (Fig 2.2c) to have a common action under loads.

Cavity wall: It is also a double leaves wall system where two parallel single-leaf are effectively tied together with wall ties. But the space between them is left as a continuous cavity or partially filled with non-load bearing thermal insulating material (Fig 2.2d).

Grouted cavity wall: wall consisting of two parallel leaves with the cavity filled with concrete or grout and securely tied together with wall ties or bed joint reinforcement.

Other types of URM walls as related to masonry construction methods and usage are shell bedded, veneer, shear, stiffening and face wall (BSI, 1996).

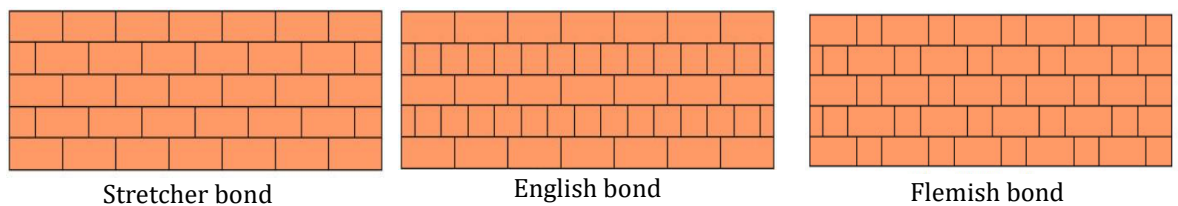


Figure 2.1. Type of URM wall bond

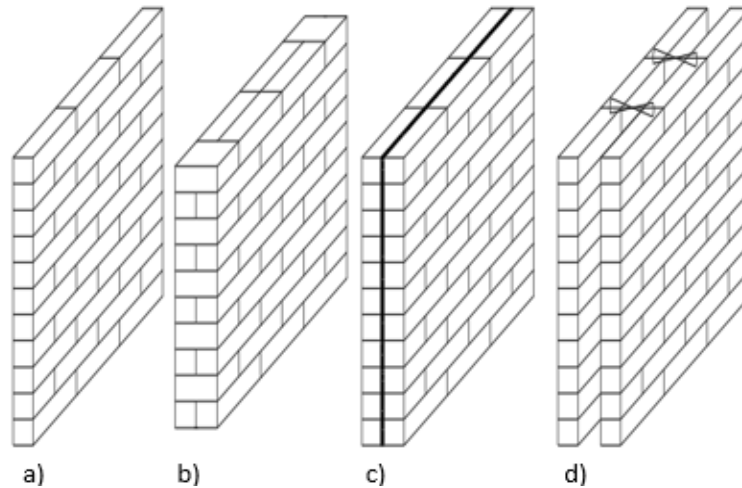


Figure 2.2. URM wall: (a) Single-leaf (b) Double wythe single-leaf (c) Double-leaf (d) Cavity wall

2.2 Structural Behaviour of URM Wall

Masonry structure is one of the simplest types of structure regarding its construction and skill requirements. Nevertheless, masonry is a complex construction material to understand in term of its structural response and mechanical properties. The complexity is because correct behaviour assessment of masonry structure is difficult (Costa et al., 2011). Its behaviour is often influenced by the quality of materials used, workmanship, and the bond pattern (Wang et al., 2016). It is quasi-brittle in nature, hefty in self-weight, contains loose components, has low tolerance to oscillation and thus undergoes sudden brittle failure without much warning to the occupants (Priestley, 1985; Lourenço et al., 2017). Therefore, in case of sudden failure induced by hazards, occupants of URM structures do not have enough time to run for safety. Hence, detail consideration for retrofit of old URM walls is highly encouraged to ensure that they can perform their highly sought energy absorption and force relieving roles against failures.

2.3 Failure Modes of URM Wall

The failure of URM walls can lead to partial or global collapse of the walls in out-of-plane due to bending or in-plane due to shear (Pabaraharan, 2008; Nazir, 2015). URM walls have considerable compressive strength under vertical loading, but they are relatively weak in tensile strength to resist lateral (out-of-plane) loads (Ismail and Khattak, 2019). They are weak against overpressure from blast effect induced by explosion or earthquake, snow-avalanche for habitation in a

mountain area, extreme wind, and mostly lateral (out-of-plane) loading. Previous occurrences reported by Jorgustin (2011), Costa et al. (2011) and Pan et al. (2016) shown that URM walls have exhibited their extreme vulnerability in the event of excessive out-of-plane loading. The failure mode of URM walls is often brittle due to their limited ductility (Ismail and Khattak, 2019). URM wall failures can happen in quite many of the in-plane and out-of-plane modes. For instance, cracks can develop along bed joint in flexure due to out-of-plane forces acting normal to the axial plane or diagonal cracks can occur due to in-plane forces acting parallel to the axial plane of the wall (Bui et al., 2010; Costa et al., 2011; Lin, et al., 2016).

Generally, the failure of URM wall is attributed to structural irregularity, poor connections between orthogonal walls and between walls, inadequate rigid floor diaphragms to attain box behaviour, and inadequate structural integrity (Magenes and Calvi, 1997; Ingrid, 2016). Depending on the response of URM structures, the failure mechanism of masonry building can be local (mode I) or global (mode II) (Fig. 2.3). The mode I failure mechanisms is generally associated with an out-of-plane failure of a structural element (local damage) which are caused due to lack of adequate anchorage of walls and diaphragm (Florio, 2010). Meanwhile, the forces acting in-plane with the wall usually causes the mode II failure and is typically marked by inclined cracks associated with shear forces that often result in an “X” pattern. When a full “X” crack occurs in the structure, the triangular sections of the “X” can become unstable, leading to collapse (Decanini et al., 2004).

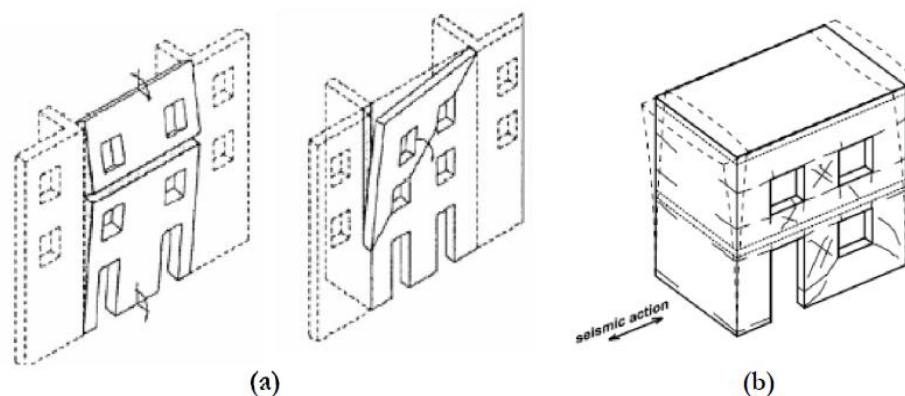


Figure 2.3. Failure mechanism modes; (a) Mode I: local collapse mechanism (D'Ayala and Speranza, 2003), (b) Mode II: global collapse mechanism (Magenes and Calvi, 1997).

2.3.1 In-Plane Failure Modes of URM Wall

Shing et al. (1991), Davidson and Brammer (1996) and Nazir (2015) concurred that URM walls exhibit three simple forms of in-plane failure, as shown in figure 2.4. The wall geometry influences these failure mechanisms i.e. the ratio of wall height to its length (H/L) and layout of joints (Brunner and Shing, 1996; Minaie, 2009). As deduced from Nazir (2015), a shorter wall ($H/L \ll 1.0$) tends to fail as bed joint sliding shear (Fig 2.4a). While a short wall ($H/L \leq 1.0$) tends to fail due to diagonal cracking induced by the principal tension perpendicular to diagonal strut (Fig. 2.4b). For walls with ($H/L > 1$), flexural failure is the most common failure exhibited (Fig 2.4c).

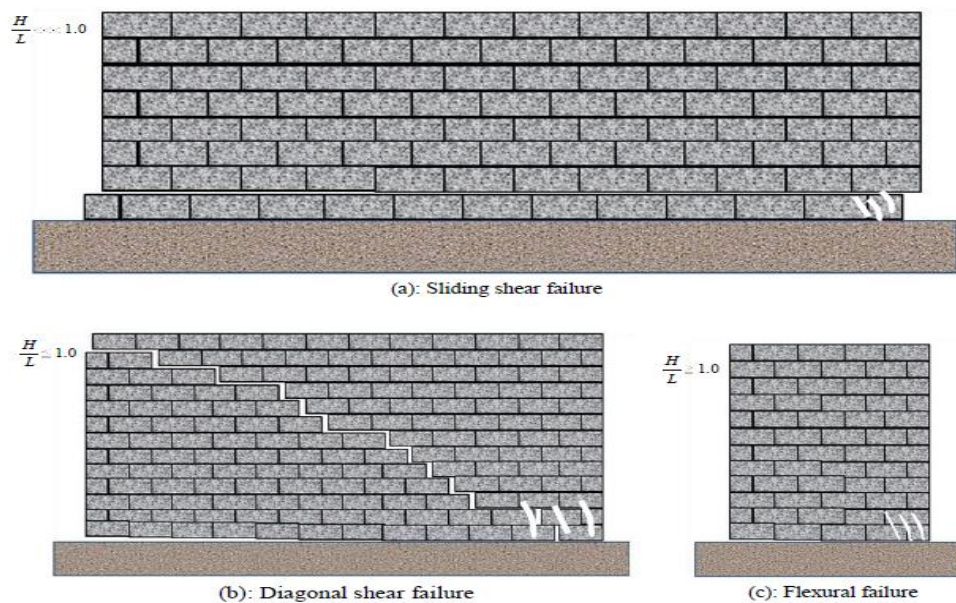


Figure 2.4. In-plane failure modes of URM (Nazir, 2015)

2.3.2 Out-of-Plane Failure Modes of URM Wall

Either one-way or two-way bending characterises the out-of-plane failure of URM walls. The bending is such that the wall will bend either in or out of its original plane. These can result in a partial or total collapse of the wall (Fig. 2.5). It is the most devastating failure mode in URM walls (Lin et al., 2016). Lourenço et al. (2017) also stated that walls collapsing in the out-of-plane represent a major hazard in the failure of URM building. The major cause of out-of-plane failure is due to the lack of tensile resisting elements in URM wall when loaded in the out-of-plane direction. Other causes are connection failures between perpendicular walls or between walls and diaphragms, presence of large spaces inside URM

buildings, insufficient connections to transverse structural elements. Costa et al. (2014) and Lin et al. (2016) enumerated that wall thickness, slenderness ratio, wall to diaphragm connections are the key parameters in assessing the out-of-plane capacity of URM walls. Furthermore, the strength of masonry wall of a given type will be influenced by the eccentricity of vertical loading and the slenderness ratio when buckling failure of the masonry wall is involved as highlighted in the study of Hendry (1998) and Sandoval and Roca (2012). The impact of the slenderness ratio of the masonry wall on the load-carrying capacity of the walls is such that an increased slenderness ratio reduces the load capacity of the wall (Hendry, 1998). The study of Sandoval and Roca (2012) expatiated that walls with lower stiffness will respond more drastically to the increase in the slenderness ratio of the wall. For the eccentricity of the vertical load, the main failure of the masonry will be by crushing when masonry wall is subjected to compression load with null eccentricity. However, if the vertical load is applied with a higher eccentricity, the failure will be due to instability resulting in buckling (Hendry, 1998; Sandoval and Roca, 2012).



Figure 2.5. Out-of-plane failure modes of URM (De Santis et al., 2015)

Similarly, BSI (1996) maintained that flexural loading as a result of face-loads on walls in the out-of-plane direction is the worst case. This flexural loading can cause the bending of the wall to have a plane of failure either parallel or perpendicular to the bed joints (Fig. 2.6). The flexural failures of masonry wall occur due to either stress exceeding the tensile strength of the unit or that of unit-

mortar bond strength. Considering failure where the induced stress exceeds the unit-mortar bond strength (i.e strong unit - weak joint combination), the failure with the plane of failure parallel to the bed joint is the most devastating. This is because in masonry with weak mortar, the ability to withstand tensile stressing (tensile bond strength) in the bed joint zone is generally very slight (low adhesive strength between the mortar and the unit, edge debonding of the mortar due to shrinkage, incomplete mortaring of the bed joint). Meanwhile, for the failure to occur perpendicular to the bed joint, the failure will pass through the bed joint and meet up with the unit, which is stronger before moving to the head joint (Fig. 2.6b(ii)), this requires higher stress than the failure parallel to bed joints.

According to BSI (1996), the characteristic flexural strength of masonry either with the plane of failure parallel or perpendicular to the bed joint may be determined by tests following EN 1052-2 provisions as later done in this thesis. Also, it may be established from an evaluation of test data based on the flexural strengths of masonry obtained from appropriate combinations of units and mortar using coefficients in tables under section 3.6.3 of BSI (1996).

Interestingly, using the tables mentioned above, the characteristic flexural strength of masonry with the plane of failure parallel to the bed joint (f_{xk1}) is smaller than its contemporary with failure perpendicular to the joint (f_{xk2}). For instance, using a combination of clay masonry unit and general-purpose mortar of strength greater than 5N/mm^2 , f_{xk1} is 0.1N/mm^2 while f_{xk2} is 0.4N/mm^2 . Clearly, this supported the observation that the failure plane parallel to the bed joint is the weakest and the most devastating failure mode in masonry walls with strong unit-weak joint combination.

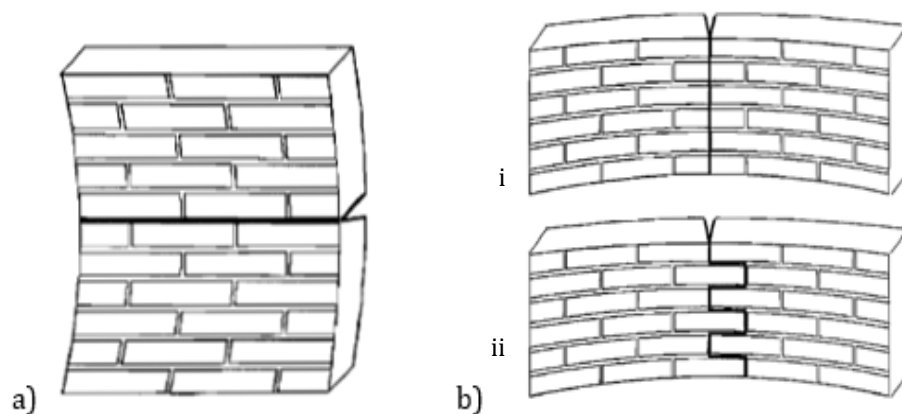
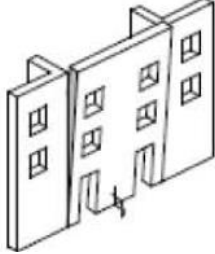
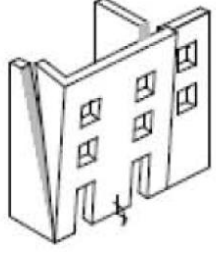
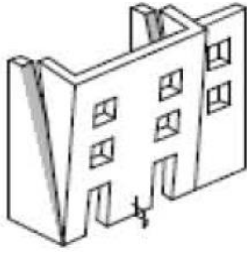
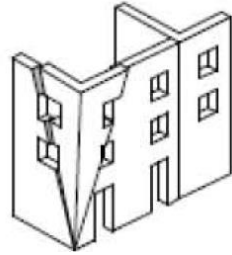
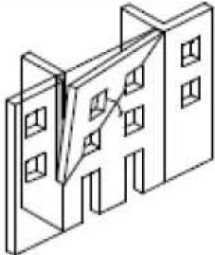
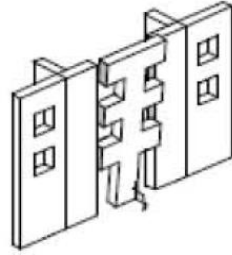
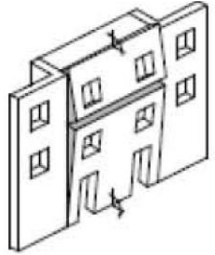
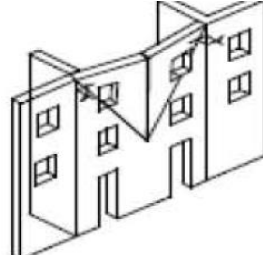


Figure 2.6. URM failure plane: (a) parallel to bed joints, (b) perpendicular to bed joints (BSI, 1996)

Furthermore, D'Ayala and Speranza (2003) identified that the development of out-of-plane failure mechanism in URM building depends on the quality and strength of the connections with the other elements of the structure, party walls, internal load-bearing partitions, floors, and roof structures. D'ayala and Speranza (2002) had earlier developed a procedure called FaMIVE (Failure Mechanism Identification and Vulnerability Evaluation). FaMIVE identified the different type of out-of-plane damages found in buildings with pre-existing seismic damages. As such, the various type of out-of-plane failure mechanism and the possible collapse causes were reviewed as shown in table 2.1.

Table 2.1: Out-of-plane failure mechanism by FaMIVE (D'ayala & Speranza, 2002)

<p>A- Vertical overturning: insufficient connection at the edges of the wall to generate restraint by the party wall</p> 	<p>B1- Overturning with one side party wall: sufficient connection of facade wall to one party wall to involve it in the overturning</p> 
<p>B2- Overturning with two sides party walls: sufficient connection to involve, beyond the facade wall, both party walls into the overturning</p> 	<p>C- Corner overturning around a horizontal hinge and orthogonal to the corner bisector plane. Occurs when the corner of the building is free, without any adjacent structures</p> 
<p>D- Partial overturning, for which only a portion of the facade is subjected to overturning and the party walls are not involved directly in the mechanism</p> 	<p>E- Vertical strip overturning: considered when due to the window layout, there might be a solution of integrity within the facade plane leading to partial failures</p> 
<p>F- Vertical arch: occurs when due to the presence of ties, the vertical strips of the facade tend to deflect out-of-plane, being restrained at bottom and top</p> 	<p>G- Horizontal arch occurs when the facade span is rather wide, and internal bearing walls exert none or minimal restraining action</p> 

2.4 Structural Retrofit of URM Wall

This research work is on the structural retrofit of URM walls to counter the out-of-plane failure mechanisms in URM walls. Therefore, this section presents a concise review of the existing retrofit techniques of URM walls classified as shown in figure 2.7 below.

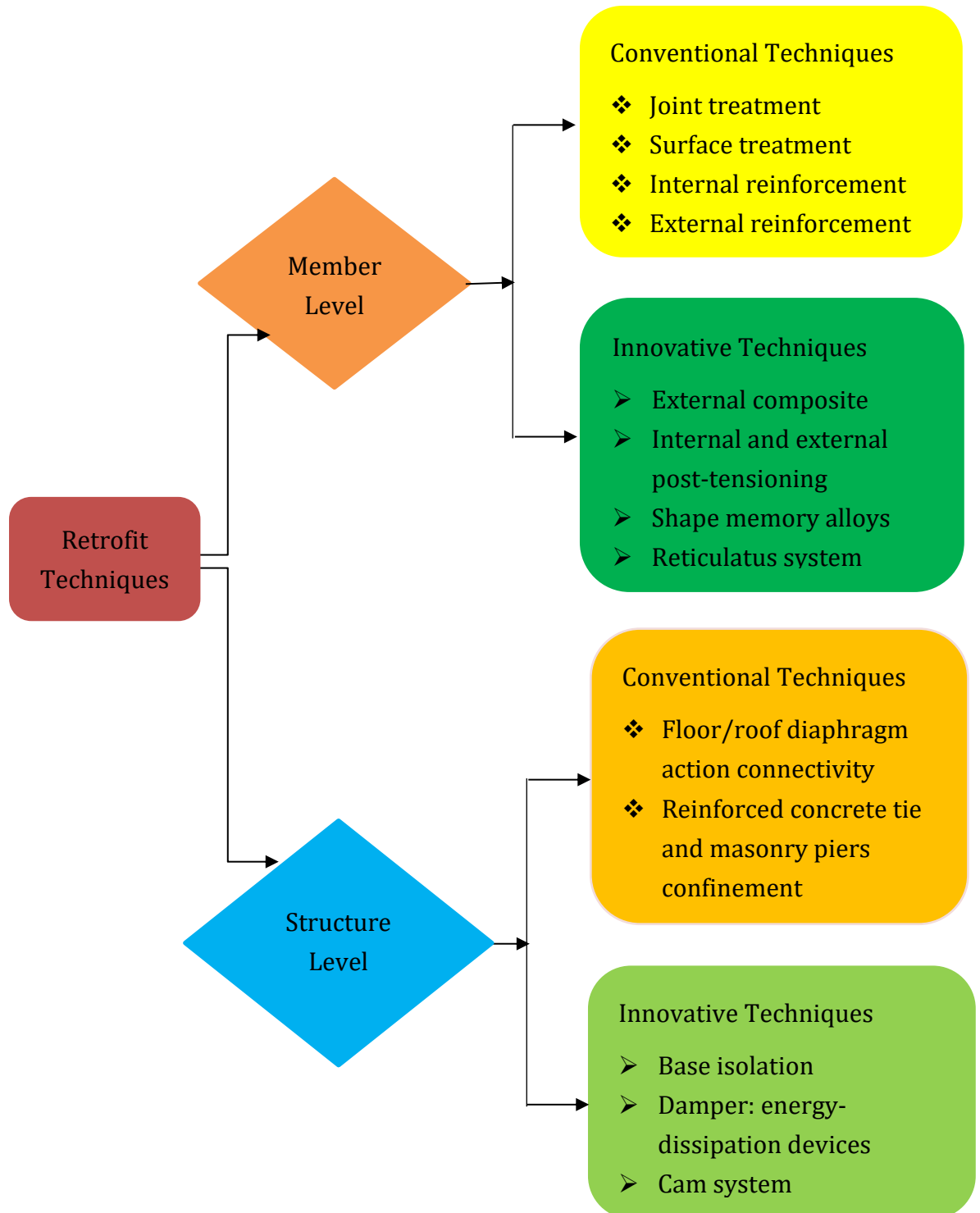


Figure 2. 7. Classification of retrofit techniques

Structural retrofitting is a process of modifying or increasing the structural capacity and ductility of existing buildings. In the case of URM structures, retrofits are used to offer some structural upgrade or structural damage control for existing URM structures. Over the years, several retrofit techniques have evolved to improve the capacities of masonry structures in resisting excessive out-of-plane loading, including earthquakes. The techniques were broadly divided into two categories; (i) member level: retrofit consideration for particular members of the building such as walls, floor or roof and (ii) structure level: retrofit consideration to improve the integrity and overall response of the whole building (Izmir and Erberik, 2015; Binda and Cardani, 2015). Under each level of intervention is subgroup classified as conventional or innovative technique as shown in figure 2.7. The subsequent sections 2.4.1 and 2.4.2 reviewed the retrofit techniques under both member level and structure level retrofit respectively.

2.4.1 Member Level Retrofit

Member level intervention mainly entails giving special consideration to retrofitting individual members such as floor and wall of an existing URM building. The process involves crack repairing, repointing, rebuilding of weakened material, and external supplemental support to a structural member. The main benefit of member level retrofit in URM building is to bring the members to a condition that the members will be sufficient for the intended structural service (Izmir and Erberik, 2015). As such, the retrofit technique being developed in this research is a member level retrofit scheme that considers the application of timber panel in retrofitting URM wall. Here, the existing member level retrofit methods are being reviewed as follows in sections 2.4.1.1 and 2.4.1.2.

2.4.1.1 Conventional Techniques

2.4.1.1.1 Joint Treatment

This method is one of the earliest member level intervention techniques in retrofitting URM structures. Joint treatment (Fig 2.8) is most appropriate in structures where the quality of the masonry units is still very good, but the mortar joint is weak. Wang et al. (2018) indicated that joint treatment is ideal in URM walls that have experienced some voids and cracks due to ageing or chemical and

physical deterioration. The main advantages of joint treatment are its ease of application with minimal cost and suitability for the preservation of historic structures where the aesthetic or historical value of the structure is of high priority. Joint treatment techniques involve approaches such as repointing, grout and epoxy injection, and the technologically advanced micro / fibre reinforced mortar system.

Repointing: This is the most used traditional technique in treating masonry joint. It is a process of replacing or refilling the mortar joints by a new bonding material to restore the original integrity of the URM wall (ElGawady et al., 2004). Repointing is often ideal in retrofitting multi-leaves masonry walls to repair the poor connection between different layers of the wall. It is also a good method in filling the voids in the dry rubble stone's inner core (Wang et al., 2018).

Grout and epoxy injection: This is a widely used technique to repair cracked/damaged masonry structures through the injection of new mortar. It is very effective in restoring the initial stiffness and strength of masonry (Wang et al., 2018). Gigla and Wenzel (1997) stated that the compatibility of the newly introduced epoxy/grout injection to the existing materials is crucial because the injection of an incompatible grout mix causes considerable damage. Also, ElGawady et al. (2004) pointed out that the effectiveness of this technique depends on the types of injection material and the techniques of injection used. In line with the claims submitted by Gigla and Wenzel (1997) and ElGawady et al. (2004) is an observation from Manzouri et al. (1996) works where the use of a high strength epoxy materials together with weaker units in existing masonry alter the stress distributions within the structures under loading. Clearly, this combination is deemed structurally incompatible as the basic characteristics of masonry structures are strong units and weaker joints. To avoid this issue of incompatibility, the most widely used retrofit injections for URM structures are cement-based grouts (Hamid et al., 1999; Chuang and Zhuge, 2005).

Micro/Fibre reinforced mortar system: This is a high-performance strengthening and force protection system designed for extreme load resistance and energy absorption. It combines an infusible ultra-high-performance grout with a densely layered micro steel or fibre reinforcement system (Alkhrdaji, 2013). Erdogmus (2015) studied the potential use of fibre reinforced mortar

(FRM) in the rehabilitation of existing masonry structures as joint reinforcement. The study established that masonry joint reinforced with fibre or micro reinforced mortar offers a considerable increase in masonry's flexural strength, toughness, energy absorption, and ductility during excessive loading.

However, Pierre et al. (1999) had earlier contended that microfibres reduce the compressive strength of the mortar due to increases in the air content of the mixture compared to the normal plain mortar. Also, Banfill and Forster (2000) highlighted that the new materials applied to historic masonry buildings could cause deterioration due to the difference in existing mortars and new mortars. These are parts of reasons why American Concrete Institute (ACI) does not yet recognise the pronounced enhancements that even the most popular and well-researched fibre reinforcement can provide for the structural behaviour of masonry (ACI, 2014). In the meantime, to ensure a successful retrofit of URM structures that will not damage the existing structure using FRM, Erdogmus (2015) recommended that the new reinforced mortar must be prepared to be compatible with the existing mortar and masonry units. When carried out properly, FRM otherwise branded as steel-reinforced grout (SRG) by De Santis et al. (2015) provides substantial improvements in the out-of-plane capacity of masonry walls and may be an effective option to traditional retrofit methods. The prerequisite to using FRM or SRG in the retrofit of historic masonry wall joint is the assessment of the existing mortar's type, strength, and engineering properties (Erdogmus, 2015).

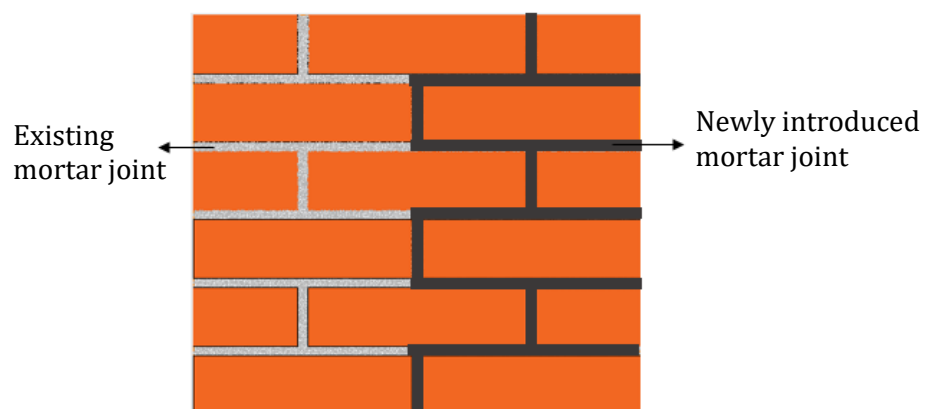


Figure 2. 8. Joint treatment of URM walls

2.4.1.1.2 Surface Treatment

This method involves enlarging existing URM walls with the addition of new reinforced mortar layer or any other suitable coating materials to one or both faces of the wall. The additional thickness achieved by the retrofitted wall leads to improved strength and stiffness of the walls (Wang et al., 2018). The surface treatment is common and easy to apply, but it is time-consuming and alters the historical appearance and aesthetic of the existing structures. Thus, it is not suitable for historical heritage (ElGawady et al., 2004; Wang et al., 2018). Surface treatment techniques (Fig. 2.9) are classified based on the materials used. As such, coating, elastomeric spray, shotcrete overlay, reinforced plaster, ferro cement and engineering cementitious composite are the known techniques used in retrofitting URM walls surface.

Coatings for URM walls: This is an application of coatings of thin cement-plaster on the surface of existing URM wall to improve its structural performance. Coating URM walls involves the use of anchors embedded into drilled holes on the existing walls (Abrams, 1998) to resist the interface shear stresses between the coating and the wall surface. The size and spacing of the anchors to be provided depends on the thickness of the proposed coating. Abrams (1998) suggested that a 6mm diameter bolt spaced at 450mm horizontally and vertically across the wall is appropriate for 25mm thick coating.

Elastomeric spray: This is a relatively emerging concept of retrofitting URM wall over the last two decades. It involves the application of urea or polyuria-based coating directly to the rear face of an existing URM wall up to about 15mm thick. Upon drying, the applied coating results in a tensile membrane which thus augments the flexural capacity of the old URM wall. It also reduces the risk of wall spalling. Ward (2004) confirmed that the use of an elastomeric spray on the wall was successful in reducing wall spalling when the retrofitted system was exposed to blast pressures up to 35psi and impulses of 215psi-ms. However, elastomeric spray cannot be used on load-bearing walls without the support of another load-bearing system. This view is also supported by ElGawady et al. (2004).

Shotcrete overlays and reinforced plaster: This is a low-cost technique for retrofit of URM walls. It is carried out by creating composite behaviour

between the old URM wall and new mortar via horizontal shear transfer through the installation of connector links (steel dowels or nails). An arrangement of connector links drilled through the wall thickness and steel wire mesh will be covered by rich mix of cement-sand mortar to thicken the existing wall for more robustness and redundancy (Ward, 2004). Robustness is the ability of buildings to deal with hazards in a way that is proportionate to the original causes while redundancy is the ability to transfer loads into alternate areas. Nepal Building Research Institute (NBRI) has found enlargement and overlay on old masonry walls effective because many masonry buildings retrofitted with this approach have performed well during recent earthquakes in Nepal (NBRI, 2016). NBRI ascertained that for good results to be achieved, the placement technique should ensure intimate contact between the existing masonry wall and the new cement mortar applied (NBRI, 2016).

Ferro cement: This is a surface treatment method where composite material such as mortar reinforced with light steel fabric/mesh is applied on the wall surface. It is very effective in avoiding expulsion in the out-of-plane direction of masonry panels and also reducing the global in-plane damages (Wang et al., 2018). Concisely, its application is very effective in improving wall height to thickness ratio which thus leads to a more rigid wall. The application of Ferro cement consists of closely spaced multiple layers of hardware mesh of fine rods with reinforcement ratio of 3-8% completely embedded in 10 - 50mm thickness of high strength (15-30MPa) cement mortar layer (ElGawady et al., 2004). Ferro cement application is majorly through manual labour, and it is thus cheap to adopt in the developing countries where the labour cost is relatively inexpensive.

Engineering cementitious composites (ECC): ECC is mainly used in retrofit of masonry for achieving improved ductility level to avoid brittle failure of masonry walls. ECC material composition is very similar to fibre-reinforced mortar composition (cement, sand, water, fibre, and a few chemical additives) but ECC does not have a large volume of fibre. Mainly, its application is to provide tension and flexural resistance that is lacking in the masonry wall. Martins et al., (2015) investigated the application of ECC for preventing brittle failure and concluded that the ductility of ECC retrofitted URM wall has been enhanced.

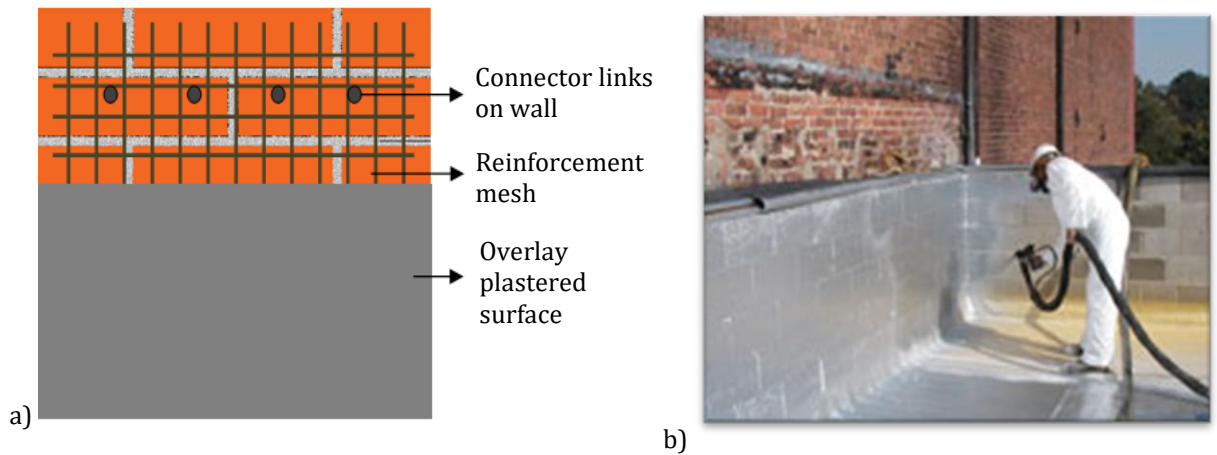


Figure 2.9: Surface treatment of URM wall: (a) Drawing (b) Application (Ward, 2004)

2.4.1.1.3 External Reinforcement

Supplemental strong back: This is an installation of external supplemental support to masonry structures to provide additional gravity support or seismic resistance. The supplemental support may be in the form of corbels installed under the location where the structural capacity upgrade is required. Jansen and Tilly (1999) submitted that seismic strengthening of masonry wall is sometimes carried out by bolting vertical steel channel girders to the wall externally. Steel reinforcements such as wind posts to safeguard URM wall against damages from the abnormal horizontal forces can also be used (Dawson, 2015). Recent investigation on the application of supplemental steel on URM are rare due to the noted challenges of cost and increased dead load on the existing structures (Lantz et al., 2016). The method requires regular maintenance via coating. Thus, it is an unappealing method in historical buildings because of its appearance (Fig. 2.10).



Figure 2.10: Externally strengthen wall with supplemental steel (Jansen & Tilly, 1999)

Steel column and plate: This is another robust form of retrofit technique different from the supplemental steel system. The approach involves securing some steel columns behind the wall and connecting them into the building frame at the floor and ceiling level at a regular interval (Fig. 2.11). The steel plates are used to tie steel columns flanges together, thereby generating an in situ tensile membranes capable of resisting considerable seismic loads (Lantz et al., 2016). This method is appropriate where load-bearing walls must give support to the floor above. In term of the applicability, the method requires minimal preparation of the internal surface. Still, the engineering and the installation process is demanding, particularly as each connecting weld must be sound, and the construction details can be problematic (Ward, 2004).

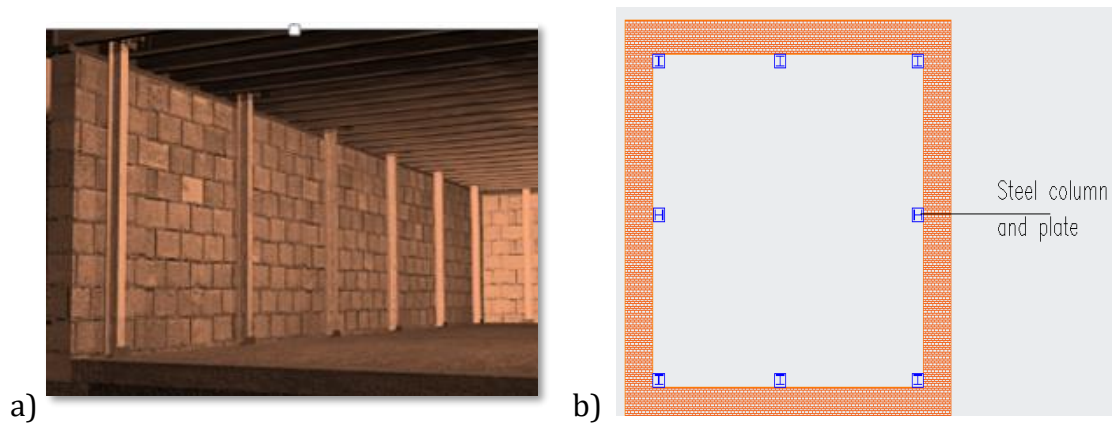


Figure 2.11: Steel column and plate behind the wall: (a) Elevation (Ward, 2004) (b) Plan view

2.4.1.1.4 Internal reinforcement:

Internal reinforced concrete (RC) skin: The emergent of seismic design codes to design RC structures that can resist greater seismic loads has made it possible to retrofit old masonry by incorporating an internal RC skin into the building. The overall aim is to improve the robustness of the existing URM building. The structural RC will be used to strengthen the building frame to resist the huge loads and prevent building collapse. This method is useful where the anticipated loads are so large, and the existing URM is so weak that it is practically impossible to achieve the required upgrade using any of the conventional retrofit techniques. Seible et al. (1997) highlighted that a well-constructed RC structural member with adequate shear reinforcement, development length, lap-splicing and steel continuity through the joints can proffer a considerable increase in seismic capacity of old masonry when integrated. However, ElGawady et al.

(2004) stated that before the implementation of this retrofit solution, a full structural analysis is required to determine whether it is necessary to underpin the foundations to resist the additional dead loads. These extra tasks make the approach very demanding and expensive. Berset et al. (2011) supported this by submitting that the construction and sequence of the concreting works required for internal RC skin sometimes might be difficult and complex. Where the method is deemed practicable and best, it important to do the RC skin symmetrically (fig. 2.12a) to avoid failure due to non-symmetrical bracing (fig. 2.12b).

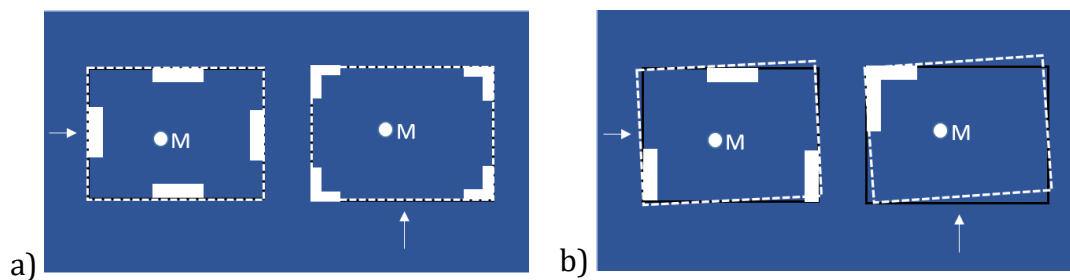


Figure 2.12: Internal RC concrete skin (a) symmetrical (b) non-symmetrical

Durisol block: A proprietary invention branded as durisol block provides a variation of the internal concrete skin. Durisol is a hollow concrete block made of mineralised wood shavings as aggregates, instead of sand and stone (Durisol, 2014). Durisol block has been used as a convenient solution to retrofit URM structures to offer some improvement in structural capacity of old URM. However, Berset et al. (2011) explained that the durisol walling system has limited ability to absorb shear forces from a seismic impact and also have relatively low weight preventing it from generating a sufficiently high force to divert the shear forces into compressive force. Therefore, structural reinforcement may be required to strengthen the durisol walling system to resist the huge dynamic loads.

2.4.1.2 Innovative Techniques

Fibre-reinforced polymer (FRP) composite: FRP is an innovative retrofit solution with externally bonded composites. The methods which have been developing over the last few decades offer significant strength improvement with minimum thickness, no variation to the original structural geometry and no mass increase (Willis et al., 2010). These advantages are the major drawbacks of the conventional methods of retrofitting which were overcome using FRP. As such, the use of FRP for strengthening and retrofit is gaining more popularity

among design professionals. FRP composite materials comprise of high strength continuous fibres, such as glass, carbon, aramids or steel wires, embedded in a polymer matrix (Alkhrdaji, 2013). Several studies on using FRP for increasing structural capacity of masonry walls (Fig 2.13) have established that FRP provides high-strength, lightweight, and economical structural retrofits solution for URM structures (Nanni and Tumialan, 2003; Saadatmanesh, 2014; Corradi et al., 2015).

While others are looking at FRP increasing popularity, De Santis et al. (2015) have submitted that inadequate fire-resistance, unidirectional behaviour, and higher cost (material cost of epoxy and FRP sheets, and high cost of skilled labour applying the FRP materials) are some of the drawbacks of using FRP for strengthening and retrofitting of masonry structures.

Regardless of the various benefits of using FRP in retrofit and new construction submitted by many researchers, the fact that regulatory authorities (such as American Concrete Institute (ACI), Soprintendenze in Italy, English Heritage in England, Conservation Régionale des Monuments Historiques (CRMH) in France, etc.) do not yet recognise the use of FRP composites as a complete retrofit solution for historical structures means the technique is not entirely problem-free (ACI, 2014; Borri et al., 2014; Corradi et al., 2015). An observer reported that FRP wraps used in retrofit of a masonry structure failed during an earthquake in Italy, the failures were attributed to the sharp edges of the masonry wall which torn the FRP apart during the earthquake. Corradi et al. (2015) expounded that some of the drawbacks in the use of FRP composite in retrofitting of monuments are attributed to the use of organic resins (epoxies) to bind or impregnate the fibres. The problems of using organic resins are poor behaviour of epoxy resins at temperatures above the glass transition temperature, high cost of epoxies and potential hazards to worker. Epoxy resins also prevent water-vapour permeability and possess very low fire resistance. Therefore, in many places such as Italy, England and France, heritage conservation authorities do not permit extensive use of epoxy adhesives on historical listed buildings or monuments (Corradi et al., 2015).

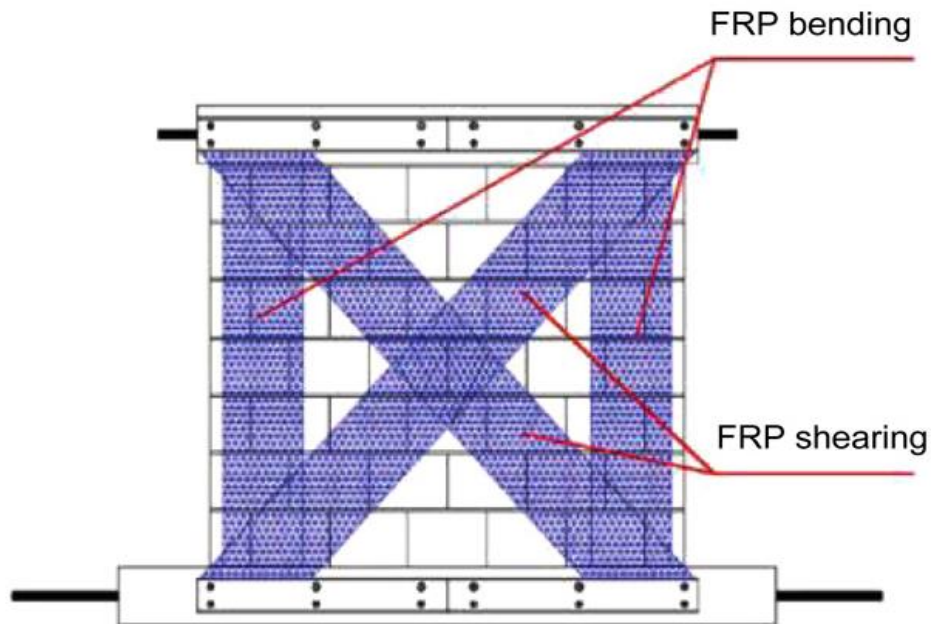


Figure 2.13: FRP strengthening approach on masonry wall (Wang, et al., 2018)

Internal and external post-tensioning: Post-tensioning is used externally in enlarged section and internally in drilled/cored holes (Daly and Witamawan, 1997). The basic constituents of the system are the steel tendons, cementitious grout, and a sock to hold the grout. In this method, ducts are created in the existing masonry wall, steel tendons or strands will then be fed and tensioned through the ducts. The tensioned strands to the required stress will then be anchored to the wall and sealed with grouting (fig 2.14). The steel tendons are primarily required to provide long term durability and increase the ductility of the old wall against seismic resistance (Jansen and Tilly, 1999). Whereas, the grout which could be either cementitious or epoxy-based material is very important to protect the tendon in the duct against corrosion (Biggs, 2003). The main function of the sock is to encompass the grout and prevent any loose brickwork being displaced by the injection pressures. The sock also allows ordered seepage of grout to enable a structural connection within the surrounding brickwork (Post Tensioning Institutes, 2006)

Bailey et al. (2015) assessed the performance of two stone masonry buildings retrofitted by post-tensioning during the February 2011 Canterbury earthquakes. Their study concluded that the post-tensioning retrofit system significantly improved the in-plane and out-of-plane wall strength and the ability to limit

residual wall displacements in the retrofitted building. This implies that the post-tensioning system is highly effective in seismic retrofitting.

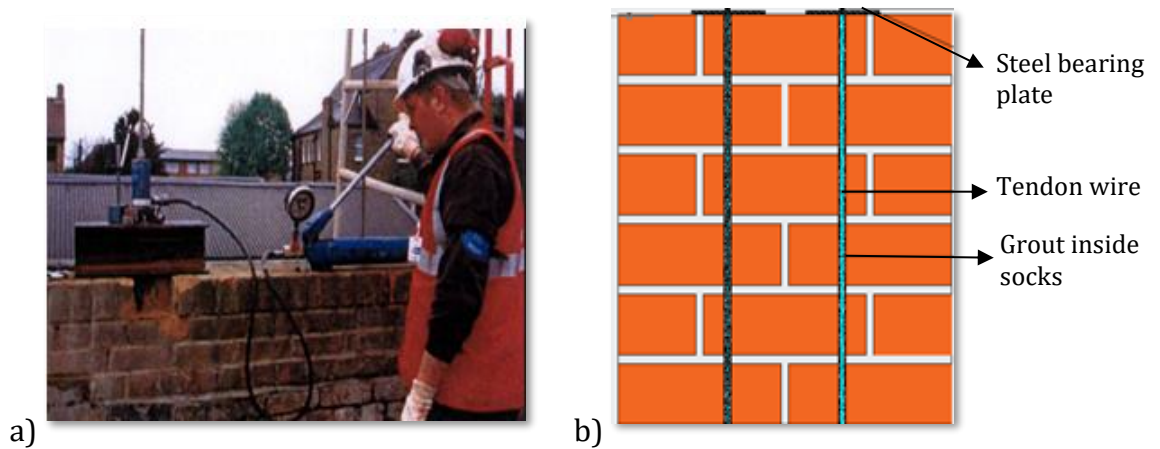


Figure 2.14: Post-tensioning of URM wall; a) Application (Jansen & Tilly, 1999) b) Schematic

Shape memory alloys (SMAs) for retrofitting of URM: SMAs sometimes referred to as smart metal is described as a distinct type of metal alloys that are capable of recovering from apparent permanent strains when they are heated above a certain temperature. They can be used to generate motion or force and can store the deformation energy (Jani et al., 2014). Shrestha (2011) corroborated that SMA are highly super elastic and possess shape recovery property on unloading. SMAs are also capable of dissipating energy, limit force transmissions, and reducing or eliminating residual deformations. Due to this auspicious property which helps to stabilise retrofitted masonry during and after excessive action, SMA finds its way into the historical masonry retrofitting space. As reported, one of the first documented application of SMAs in retrofitting masonry was done on S. Giorgio Church Bell Tower (Fig 2.15) by Indirli et al. (2001). The process is similar to the post-tensioning procedures earlier described with the introduction of the smart metal of 1mm diameter as the material. After that, there several other retrofit projects that have considered using SMAs to retrofit historical masonry constructions (Chrysostomou et al., 2008; Paret et al., 2008; Martelli, 2008). However, the high cost of SMA material and the intense technical details involved in its machining has hampered their wide-spread use in retrofitting of historical URM constructions.

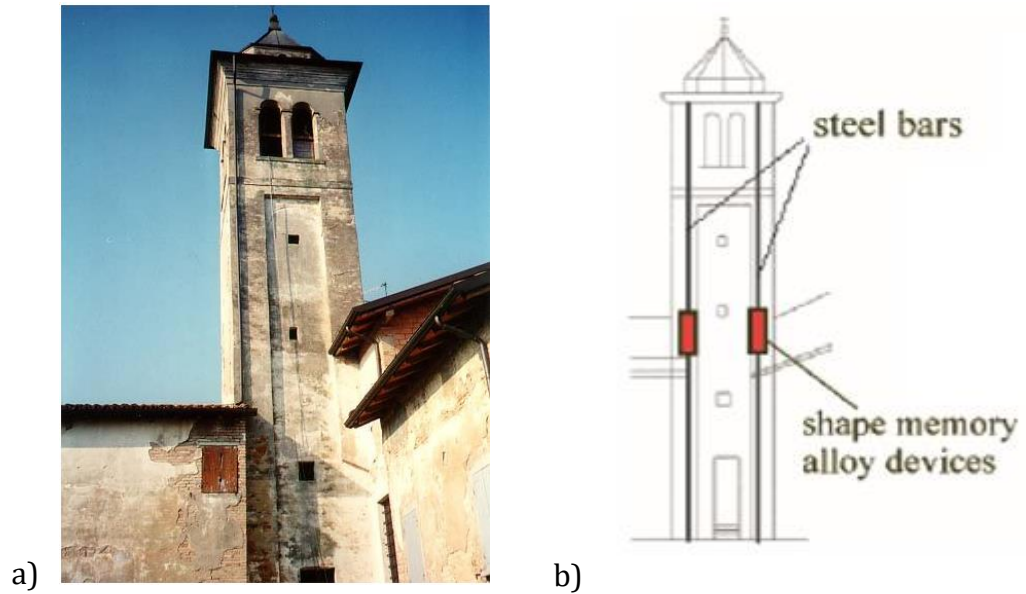


Figure 2.15: St. Giorgio bell tower retrofitted with SMA: (a) general view (b) retrofit location
(Indirli et al., 2001)

Reticulatus system: Reticulatus is an innovative retrofit technique that was first introduced at the University of Perugia, Italy as a repair and preventive technique for retrofitting rubble stone masonry (Borri et al., 2008). The obvious advantage of this technique (Fig 2.16) is that the fair-faced masonry was kept as existing after the application. Technically, the method provided a cross-interlock especially for rubble masonry and supplied resistance to tensile strength for normal lateral forces (Borri et al., 2008; Fonti et al., 2017). The system comprises of two components (continuous mesh cords and transverse bars) which are embedded in the mortar joints. The continuous mesh cords which are made of rope, high strength steels or a composite such as polyethylene (Castori et al., 2016) are inserted in the mortar joint by anchoring it to the wall using transverse metal bars (such as threaded rods and eyebolts).

Fonti et al. (2017) explained that the first requirement of this method is that the mesh cords must be arranged in a vertical and horizontal direction. These must be accurately settled by following the masonry pattern, thus forming an approximately square mesh. The desired cross interlock will be obtained by anchoring the nodes of the mesh cords to the already settled transverse connector in the mortar joint.

Castori et al. (2016) reported that this technique exhibited an increase in shear strength of up to 170% compared to unreinforced reference panels when used on

old masonry that have low quality of the pre-existing mortar. However, Csikai, et al. (2014) pointed out that the increase in the maximum applied bending force in the cracking limit point and the initial stiffness only could be achieved if appropriate pretensioning of the reinforcing grid/cords is done.

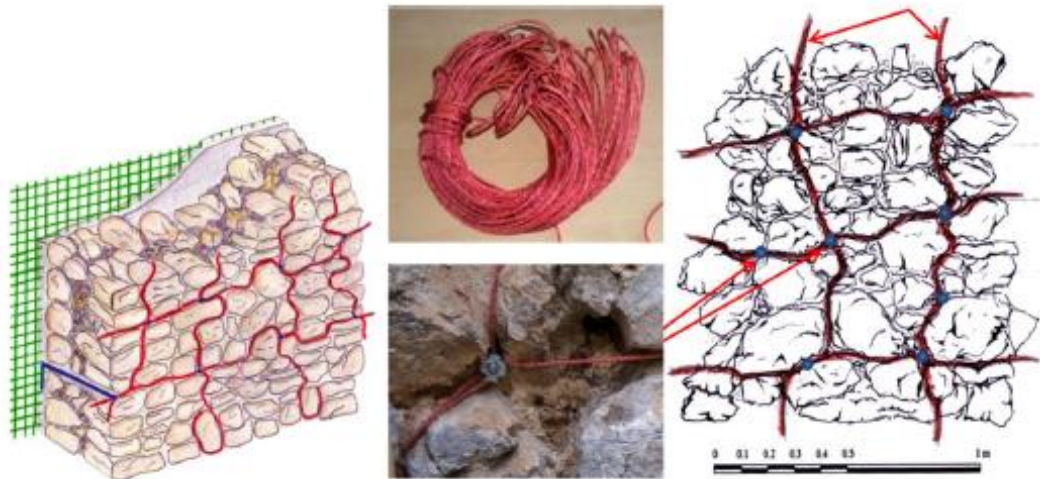


Figure 2.16: Reticulatus system showing the reinforcement idea and pattern (Fonti et al., 2017)

2.4.2 Structure Level Retrofit

2.4.2.1 Conventional Techniques

2.4.2.1.1 Floor/Roof Diaphragm Action Connectivity

The connection between walls and floor/roof of a masonry structure is crucial in transferring lateral action to the walls of any structure under horizontal load (out-of-plane). This had led to the emergent of structure level intervention techniques that can hold all the building components together such that they behave like a box under loading. This is achieved through various means that can tie all structural and non-structural elements in a masonry building together so as to provide the building with improved structural integrity (da Porto et al., 2018). Improved diaphragm action in URM can be achieved by any of figure 2.17 (a) adding wooden plank in orthogonal direction on top of an existing floor of masonry with a proper connection to the wall of the floor (b) applying metallic bracing belts or bars (c) fixing metallic ties at the extrados of floor to improve the stiffness of existing building (Valluzzi et al., 2008).

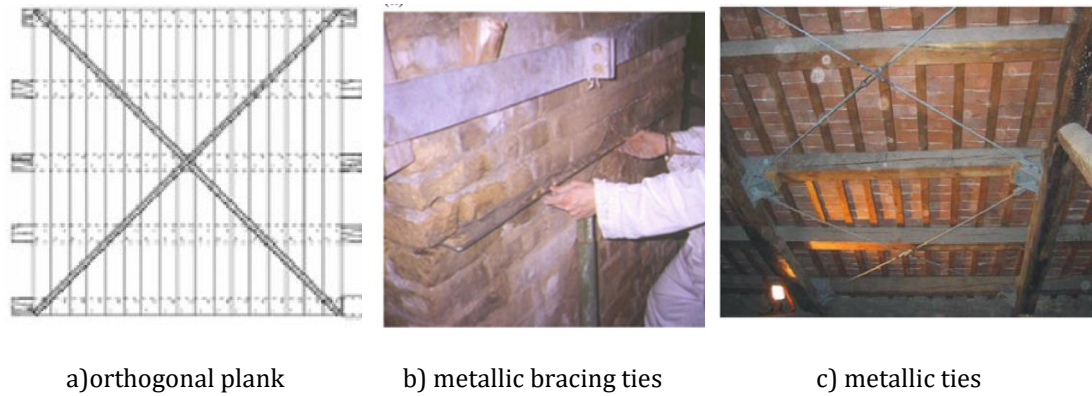


Figure 2.17. Floor/Roof diaphragm strengthening intervention

2.4.2.1.2 Reinforced Concrete Tie and Masonry Confinement

This is the process of providing confinement for existing masonry walls using a reinforced concrete column or by building masonry pier which can be reinforced or plain masonry. The confinements are usually placed at wall corners and intersection (Fig. 2.18). This method is widely recognised in masonry construction in Europe (BSI, 2004). It is also one of the most used masonry construction systems for both new masonry buildings and in retrofitting of existing masonry building in Asia and Latin America.

The vertical RC or masonry tie columns which confine the walls at all corners and wall intersections is the main feature of the confinement technology. This retrofit approach has deep-rooted success in the earlier study of Zezhen et al. (1984) where the results show that the tie column connected with a tie beam have significant positive effect on walls behaviour. Also, Karantoni and Fardis (1992) and Chuxian et al. (1997) agreed that confinement prevents disintegration, improves ductility and energy dissipation of URM buildings. However, for the confinement to be effective, tie columns should connect well with tie beam along the walls at floors levels (ElGawady et al., 2004). More so, Brzev (2014) reported that URM building confined with RC columns remained undamaged in the 8.0 magnitudes earthquake in 2007 in Pisco while many other masonry buildings around experienced severe damage and collapse (fig. 2.19).

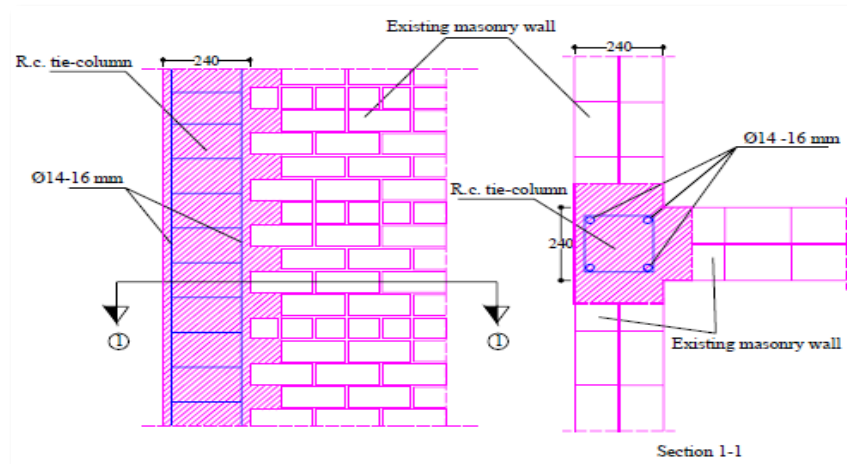


Figure 2.18: RC column confinement in masonry wall (ElGawady, et al., 2004)



Figure 2.19: Performance of RC confined masonry in 2007 Pisco earthquake (Brzev, 2014)

2.4.2.2 Innovative Technologies

2.4.2.2.1 Base isolations

Base isolation is an innovative structural level intervention strategy mainly used to modify the response of structure for seismic risk mitigation. Like every other retrofit technology, the motive of base isolation technique is to reduce the potential for heavy structural damage or collapse and not to earthquake proof. The main concept of the technology is to isolate the superstructure from the substructure using isolation device such as elastomeric bearing (Matsagar and Jangid, 2008). This isolation system will alter the behaviour of the building during an earthquake as shown in figure 2.20.

The advantage of base isolation compared to conventional methods discussed earlier is by reducing the seismic forces transmitted into the structure. Base

isolation continues gaining more popularity in the retrofit of cultural heritage in seismically active regions. As such, the Eurocode 8 now contains two chapters devoted to the seismic isolation of buildings and bridges. Ferraioli and Mandara (2016) claimed that the inclusion of these two chapters in Eurocode 8 had produced a significant effect in promoting the general application of seismic isolation to even ordinary residential and commercial buildings.

Several historic buildings including the Oakland city hall, San Francisco city hall and Salt Lake City hall have been retrofitted by insertion of base isolators at foundation level (Melkumyan et al., 2011). Base isolation protects the contents, secondary structural features, and the main structure. The safety of occupants and passers-by is also enhanced using base isolation (Ferraioli & Mandara, 2016). Base isolation reduces the inter-storey drift in superstructures when compared to the fixed-base structures (Ferraioli et al., 2010).

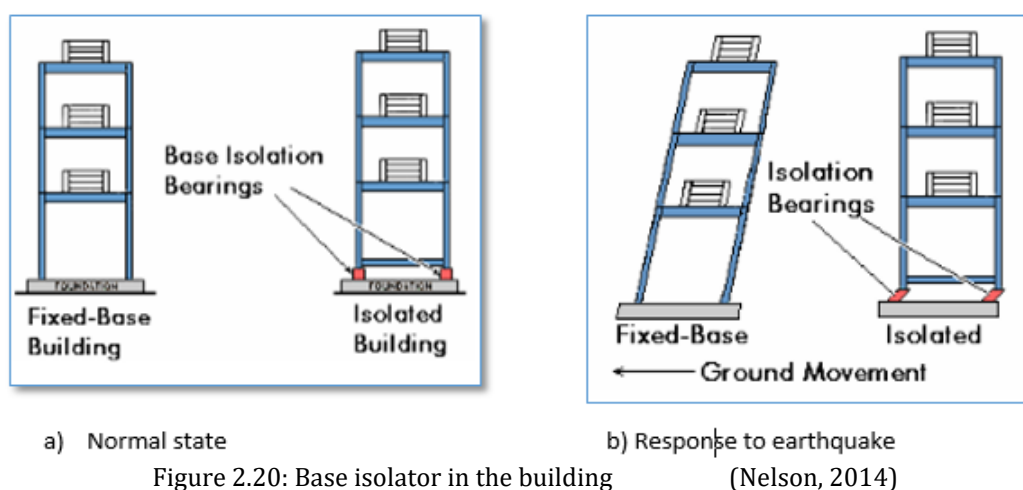


Figure 2.20: Base isolator in the building (Nelson, 2014)

2.4.2.2.2 Energy- dissipation devices

Seismic energy dissipation devices, otherwise known as dampers, are generally devices that deaden and depress the earthquake energy in building (Fig. 2.21). Its primary purpose is to reduce and dissipate the earthquake's energy as it enters the building, thereby leading to a significant reduction in building deformation and damages during an earthquake. Many studies have been carried out to investigate the effectiveness of the energy dissipation device in seismic retrofitting. For instance, Branco & Guerreiro (2011) studied the efficacy of viscous dampers on a building that was built in 1911 in Lisbon. They concluded that viscous dampers have a noticeable beneficial effect through the reduction of the displacements of each floor. Recently, Asteris et al. (2014) and Chrysostomou

et al. (2015) have established that the use of dampers leads to a greater reduction of seismic vulnerability of URM buildings compared with traditional retrofitting techniques.

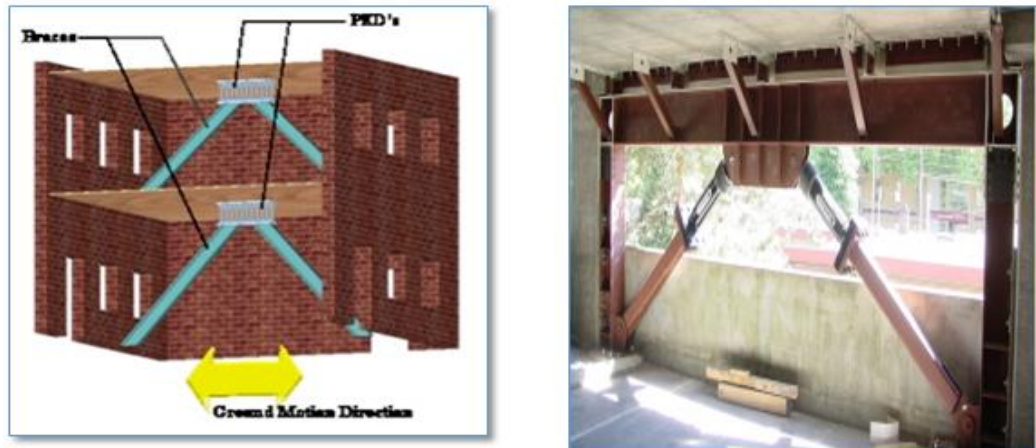


Figure 2.21: Seismic energy dissipation in building

(Staaleson, 2014)

2.4.2.2.3 Cam system

CAM system are innovative three-dimensional tying system developed to tie masonry together to achieve a good compaction of masonry parts. Dolce et al. (2001) have the patent for CAM system called (Masonry active\tying). The system uses stainless steel ribbons to tie masonry with loops passing through transverse holes (Fig. 2.22). The loops are closed with a special tool which can apply a calibrated prestress to the ribbon. Dolce et al. (2001) applied this technique on seismic upgrading of a building, damaged by the Umbria '97 earthquake. The application results in improved connections between different structural elements of the building. Dolce et al. (2001) then substantiated the effectiveness of this CAM system by conducting a series of test on masonry panels. They report a 50% increase in strength of the panel and 60 times increment in dissipation energy when the panel is retrofitted with the CAM system.

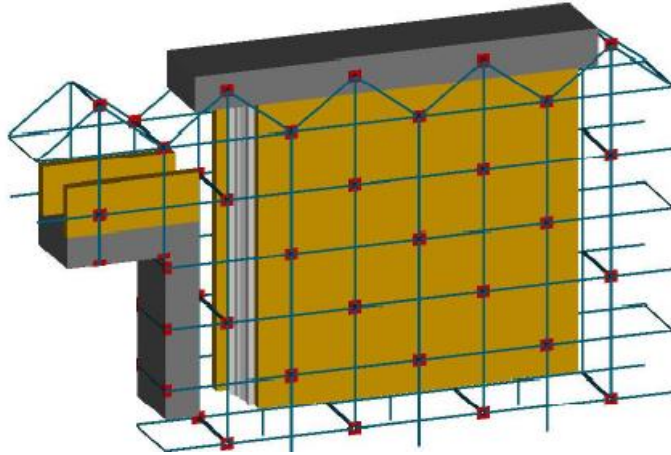


Figure 2.22: CAM arrangement in URM wall (Dolce et al., 2001)

2.5 Evaluation of Different Retrofit Techniques

Table 2.2 summarises the details of the reviewed retrofit techniques. The efficiency, applicability, merit, and the challenges of each of the identified retrofit technique were summarised as shown in table 2.2 below.

Table 2.2: Summary of retrofit techniques

Techniques		Efficiency	Applicability	Merits	Challenges
Joint Treatment	Repointing	Restore initial stiffness	Suitable where the qualities of the masonry units are still very good, but the mortar joint is poor.	Ease of application	No major increment in initial stiffness
	Grout and epoxy injection	Increase the lateral strength Improve out-of-plane stability		Minimal cost No additional load	
	Micro/Fibre reinforced mortar	Improve flexural strength		No aesthetic or historical impact	
Surface Treatment	URM coating	Improve lateral resistance	Suitable to upgrade both in-plane and out-of-plane capacity of masonry in developing countries where labour cost is relatively cheap.	Low technology	Time-consuming
	Elastomeric spray	Improve energy dissipation		Minimal cost	Aesthetic or historical impact
	Shotcrete overlays	Improve out-of-plane stability		where labour cost is cheap	Reduces functional space
	Reinforced plaster	Improve lateral strength		Major increment in initial strength and resistant	Disruption of occupancy usage
	Ferro cement	Reduce the risk of wall spalling	Not suitable for historical heritage.		
	Engineering cementitious composites (ECC)	Increase robustness and redundancy			

	Techniques	Efficiency	Applicability	Merits	Challenges
External Reinforcement	Supplemental strong back	Improve lateral resistance Improve tensile strength Improve rigidity Improve ductility	Ideal where walls are expected to resist a high horizontal load. Suitable for medium-rise building.	Ease of alteration Minimal internal preparation Provide additional support to floors	Additional load Space reduction Aesthetic and architectural impact Regular maintenance Installation is demanding Requires good connection design
	Steel column and plate				
Internal Reinforcement	Reinforced concrete skin	Increase robustness and redundancy Improve energy dissipation Improve ductility	Suitable for low and medium-rise building in a high seismic zone where the anticipated loads are so large, and the existing URM is so weak.	Available design guides in design codes, e.g. EC8 RC elements can be designed for specific seismic loads	Not easy to integrate Additional heavy load Occupancy usage disruption Requires full structural analysis before application
	Durisol block	Increase strength			

Techniques	Efficiency	Applicability	Merits	Challenges
Fibre-reinforced polymer (FRP) Composite	Enhances ductility	Suitable for main resisting elements such as columns, walls, arches and vaults but not good at sharp edges	No variation to the original geometry	Inadequate fire-resistance, Unidirectional behaviour High cost of materials Limited efficiency as a result of de-bonding
	Improves energy dissipation		No additional load	
	Improves flexural strength		Ease of application	
	Increases lateral resistance		Resistance to corrosion	
	Enhances shear capacity		No loss of space	
Internal and external post-tensioning	Improve lateral resistance	ACI 530-02 currently limit post-tensioning in retrofitting to low rise masonry wall in moderate seismic zone	No additional load	Requires skilful professionals Corrosion may break tendon untimely Anchorage failure and energy losses due to creep and friction
	Increase strength		No loss of functional space	
	Increase stiffness		High speed of construction	
	Improve ductility			
Shape memory alloys (SMAs) for retrofitting of URM	Restores deformation	Suitable for low and medium-rise masonry wall in moderate seismic zone	Stabilises retrofitted masonry during and after excessive action	High cost of SMA material Requires intense technical details
	Improve energy dissipation			
	Reduces deformation			

Techniques	Efficiency	Applicability	Merits	Challenges
Reticulatus system	Improves tensile strength Increases shear strength Improves integrity Increases initial stiffness	Suitable for historical heritage because the fair-faced masonry was kept as existing after application	Can be used for both repair and prevention Increased the connection between panels	Slow due to tedious installation Inappropriate strap pointing
Floor/Roof Diaphragm Action connectivity	Improves structural integrity Provides lateral support Resists out-of-plane forces Improves pull-back force	Suitable for upgrading the global strength of multi-storey building in high seismic Zone	Transfer all horizontal load to lateral resisting elements Tie all structural and non-structural elements together	Complexity in design and implementation
Reinforced Concrete Tie and Masonry Confinement	Improve rigidity Improve energy absorption Prevent disintegration Improve lateral resistance Improve ductility	Suitable for low and medium-rise building in a high seismic risk zone	Prevent total collapse of building Low level of construction skills Available design guides in codes	Disturb the existing occupancy during the retrofit Not easy to integrate

Techniques	Efficiency	Applicability	Merits	Challenges
Base isolation	<p>Reduces inter storey drift</p> <p>Reduces seismic forces demand on the superstructure</p> <p>Increases energy dissipation</p> <p>Increases vertical stiffness</p> <p>Reduces displacement and rocking</p>	<p>Suitable to modify the response of complex structures and building that must remain functional after an earthquake (hospital) in high seismic zone</p>	<p>Safety is enhanced</p> <p>Improves performance against ground excitation</p> <p>Isolators require no maintenance during service life</p>	<p>Instability of elastomeric bearing under increased load</p> <p>Complex and costly</p> <p>Cannot be used in building on loose soil</p> <p>Less effective for light and flexible structures</p>
Energy- dissipation device	<p>Improves lateral resistance</p> <p>Restores stiffness</p> <p>Increases energy dissipation and dampen the motion of building</p>	<p>Suitable for high rise building, complex structures in high seismic zone</p>	<p>Energy dissipation is concentrated at a designed location</p> <p>Can be replaced easily after an earthquake</p>	<p>Complex and costly</p> <p>Sensitive to ductility ratio</p> <p>Requires proper design and selection of damper</p>
Cam system	<p>Improves transverse link</p> <p>Increases strength</p> <p>Increases ductility</p> <p>Improves connection</p>	<p>Ideal for upgrading the global integrity of the medium-rise building in moderate seismic Zone</p>	<p>Guaranteed continuity in CAM</p> <p>CAM technology is little intrusive and reversible</p>	<p>Limited efficiency in irregular masonry</p> <p>Time-consuming</p>

2.6 Previous Experimental Studies on Out-of-Plane Behaviour of URM Walls

The review of previous experimental tests on out-of-plane behaviour of URM walls was carried out to understand the out of plane behaviour and performance of some existing retrofit techniques. Table 2.3 presents the details of previous experimental works reporting for each of them, the geometry, boundary conditions of the URM walls tested, the loads applied, and the testing procedure.

While some of the selected works like that of Maheri et al. (2008), Derakhshan et al. (2009), Costa et al. (2014) and Maccarini et al. (2018) only focused on characterising the out-of-plane behaviour of plain URM walls, majority of the reviewed works investigated the out-of-plane structural performance of URM walls retrofitted with different techniques and materials such as expansive epoxy known as Bisfoam-3 by Zeiny and Larralde (2010), Carbon Fibre Reinforced Polymer (CFRP) by Bui et al. (2010), Tyfo-S fibre fabric wrap by Reinhorn and Madan (1995), Polymer Textile Reinforced Mortar (TRM) by Ismail and Ingham, (2016), Engineered Cementitious Composite (ECC) shotcrete by Lin et al. (2016) and Glass Fibre Reinforced Polymer (GFRP) by Gattesco and Boem (2017). More so, Costa et al. (2011) investigated the effectiveness of strengthening the connection between the URM walls of existing masonry building using a mechanical system. More relevantly to this study, Sustersic and Dujic (2014) performed quasi-static cyclic testing on URM wall to investigate the application of Cross Laminated Timber (CLT) panels as a strengthening system for existing URM wall against seismic force.

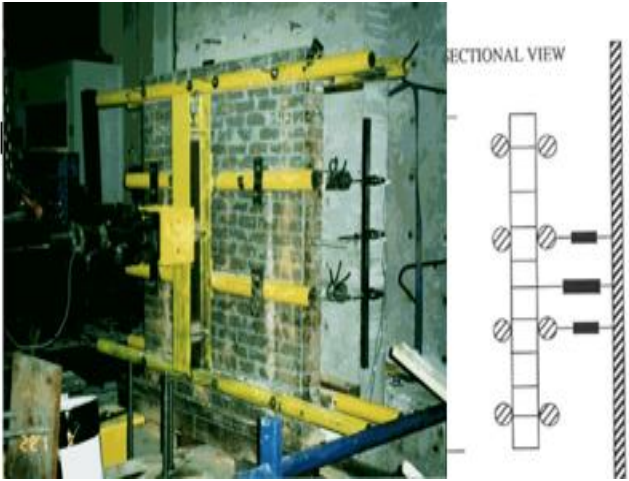
As deduced from the review of the selected experimental works, the most common geometry of the URM walls tested is a free-standing wall panel without any party walls at the edges of the wall to generate restraint. All reviewed experiments excluding that of Bui et al. (2010) have been carried out on wall panels without returning walls at the corners. Although Bui et al. (2010) geometric configuration is ideal for reproducing the in-situ condition of a portion of a typical load-bearing wall including corners, evidence from the previous works has shown that test on panels without corners is a good indication in assessing the out-of-plane capacity

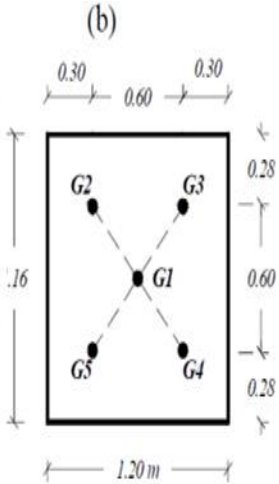
of URM wall. Hence, the walls tested in this study were without returning walls at the corner.

Moreover, the general boundary conditions assumed in the reviewed testing works were restraints at the top and bottom of the wall. Because of this restrained boundary condition, the observed failure mechanisms when walls were loaded in out-of-plane either as a uniform or point load is generally characterised by vertical arching which has been termed as failure mechanism type F in FaMIVE (Table 2 .1). This type of out-of-plane failure mechanism occurred in all the tests reviewed because of the restraint at the top and bottom of the wall, which allowed the vertical strips of the wall panel to deflect in the out-of-plane.

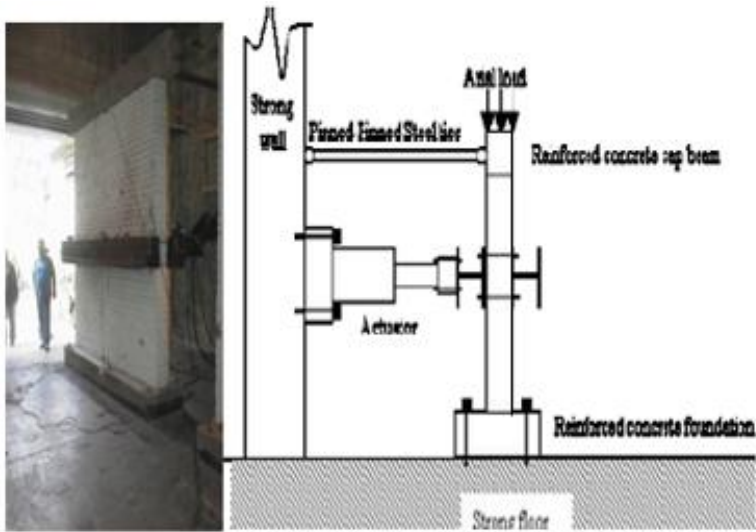
The observed failure of walls from the tests is considered as first-mode of failure and the least desirable in historical buildings causing dramatic consequences (Solarino et al., 2019). As such, this study aims to propose a retrofit technique that will improve the performance of URM wall against this type of out-of-plane failure. It is thus imperative to assess the out-of-plane performance of plain and retrofitted URM wall to evaluate the improvement due to the application of the proposed retrofit technique. To do this, test setup which is similar to that of Maheri et al., (2008) and Gattesco and Boem (2017) which is according to provisions of ASTM E-72 was adopted in this research (see chapter 3 for detail of the full experimental works).

Table 2.3: Summary of Previous Out-of-plane Testing of URM wall

Geometry (l x h x t) m	Test Description	Connection		Loading	
		Base	Wall	Vertical	Horizontal
1.8 x 1.8 x 0.2	Out-of-plane test was performed on double wythe single leaf URM wall placed on 3 inches pipe positioned on the web of I-section on floor. The walls were loaded out-of-plane in two equidistant locations from the end support through the pipe interfaces using a single hydraulic actuator. A spreader beam was placed in between the pipes and actuator to simulate three-point loading. Applied load and corresponding displacements at the load points and mid-height were evaluated.	The wall was constructed on a structural steel plate.	Specimen wall bonded to a steel plate with mortar was rested on a 3ins pipe to induce pin support. The top and the two vertical edges of the wall were free.	Free i.e no pre-compression load applied.	Three-points loading through hydraulic actuator was applied in the middle.
Reference					
(Reinhorn & Madan, 1995)					

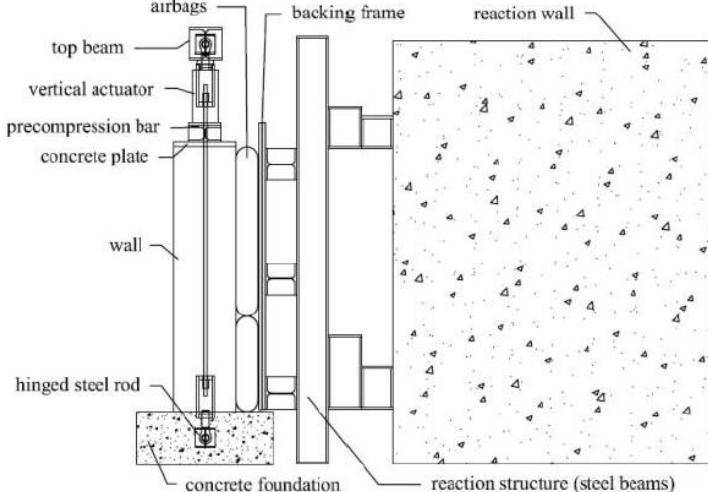
Geometry (l x h x t) m	Test Description	Connection		Loading	
		Base	Wall	Vertical	Horizontal
1.2 x 1.2 x 0.11	<p>The test setup consists of a loading frame, against which a horizontally placed hydraulic jack exerts the out-of-plane load on the specimens. The value of the applied load was determined through a ring load cell at the wall centre. Five mechanical dial gauges were used to record the deflections of each specimen. The locations of these gauges are such that there are three in each diagonal, as shown below.</p>	Strong steel beam base on the laboratory floor.	The wall was bounded by structural steel member in all the four edges (interior Panel).	The wall carried no extra vertical loads apart from the self-weight of the wall and confining steel member.	Point load was applied at the wall centre through the actuator.
Reference					
(Maheri et al., 2008)					

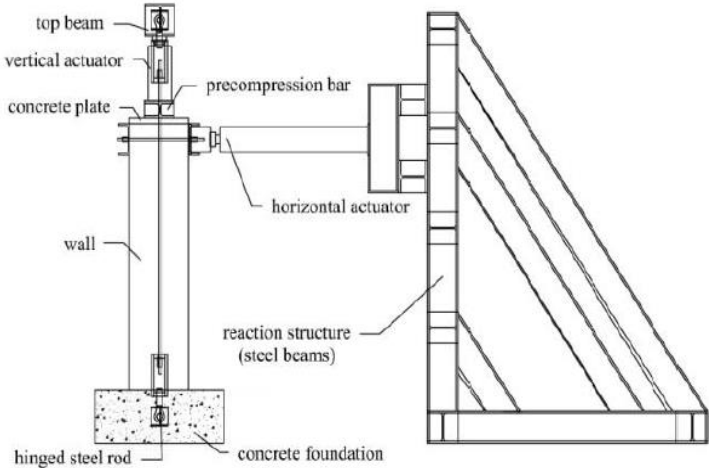
Geometry (l x h x t) m	Test Description	Connection		Loading	
		Base	Wall	Vertical	Horizontal
1.2 x 3.5 x 0.22	Masonry wall specimens subjected to out-of-plane uniform loading were tested. Specimens were tested with simply supported boundary conditions, with and without pre-compression load to indicate walls with and without top floor load. The simply supported condition was achieved by restraining the horizontal movement of the walls at top and bottom using steel angles. Displacement and load capacity of walls were recorded.	The existing strong floor of the laboratory was used as the wall base.	The bottom of the wall was mortar bonded to the floor. Both sides of the wall were restrained using steel angle at top and bottom. The two vertical edges were free.	Wall with no vertical load and another with up to 6KN vertical load were tested.	Uniform load was applied on the out-of-plane by using an airbag.
Reference					
(Derakhshan et al., 2009)					

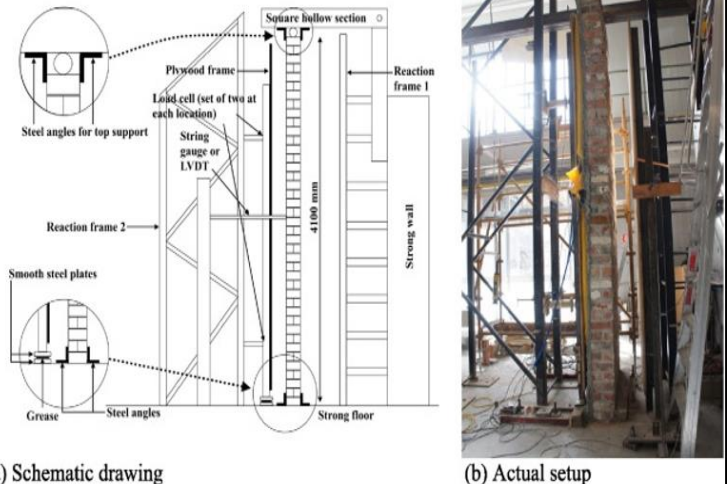
Geometry (l x h x t) m	Test Description	Connection		Loading	
		Base	Wall	Vertical	Horizontal
3 x 3 x 0.25	Test wall specimens were subjected to out of plane loading using a cyclic displacement control test through the actuator. Also, the axial load from a concrete header beam placed on top, the weight of the two steel beams in the middle, and the self-weight of the wall were applied. During testing, applied load and wall displacement were continually monitored and recorded.	RC strip footing connected to a strong floor with three long bolts at equidistant on both side of the wall.	The bottom of the wall is fixed with mortar to RC footing while the top is restrained with the vertical load. The two edges were free.	Concrete beam to impose axial load due to a light roof.	Cyclic displacement with 10secs as the period of one cycle applied on out-of-plane using an actuator.
Reference					
(Zeiny & Larralde, 2010)					

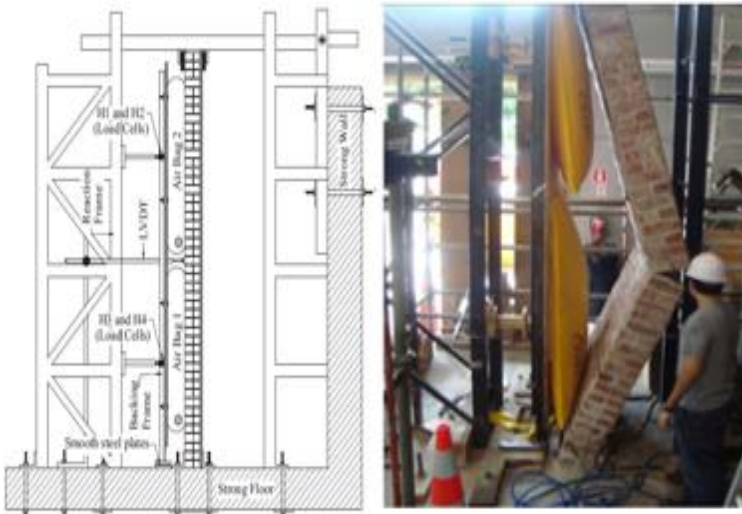
Geometry (l x h x t) m	Test Description	Connection		Loading	
		Base	Wall	Vertical	Horizontal
2.9 x 2.0x 0.2	URM walls having two corners were constructed and tested. The main wall was subjected to a quasi-static loading of uniform pressure applied to the outside face, using inflatable cushions backed with the existing reaction frame. A calibrated pressure transducer was used to control and measure the applied water pressure. The out-of-plane displacement of the structure was measured using nine linear variable differential transducers (LVDT).	RC slab on the existing floor of the laboratory.	The top is free while the bottom was mortar bonded to the RC slab. The vertical edges were restrained with inner walls.	The top of the wall is free (no vertical load).	Out-of-plane uniform pressure applied using six inflatable cushions backed on supporting frame.
Reference					
(Bui et al., 2010)					

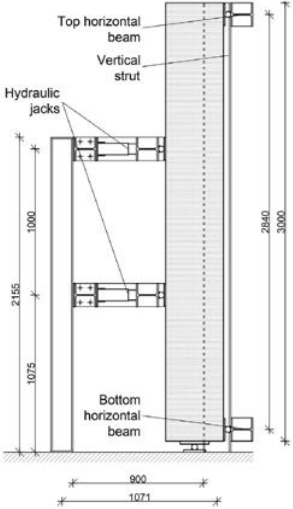
Geometry (l x h x t) m	Test Description	Connection		Loading	
		Base	Wall	Vertical	Horizontal
2.17 x 5 x 0.25	In-situ tests on existing traditional 2-storey masonry building abandoned after the 1998 Azores earthquake to study its out-of-plane behaviour. The test involved placing a load actuator in the given building perpendicularly to the wall panels to be tested to impose monotonic or cyclic out-of-plane loads under controlled displacement conditions. The test was monitored using draw-wire displacement transducers.	The building foundation which has been partially buried due to the natural soil level above the foundation is the base.	Wall fixed to the base at the bottom and freed at the top. The corner walls at the two edges restrained the panel.	The walls do not carry any vertical load since there is no roof on the wall anymore.	The concentrated load was placed perpendicular to the panel to simulate the out-of-plane loading.
Reference					
(Costa et al., 2011)					

Geometry (l x h x t) m	Test Description	Connection		Loading	
		Base	Wall	Vertical	Horizontal
1.3 x 2.5 x 0.65	The test involved the application of uniformly distributed surface load on SACCO stone masonry wall using a system of nylon airbags which reacts against a backing frame connected to the reaction wall. The level of pressure inside the airbags and the top displacement of the specimen continuously acquired through a data acquisition system to evaluate the out-of-plane performance of the wall.	RC footing was provided on a strong floor.	The bottom of the wall is fixed to RC footing while the top is restrained with a pre-compression load. The two edges were free.	The wall carried precompression force of (0, 52, and 140kN) to represent different loading on the wall.	Uniform load was applied on the wall surface by controlling the pressure inside the airbag.
Reference					
(Costa et al., 2014)					

Geometry (l x h x t) m	Test Description	Connection		Loading	
		Base	Wall	Vertical	Horizontal
1.3 x 2.5 x 0.65	The second phase of Costa et al. (2014) work is the application of a horizontal line load through a displacement controlled hydraulic actuator. The actuator reaction was provided by a stiff steel structure, anchored to the test slab. Top displacement and load were also recorded. The results were compared to the previous setup, where a uniform load was applied. The two set up shows similar envelope curves and strength.	RC footing was provided on a strong floor.	The bottom of the wall is fixed to RC footing while the top is restrained with a pre-compression load. The two edges were free.	The wall carried precompression force of (0, 52, and 140kN) to represent different loading on the wall.	Horizontal line load at the top of the wall using actuator was applied.
Reference					
(Costa et al., 2014)					

Geometry (l x h x t) m	Test Description	Connection		Loading	
		Base	Wall	Vertical	Horizontal
1.2 x 4.1 x 0.23	The test was set up to be able to predict the out-of-plane behaviour of as-built unreinforced clay brick masonry walls expected in URM buildings with floor diaphragms typically flexible and provide little restraint against potential wall rotation. Airbags were inserted at the back of the wall to provide a UDL horizontal pressure simulating out-of-plane loads. LVDT was connected to the wall at mid-height to measure wall displacement.	The existing strong floor of the laboratory was used as the wall base.	Two sets of steel angles fixed horizontally to restrain the wall top and bottom at both sides. The two vertical edges were free.	No axial overburden load applied to any of the walls.	Uniform distributed load with airbags was applied.
Reference	 <p>a) Schematic drawing</p> <p>b) Actual setup</p>				
(Lin et al., 2016)					

Geometry (l x h x t) m	Test Description	Connection		Loading	
		Base	Wall	Vertical	Horizontal
1.2 x 3.7 x 0.22	<p>These test walls were subjected to out-of-plane uniform pressure using pressure airbags backed by strong reaction frame. The set up was similar to that of Lin et al. (2016), where walls were loaded until the wall collapsed.</p> <p>To evaluate the out-of-plane capacity of the wall, the lateral displacement and applied lateral force were measured using LVDT and load cell connected to the data acquisition unit.</p>	Strong laboratory concrete floor	<p>The bottom of the wall was mortar bonded to RC floor and restrained at top and bottom using steel angle at both sides.</p> <p>The two vertical edges were free</p>	No vertical load applied.	Uniform load was applied on the out-of-plane by controlling the air pressure in the bag.
Reference					
(Ismail & Ingham, 2016)					

Geometry (l x h x t) m	Test Description	Connection		Loading	
		Base	Wall	Vertical	Horizontal
1.0 x 3.0 x 0.25	The setup is a four-point bending test where loads are applied at the thirds of the wall height by two hydraulic jacks. Two horizontal beams, connected by vertical struts, were placed in contact with the top and bottom ends of the wall face on opposite sides of loads to restrain the wall. Applied load and displacements at the top, bottom and mid of the wall were monitored through an electronic data acquisition unit.	The specimen was built on steel plate	The steel plate at the bottom of the wall was placed on a circular pipe to induce pin support to allow for wall rotation.	No vertical loading considered	Horizontal point loads applied in the first and second third of the wall height using hydraulic actuators.
Reference	 				
(Gattesco & Boem, 2017))					

2.7 Numerical Modelling of Masonry Structures

Computational numerical analyses can predict the behaviour of structures to the applied load. Numerical analyses are based on different theories such as finite element model (FEM), discrete/distinct element methods (DEM) or particle flow code (PFC), among others (Lourenco, 1996; Asteris et al., 2015; Zhang, et al., 2016). FEM-based models are the most widely used due to the availability of many analysis software that operates based on this theory. Therefore, the numerical modelling strategy employed in this study will be based on FEM.

Many researchers who have previously worked on FE modelling of masonry structures, (Anthoine, 1992; CUR, 1994; Lourenco, 1996; Maccarini et al., 2018; Portioli, 2020) agreed that numerical modelling and analysis of masonry structures posed some of the greatest challenges to structural engineers. The main difficulty has been attributed to the presence of mortar joints which act as planes of weakness, discontinuity, and non-linearity. Besides, the existence of uncertainties in the material and geometrical properties is also another concern when modelling masonry structures (Lourenco, 1996; Asteris et al., 2015; Dogariu, 2015). Despite these challenges, three modelling techniques (Fig. 2.23) have evolved.

[1] Detailed micro-modelling: It is a material level model where masonry structure is considered as a three-phase material like ideal masonry wall (Fig 2.23a). The masonry units and mortar in the joints are represented by continuum elements while the unit-mortar interface is represented by discontinuum elements as shown in figure 2.23b (Lourenco, 1996). This technique produces the most accurate results, but its analysis is computationally intensive due to the detailed level of refinement (Zucchini and Lourenço, 2004).

[2] Simplified micro-modelling: In this strategy, bricks are represented as fictitious expanded bricks by continuum elements. The bricks size is that of original bricks dimensions plus the real joint thickness. The mortar joint is also modelled as an interface with zero thickness (Fig. 2.23c). The approach leads to the reduction of the computational effort and yields a model that applies to a wider range of structures.

[3] Macro-modelling: This is structural level modelling techniques. Masonry is modelled as one phase material by smearing out masonry units, mortar and unit–mortar interface in a homogeneous continuum (Fig. 2.23d). This method has been previously adopted by Pande et al. (1989), Lourenco (1998), Zucchini and Lourenco (2004), Pena et al. (2010) and Dogariu (2015). This procedure is preferred for analysis of large-scale masonry structures, but not suitable for detailed stress analysis of a small masonry panel, due to the difficulty of capturing all its expected failure modes.

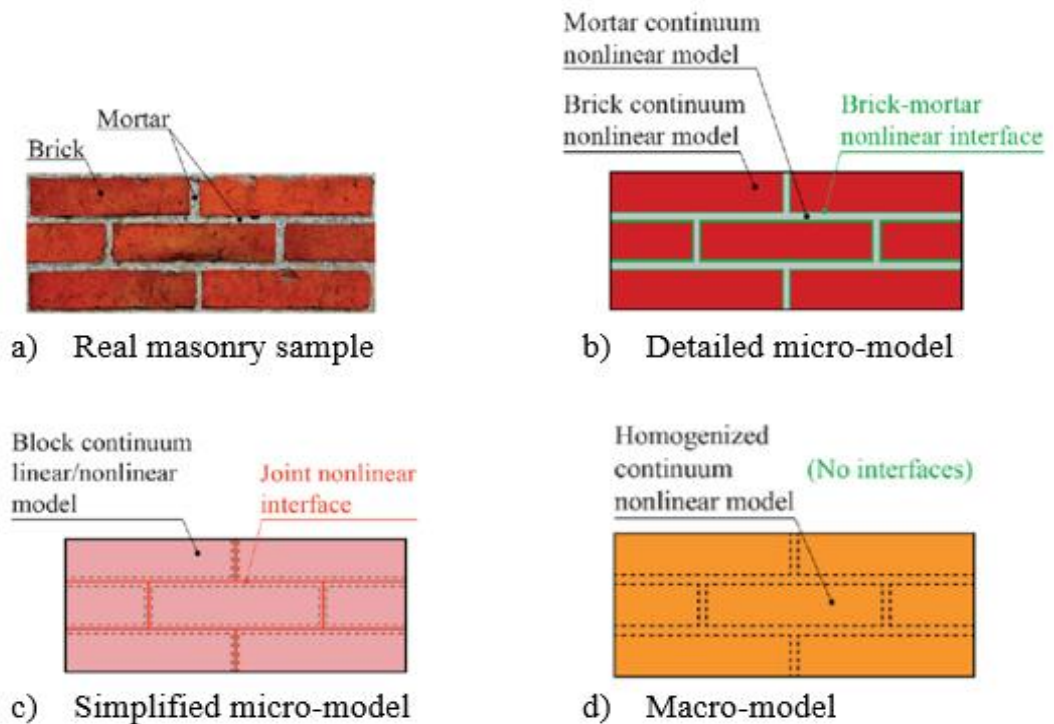


Figure 2.23. Masonry modelling techniques (a) real masonry sample (b) detailed micro-modelling (c) simplified micro model and (d) macro modelling

Meanwhile, as part of effort to make numerical analysis of masonry structures easy for engineers and researchers, Asteris et al. (2015) suggested a guideline in choosing a modelling strategy, this is summarized in figure 2.24 below.

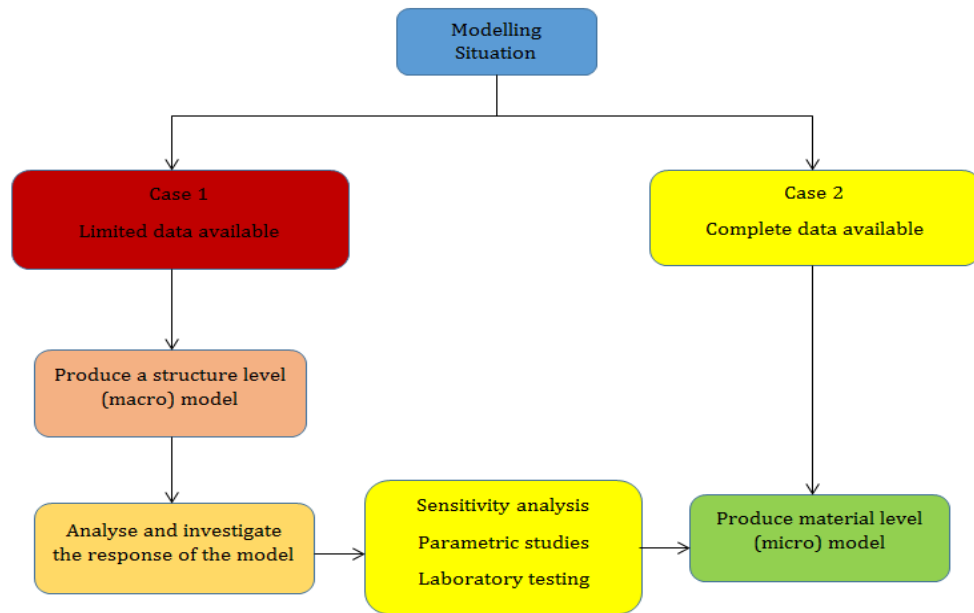


Figure 2.24. Guidelines for choosing the level of FE modelling

The choice of the method to adopt depends on the level of material information available, the level of accuracy and simplicity desired (Lourenco, 1996; Asteris et al. 2015). Macro modelling is more practice-oriented due to the reduced time and memory requirements as well as a user-friendly mesh generation (Lourenco, 1996). This type of modelling is valuable when a compromise between accuracy and efficiency is needed. On the other hand, the detailed micro-modelling technique produces the most accurate results, but it is computationally intensive due to the precise level of refinement required (Portioli and Cascini, 2016).

In this study, the detailed micro-modelling technique will be adopted to perform the numerical simulation. This is selected because the masonry specimen is small and a thorough description of the material is possible. This approach enables the combined action of unit, mortar and interface to be studied under a magnifying glass.

2.8 Summary of Review Carried Out

This section briefly summarises the knowledge and understanding gained from the review carried out, which formed bases for proposing this research work. The first section of the review focused on the structural behaviour of masonry walls. Here, the in-plane and out-of-plane failure modes of masonry wall were

discussed with emphasis on the out-of-plane failure mode of URM walls. This is because the review carried out revealed that the out-of-plane failure mode is the most devastating in URM walls and presents severe hazards for both human lives and cultural heritage in the event of structural failure.

Then, a concise review of the existing retrofit techniques used for URM walls is presented. The existing retrofit techniques were classified into both structure level and member level retrofit. The member level retrofit is the first ideal for investigating the effectiveness of a proposed retrofit technique. As such, this study will be on member level retrofit, in particular, retrofit of URM walls. The existing member level retrofit techniques are mostly in the form of joint treatment (repointing and grout injection), surface treatment (coating and reinforced plaster), internal and external reinforcement, FRP wrapping, and many other innovative techniques such as post-tensioning, CAM, and reticulatus system.

Subsequently, the review of some experimental tests on how to assess the out-of-plane performance of masonry walls was presented. From the review, it was observed that out-of-plane testing on URM wall panel without edge restraints or party walls is the most common viable means of assessing out-of-plane behaviour of masonry walls. The tests were carried out with either UDL or four-point load applied on the wall in an out-of-plane direction. The walls were tested with simply supported boundary conditions, and they are mostly according to the provision of ASTM E-72. The observed out-of-plane failure mechanisms from these reviewed test set-ups were characterised by vertical arching which has been termed as failure mechanism type F in FaMIVE. This type of out-of-plane failure mechanism occurred because the vertical strips of the tested wall panels deflected in out of plane due to the restraint at top and bottom of the wall. Vertical arching failure mechanism in URM wall will allow to establish the out-of-plane capacity of the plain wall and further allow assessing the improvement in the out-of-plane capacity of the wall due to the application of any retrofit technique.

The review revealed that the conventional retrofit techniques are very easy to apply with minimal cost, their major drawback is the inadequate increment in

the initial stiffness and higher additional dead load added to the existing structures. Meanwhile, the innovative techniques overcome these challenges but then present major challenges in the form of high cost of materials, complexity in design and implementation in existing structures. Therefore, this study aims to propose the possibility of using timber panels to retrofit old URM walls for better out-of-plane performance. The proposed OSB timber material is economical, can be easily sourced around the globe and can be considered as a sustainable material. The introduction of this retrofit approach using OSB timber panel will add to the existing masonry retrofit techniques and provide practitioners with the opportunity to choose an appropriate retrofit technique for URM structures from the available pool.

Timber is one of the oldest structural materials used in many parts of the world. Timber is highly known for its relatively higher strength to weight ratio compared to concrete and mortar coatings currently being used for retrofitting URM walls. It also has high shear strength across the grains, good aesthetic compared to FRP wrapping and steels bracing system. Despite these obvious advantages and strength of timber, the literature review shows that the potentials of timber have not been fully utilised in the structural retrofit of an old masonry building. Even though Langenbach (2007) and Pan et al. (2016) have acknowledged the seismic performance of timber-framed structure during earthquakes, there is little evidence of using timber panel to retrofit old unreinforced masonry building. The motivation for proposing this technique is that if timber-framed structure can perform well during earthquakes as identified in the literature, then timber panel might also be used to augment the out-of-plane performance of URM walls.

Indeed, timber-panels are currently being used for energy retrofits such as insulation, vapour control and airtightness in an old building (Pelenur, 2013; Giongo et al., 2017). But their application in structural retrofitting of URM wall is still not been thoroughly studied. An experimental study by Sustersic & Dujic (2014) was the only available study on the application of timber panels as strengthening system for existing buildings against seismic force. The in-plane behaviour of URM retrofitted with Cross Laminated Timber (CLT) panel was studied, and the results showed that there is a considerable increase in the

strength and ductility of the retrofitted wall. In (Sustersic & Dujic, 2014), a 100% increase in ductility when the CLT panel is connected to URM walls with a specially developed steel connection at top and bottom of the wall was observed. However, the availability of these unique connections in the open market is a concern limiting the acceptability of the techniques.

While developing this works, more recent researches (Riccadonna et al., 2019; Borri et al., 2020; Guerrini et al., 2020) involving the use of timber panel to retrofit masonry walls have emerged. Riccadonna et al. (2019) presented an experimental investigation to evaluate the application of Laminated Veneer Lumber (LVL) and CLT timber panel connected to masonry wall with screw anchor fasteners. Their study concludes that the proposed timber retrofit approach increases both the capacity and the stiffness of the retrofitted walls. Also, Borri et al. (2020) proposed the combined use of CLT panel and steel cords to reinforce rubble stone masonry walls to increase the shear response of cracked stone masonry wall panels while also improving the energy performance of the building. The study of Borri et al. (2020) found that the proposed CLT and steel cords retrofit techniques enhanced the lateral capacity of retrofitted masonry wall panels by about 150%. Moreover, Guerrini et al. (2020) proposed masonry pier in-plane retrofit system consisting of an OSB panel connected to vertical timber strong-backs on masonry pier using anchor nails to increase the in-plane shear strength and stiffness of the masonry specimen. The significant results obtained from the Guerrini et al. (2020) is that an improved seismic performance (increase in ultimate displacement by 167% and its lateral strength by 35%) of the retrofitted wall was achieved.

The earlier and recent studies (Sustersic and Dujic, 2014; Riccadonna et al., 2019; Borri et al., 2020) proposed the application of heavy CLT and laminated veneer lumber panels of around 60mm to 80mm which might be challenging to introduce in old URM buildings. In contrast, this study aims to propose the application of an 18mm oriented strand board (OSB) type 3 panel to retrofit URM walls. OSB is regarded as a promising wood-based structural panel due to its superior strength, stiffness, workability, and competitive pricing (Chen and He, 2017). This research investigated the performance of OSB type 3 panels connected to URM wall by threaded dry rod connections and injectable chemical

adhesive anchor readily available in the European market. However, it is imperative to point out that the novelty in this proposed retrofit technique is different from the known timber-framed masonry building (Fig. 2.23). In timber-framed masonry building, the masonry wall is confined with the timber frame to enhance the stability and integrity of masonry walls for the in-plane and out-of-plane loads. But this proposed technique considers securing timber panel behind the masonry wall (Fig 2.24). In this study, 18mm thick OSB type 3 was connected to URM wall using $\varnothing 8\text{mm}/L50\text{mm}$ threaded anchor rods together with an option of plastic plug or injection mortar to investigate how the out-of-plane behaviour of the retrofitted URM wall changes under out-of-plane loading. The study has proposed to investigate only the out-of-plane performance of the proposed techniques because URM walls are more vulnerable when loaded in the out-of-plane direction and generate profuse damages upon failure.

The advantages of this proposed retrofit technique include ease of application with low level of construction skills required, minimal cost compared to fibre-based application, no heavy additional load on the existing building due to lightweight of OSB. The retrofit will create a system with the same zone of stiffness and strength as against many of the surface and joint treatment that creates different zones. It is also a reversible retrofit system and will prevent the total collapse of the building. It proffers major increment in initial stiffness, strength and resistant of the retrofitted wall system.

However, the limitation of the proposed system is that it reduces functional space in the building. It also has an aesthetic or historical impact, particularly on the external surface if used on both sides of the wall and thus not desirable in the retrofit of historical heritage.

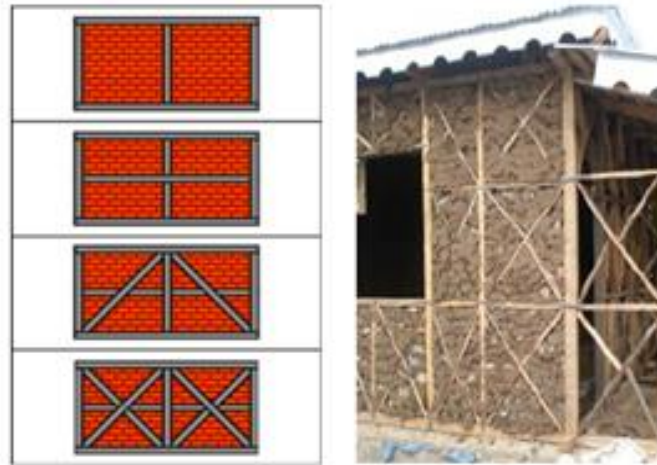


Figure 2.23: Timber confinement of URM

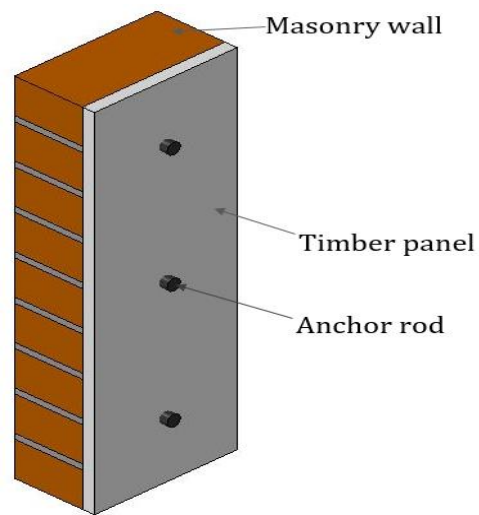


Figure 2.24: Proposed Timber panel retrofit

CHAPTER THREE- METHODOLOGY

3.0 Introduction

Here, the details of the methodology used in this study following the aim and objectives already identified in chapter 1 were presented through sequences of experimental (section 3.1) and numerical studies (section 3.2). The integrated approach adopted in this study to evaluate the effectiveness of the proposed timber-based retrofit technique has been articulated into three key stages: (1) experimental characterisation of masonry components to determine the mechanical properties of masonry brick units, mortar and masonry assemblage. This will ensure that the right material to represent the intended category of masonry walls were selected for this study. (2) out-of-plane flexural bond strength tests in the form of four-point bending testing on small scale (665 x 215 x 102.5mm) masonry prisms. This second stage helps to assess the prospect of the proposed retrofit technique and further aids the larger-scale experimental study and; (3) out-of-plane testing of 1115 x 1115 x 215mm masonry walls. The third stage is on larger-scale samples to study in details the out-of-plane performance of the proposed retrofit technique.

3.1 Experimental Program

I. Stage 1: Material Characterisation

Experimental programs were planned on brick units, mortar, and masonry assemblage as shown in stage 1 of table 3.1. The purpose is to characterise the mechanical behaviour of the masonry and its constituents.

Before designing any retrofit scheme, an understanding of the behaviour of the structure is essential. In the case of masonry wall, the mechanical properties of the constituents (i.e. masonry unit and mortar) affects its structural response under loading. Therefore, it is a general prerequisite to know the mechanical properties of the masonry unit and mortar constituents of the masonry wall before carrying out any retrofit work on the wall.

Thus, this section presents an experimental characterisation of the brick masonry components (i.e. solid fired clay brick and cement-lime mortar) that were used to construct masonry walls for investigating the efficiency of the

proposed timber-panel retrofit techniques. The solid fired clay masonry units and type N (general purpose) mortar were selected because the combination of the two is similar to what is expected in old masonry units (strong unit-weak mortar joint). The material characterisation tests also help in obtaining the strength material properties for masonry unit, mortar, and the unit-mortar interface that were used to produce detailed numerical analyses to complement the experimental tests carried out in this study.

For the material characterisation tests, an experimental program has been developed based on the components (brick unit and mortar) and assemblage (brick masonry) as shown in table 3.1. Firstly, experimental studies have been carried out to define the consistency and compressive strength of mortar and the dry density, water absorption, compressive strength, modulus of elasticity, and Poisson ratio of the brick units, all according to the relevant British standard (BS), as identified in table 3.1.

In particular, the water absorption property of the brick units is vital for the bond between the units and mortar (BSI, 2011a). If the water absorption of the brick units is too high, the bricks will absorb more water from the mortar, and the mortar will dry up quickly. This can cause dry shrinkage in mortar and reduction in strength and durability of the masonry wall specimens (Arash, 2012). Also, if the water absorption of the brick units is too low, the unit will float on the mortar bed joint, causing excessive bleeding in the mortar joints. This can cause major irregularities in the geometry of the masonry wall and reduction in the strength of the joint.

Therefore, it is important to know the water absorption of the brick units before using them. This will enable to design a right mortar mix with an optimum water content that is ideal for bonding the bricks. Having identified that the selected brick units have a low water absorption rate, hydrated lime was added to the mortar to have mortars with high water retention. This will create an improved bond as there is more contact between unit and mortar and also creates the best conditions for early hydration of cement lime mortars. Eventually, this will reduce dry shrinkage and cracking of the hardened mortar joints.

In addition, an unconventional test was used to determine the compressive strength of the assemblage (215 x 215 x 215mm masonry cubic specimen). The purpose of this test is to understand how bricks and mortar work together particularly, how the water absorption and addition of lime will affect the mechanical properties of the masonry. This test is also important because the results of the compression tests were later used to calibrate the properties of the brick units and mortar, nonlinear behaviour of the unit and joint in the developed FE models in numerical studies in section 5.

II. **Stage 2: Small-Scale Test (Flexural bond strength of masonry prism)**

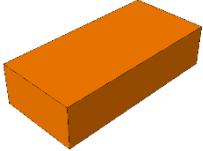
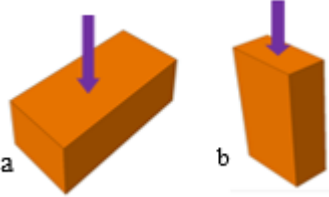
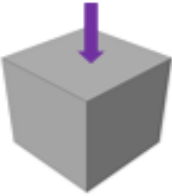
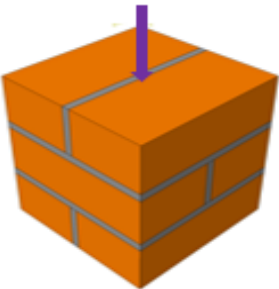
Since an experimental program with full-scale testing is expensive, small-scale testing such as the one presented in stage 2 is ideal for insight when proposing a new retrofit technique for masonry walls. In this stage, flexural bond strength test according to the provisions of (ASTM, E518-15) and (ASTM, E72 -15) was conducted on nine 615 x 215 x 102.5mm masonry prisms (MP). Three of which were tested as plain MP while the remaining six specimens were retrofitted with an 18mm thick Oriented Strand Board (OSB) timber panel using two different types of connections; C1 (adhesive anchor: a threaded dry rod with an injectable chemical adhesive) and C2 (mechanical connection: a threaded dry rod with a plastic anchor). The purpose of this test is to provide a simplified means of gathering data on the flexural strength of plain and timber retrofitted MP. Precisely, the experiment evaluates the out-of-plane performance of OSB panel in retrofitting URM prisms by comparing the toughness, flexural strength, out-of-plane load capacity, and displacement of both plain and OSB-retrofitted masonry prisms. This small-scale test helps to understand the behaviour of masonry and the connection between masonry and timber panel. It also helps to identify the best-performed connection types for the proposed application.

III. **Stage 3: Larger-Scale Test (Flexural strength of masonry wall)**

The knowledge gained from the small-scale test (stage 2) was then used to perform an out-of-plane flexural strength test on six larger-scale single leaf, double wythe solid (1115 x 1115 x 215mm) masonry walls. The purpose of this test is to achieve the research aim, which is to evaluate how the timber panel has aided the out-of-plane behaviour of the masonry wall. Table 3.1 presents the full experimental campaign for the study. For the larger-scale test, two similar specimens were tested as plain, one-sided retrofitted and double-sided

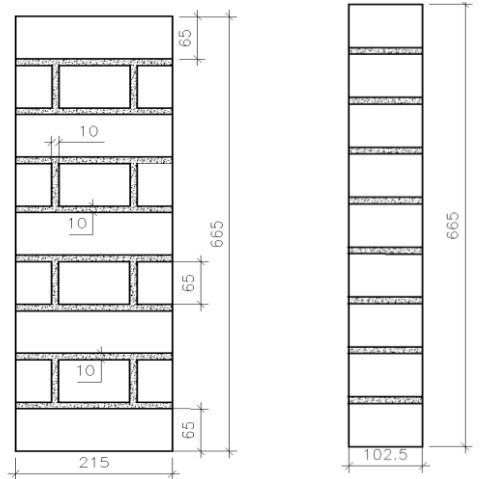
retrofitted walls. The plain wall was tested with both constant and variable pre-compression load to represent high in-plane compression usually present in URM walls. The retrofitted walls were constructed using OSB type 3 and adhesive anchor connection type (C1) that offer the most improvement in the flexural bond strength of masonry prisms identified from the small-scale test. The test program has ensured that loading has been applied on wall retrofitted with OSB timber on only tension face and on both tension and compression face of the masonry wall. This is because the type of application this study is proposing is the application of the OSB panel on the internal surface of exterior URM walls so that external historic appearance of the building is preserved. The other configuration where there will be OSB on both sides were for application on both surfaces of internal partition walls. So, specimens with OSB on the compression face only was not tested because the application of the technique on the only external surface is not envisaged.

Table 3.1 Full Experimental Program

Stage 1: Material characterisation			
Category		Properties	Relevant code
Brick		Dimension,	
		Dry density	BS EN 772-13:2000
Unit	 <p>Load on (a) bed face (b) head</p>	Water absorption	BSEN 772-21:2011
		Compressive strength,	
		Modulus of elasticity,	BS EN 772-1:2011
		Poisson's ratio	
Mortar		Dropping value	BS 4551:2005
		Consistency of fresh mortar	Flow value
		Compressive strength	BS EN 1015-11:1999
Masonry Cube		Compressive strength	unconventional test with insight from BS EN 1052-1:1999

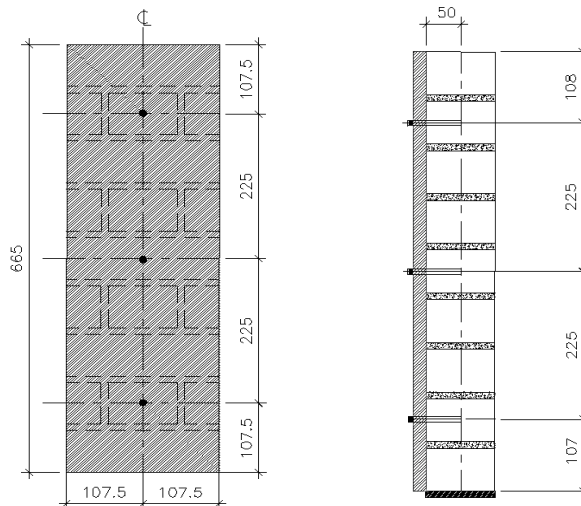
Stage 2: Small-Scale Test (Flexural bond strength of masonry prism)

Plain MP



3 plain MP specimens to be tested

Retrofitted MP

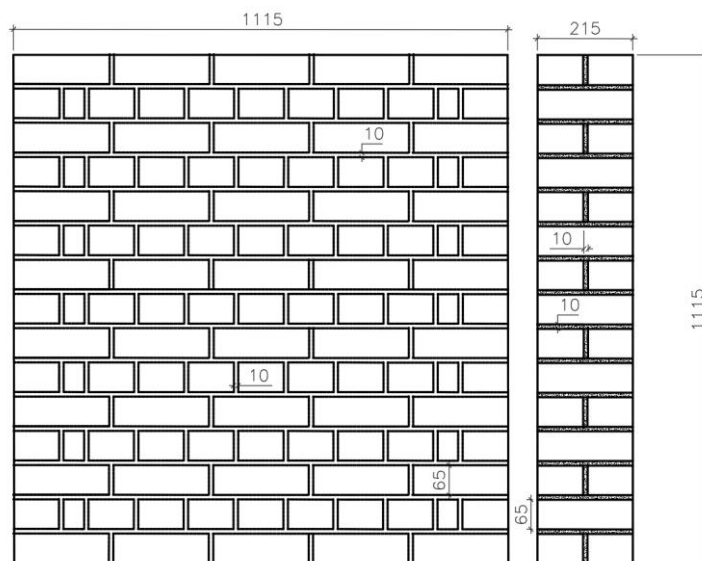


3 MP specimens retrofitted with C1: adhesive anchor

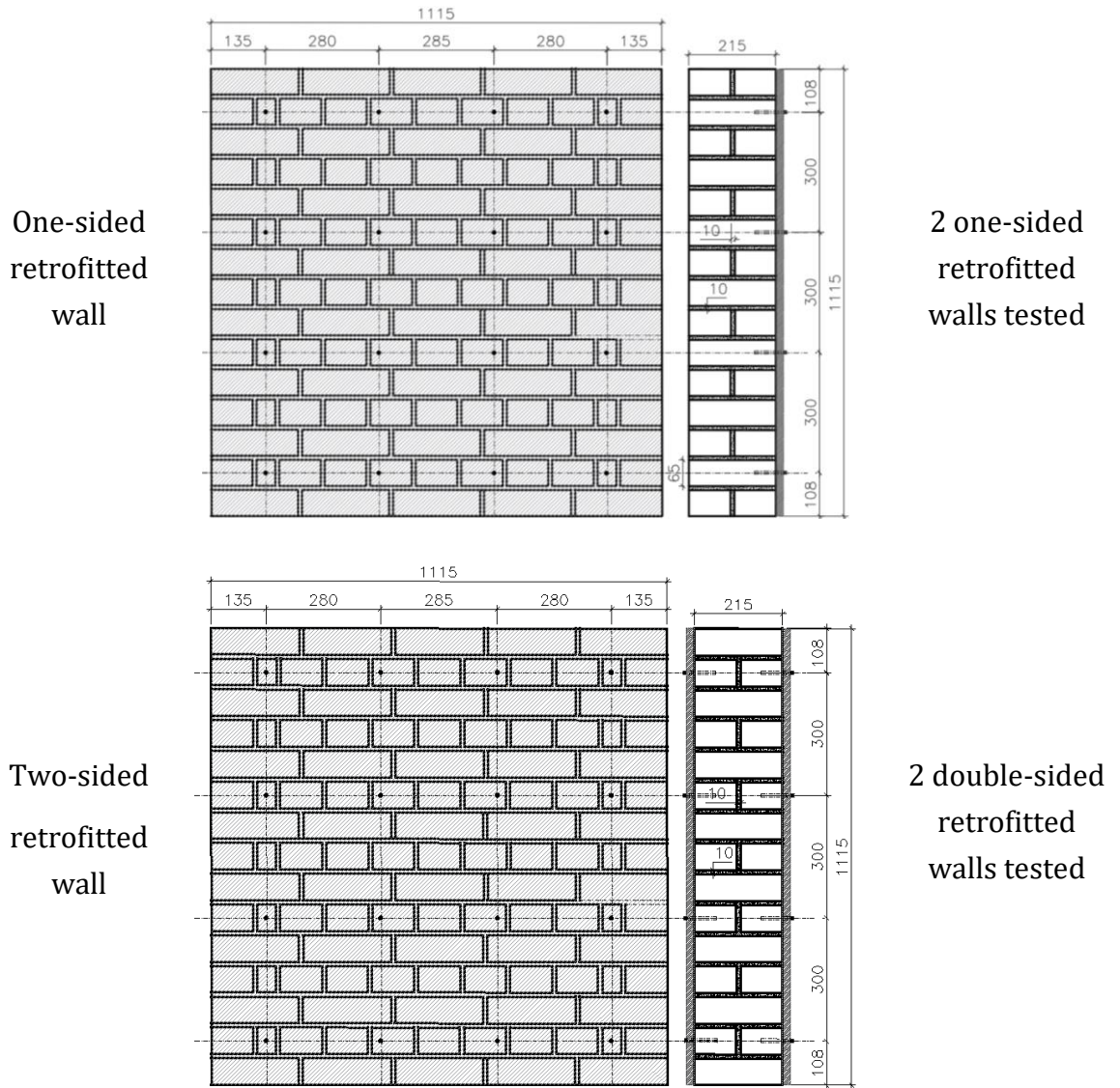
3 MP specimens retrofitted with C2: mechanical connection

Stage 3: Larger-Scale Test (Flexural strength of masonry wall)

Plain wall



2 plain wall specimens tested



Note: all dimensions are in mm

3.2 Materials

Four components which are brick unit, mortar, timber panel and connections were used for the experimental works in this study. The properties of these materials are briefly presented here. The full details of the properties of the materials including the tests used to determine them were presented under materials characterisation section in chapter four (section 4.1).

- I. **Brick Unit:** Engineering class B solid fired clay bricks with UK standard size 215 x 102.5 x 65mm were used to construct all test specimens. Before the construction of the test specimens, samples of the brick unit were randomly selected and tested to determine the conformity of the physical properties

of the brick to the manufacturer's specification. The characterisation tests were also to determine the suitability of the brick unit samples for the proposed experimental campaign.

- II. Mortar:** Type N (general purpose) mortar mix with a ratio of 1:1:6 (Type II Cement: aerial lime: sand) by volume was used to construct the specimens with 10mm thick nominal mortar joint. The fresh mortar sample was tested for consistency and hardened mortar cubes were also tested for strength.

The combination of the mortar specification and the selected brick unit represents a strong unit-weak mortar joint which is similar to what is expected in old masonry units.

- III. Timber Panel:** An 18mm thick oriented strand board (OSB) type 3, which is a load-bearing engineered wood-based panel for use in humid conditions, was selected for this study. The OSB is manufactured from strands of wood which are bonded together with a synthetic resin.

- IV. Connections:** Two types of connection systems from Fischer ® group were selected for this study. The selected connections were made of A4 (1.4401 or 316) stainless steel. The connections are classified as connection type 1 and type 2. Type 1 is an adhesive anchor connection system which is a combination of FIS V 360 S injection mortar and FIS A4 anchor rod. While type 2 is a mechanical connection system which is a combination of Fischer frame fixing SXS plastic plug made of high-quality nylon and FUS A4 anchor rod.

3.3 Numerical Analysis Program

The numerical analysis was planned to complement the experimental works. The purpose of this is to expand the experimental study to evaluate the efficiency of the proposed timber-based retrofit for URM walls. Abaqus/CAE, or "Complete Abaqus Environment" (Simulia, 2014) was used for both modelling and analysis performed in the numerical studies. Figure 3.1 below schematically represents the full numerical analysis performed in three stages to follow suit with the experimental works identified in section 3.1.

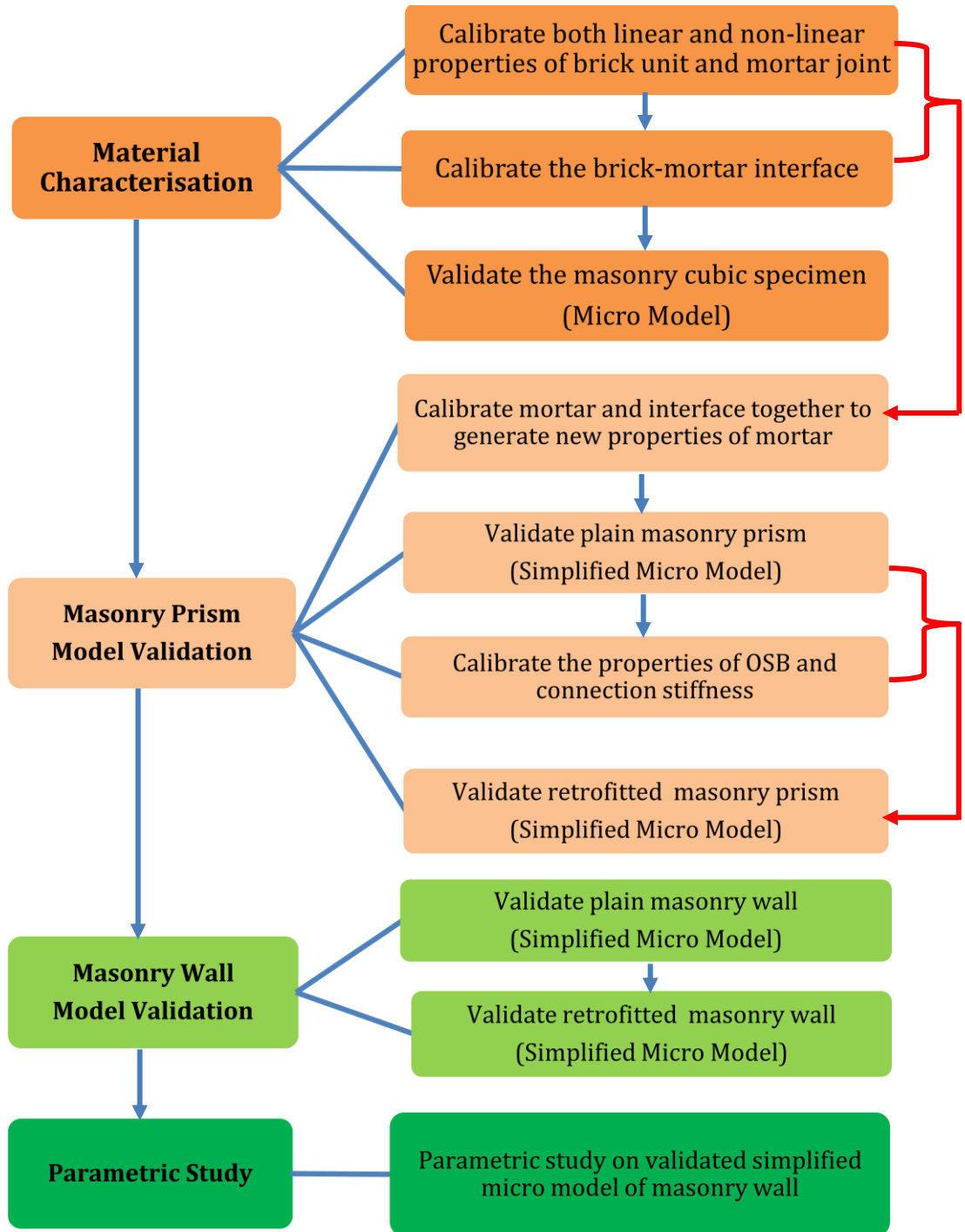


Figure 3.1. Full numerical analysis program

The first section in figure 3.1 is material characterisation which is the numerical simulation of the compression test on the masonry cubic specimen presented in section 4.1. The purpose of this is to obtain accurate mechanical properties of the unit, mortar and the interfacial properties of the unit-mortar joint that is necessary to produce detailed micro-modelling of masonry structures. To

achieve this, a complete description of each component was done based on the experimental results of compression tests on brick units, mortar, and the masonry cubic assemblage in section 3.1. Basically, this was done in three steps as can be seen from figure 3.1 with leading arrows connecting the steps. The linear properties of the unit and joint were directly obtained from the experiments and the non-linear post-peak behaviour of the compressed brick and mortar were characterised using the concrete damaged plasticity model in ABAQUS. After that, the brick-mortar interface was calibrated and then the model for the masonry cubic specimen was finally developed and calibrated against the experimental results to obtain strength material properties for the unit, mortar and interface that will be used to analyse the out-of-plane response of masonry panels retrofitted with the proposed technique.

Secondly, the numerical simulation of the flexural bond strength test on small-scale masonry prism described in section 4.2 is presented as masonry prism model validation (Fig. 3.1). The purpose of this section is to develop a FE model that will capture the damage and failure pattern of the masonry prism (MP) tested in the laboratory. This stage was done in two steps; (i) validation of the plain MP using the already calibrated properties of the brick units and new properties that lumped the properties of mortar and the interface together, (ii) validation of the retrofitted MP, here the properties of the retrofit materials which are the OSB panel and the connections were calibrated and the components were added to the already validated plain MP model to generate the retrofitted model. The model was created with all the components in the four-point loading test properly modelled to obtain the best accurate results from the finite element analysis. The full description of the model, material properties and the interaction of the components considered in the model are described in section 5.2.

More so, the numerical simulation of the out-of-plane loading test on the larger-scale masonry wall presented in section 4.3 was then carried out in the third step of figure 3.1. The process follows the preceding stage with the plain wall model first validated and then the retrofitted wall was modelled with the addition of OSB panel and connections. At each stage of the simulation, the developed models were validated using the experimental data.

Finally, parametric studies to assess the model capability to simulate URM walls retrofitted with different OSB panel thickness, application side, and connection layout were carried out.

3.4 Summary

The main approaches to this study are numerical and experimental study. The focus is to obtain an accurate assessment of the proposed retrofit technique through a thorough investigation. This chapter has briefly presented the research approach, which involves the full tests carried out and the scheme for the numerical works that were done to complement the experimental works. The full description of the experimental works including the materials, specimen construction, test matrix, test setup, instrumentation and the experimental results for each stage of the test program identified in table 3.1 is presented completely in the following chapter four.

Similarly, the numerical works including the description of finite element models, input material parameters, analysis methods, mesh sensitivity analysis and the obtained results from the validated model and parametric study were presented in chapter five.

CHAPTER FOUR – RETROFIT OF URM WALL WITH TIMBER PANEL: EXPERIMENTAL STUDY

4.0 Introduction

This chapter presents the full experimental work carried out to evaluate the efficiency of the proposed timber-based retrofit of URM walls. The experimental work as previously identified in table 3.1 was divided into three main sections, which are material characterisation, small-scale test on masonry prisms, and larger-scale test on masonry walls.

Here, the details of the experimental tests comprising the materials, specimens' construction, test setups, methodology, and the obtained test results are presented under each section.

4.1 Material Characterisation

4.1.1 Characterisation of Brick Units

Engineering class B solid fired clay bricks (UK standard size 215 x 102.5 x 65mm) manufactured by Weinberger were used for constructing the masonry specimens for this study. The properties of the brick units depend mainly on the constituent soils and manufacturing process, which varies from place to place. So, the source of the bricks was kept the same throughout the experimental campaign to ensure that the bricks were of the same quality. However, experimental tests were conducted on the bricks to determine the conformity of the bricks to the manufacturer's specifications and their quality before using them. The obtained properties of the brick units from the test carried out were the dimension, dry density, water absorption, compressive strength, modulus of elasticity, and Poisson's ratio of the brick units.

4.1.1.1 Dimension of Brick Units

Six brick units were selected randomly, and meter rule was used to measure the length, breadth, and height of the bricks (Fig. 4.1a) as recorded in table 4.1. Due to the manufacturing variations, all brick units were not of the same dimension, but the variation in the size is not more than 2mm in any of the selected bricks.

This will not affect the properties of the brick unit because the variations fall within the allowable dimensional tolerance specified in BSI (2011a).

4.1.1.2 Dry Density of Brick Units

In addition to the dimension of the brick units obtained earlier, the six chosen bricks were weighed using an electronic weighing balance (Fig. 4.1b) to get their gross mass. After that, the samples were then dried in a ventilated oven (Fig. 4.1c) at 100°C temperature for 48hrs to ensure that the difference in mass is less than 0.2% of the gross mass, an indication that the constant mass of the samples has been reached (BSI, 2000). The dry density (γ_{du}) was calculated based on the dry weight and volume of bricks as recorded in table 4.1.

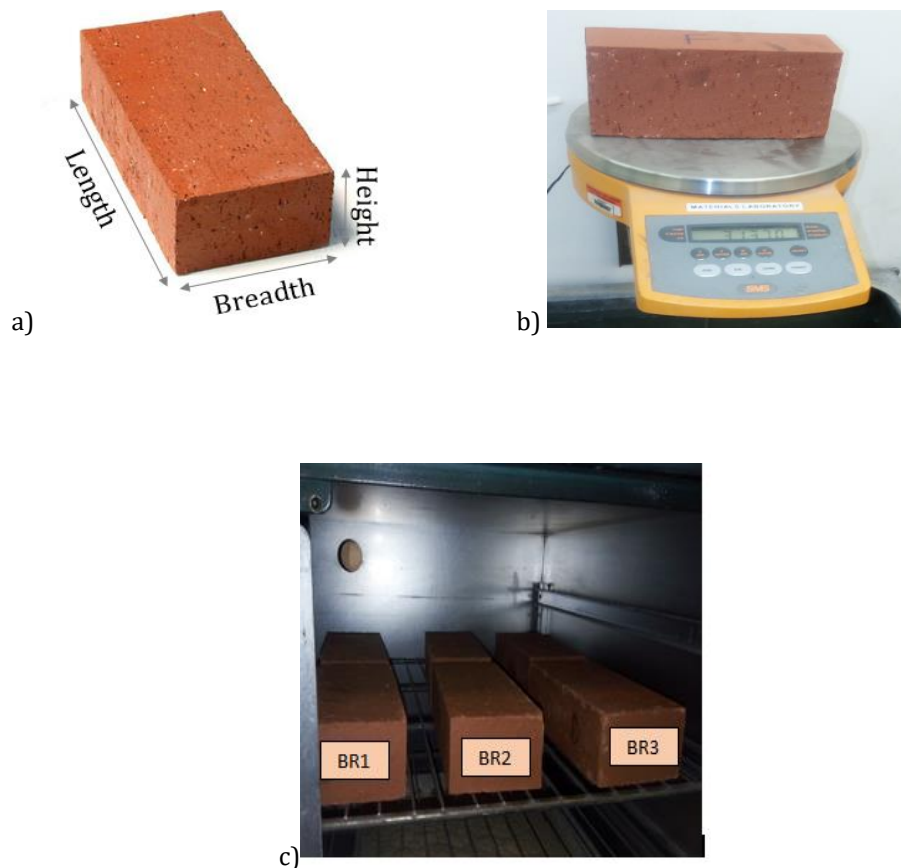


Figure 4.1. Brick unit samples; (a) Measuring (b) Weighing (c) Drying inside an oven

Table 4.1: Dimension and dry density of brick units

Label	Dimension ($l \times b \times h$) m	Volume V_u (m ³)	Dry weight M_{du} (kg)	Dry density M_{du}/V_u	Av. γ_{du} (kg/m ³)
BR1	0.214 x 0.103 x 0.065	0.0014	3.146	2196	2195 (cov = 0.3%)
BR2	0.215 x 0.102 x 0.064		3.134	2188	
BR3	0.213 x 0.103 x 0.065		3.153	2200	
BR4	0.215 x 0.102 x 0.065		3.150	2199	
BR5	0.215 x 0.102 x 0.065		3.152	2200	
BR6	0.214 x 0.103 x 0.065		3.131	2189	

4.1.1.3 Water Absorption of Brick Units

The water absorption property of the brick units is vital for the bond between the units and mortar (BSI, 2011a). If the water absorption of the brick units is too high, the bricks will absorb more water from the mortar, and the mortar will dry up quickly. This can cause dry shrinkage in mortar and reduction in strength and durability of the masonry wall specimens. Also, if the water absorption of the brick units is too low, the unit will float on the mortar bed joint, causing excessive bleeding in the mortar joints. This can cause major irregularities in the geometry of the masonry wall and reductions in the strength of the joint (Arash, 2012).

Therefore, it is important to know the water absorption capacity of the brick units before using them. This will enable to design a right mortar mix with an optimum water content that is ideal for bonding the bricks. For these reasons, the water absorption of the selected brick units was determined according to provisions of (BSI, 2011b). After the constant mass of brick samples has been achieved in section 4.1.1.2, the selected six bricks were then immersed in a cold-water tank where water freely circulated on all the sides of the samples (Fig. 4.2). After 24hrs, the bricks were removed from the water tank, and surface water was wiped off with a damp cloth from the bricks. Then, the saturated bricks were weighed within 2mins after removal from water. The increase in the mass of the bricks gives the bricks water absorption as recorded in table 4.2.



Figure 4.2. Brick samples immersed in water

Table 4.2: Water absorption of bricks

Label	Dry weight	Wet weight	Water absorption (W_u)	Av. W_u (%)
	M_{du} (kg)	M_{wu} (kg)	$\frac{M_{wu} - M_{du}}{M_{du}} \times 100\%$	
BR1	3.146	3.266	3.8	3.9 (cov = 5%)
BR2	3.134	3.255	3.9	
BR3	3.153	3.269	3.7	
BR4	3.150	3.281	4.2	
BR5	3.152	3.274	3.9	
BR6	3.131	3.262	4.2	

4.1.1.4 Compressive Strength of Brick Units

The compressive strength (f_b) of the brick units affects the behaviour of the masonry wall under loading, and it is an essential property for designing any retrofit for masonry walls. Therefore, the compressive strength of the selected six bricks was determined according to (BSI, 2011a). Each brick unit was conditioned back to a constant mass (BSI, 2011a). The samples were dried in a ventilated oven at 100°C temperature for 48hrs to ensure that the difference in mass is less than 0.2% of the gross mass, an indication that the constant mass of the samples has been reached. After that, the brick was laid and centred on the platen of a 5000kN capacity compression-testing machine with 2mm thick plywood placed on top and bottom face of the brick. In order to estimate the strength of the brick in two orientations, three bricks each were loaded on the header (BR1-BR3) and bed face (BR4-BR6) as shown in figure 4.3(a) and (b) respectively. After that, a uniformly distributed load was applied gradually in

equal increments of 4kN/sec up to the failure (splitting) of the brick units. The loading and the results were monitored using a data logger connected to the compression-testing machine and f_b for each tested brick was calculated from the failure load and loaded area of the brick unit, as shown in table 4.3.

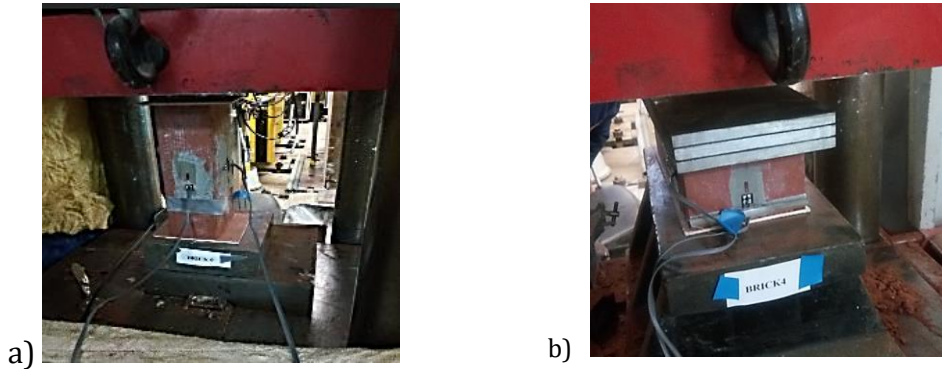


Figure 4.3. Compression test; a) load applied on header b) load applied on the bed face

Table 4.3: Compressive strength of bricks

Label	Max. Load	Area A (mm ²)	Compressive strength (f_b)	Av. f_b (N/mm ²)
	P_{max} (N)		$\frac{P_{max}}{A}$ (N/mm ²)	
BR1	739800		111.04	106 (cov = 5%)
BR2	664199	6663	99.69	
BR3	715000		107.32	
BR4	1898971		86.17	87.9 (cov = 1.8%)
BR5	1948115	22038	88.40	
BR6	1965100		89.17	

4.1.1.5 Modulus of Elasticity and Poisson's Ratio of Brick Units

The modulus of elasticity (E_b) and the Poisson ratio (μ_b) are important properties of the brick unit that measure its stiffness. They are essential for characterising masonry wall and unavoidable for performing numerical analysis on masonry structures. So, this study determined both properties (E_b & μ_b) alongside with the compressive strength of the brick units. E_b and μ_b were only determined for bricks loaded in bed face (BR4- BR6) because the masonry bond pattern considered in this study were all constructed with brick laid in bed face.

E_b was determined using the stress-strain relationship obtained from the axial compression test. Before placing the bricks under the compression-testing

machine, FLA-5-11 strain gauges were fixed in the longitudinal and along lateral direction on each brick unit as shown in figure 4.4 to record the strain values in the bricks under axial compression. The stress and corresponding strain for each unit were then calculated as shown in table 4.4. E_b was calculated by considering values between 30% and 60% of the maximum stress (σ_{max}) according to (Vasconcelos & Lourenço, 2009) and (Oliveira, et al., 2012).

The Poisson's ratio was calculated by plotting the lateral strains against longitudinal strains for each brick (Fig. 4.5). Best line of fit for each brick unit was then plotted to determine the relationship between the lateral and longitudinal strain. Referring to figure 4.5, the strains plot for BR5 is too scatter and the line of fit does not seem best. Hence the result was discarded and μ_b was calculated using results for BR4 and BR6.

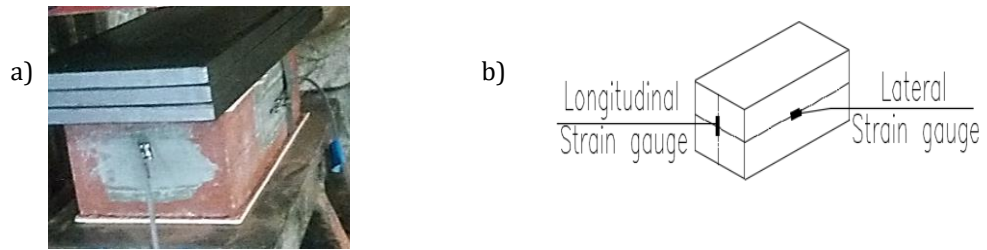


Figure 4.4. Strain gauges on the brick; a) As fixed (b) Drawing scheme

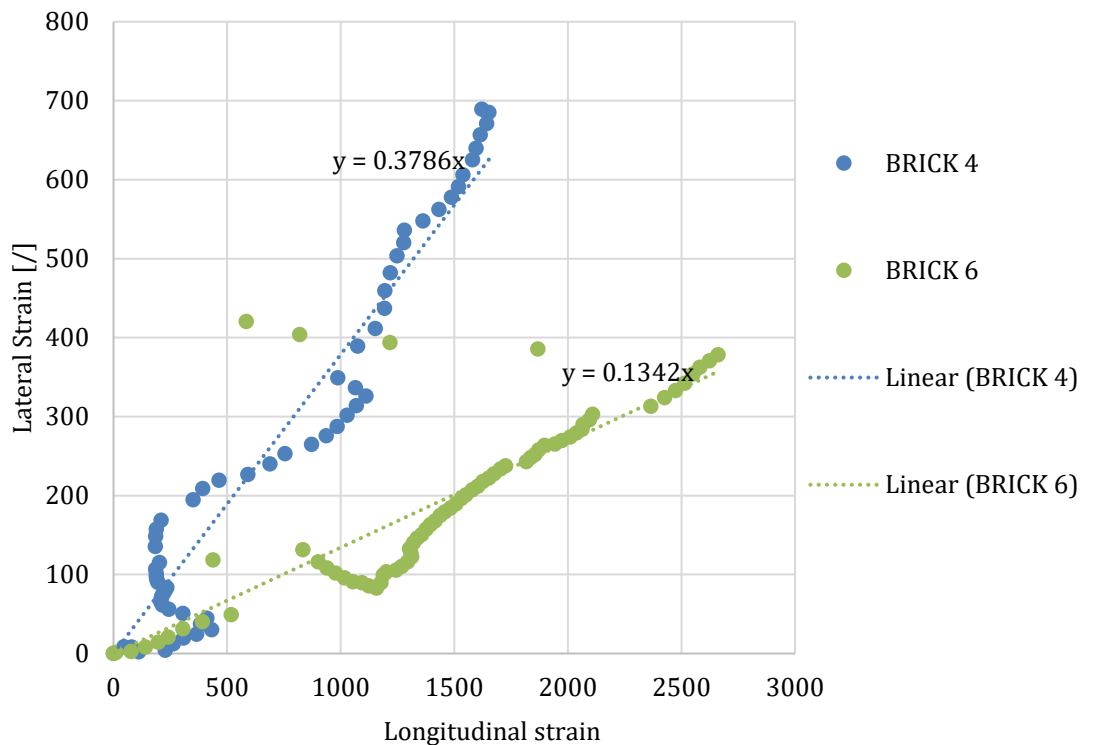


Figure 4.5. Lateral vs longitudinal strain for brick [μ]

Table 4.4: Modulus of elasticity and Poisson ratio of bricks

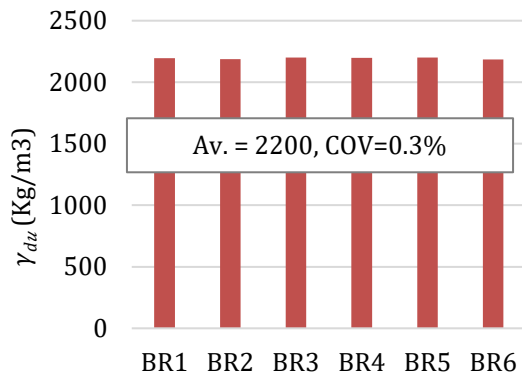
Label	σ_{max} (N/mm ²)	$\sigma_{60\%}$ (N/mm ²)	$\varepsilon_{60\%}$ (10 ⁻⁶)	$E_b = \frac{\sigma_{60\%}}{\varepsilon_{60\%}}$	Av. E_b (N/mm ²)	μ_b	Av. μ_b
BR4	86.17	51.70	1517.93	34060.75		0.379	
BR5	88.40	53.04	1711.31	30993.79	32500	-	0.26
BR6	89.17	53.50	1642.92	32565.37		0.134	

4.1.1.6 Mechanical Properties of Brick Units

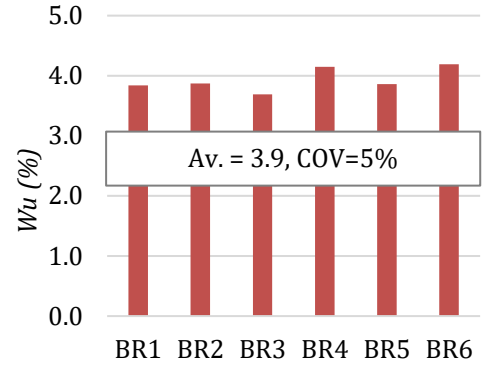
Figure 4.6 presents the graphical representation of the average value of the mechanical properties of the brick units obtained from the experimental tests carried out on the selected brick units. In complementary, table 4.5 compares the obtained brick properties from the experiments to the values declared by the manufacturer except for E_b and μ_b that were compared with the values reported in Vasconcelos & Lourenço (2009), Oliveira et al. (2012) and Italian Code for Constructions (DM 14.1.2008). The purpose of this comparison is to establish if the bricks qualities conform to the manufacturer specifications and also to determine if they are good enough to be used for this study.

For comparing the compressive strength (f_b), modulus of elasticity (E_b), and Poisson's ratio (μ_b), the average of the values obtained for BR4, BR5, and BR6 were considered because the bricks were loaded in bed face as already explained in section 4.1.1.5.

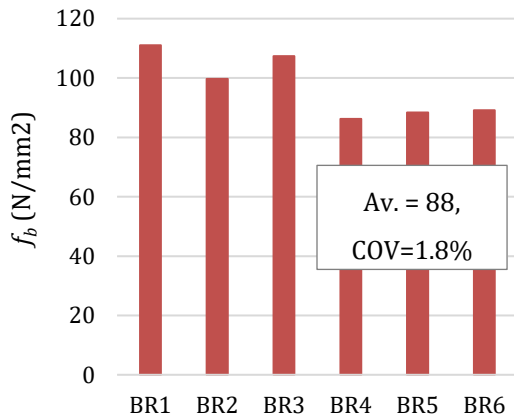
Generally, the obtained properties of the bricks indicate that the selected bricks are of good qualities and conform to the declared specifications from the manufacturer. Therefore, the brick units are acceptable for the proposed experiment. Hence, all the bricks used in this study were sourced from the same manufacturer (Wienerberger Ltd).



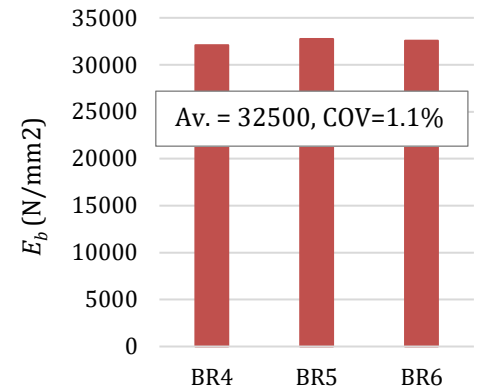
a) Density of brick units



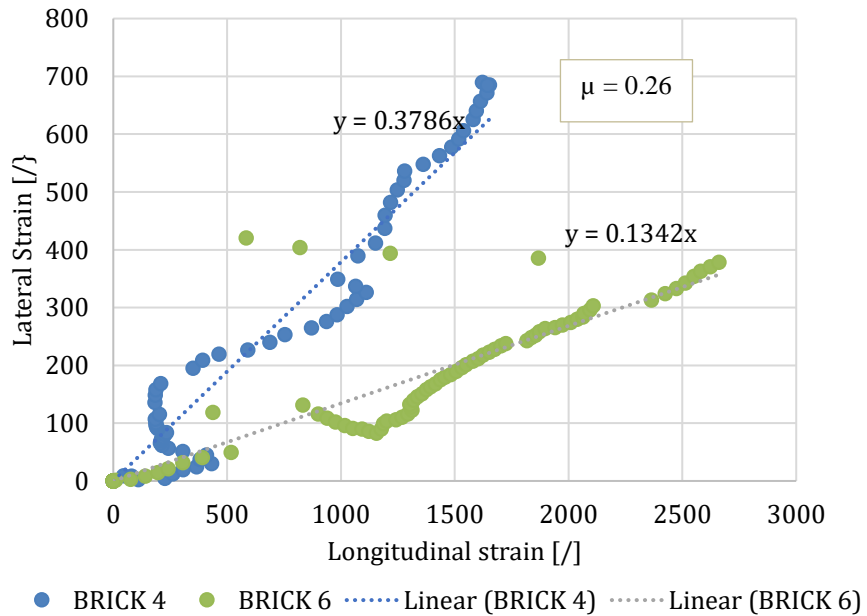
b) Water absorption of brick units



c) Compressive strength of brick units



d) Modulus of elasticity of brick units



e) Poisson's ratio of brick units

Figure 4.6. Summary of mechanical properties of brick units

Table 4.5: Mechanical properties of brick units

Property	Values		Requirement
	Experiment	Manufacturer	
γ_{du} (kg/m ³)	2200	2310	shall not be less than 2079kg/m ³ i.e 90% of specified density (BSI, 2000)
W_u (%)	3.9	≤ 7	shall not be more than manufacturer limit (BSI, 2011b)
f_b (N/mm ²)	87.9	75	shall be not less than the declared compressive strength (BSI, 2011a)
E_b (N/mm ²)	32500	≤ 34000	between 3500 and 34000 for different types of clay unit (DM 14.1.2008)
μ_b [°]	0.26	0.15-0.40	range for clay unit (Lourenco, 1996)

4.1.2 Characterisation of Mortar

Mortar can be described as a mixture of binder materials (cement and/or lime) and inert material (e.g. sand) with the addition of water to form a smooth paste. The quality of the mortars used in bonding brick units together is essential in masonry construction. In this study, type N (general purpose) mortar mix with a ratio of 1:1:6 (cement: lime: sand) was prepared. This ratio was converted to weight as the materials were batched in weight. The amount of water to be added to the mix proportion was not mentioned in masonry standard codes. Hence the optimum water content, which gives a working consistency was found by trial and error using the dropping ball test in section 4.1.2.1 described in (BSI, 2005). After the mortar mix ratio and water/binder ratio has been determined through trial mixes, these ratios were then used to prepare all mortar used in the experimental works. For consistency, the dropping ball test and flow table test were conducted on all the batches of the fresh mortar used throughout the experimental campaign. Also, samples of mortar cube were prepared from all batches of mortar, and the compressive strength of the hardened mortar cubes was determined.

4.1.2.1 Consistency of Fresh Mortar (Dropping ball test)

To ensure the consistency of mortar used in the preparation of masonry sample specimens throughout the experimental campaign, dropping ball test was carried out for all the mortar used in the specimens. The test was carried out according to the provisions of (BSI, 2005) using dropping ball apparatus consisting of the stand, acrylic ball, ring mould (\varnothing 100 x 25mm), rubber suction hand pump, and a dial Indicator as shown in figure 4.7. The test procedures are:

- ❖ The ring mould was filled with fresh mortar to level with the top of the mould
- ❖ The acrylic ball on the suction rubber was then allowed to fall freely through a height of 250mm to strike the surface of the mortar in the mould
- ❖ The tip on the dial indicator was then wound down to allow the tip to touch the acrylic ball
- ❖ After that, the penetration of the ball was measured from the dial indicator to the nearest 0.1mm and recorded as shown in table 4.6
- ❖ As required, the consistency of the fresh mortar was adjusted to a penetration of 10 ± 0.5 mm.

The target dropping value of 10 ± 0.5 mm must be achieved before accepting the mix ratio. In trial mixes, the 10 ± 0.5 mm dropping value was achieved after the third trials as detailed in table 4.7. The water binder ratio that gives the dropping value of 10 ± 0.5 mm was then adopted as the water ratio for the mix throughout the experimental campaign. This test was carried out on all the mortar used throughout the experimental campaign, and the records are presented in appendix 4.1.



Figure 4.7. Test setup for dropping ball test

Table 4.6: Dropping test value of fresh mortar

Trial No	Cement (kg)	Lime (kg)	Sand (kg)	W/binder ratio	Dropping test value (mm)
1	1.00	0.67	6.20	0.60	7.20
2	1.00	0.67	6.20	0.90	9.30
3	1.00	0.67	6.20	0.96	10.20

4.1.2.2 Consistency of Fresh Mortar (Flow table test)

Flow table test is the most recommended test on fresh mortar for bonding masonry unit, and it was carried out on the mix ratio that gives the targeted dropping value for all masonry samples preparation. The flow table test was carried out according to (BSI, 1999b) by using a mould, flow table disc, tamper rod, and metre rule. The test procedures were as explained below:

- ❖ The flow table disc and the mould were first deeply cleaned and wetted
- ❖ The mould was then placed in the centre of the flow table disc and filled with fresh mortar in two equal layers. Each layer was tamped 10times with a tamping rod to ensure uniform filling of the mould
- ❖ The excess mortar was skimmed off the mould with a palette knife and any water around the bottom edge of the mould was removed
- ❖ After approximately 15s, the mould was slowly raised vertically, and the mortar on the disc was spread out by jolting the flow table 15times at a constant frequency of approximately one cycle per second
- ❖ After that, the flow of the mortar was measured in two directions at right angles to each other using rule (Fig 4.8), and the mean was found in table 4.7.

Table 4.7: Flow test value of adopted mix

Trial No	Cement (kg)	Lime (kg)	Sand (kg)	W/binder ratio	Flow test Value (mm)		
					Dir 1	Dir 2	Mean
3	1.00	0.67	6.20	0.96	167.5	167.0	167.25

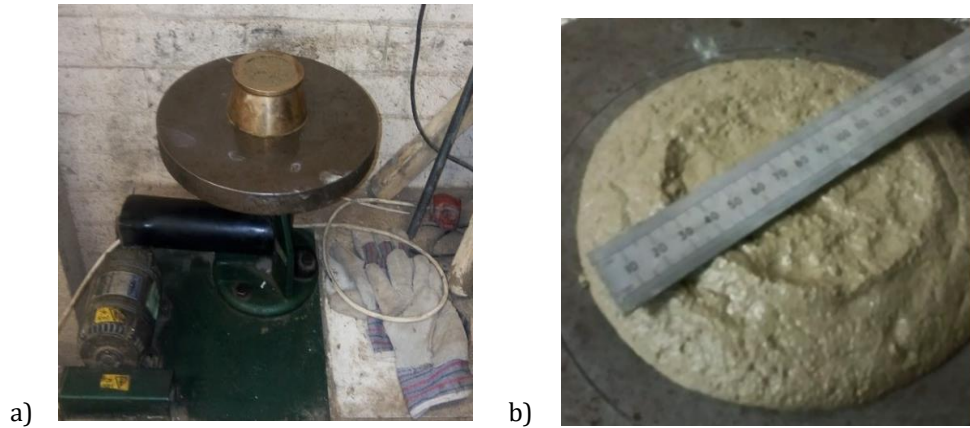


Figure 4.8: a) Test setup for flow table test, b) Mortar flow measurement

4.1.2.3 Compressive strength test of hardened mortar

The compressive strength of hardened mortar was determined according to (BSI, 1999c) under the universal compression-testing machine. At least three samples of 100 x 100 x 100mm (M1-3) or 50 x 50 x 50mm(M4-6) cubes were prepared from each batch of mortar and cured under the same condition with the masonry specimens. Usually, the cubes were removed from the mould after 24hours and covered with polythene sheet for 14days and then left open for the next 14days in the laboratory. This is to keep the curing condition of the mortar the same with the masonry specimens as will be discussed later in the subsequent section. After 28days, the hardened mortar cubes were tested under compression testing machine to determine the compressive strength of the mortar (f_m) as shown in figure 4.9. The mortar cube specimens were carefully aligned under the machine with the centre of the ball-seated platen so that a uniform seating is obtained. Thereafter, a uniformly distributed load was applied gradually in equal increments of 1kN/sec continuously up to the failure of the mortar cube. f_m was then calculated from the failure load and loaded area of the mortar cube, as shown in table 4.8.



Figure 4.9: Compressive strength test of hardened mortar

Table 4.8: Compressive strength of mortar

Label	Max. Load P_{max} (N)	Area A (mm ²)	Compressive strength $(f_m) \frac{P_{max}}{A}$ (N/mm ²)	Av. f_m (N/mm ²)
M1	72300		7.23	
M2	70700	10000	7.07	7.11
M3	70300		7.03	(cov = 1.5%)
M4	17600		7.04	
M5	17700	2500	7.08	7.06
M6	17670		7.07	(cov = 0.3%)

4.1.2.1 Mechanical Properties of Mortar

From the tests conducted on both the fresh and the hardened mortar, the mix ratio of 1:1:6 with water binder ratio of 0.96 gives the dropping value of 10.2mm, and the corresponding mean flow value is 167.25mm. This mean value is the flow value for the mortar sample, and since the individual flow values from the two directions do not deviate from their mean value by up to 10%, the result is satisfactory as deduced from (BSI, 1999b). Also, the consistency of mortar is good as this agrees with the ideal flow value (150-175mm) for mortar joints, as derived from (Haach, et al., 2007) as shown in figure 4.10. The hardened mortars have an average compressive strength of 7.1N/mm² (Fig. 4.11).

To maintain the consistency of all specimens constructed throughout the experimental campaign, dropping ball test, flow test, and compressive strength of hardened mortar samples were carried out on all the mortar used in this experimental study and the records of the result are presented in appendix 4.1.

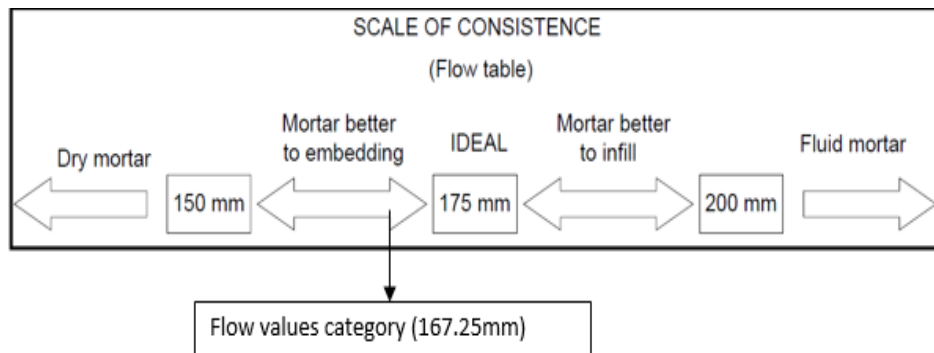


Figure 4.10: Consistency of fresh mortar

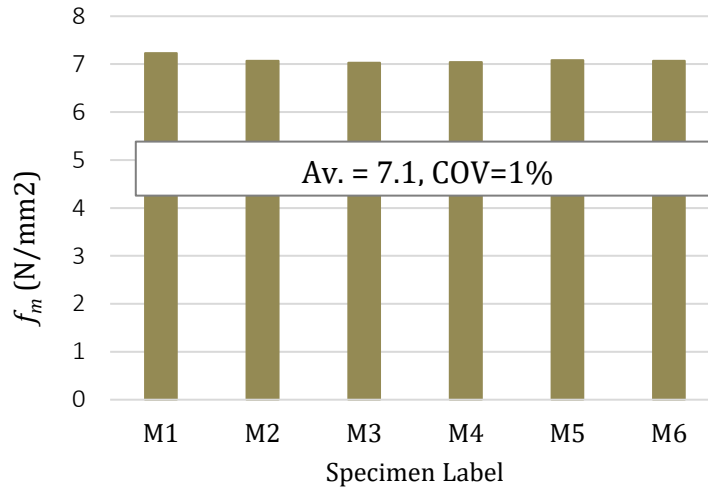


Figure 4.11. Compressive strength of mortar

4.1.3 Characterisation of Masonry Cubic Specimen

In order to understand how the selected brick units and the adopted mortar mix ratio work together, the compressive strength of masonry cubic (MC) specimen was obtained experimentally in section 4.1.3.1 through an unconventional test developed according to previous tests carried out by (Arash, 2012) with insight from (BSI, 1999a). The rationale behind this unconventional test was based on testing the compressive strength of cubic specimens. As such, masonry cubic specimen was prepared by bonding the brick units with mortar. In complementary, the compressive strength of the masonry cubic specimen was also determined by empirical calculation in section 4.1.3.2 using equations given in (BSI, 1999a).

4.1.3.1 Compressive Strength of MC Specimens: Experimental

Six masonry cubic specimens (MC) of 215 x 215 x 215mm were prepared using masonry brick units from the same stock as the ones tested earlier and a 10mm thick mortar joint with the mix ratio described above. The MC specimens were constructed using English bond consisting of alternate rows of headers and stretchers (Fig. 4.12a) which is the oldest form of brick bond popular in the UK until the late 17th century (Anon, 2009). The MCs were prepared in the laboratory, and horizontal level surface is ensured by using a bubble level during construction. After the construction, each sample was wrapped with polythene sheet for 14days (Fig. 4.12b) to prevent quick loss of moisture to avoid dry

shrinkage in the joint. Thereafter, the samples were opened and cured for further 14days in the laboratory to allow the samples to achieve their standard strength. After the curing of the samples has been completed in 28days, the specimens were then ready to be tested under the compression-testing machine. However, before testing the specimens, four linear variable displacement transducers (LVDT) were attached to the samples as shown in figure 4.13 to measure the deformation of the MC during testing. After that, the specimens were carefully aligned with the centre of the ball-seated platen, under the compression-testing machine with 2mm thick plywood placed on top and bottom of the MC under the compression-testing machine. A uniformly distributed load was applied gradually in equal increments of 4kN/sec continuously up to the failure of the specimens. The compressive strength of MC was then estimated from the failure load and loaded area of MC, as presented in table 4.9.

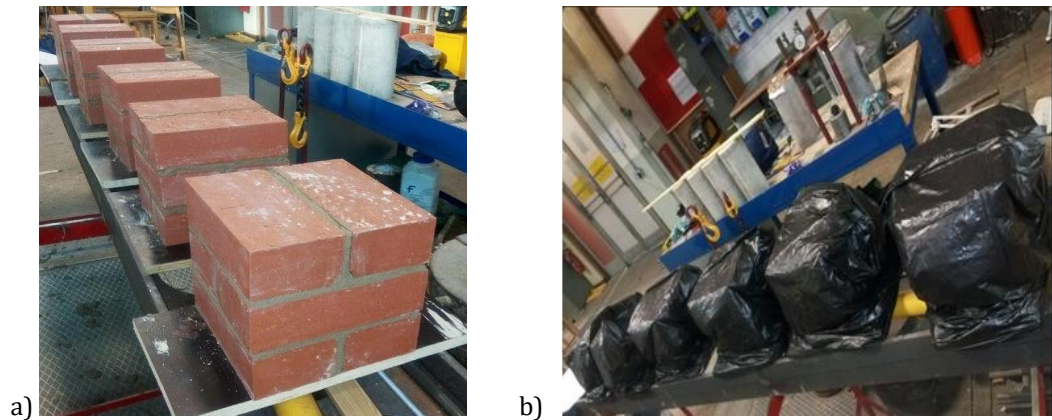


Figure 4.12. Masonry cubic specimens; (a) bonding (b) curing

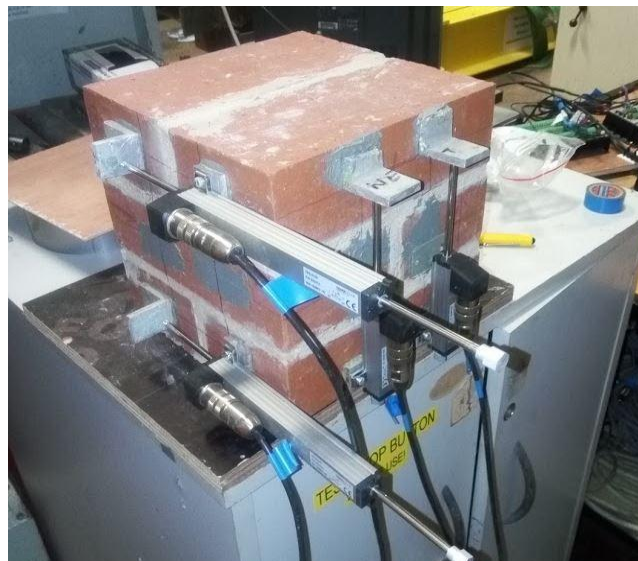


Figure 4.13. Masonry cubic specimens with LVDTs attached

Table 4.9: Compressive strength of masonry cubic specimen

Label	Max. Load	Area A (mm ²)	Compressive strength (f_{mc})	Av. f_{mc} (N/mm ²)
	P_{max} (N)		$\frac{P_{max}}{A}$ (N/mm ²)	
MC1	2302699	46225	49.82	46.4 (cov = 4.8%)
MC2	2078800		44.97	
MC3	2120699		45.88	
MC4	2055399		44.47	
MC5	2075300		44.90	
MC6	2245100		48.57	

4.1.3.2 Characteristic Compressive Strength of MC Specimen

The characteristic compressive strength of the masonry specimen (f_k) was calculated according to section 10.2 of BS EN 1052-1:1998 as larger of (a) or (b)

(a) The smaller of $f_k = \frac{f_d}{1.2}$ or $f_{i,min}$;

$$f_d = f_i \times \left(\frac{f_{bd}}{f_b}\right)^{0.65} \times \left(\frac{f_{md}}{f_m}\right)^{0.25} \quad (4.1)$$

Where:

f_d : is the normalised compressive strength of masonry specimen

f_i : is the measured compressive strength of masonry specimen

f_{bd} : is the specified compressive strengths of the masonry unit (75N/mm²)

f_b : is the mean compressive strengths of the masonry unit (87.9N/mm²)

f_{md} : is the specified compressive strengths of the mortar (7N/mm²)

f_m : is the mean compressive strengths of the mortar (7.1N/mm²)

First, the mean compressive strength of the MC was converted to the normalised masonry strength relevant to the specified unit and mortar strengths using equation 4.1 (BSI, 1998). This is necessary because the compressive strength of the masonry units and the mortar at the time of testing deviate from their specified values.

$$\text{Therefore, } f_d = 46.4 \times \left(\frac{75}{87.9}\right)^{0.65} \times \left(\frac{7}{7.1}\right)^{0.25} = 41.7\text{N/mm}^2$$

$$\text{Hence, } f_k = f_d/1.2 = 34.8\text{ N/mm}^2$$

(b) 5% fractile values gives; $f_k = 34.07\text{N/mm}^2$

The result from option (a) is higher than (b), so the characteristic compressive strength (f_k) of the MC specimen is taken as 34.8N/mm^2 .

Besides, the characteristic compressive strength of the MC specimen can be calculated using the properties of the constituents (i.e. brick units and mortar) according to equation 4.2 provided in (BSI 1996)

$$f_k = K \times f_{b,m}^\alpha \times f_m^\beta \quad (4.2)$$

f_k : is the characteristic compressive strength of masonry specimen

$f_{b,m}$: is the normalised mean compressive strength of the masonry unit, in the direction of applied action.

f_m : is the compressive strength of the mortar (7.1N/mm^2)

α and β : are constants for general-purpose mortar, which are 0.7 and 0.3 respectively

K: is a constant, function of the type of units and mortar.

In order to apply equation 4.2, the mean compressive strength of the unit obtained from the test is first converted to normalised mean compressive strength ($f_{b,m}$). Because the samples were oven-dry, the average strength obtained from the test is multiplied by a factor of 0.8. This is to obtain the strength of the unit relevant to air-dry conditioning (BSI 2011). After that, the equivalent mean strength was then multiplied by shape factor (0.685) obtained from table A.1 of BS EN 771-1:2011.

$$\text{Therefore,} \quad f_b = 0.8 \times 87.9 \times 0.685 = 48.17\text{N/mm}^2$$

Meanwhile, K is taken from table 3.3 of BSI 1996 as 0.55 for group 1 clay masonry unit and general-purpose mortar.

$$f_k = 0.55 \times 48.17^{0.7} \times 7.1^{0.3} = 17.95 \text{N/mm}^2$$

The calculated characteristic compressive strength of MC (f_k) from the property of the constituents equals 17.95N/mm^2 . This characteristic value of 17.95N/mm^2 is 52% of the characteristic compressive strength value gotten experimentally. The characteristic compressive strengths obtained from tests

on MC specimens were higher than the strengths calculated using the constituent strength (equation 4.2), suggesting that equation 4.2 is too conservative. This is supported by the claim that the unit strength method yields more conservative strengths when compared to the prism test method, especially at the higher range of masonry unit strengths (NCMA TEK 18-1B). Also, this is similar to what has been observed in previous studies by (Phipps, et al., 2001) and (Arash, 2012). (Phipps, et al., 2001) went further by increasing the value of K to 0.78 to match their experimental observation. Their work later proposed a change in the coefficient (K) found in BSI, 1996. However, more detailed experimental data will be required to make such a significant contribution to the evolution of code.

4.1.4 Failure Mode of Masonry Units and Masonry Cubic Specimens

Figure 4.14 below presents the failure images of both the brick units and the MC specimens after testing. Monitoring the failure pattern of both the units and MC by eyes during the test was very difficult because the test rig was enclosed to avoid injuries. However, adequate cameras were provided to capture the entire testing.

The observation shows that the failure modes of both the units and MC are brittle. A view through the casement and video recorded during the tests indicated that the failure of the brick units (Fig. 4a) started with a vertical crack along the height of the bricks causing high tensile stress in the bricks which make them fail i.e. be broken in the end.

For the MC specimens, the failure was characterized by vertical splitting cracks appeared first in the central unit and extended to the other units as the stress increased. This observation is similar to what was reported by Vasconcelos & Lourenço (2009) and Mohamad and Chen (2016). This failure pattern is due to the presence of the vertical joints and the lateral expansion of the mortar inducing high tensile strength in the bricks. The splitting of MC on the side faces caused the attached LVDTs on the MC sides to fall off, which make recording the continuous deformation of MC difficult because the compression machine does not have an inbuilt LVDT.

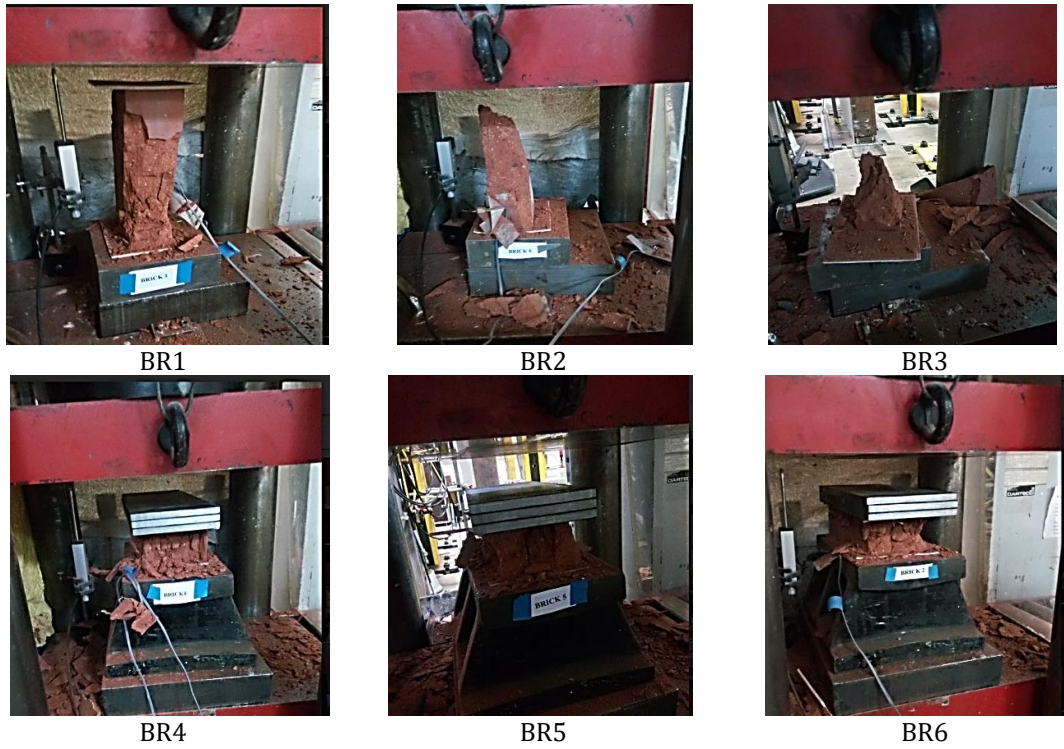


Figure 4.14a: Failure modes of brick units



Figure 4.14b. Failure of masonry cubic specimens

4.2 Small-Scale Test: Flexural Bond Strength of Masonry Prism

In this section, flexural strength of masonry prisms (MP) has been obtained from four-point bending test conducted on MPs according to the provisions of (ASTM, E518-15) and (ASTM, E72 -15). This test helps to gather data on the flexural strength of plain unreinforced MP and MP retrofitted with timber panel using two selected connection types identified earlier in chapter 3. The test was carried out before the larger-scale experimental works described later in section 4.3. The small-scale test helped to understand the behaviour of masonry and the connection between masonry prism and timber panel proposed for retrofitting masonry wall. The test provided an insight on the effectiveness of the proposed timber panel retrofit on flexural behaviour of masonry prisms, and it also enabled the design and implementation of the larger-scale test to be straightforward.

4.2.1 Test Specimen Characteristics

The section describes in detail, the materials and the construction process for building the tested MP specimens. The section is subdivided into material sections and specimen construction sections.

4.2.1.1 Materials

In addition to Engineering class B solid fired clay bricks with UK standard size 215 x 102.5 x 65mm and Type N (general purpose) mortar mix with a ratio of 1:1:6 (Type II Cement: aerial lime: sand) that have already been fully characterised in section 4.1, two other materials which are oriented strand board (OSB) and connections were used for preparation of specimens. Manufacturer data sheets were used to obtain the mechanical properties of OSB and the adopted connections. The properties of the materials are summarised below:

❖ Oriented Strand Board (OSB)

18mm thick OSB type 3 (Fig. 4.15a), which is a load-bearing engineered wood-based panel for use in humid conditions, was selected for this study. The OSB is manufactured from strands of wood, which are bonded together with a synthetic resin. The strands are pressed together in layers. From the manufacturer's specification, the board has an average density of 650kg/m³, internal bond

strength of 0.3N/mm^2 , and modulus of elasticity of 3500N/mm^2 and 1400N/mm^2 for both bending in major and minor axis respectively. The OSB type 3 that was used in this study can achieve a Euro class D fire rating under the new Euro class system for the reaction to fire of materials. OSB panel can resist a small flame attack without substantial flame spread for an extended period (Anon, 2018). Also, they are capable of undergoing thermal attack by a single burning item with sufficiently delayed and limited heat release.

❖ Connections

Two types of connections were used in this study. The OSB panel was securely connected behind the masonry prism using two types of anchor systems selected from available products by Fischer® group. Fischer anchor systems have a long reputation in providing connections and fixings to masonry. Consequently, two different anchor systems were selected from Fischer® products by considering masonry as the base material, manual cleaning procedures of holes drilled, economy, the recommended design tensile resistance (N_{rd}), and the configuration of the anchors. The criteria for selecting these connection types are guided by the requirements of European Technical Approval (ETAG, 029) which ensure that the selected anchorages are fit for use in solid masonry subjected to either static or quasi-static loading, which was tested in this study. The strength of both the masonry unit and mortar were considered in the selection of the anchor diameter. The spacing of the anchors is provided to meet the minimum allowable spacing and edge clearance as specified in the ETAG 029. The selected connections were made of A4 (1.4401 or 316) stainless steel classified as follows;

- I. Connection Type 1 (C1): This is an adhesive anchor connection system herein referred to as C1. It is a combination of FIS V 360 S injection mortar and FIS A4 anchor rod. FIS V 360 S is a high-performance injection mortar which is approved for fixings in both perforated and solid bricks. The selected FIS A4 anchor (Fig 4.15b) has 8mm diameter with 1.29kN permissible tensile load.
- II. Connection Type 2 (C2): This is a mechanical connection system classified as C2 in this study. C2 is a combination of Fischer frame fixing SXS plastic plug made of high-quality nylon and FUS A4 anchor rod. The diameter of the anchor rod is 8mm with a permissible tensile load of 1.39kN (Fig. 4.15c).



Figure 4.15. Material (a) OSB timber, (b) Adhesive anchor, (c) Mechanical anchor

4.2.1.2 Test Specimen Construction

The MP test specimens were constructed as 9 courses stacked bonded prisms, 215 x 102.5 x 665mm with mortar joints of 10 ± 1.5 mm thickness, as shown in figure 4.16. The size of MPs constructed allowed the specimens to meet the minimum height of 460mm required according to clause 6.1 of ASTM E518-15 without cutting brick units in height. The test specimens were constructed using English bond consisting of alternate rows of headers and stretchers.

The construction of the MP started by laying the first course of the brick unit on a 10mm thick flat metal plate with the use of mortar. Subsequently, all the remaining 8 courses were laid on top of one another with a full-face mortar bed on all other units without furrowing (i.e with no groove or hole in the mortar bed). During the construction of all test specimens, the mason used a plumb line and level to align the vertical face of each specimen. In all cases, the test specimens remained in construction position for 21days after construction to avoid disturbing the setting of the specimens.

The standard curing procedures were adopted for all specimens by wrapping them with a polythene sheet for 14days. After that, they were stored in the laboratory air for further 14days as in the case of masonry cubic specimens described in section 4.1.3. Samples of mortar cubes were taken from the mortar mix prepared for each specimen and cured under the same condition with the test prism to monitor the quality control.

Before the construction of the specimens that were retrofitted with OSB timber panel, the brick units in the predetermined connection locations (Fig. 4.17) were pre-drilled. The purpose of predrilling these bricks before bonding is to avoid

disturbing the joint of the specimens after the construction, which might have caused the failure of the joint before testing.

The selected OSB type 3 timber panel was fixed to the masonry prism to apply the proposed timber-based retrofit technique (Fig. 4.17). The retrofit was applied after the specimens have cured for 21 days to allow for curing of the connection for further 7 days before testing. All the test specimens and the mortar cubes prepared during their construction were tested at 28 days.

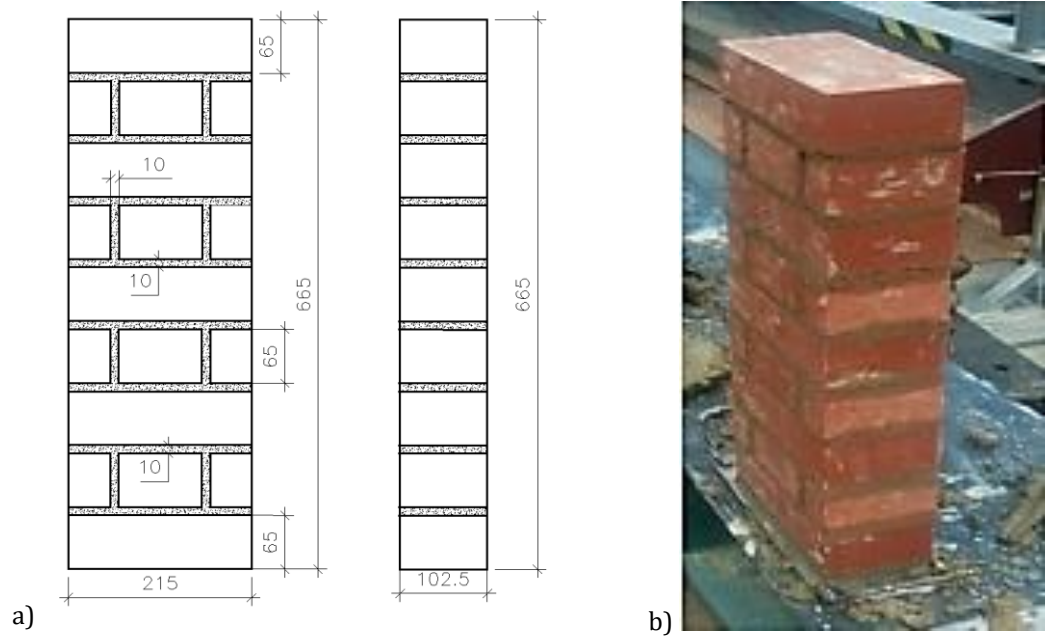


Figure 4.16. Plain masonry prism specimen a) Drawing (all dimension in mm) b) As-built specimen

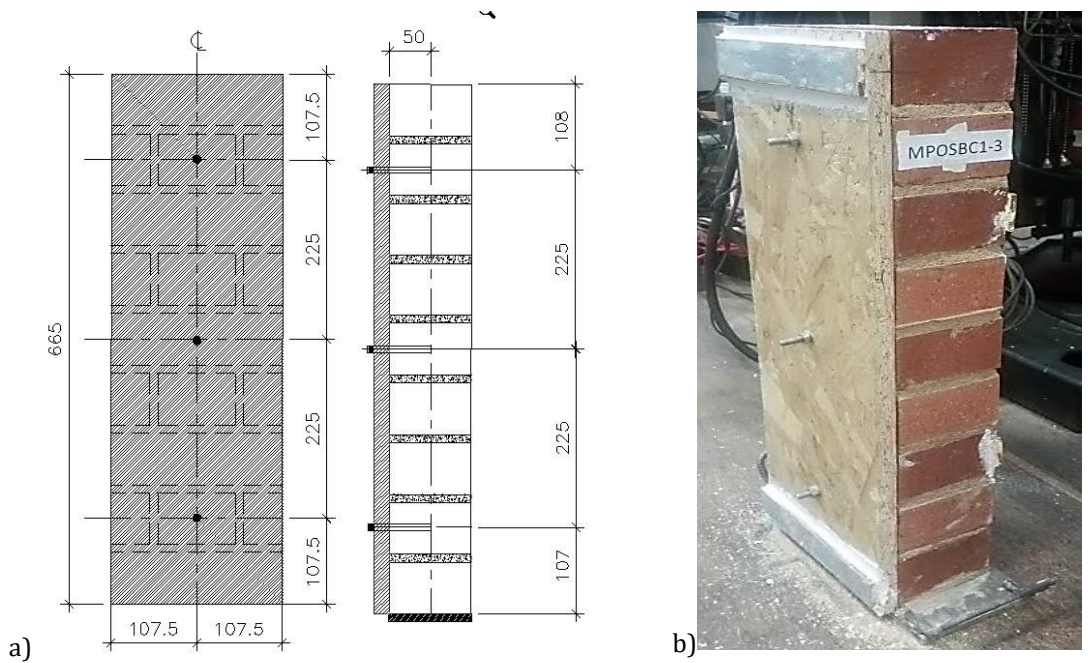


Figure 4.17. Retrofitted masonry prism specimen a) Drawing (all dimension in mm) b) As-built

4.2.2 Test Program/Matrix

Nine single leaf masonry prisms (MPs) were tested in the laboratory under four-point bending test using a quasi-static monotonic loading scheme. The small-scale experimental campaign presented in table 4.10 involved testing: (a) three samples of plain MP to serve as references to measure the effectiveness of the proposed retrofit techniques, (b) three samples of retrofitted MP, each retrofitted with 18mm thick OSB type 3 timber panel using adhesive anchor connection (C1), and (c) three samples of MP retrofitted with 18mm thick OSB type 3 using mechanical connection (C2).

Table 4.10: Test program specimen identification

Specimen Label	Description	Connection Type	Quantity
MP00-1		-	1
MP00-2	Plain specimen		1
MP00-3			1
MPOSBC1-2			1
MPOSBC1-2*	Retrofitted specimen	C1	1
MPOSBC1-3			1
MPOSBC2-1			1
MPOSBC2-2	Retrofitted specimen	C2	1
MPOSBC2-3			1

MP00 stands for Plain Masonry Prism

MPOSBC stands for Masonry Prism retrofitted with OSB panel

C1 stands for connection type 1, i.e. adhesive anchor connection

C2 stands for connection type 2, i.e. mechanical connection

MPOSBC1-2* was constructed to replace the damaged MPOSBC1-1

4.2.3 Test setup and Procedures

The MP specimens constructed on the 10mm thick steel plate were tested in the test rig, as shown in figures 4.18 and 4.19. All the nine specimens were tested with simply supported boundary condition with no vertical pre-compression load. The specimen on steel plate was rested on 25mm diameter cylindrical

roller clearly identified in figure 4.19b with the axis of the roller parallel to the face of the specimen to allow it to freely rotate around its base while deflecting out-of-plane and prevent restrained end condition. At the back of the specimen, 25 x 5mm thick metal plate was fixed across the middle of the top and bottom brick unit each. This 5mm thick plate provided a smooth contact for the Ø25mm supporting rollers fixed on an existing steel reaction frame in the laboratory (Fig. 4.19c). On the front side of the specimen, two others 25 x 5mm thick metal plates were fixed at 1/4th and 3/4th of the height of the specimen each to provide a contact for which the loading roller rest as identified in figure 4.19c.

The loading of the specimens is such of a four-point testing arrangement where the loads were applied on the specimen using a Hi-force hydraulic jack (4.20a) and distributed through a spreader beam. The spreader beam spanned between two Ø25mm cylindrical rollers placed across 1/4th of the height from top and bottom support of the specimen. The direction of the load application is perpendicular to the specimen surface. The applied load on the prism were monitored using a 200kN capacity ring load cell (Fig. 4.20b). Simultaneously, 4 linear variable displacement transducers (LVDTs) were used to record the deflections of the specimen along the centre, mid-top and bottom. The locations of these LVDTs are shown in figure 4.20c. All the LVDTs were fixed on an independent steel tripod stand, which was not connected to the rig (Fig. 4.20d).

The force and the displacements were real-time monitored by connecting the load cell and LVDTs to an electronic acquisition unit interfaced with a computer. The test was load controlled, and the loading scheme is such that an initial load of 200N increments at every two minutes up to the occurrence of first cracks was applied. This loading rate represents 1/10th of the expected maximum load. The load increment was chosen so that a sufficient number of readings will be obtained to determine definitely the load-deformation curve (ASTM E72-15). After the first crack appeared, the loading was increased continually at a rate of 2N/sec up to the cracking/failure of MP specimens.

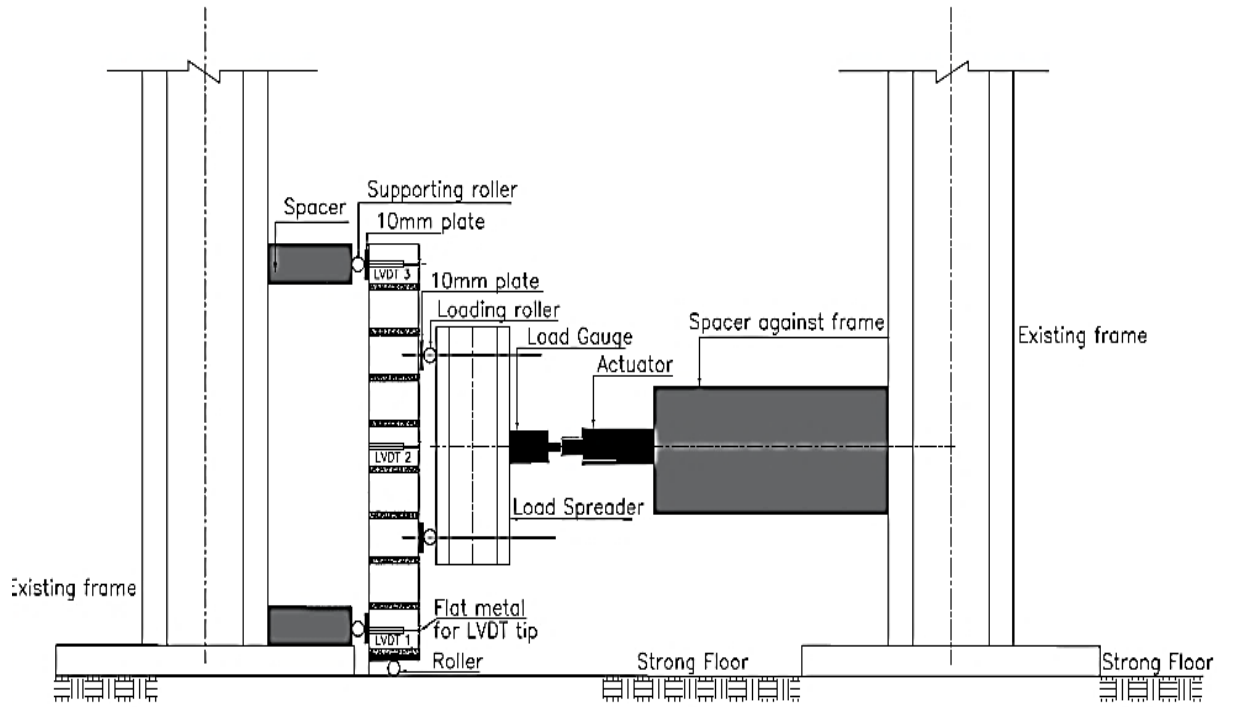


Figure 4.18. Small-scale test setup (drawing)

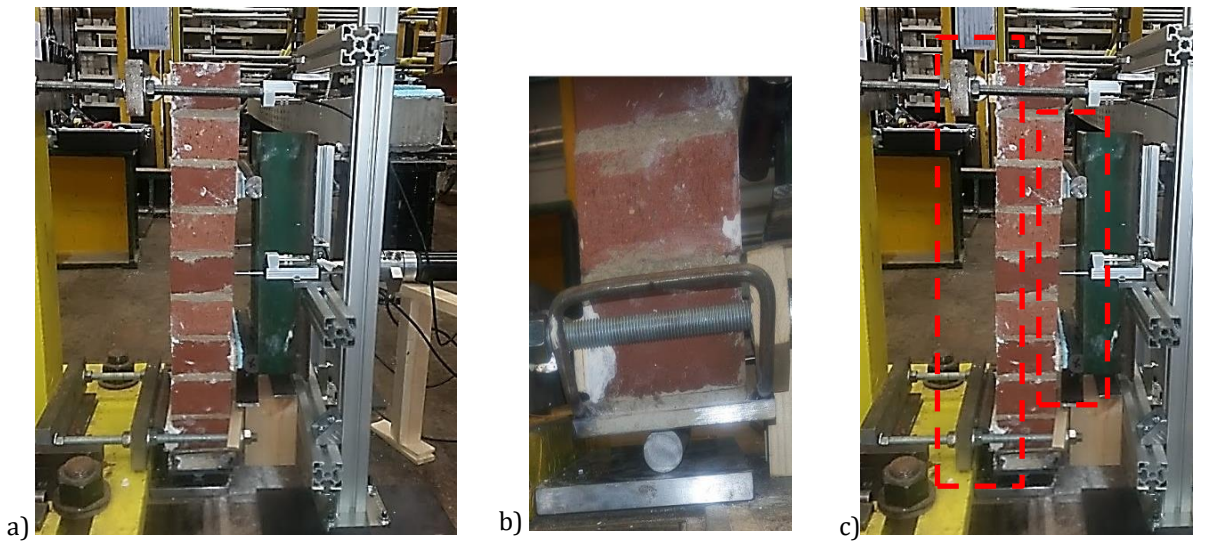


Figure 4.19. Test setup: (a) As built, (b) Roller under MP, (c) Roller contact at the front and back of MP



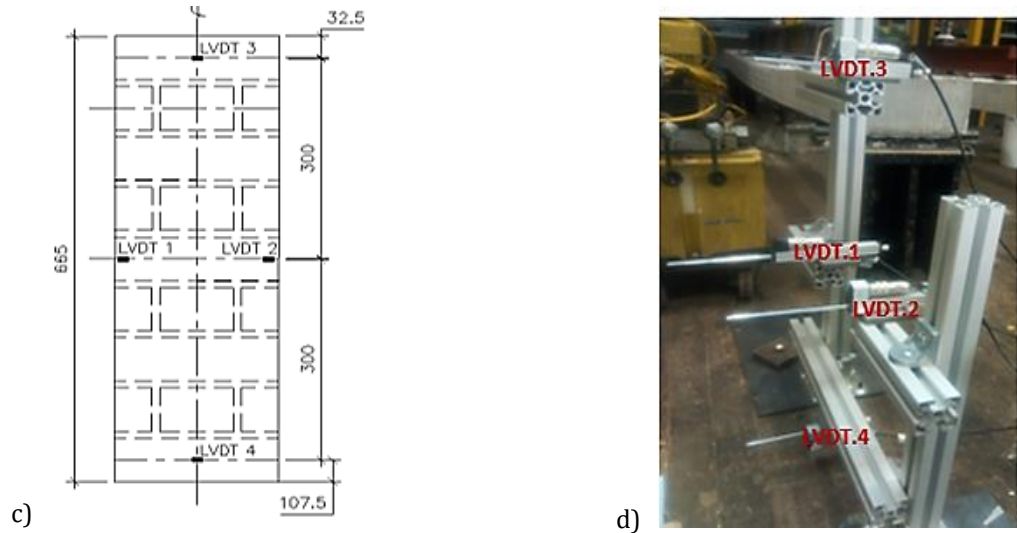


Figure 4.20. Instrumentation: (a) Hydraulic jack; (b) Load cell; (c) LVDTs position; (d) LVDTs on frame

4.2.4 Test Results

The test specimens were tested to failure with the load and corresponding out-of-plane displacements monitored. The experimental results were then expressed in term of load-displacement curve, which represents the relationship between the applied out-of-plane loads and the net out-of-plane displacement in the mid-height of the test specimens.

4.2.4.1 Out-of-plane Displacement

In order to estimate the net displacement in the specimen mid-height, the average value of horizontal displacement at the top and bottom of the specimen was removed from the mean value of the displacement measured at the specimen mid-height using equation 4.2.

$$d_{net} = \left(\frac{d_1 + d_2}{2} \right) - \left(\frac{d_3 + d_4}{2} \right) \quad (4.2)$$

Where; subscript 1, 2, 3 & 4 refers to LVDT's position as shown in figure 4.20c.

The average displacement at the top and bottom of the specimen deducted from the average displacement at the mid-height of the specimen accounted for the unexpected little displacement at the top and bottom of the MP prisms. A typical load-displacement curve for specimen MP00-1 showing load vs displacement measured by all the four LVDTs is shown in figure 4.21. LVDT.1 plot is overlaid by LVDT.2 because the displacement recorded by the two LVDTs are the same. It can be observed from the curve that the specimen did not exhibit any significant displacement (0.29mm) before the peak load. Then suddenly, after the crack

occurred, the brick separated from the joint, and the displacement jumped from 1mm to 9mm.

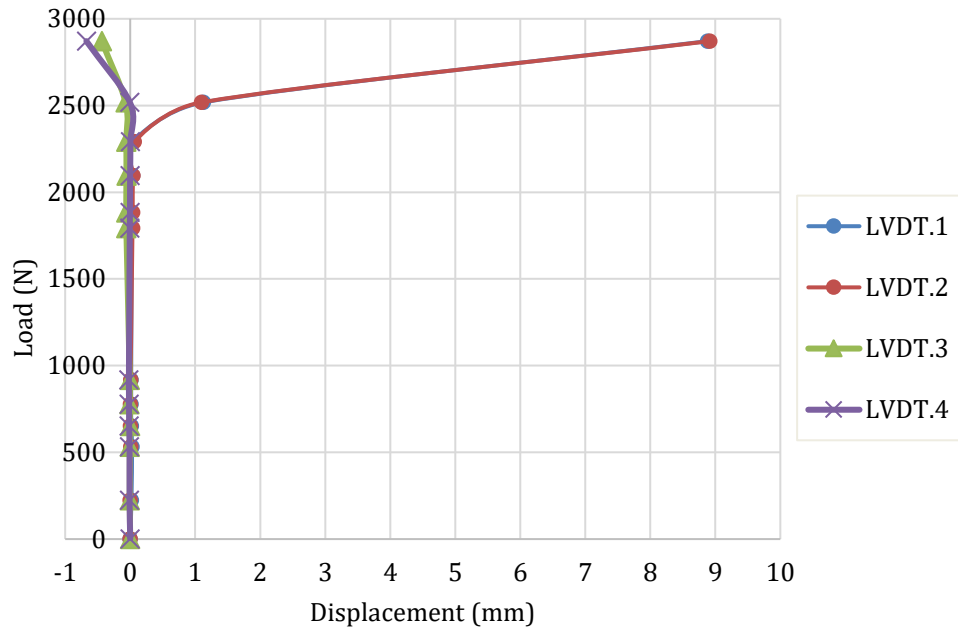


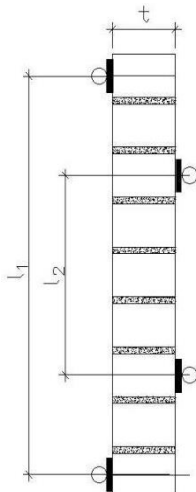
Figure 4.21. Typical load-displacement curve

Figure 4.21 above presented here the displacement measurements for all the four LVDTs for only specimen MP00-1. The curve showing the load vs displacement measured by the four LVDTs for all other specimens is presented in appendix 4.2. In the subsequent sections, only the load vs net out-of-plane displacement for each specimen was shown.

4.2.4.2 Flexural Strength

The flexural strength of the masonry prism was determined using equation 4.3

$$f_x = \frac{3P_{max}(l_1 - l_2)}{2bt^2} \quad (4.3)$$



Where;

f_x : Flexural strength of masonry prism

P_{max} : The maximum load applied to the specimen

l_1 : Distance between back supports (outer bearing)

l_2 : Distance between the loadings supports (inner bearing)

b : Width of specimen

t : Thickness of specimen

Figure 4.22a: Dimension on the prism

However, equation 4.3 is only valid if the neutral axis of the section is in the centre and used for the plain masonry prisms only. In order to obtain the flexural strength for the retrofitted MP with the OSB added, the equation of bending (Eqn 4.4) is employed.

$$\frac{M}{I} = \frac{\sigma}{y} \quad (4.4)$$

$$M = \frac{P_{max} * l}{4}$$

$$I = \frac{b * t^4}{12}$$

$$y = \frac{t}{2}$$

Where;

M : Maximum moment applied on the section

σ : Flexural strength of section (i.e f_x)

I : Moment of inertia of the section

y : Depth to the neutral axis of the section

Equation 4.4 is first employed for the plain MP and the difference between the flexural strength calculated and the experimental result is only 6%. Therefore equation 4.4 is then extended to calculate the flexural resistance of the retrofitted MP (Table 4.10). In order to use equation 4.4 for the retrofitted MP, the section is converted to an equivalent section because of the composition of the retrofitted MP with two parts having different stiffness. An equivalent thickness of the OSB with respect to the masonry is obtained by multiplying OSB thickness (t_{osb}) by a factor (n) which is the ratio of Young's modulus of the OSB to the masonry (Fig. 4.22b). After that, the neutral axis of the retrofitted section is calculated from the new thickness of the equivalent section. The new properties of the equivalent section were then used in the equation of bending to determine the flexural strength of the retrofitted specimens.

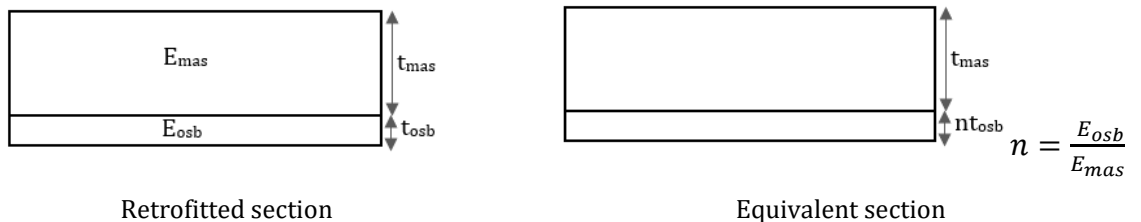


Figure 4.22b: Equivalent section for the retrofitted prism

4.2.5 Observed Failure Pattern

4.2.5.1 Failure Pattern of Plain MPs

The failure mode of the plain MP specimen is quasi-brittle with plain MP showing little deformation (0.29mm) before the separation of the brick unit from the mortar (Fig. 4.24). This type of behaviour shows that during the first part of the tests, the plain MP specimens did not exhibit any damage as also observed in similar works by Gattesco and Boem (2017) and Lin et. al (2016). After this crack had appeared in the unit/mortar interface, the deformation measured in LVDT 1 & 2 jumped up significantly. This jump indicates a brittle failure of the plain MP specimens (Fig. 4.23). The failures were sudden and always started with the formation of a crack opening in one of the bed joints at the tensile face of the specimen (i.e. the side opposing the loading face). Subsequently, the crack that occurred in the single bed joint propagated throughout the specimen thickness so that the unit-mortar interface was completely separated in all cases.

The failure occurred within the loading span (i.e. the inner bearing) for all tested specimens except for MP00-2 (Fig. 4.23b). Thus, the result of MP00-2 was discarded because one of the acceptability criteria of the test is that the failure must occur within the inner bearing (ASTM E518 -15; ASTM E72 -15; BSI, 1999).

The load-displacement curve for MP00-1 and MP00-3 is shown in figure 4.24, having discarded the result for MP00-2. The inference from the figures 4.24 shows that the specimens remain undamaged for up to 80% and 85% of the average failure load (2857N) for MP00-1 and MP00-3 respectively. However, as the loading increment continues, the specimen peak load and corresponding net out of plane displacement of the damaged specimen at the mid-height were then recorded as (2871N, 8.34mm) and (2843N, 9.62mm) for MP00-1 and MP00-3 respectively. A new specimen to replace MP00-2 was not constructed because the results of MP00-1 and MP00-3 compared fairly well.

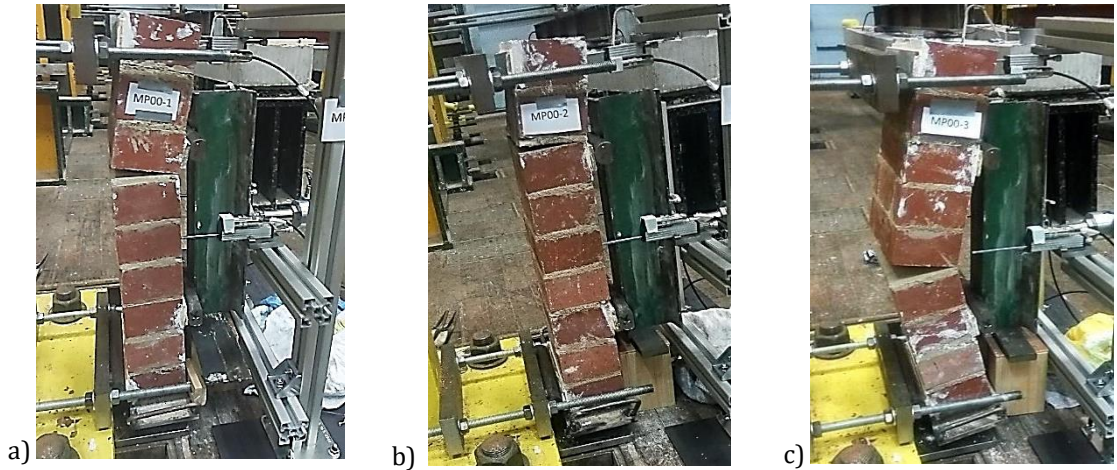


Figure 4.23. Failure pattern of (a) MP00-1; (b) MP00-2; (c) MP00-3

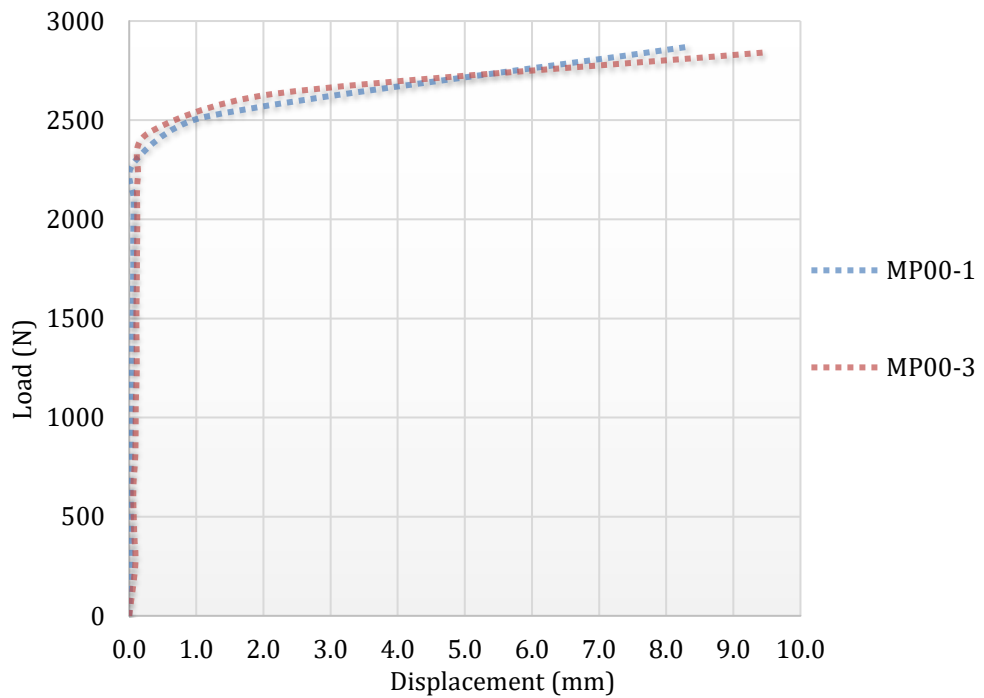


Figure 4.24. Load displacement curve for plain specimens

4.2.5.2 Failure Pattern of Timber Retrofitted MPs

Similar to the plain MP, the retrofitted specimen (MPOSB) showed little deformation (0.5mm) before the appearance of the first crack, which is also in the bed joint within the inner bearing. This first crack appeared at an average load of 3640N and 3590N for MP retrofitted with adhesive anchor connection (C1) and mechanical connection (C2) respectively. As the loading continued, other cracks appeared in the bed joints parallel to the first crack still within the inner bearing (Fig. 4.25 & 4.26). As the applied load increased, the first crack to appear failed completely at an average load of 5330N for C1 and 5280N for C2.

Meanwhile, since the first crack appeared in the specimens, the effect of the application of the timber panel at the back of the MPs caused the formation of other cracks in the specimens. Unlike plain MPs, the retrofitted specimens remained unseparated after the first crack. In order to ensure that the maximum load capacity of the retrofitted specimen is obtained, the loading continued until the timber panel at the back failed (broken). At this failure point, the corresponding load vs net out-of-plane displacement for all specimens including the plain MPs were plotted for comparison in figure 4.27. On the load-displacement curve shown in figure 4.27, the points at which each crack developed were identified with numerals corresponding to the ones labelled on the specimens' image in figure 4.25 and 4.26 testing. The labels are boxed with the same ink colour as shown on the graph in figure 4.27. The average maximum load and corresponding displacement at failure are (21068N, 18.74mm) and (14407N, 15.24mm) for MPOSBC1 and MPOSBC2 respectively. Notably in figure 4.27 is the strange behaviour of MPOSBC2-3 at around 4000N applied load. This behaviour is because of the manual application of load in which the increment in the applied load at this point is high which cause the sudden jump in the displacement. However, to avoid this kind of variation, an automatic loading program was written for the larger-scale test described in section 4.3.

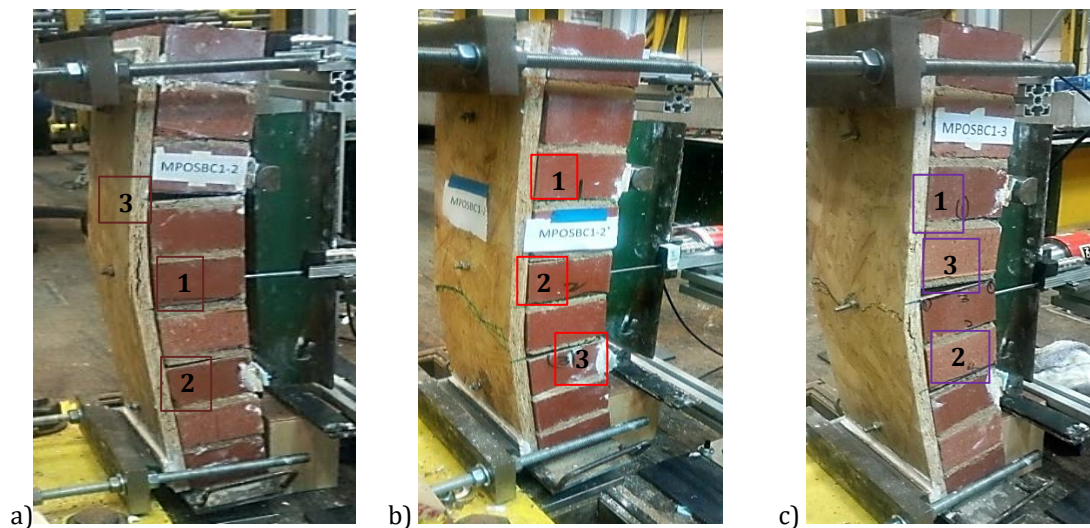


Figure 4.25. Failure pattern of (a) MPOSBC1-2 (b) MPOSBC1-2* (c) MPOSBC1-3

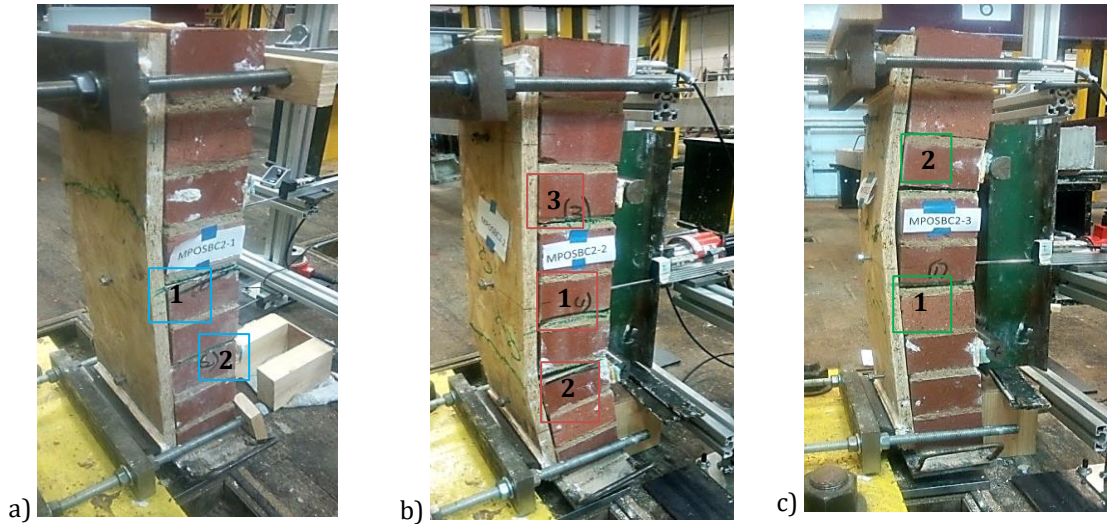


Figure 4.26. Failure pattern of (a) MPOSBC2-1 (b) MPOSBC2-2 (c) MPOSBC2-3

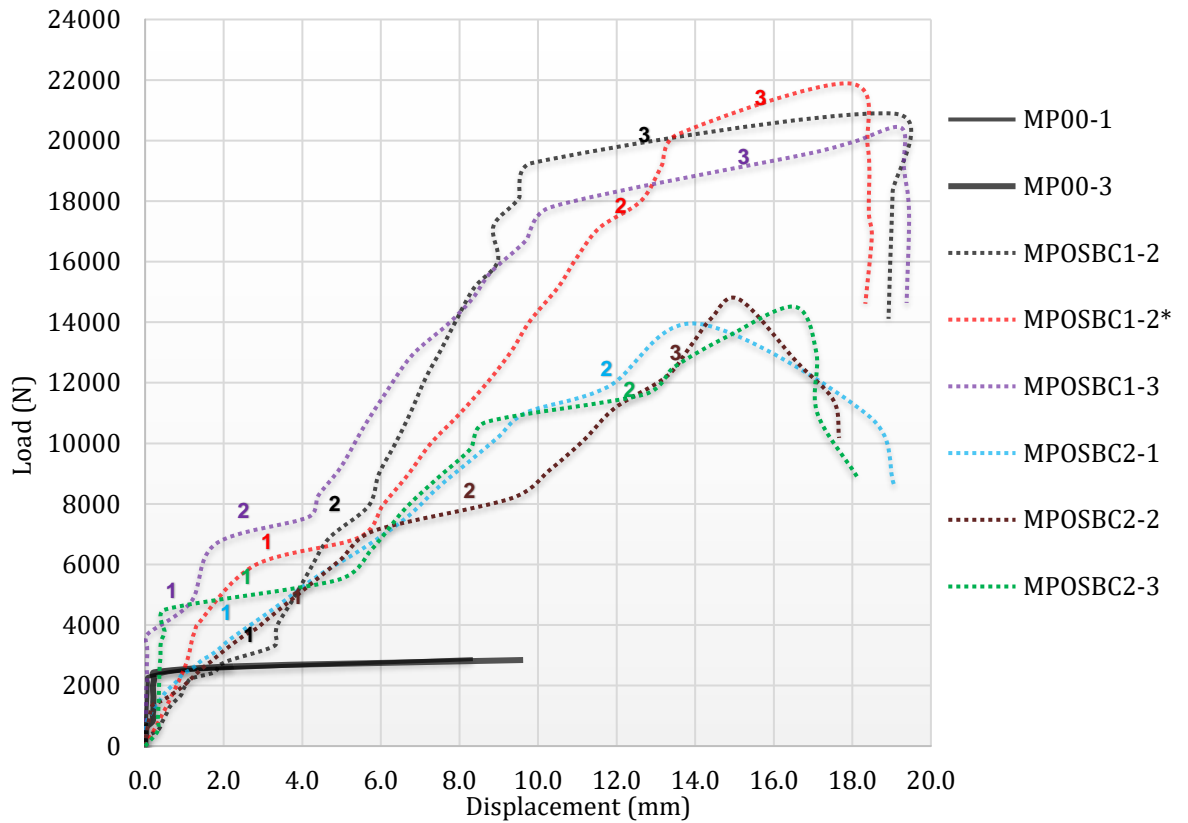


Figure 4.27. Load displacement curve for plain and retrofitted specimens

4.2.6 Evaluation of Performance of the Proposed Technique

The maximum load, corresponding displacement at failure, flexural strength, and toughness of the tested specimens is presented in table 4.11. The toughness (i.e. energy absorbed) of the specimens is estimated from the load-displacement curve (Fig. 4.27) using the method based on ASTM 1609. This toughness is estimated as the overall (i.e. the total area under the load-displacement curve) and the limiting toughness. The limiting toughness is the area under the curve up to a limited displacement of span/250 (BSI, 1996). This is done to understand

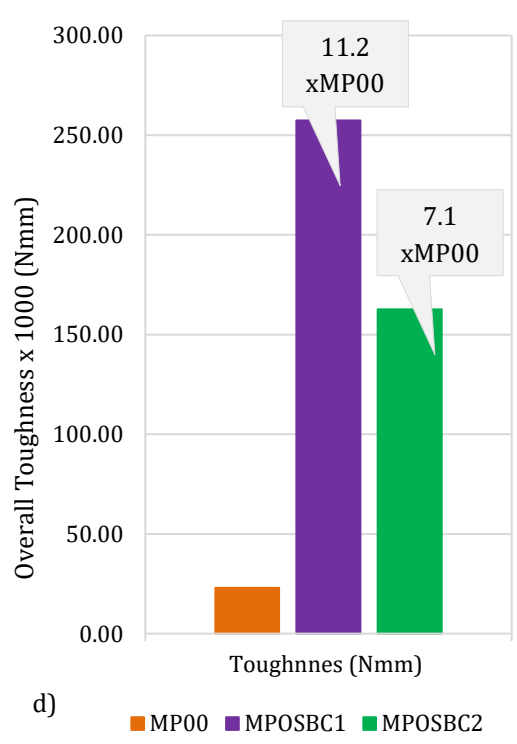
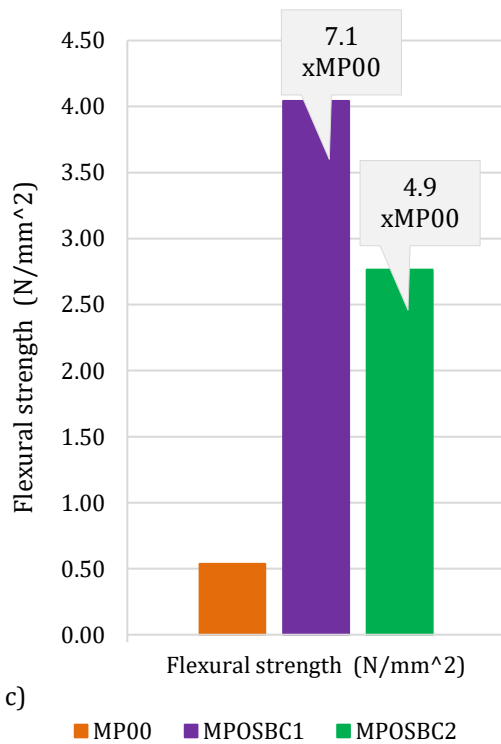
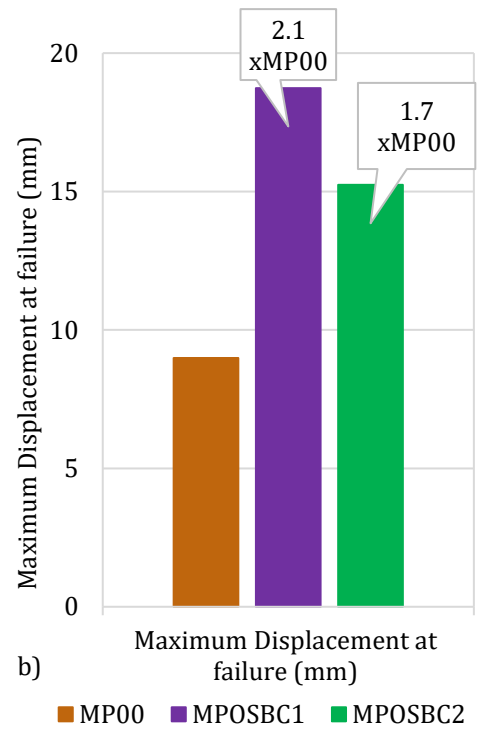
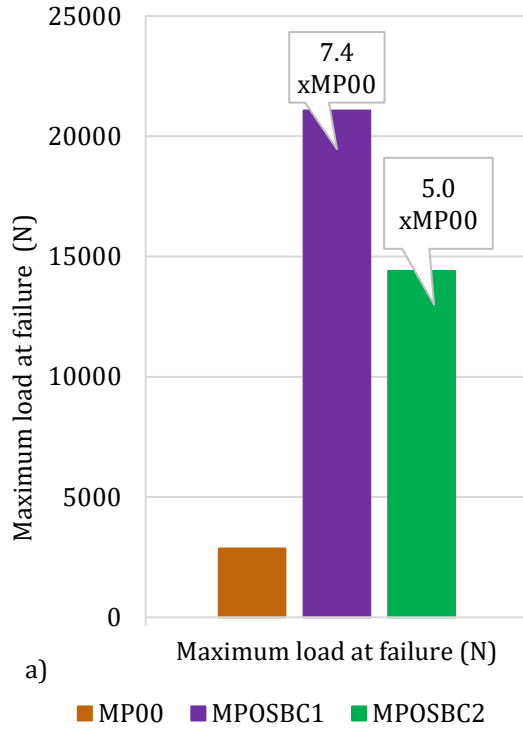
the toughness gained by the specimens when undergoing an acceptable displacement without adverse effect. Because the masonry specimens deflected excessively during testing to get to the failure of the OSB (i.e. overall) which is in contradiction to BSI 1996 recommendation “*Masonry walls subjected to lateral loads shall not deflect adversely under such loads*”. Therefore, this excessive deflection is not acceptable in the real situation because this can cause visual distress to the users of the building and can lead to damage of building parts. Thus, the limiting toughness actually estimates the improvement due to the retrofit application in the acceptable range.

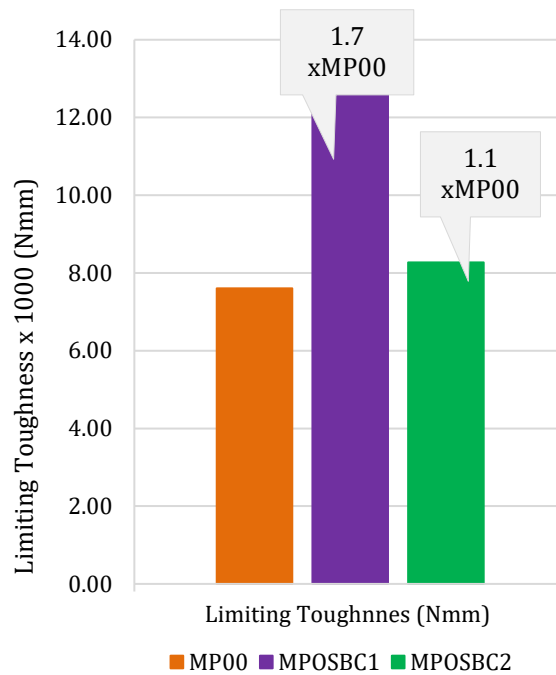
Table 4.11: Summary of flexural strength test results

Specimen Label	Max. load at failure (N)	Displacement at failure (mm)	Flexural strength (N/mm ²)		Toughness (Nmm)	
			Exp.	(Bending theory)	Limiting	Overall
MP00-1	2871	8.34	0.54	0.57	7600	22700
MP00-3	2843	9.62	0.53	0.57	7600	23200
Average	2857	8.98	0.54	0.57	7600	25800
MPOSBC1-2	20889	19.07	-	4.01	12200	258000
MPOSBC1-2*	21890	17.91	-	4.20	14000	254000
MPOSBC1-3	20424	19.24	-	3.92	11600	260000
Average	21068	18.74	-	4.04	12600	257333
MPOSBC2-1	13950	14.07	-	2.67	8600	164000
MPOSBC2-2	14760	15.12	-	2.83	8000	158000
MPOSBC2-3	14510	16.54	-	2.78	8200	166000
Average	14407	15.24	-	2.76	8267	162667

In table 4.11, the average value of each property for each group of the specimen (i.e. MP00, MPOSBC1 and MPOSBC2) was evaluated and compared in figure 4.28. The comparison shows that the maximum load that can be attained in MP when retrofitted with OSB panel is 7.4times and 5times that of plain MP for connection type C1 and C2 respectively (Fig. 4.28a). The retrofitted MPs were able to take more loads by displacing more without sudden failure (Fig. 4.28b). The increased out-of-plane displacement is 2.1times and 1.7times that of plain MP for sample

retrofitted with C1 and C2 respectively. Similarly, the increment in the flexural strength (Fig. 4.28c) is also significant when MP is retrofitted with OSB panel. C1 offered the most increment in the load capacity and flexural strength.





e)

Figure 4.28. Performance in term of (a) Load Capacity (b) Displacement (c) Flexural strength (d) Overall Toughness (e) Limiting Toughness

Further analysis of the data presented in figure 4.28 reveals that the toughness gained due to the retrofit application when taken up to the failure of the OSB is enormous. An improvement of 11times and 7times that of plain MP is recorded for connection type 1 and 2 respectively (Fig. 4.28d). However, having established the need for consideration of performance at the limiting displacement, the analysis shows that the application improved the toughness by 1.7times that of the plain wall for C1 and little increment of 1.1times plain wall for C2. Even though the increment in the load capacity of the retrofitted specimens at this limiting displacement is about 3times and 2times that of the plain wall for C1 and C2 respectively. Still, C1 offers the most improvement in the toughness gained at both the limiting displacement and overall failure.

4.3 Larger-Scale Test: Flexural strength of masonry wall

The application of oriented strand board type 3 (OSB/3) as a prospective retrofit material for URM walls has been introduced in section 4.2, with evidence of improving the flexural performances. This section presents larger-scale experimental works on 1115 x 1115 x 215mm double wythe single leaf URM walls to validate the observations in the small-scale test. Here, the quasi-static out-of-plane loading test was carried out on plain masonry wall specimens,

single-sided retrofitted masonry walls and double-sided retrofitted masonry walls. The flexural and displacement capacities were evaluated in both plain and retrofitted specimens, and the results were analysed.

As previously mentioned, that the small-scale test enabled the setup and execution of the larger-scale test, the description of the experimental works and results of the larger-scale test follows the same pattern of subheadings as in the small-scale test described in section 4.2.

4.3.1 Test Specimen Characteristics

4.3.1.1 Materials

The materials used for the experimental works here are the engineering class B solid fired clay bricks with UK standard size 215 x 102.5 x 65mm, type N (general purpose) mortar mix with a ratio of 1:1:6 (Type II Cement: aerial lime: sand), 18mm thick OSB type 3 and adhesive anchor: threaded dry rod with injectable chemical adhesive (C1). These materials are exactly the same as the one used for the small-scale test. The only exception here is that only the adhesive anchor connection type (C1) was used. C1 has been identified as the best-performed connection from the small-scale test described earlier.

4.3.1.2 Test specimen construction

Single leaf, double wythes URM wall specimens of 1115 x 1115 x 215mm (length x height x width) were constructed. The geometry of the walls is such that each of the two wythes of the walls has 15 courses with each course having 5 units of brick bonded together by 10mm thick mortar joint. The walls were built in English bond consisting of alternate rows of headers and stretchers, which is the oldest form of brick bond popular in the UK since the late 17th century. The bonding pattern is such that the joints between the stretchers are centred on the headers in the course above as can be seen from the plan sketches of first and second courses of the bonding pattern in figure 4.29 and image in figure 4.30.

Before the construction of the retrofitted wall specimens, brick units in particular locations were pre-drilled and bonded in the pattern to have a connection layout, as shown in figure 4.31. The connection layout ensured that the spacing of the connection has 50mm as minimum edge clearance and 250mm as the minimum spacing between two connections.

All test specimens were constructed on 1315 x 150 x 350mm (length x height x width) reinforced concrete (RC) footing with 1mm thick polymer (nylon) placed on top of the RC footing to prevent the bottom of the wall from bonding to the RC to avoid toe crushing failure during testing. The wall specimens (Fig. 4.32) were constructed and tested in place, no movement of the wall to prevent any significant disturbance of the wall. All masonry wall specimens were cured by wrapping them with a polythene sheet for 14days and then cured for further 14days in the laboratory in the open air. For the retrofitted masonry wall, the OSB timber panel was fixed to the masonry walls after 21days to allow for curing of the injection mortar in the connection point.

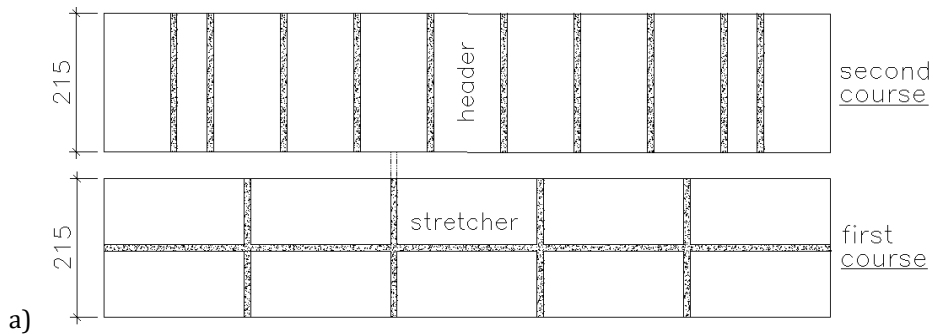


Figure 4.29. Wall specimen bonding pattern (plan drawing)



Figure 4.30. Wall specimen bonding pattern (image during construction)

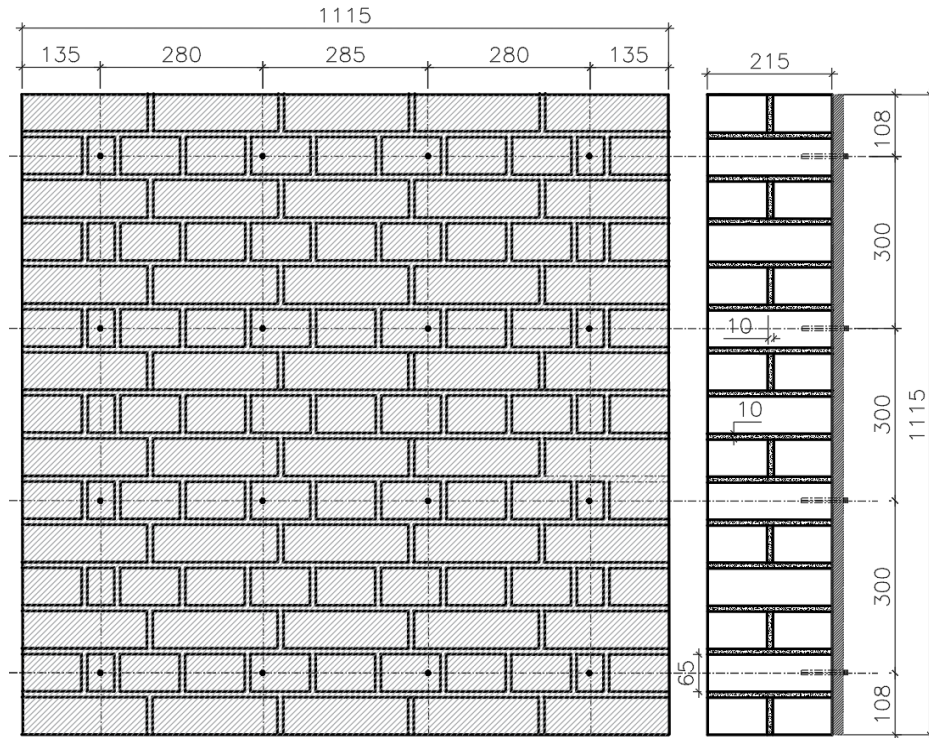
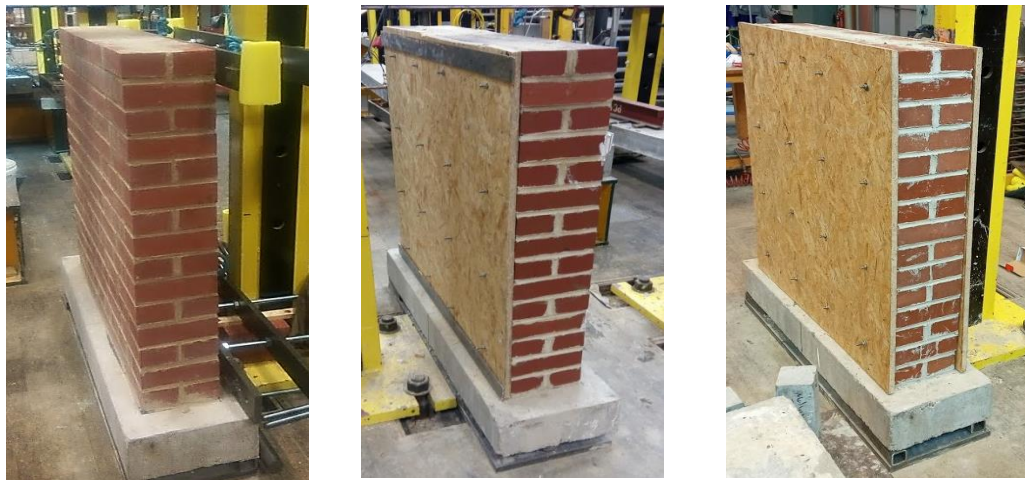


Figure 4.31. Typical connection layout for retrofitted wall specimens (all dimensions in mm)



Plain wall

1-sided retrofitted wall

2-sided retrofitted wall

Figure 4.32. Masonry wall specimens (As-built)

4.3.2 Test Program/Matrix

Out-of-plane load control tests have been performed on six masonry wall specimens, as indicated in Table 4.12. Two walls identified as PW1115-1 and PW1115-2 were tested as plain specimens. PW1115-1 was tested with a vertical pre-compression load that varied as the applied out-plane load increased while PW1115-2 was tested with a constant vertical pre-compression load. For the retrofitted specimens, two samples were tested as single-sided retrofitted samples while the last two walls were tested as double-sided retrofitted wall

sample. An 18mm thick OSB type 3 and adhesive anchor system (C1) were used to retrofit the URM wall specimens. The test program has ensured that loading has been applied on wall retrofitted with OSB timber on only tension face and both tension and compression face of the masonry wall. This is because the proposed technique is to apply the OSB panel on the internal surface of exterior URM walls so that external historic appearance of the building is preserved. The other retrofit configuration is the application of the OSB panel on the outer surface of exterior URM walls with the combination of plaster, brick-polymer based imitating finishing or clay tiles. The configuration where we have the OSB on both sides were for application on both surfaces of walls when heritage preservation is less stringent, and the solution is feasible.

Table 4.12: Test program for larger-scale test

Specimen Label	Description	Connection Type	Quantity	Pre-compression loading
PW1115-1	Plain specimen	-	1	Variable
PW1115-2			1	Constant
1SRW1115-1	single-sided retrofitted	C1	1	Constant
1SRW1115-2			1	
2SRW1115-1	double-sided retrofitted	C1	1	Constant
2SRW1115-2			1	

PW stands for Plain Masonry Wall

1SRW stands for Masonry wall retrofitted with OSB panel on one side

2SRW stands for Masonry wall retrofitted with OSB panel on two sides

C1 stands for Connection type 1 (Adhesive Anchor Connection)

4.3.3 Test setup and Procedures

The general test setup (Fig. 4.33 & 4.34a) was designed to replicate a four-point loading test arrangement, which is suitable for assessing the flexural behaviour of masonry wall as described in ASTM E72-15. Each wall specimen was tested by applying an out-of-plane load in the middle section of the wall to induce an approximately constant flexural stress in the central area of the wall. The load was applied to each tested specimen using a hydraulic ram and was distributed through a steel spreader arrangement in the central area of the wall (Fig. 4.34b).

The spreader arrangement spanned between the fourth course from the top and bottom of the wall specimen. All specimens were tested with simply supported boundary condition and a vertical pre-compression load on top of the walls.

The simply supported boundary condition of the test specimen was achieved by supporting the back of the wall specimen across the middle of the top and bottom course with supporting steel frames. The support frames were connected to an existing stanchion as a reaction frame at the top and bottom of the wall (Fig. 4.34c). Ø25mm roller was placed between the back face of the wall and the supporting steel plate on the reaction frames to provide for smooth distribution of load action across the length of the wall and avoid point contact. On the front side of the specimen, two number of 50 x 5mm thick metal plates were fixed at 1/4th and 3/4th of the height of the specimen each to provide a contact for the roller on the steel load spreader arrangement.

Meanwhile, all the test arrangements were carried out while the specimen constructed on the RC footing still rested on the four 60mm square pipes placed at each corner of the RC footing. These square pipes ensured that the wall was stable during preparation and also allowed the placement of 50mm diameter roller under the specimen before the start of the load application. Once the setups were completed, the 50mm diameter roller was slide under the specimen, and the four 60mm square pipes were removed. This allowed the wall specimen to rest on the 50mm diameter cylindrical roller (Fig 4.34d), with the axis of the roller parallel to the specimen's face to allow it to freely rotate around its base while deflecting out-of-plane and prevent restrained end condition.

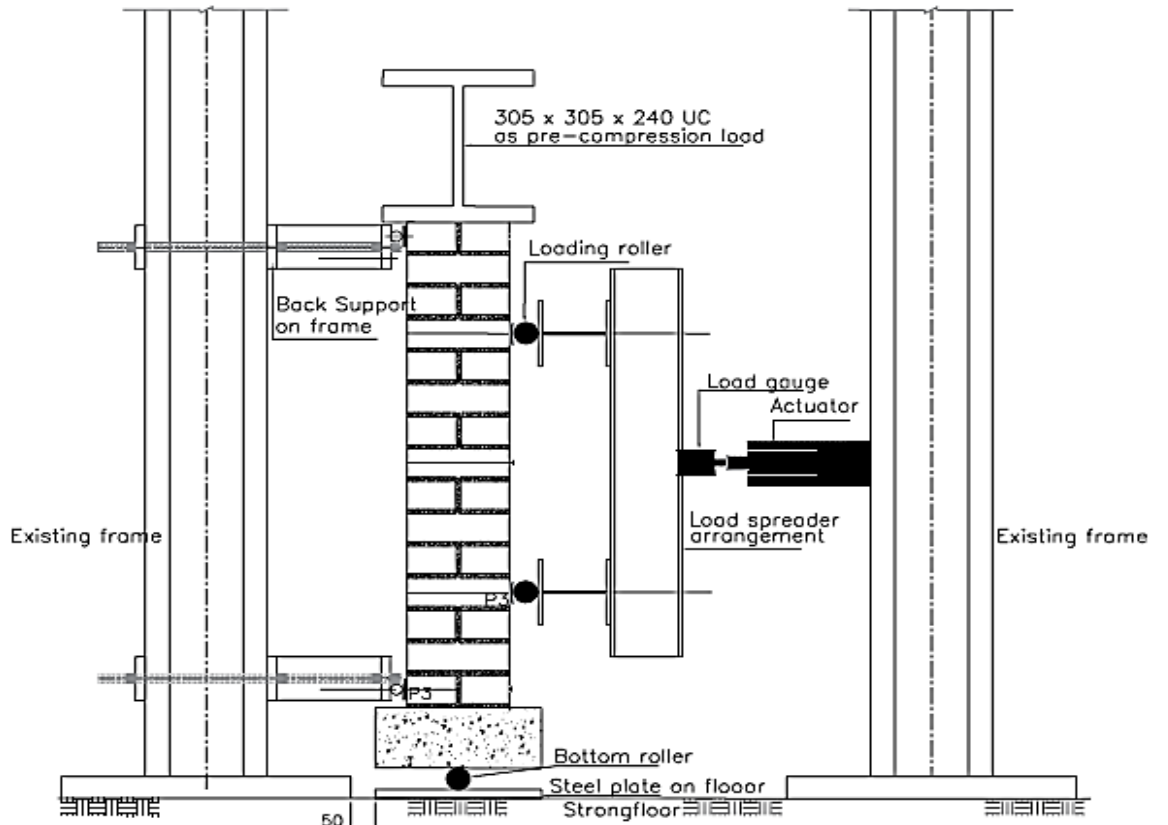


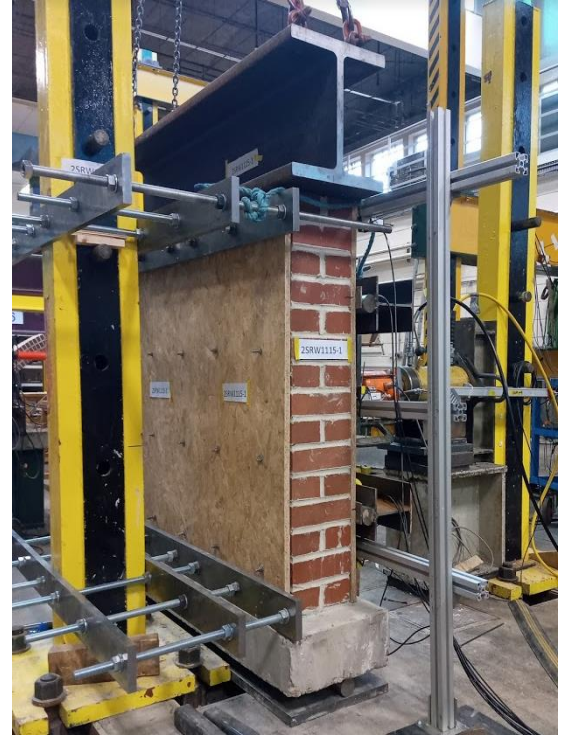
Figure 4.33. Larger-scale test arrangement (drawing scheme)



Figure 4.34a. Larger-scale test arrangement (Side view showing the general arrangement)



b) front view showing loading area



c) Back view showing upper and lower support



d) Roller under wall specimen

Figure 4.34. Larger-scale test arrangement (As-built)

4.3.3.1 Loading Procedure

The loading is such of a four-point testing arrangement where the load was applied on the specimen using a hydraulic ram and distributed through a spreader beam arrangement. The spreader beam spanned between two $\text{Ø}25\text{mm}$ cylindrical rollers rested on 5mm metal plate placed at 1/4th of the height from top and bottom support of the test wall specimen. The direction of the load application was perpendicular to the wall specimen surface. The test was load controlled, and the loading scheme was such that an initial load was applied continuously at a rate of $1\text{kN}/\text{min}$ for up to 5kN and then maintained the load for 5mins period. The purpose of maintaining the applied load was to allow the wall assembly to come to substantial rest before taking the next set of reading as recommended in (ASTM E72-15). Also, this helped to observe any time-

dependent deformation and load redistribution. The load steps were repeated continuously for 10kN, 15kN, 20kN, 25kN, and 30kN load and maintained for 5mins period at each load step (Fig. 4.35). After that, the load was increased continuously to the failure of the test specimen. In order to obtain the maximum capacity of the retrofitted walls, the applied load was increased continually after the first crack until additional cracks were formed in the retrofitted specimens and ultimately the timber at the back of the masonry walls were broken.

For the constant pre-compression load, a 305 x 305 x 240 UC section amounting to 3kN load was placed on top of the wall. In the case of variable vertical load (PW1115-2), a hydraulic jack was placed on top of the UC beam with an initial load of 10kN (self-weight of UC inclusive). The vertical load in PW1115-2 further increases as the applied out of plane load increases. The pre-compression load applied simulated a vertical load on the wall, which might be due to a light roof or even an upper portion of the wall.

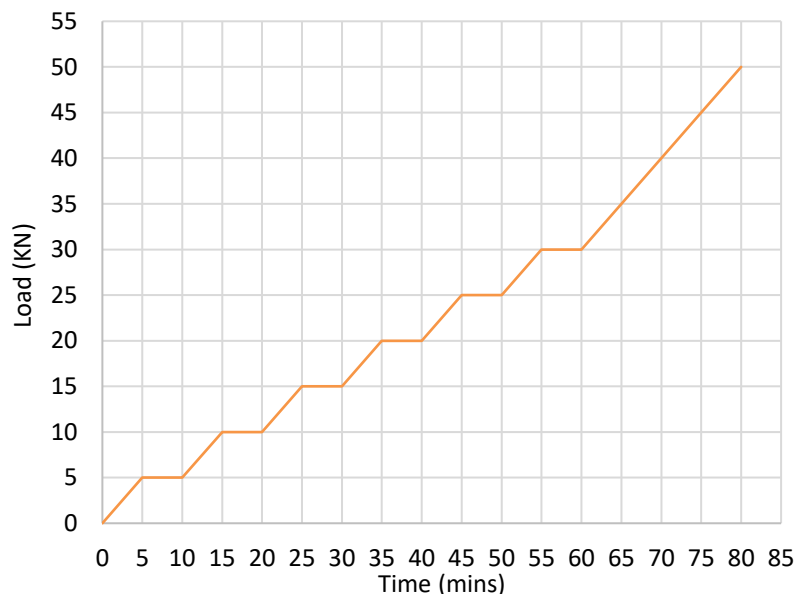


Figure 4.35. Applied out-of-plane load history.

4.3.3.2 Instrumentation

The values of the applied load on the wall were monitored using a 200kN capacity ring load cell. Simultaneously, 8 linear variable displacement transducers (LVDTs) were used to record the deflections of the test specimen along the wall centre, top and bottom. The locations of these gauges were as shown in figure 4.36. All the eight LVDTs used during the test were fixed on an independent steel tripod stand, which was not connected to the test rig. The force

and the displacements were real-time monitored by connecting the measuring equipment (load cell and LVDTs) to an electronic acquisition unit interfaced with a computer.

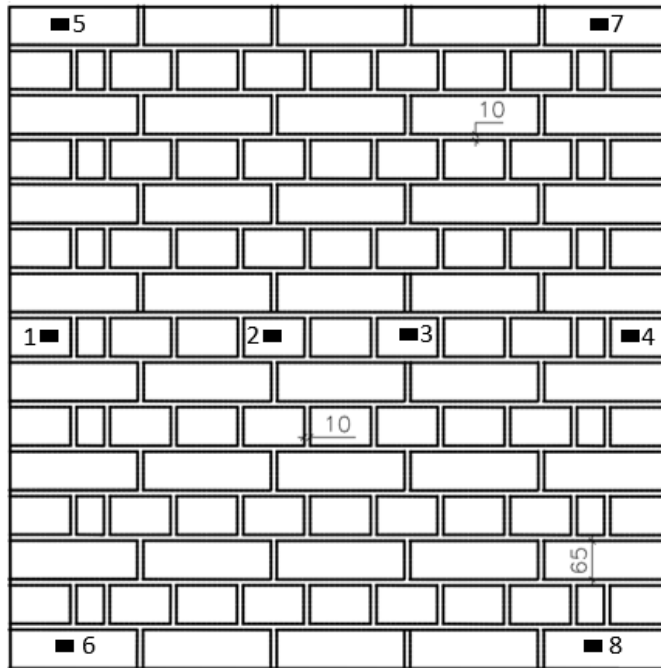


Figure 4.36. Position of LVDTs on wall specimen

4.3.4 Test Results

The experimental results were expressed in terms of load vs displacement curve representing the total applied out-of-plane load against the net out-of-plane displacement for both plain and retrofitted specimens. The maximum out-of-plane loads and the corresponding net out-of-plane displacement of the plain walls were obtained to establish the baseline for estimating the effectiveness of the proposed retrofit technique.

4.3.4.1 Out-of-plane Displacement

The net out of plane displacement in the mid-height of the wall was estimated by deducting the mean displacement recorded at the top and bottom of the specimens from the average mid-height displacement. This deduction accounted for the unexpected displacement at the top and bottom of the wall. The net out-of-plane displacement was obtained using either of the two options below because the two options give the same results.

- **Option 1:** Right and Left side

In this option, the wall was divided into two sides, the displacement on each side of the wall was estimated and averaged to give the net out-of-plane displacement of the wall as shown from equation 4.4-4.6

Considering figure 4.36,

$$d_{net/left} = \left(\frac{d_1 + d_2}{2} \right) - \left(\frac{d_5 + d_6}{2} \right) \quad (4.4)$$

$$d_{net/right} = \left(\frac{d_3 + d_4}{2} \right) - \left(\frac{d_7 + d_8}{2} \right) \quad (4.5)$$

$$d_{net} = \left(\frac{d_{net/left} + d_{net/right}}{2} \right) \quad (4.6)$$

- **Option 2:** Top, Mid and Bottom

Here, the wall was considered as a single part with three regions as the top, mid and bottom. In order to estimate the net displacement in the specimen mid-height, the average value of horizontal displacement at the top and bottom of the specimen was removed from the mean value of the displacement measured at the specimen mid-height using equation 4.7 to 4.10

$$d_{net/top} = \left(\frac{d_5 + d_7}{2} \right) \quad (4.7)$$

$$d_{net/bottom} = \left(\frac{d_6 + d_8}{2} \right) \quad (4.8)$$

$$d_{net/mid} = \left(\frac{d_1 + d_2 + d_3 + d_4}{4} \right) \quad (4.9)$$

$$d_{net} = d_{net/mid} - \left(\frac{d_{net/top} + d_{net/bottom}}{2} \right) \quad (4.10)$$

Where; d refers to displacement at a particular position of LVDT in figure 4.36.

4.3.4.2 Behaviour of Plain Masonry Wall

Figure 4.37 below presents the load-displacement curve for the two tested plain masonry wall specimens (PW1115-1 and PW1115-2). The damaged pattern after the test is shown in figure 4.38 and 4.39. The observed failure pattern in the plain walls is characterised by the sudden formation and rapid opening of the crack in the unit/mortar joint interface throughout the whole wall specimen thickness. The failure of the plain masonry wall is quasi-brittle and always started with the formation of a crack opening in one bed joint at the tensile face

of the specimen (i.e. the side opposing the loading face). Subsequently, the crack occurred in the bed joint was propagated through the perpendicular joint to the next bed joint. The crack occurred throughout the whole thickness of the wall so that the unit-mortar interface was completely separated (Fig 4.39). In the case of PW1115-1, where the pre-compression load applied varied according to the applied out of plane loading, the failure occurred across 3-bed joints as shown in figure 4.38.

The load-displacement curve in figure 4.37 shows that the two plain specimens have a quasi-linear behaviour up to about 15000N load, which corresponds to the onset of crack formation in PW1115-2. After that, the load continuously increased with a little increase in the out-of-plane displacement before the specimen failed. At the failure point, the displacement suddenly increased. This increment is due to the brittle nature of the failure pattern. The maximum load attained by PW1115-2 is 38330N and the corresponding net out-of-plane displacement at this point is 5.25mm.

From figure 4.38, specimen PW1115-1 appeared very stiff because the applied pre-compression loads keep increasing as the load increases, preventing significant out of plane displacements. However, at about 25000N load capacity, there is an onset of crack 1 in the specimen which later failed at maximum load of 39720N with a corresponding net out-of-plane displacement of 3.4mm. Then, because of the increasing pre-compression load, there is a redistribution of the stresses in the wall, which then allowed PW1115-1 to carry more out-of-plane load until another crack (crack 2) formed at 65000N applied out-of-plane load.

Clearly, the applied load on PW1115-1 has passed the normal load capacity of the wall, which is 38330N for PW1115-2. So, the loading was stopped after the failure of crack 2. This is to avoid the total collapse of the wall and damage to the instruments. It was evident that the higher pre-compression load increased the out-of-plane capacity of the wall. However, the increasing pre-compression load as the out-of-plane load increases is not realistic. Therefore, the load at the first crack of PW1115-1 (39720N) and the maximum load of PW1115-2 (38330N) were chosen as the maximum load capacity of the plain specimen. The average of these two values (39025N) was chosen as a baseline to evaluate the

effectiveness of the proposed timber-retrofit technique in both single-sided and double-sided retrofitted walls.

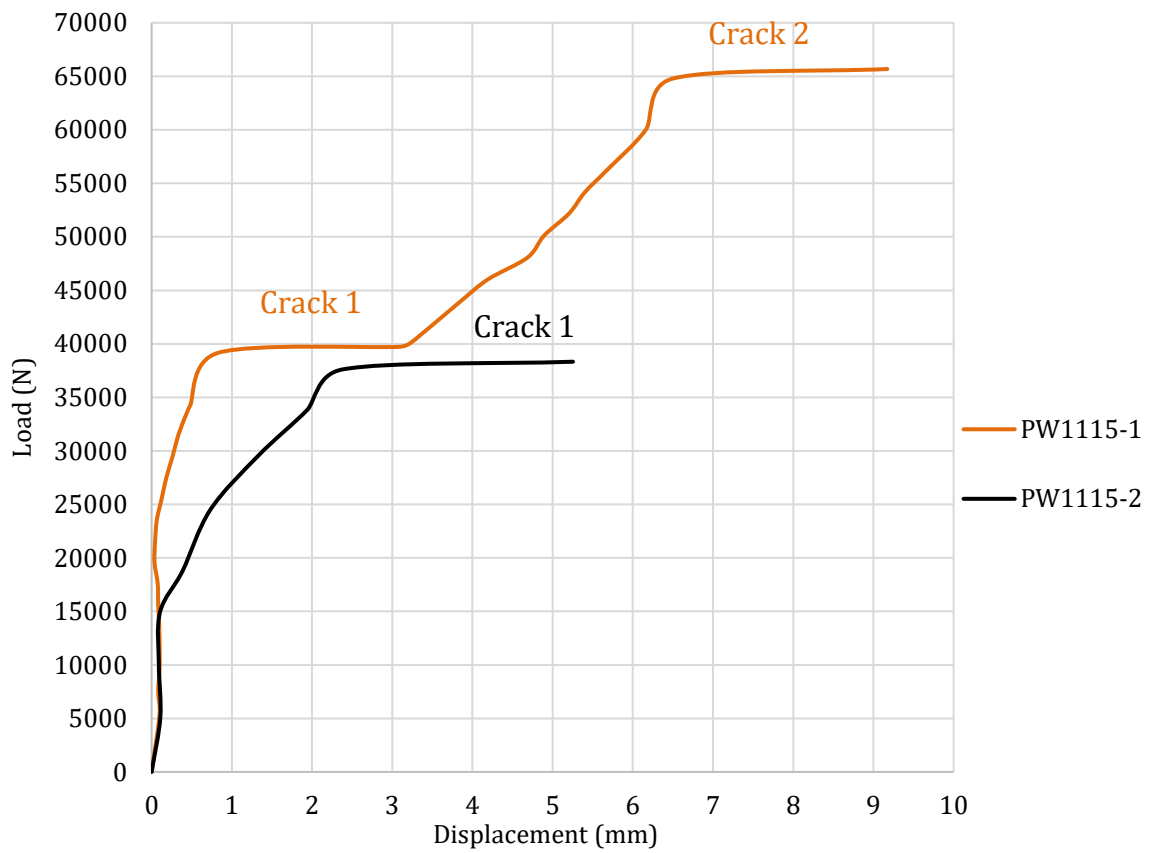


Figure 4.37. Load vs Displacement curve for plain specimens

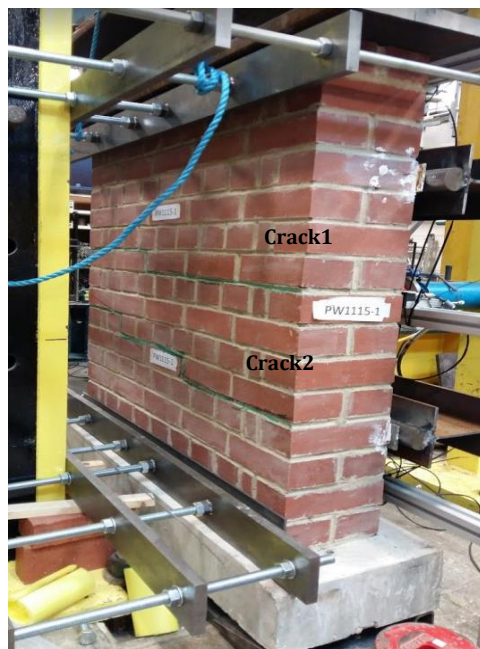


Figure 4.38. Failure pattern of PW1115-1



Figure 4.39. Failure pattern of PW1115-2

4.3.4.3 Behaviour of Retrofitted Masonry Wall

In this section, the load-displacement curve for both single and double-sided retrofitted masonry wall specimens are shown in figure 4.40. Also, the specimens damaged patterns after the test are shown in figure 4.41.

The behaviour of single-sided retrofitted masonry wall (1SRW) shows that the net out-of-plane displacement of the specimens increased with the applied out-of-plane load from the beginning. This behaviour indicates that 1SRW specimens started to deflect while remaining undamaged. The failure of 1SRW began from the tensile face with the first crack occurred in the unit-mortar interface at 54600N and 50900N for 1SRW1115-1 and 1SRW1115-2 respectively. Before the first crack appeared, the net out-of-plane displacement has reached 7.0mm and 6.2mm in 1SRW1115-1 and 1SRW1115-2 respectively.

Meanwhile, the double-sided retrofitted wall (2SRW) shows approximately no displacement (0.25mm) before the first crack occurred in the masonry part at an average load of 68714N. This implies that the addition of the timber panel on the compression face (i.e. the face where the load was applied) in 2SRW improved the lateral resistance of the 2SRW specimens. So, double-sided application means that the specimen remained undeflected and undamaged before the first crack occurred at an average load and displacement of 68714N and 4.18mm.

For the sake of comparison, the load-displacement curve of plain walls is included in figure 4.40, with PW1115-1 shows up to crack 1 formation only. This

is because the additional strength gained by PW1115-1, which led to the formation of crack -2 was due to the increased pre-compression load, which is not available on the retrofitted sample. An inference from figure 4.40 reveals that the proposed retrofit technique has substantially increased the out-of-plane load capacity of retrofitted walls. Specifically, 1SRW and 2SRW attained an average of 114622N and 120559N maximum load. Remarkably, the load capacity of the retrofitted walls before the first crack occurred is more than the maximum load capacity of the plain wall. On the load-displacement curve, the points at which the cracks occurred in the walls were indicated with numbers. This numbering corresponds to the numbers on the images from the test (Fig 4.41). For instance, crack 2 at 81765N load and a third final crack at 116444N for 1SRW1115-1.

Evidently, the proposed timber retrofit technique has improved the brittle behaviour of the plain masonry wall. Unlike the plain masonry walls, the retrofitted masonry walls remained unseparated after the first crack. This is because the application of the OSB timber has improved the out-of-plane behaviour and integrity of the retrofitted walls. The retrofitted walls displaced more in the out-of-plane direction, which then prevents their sudden collapse.

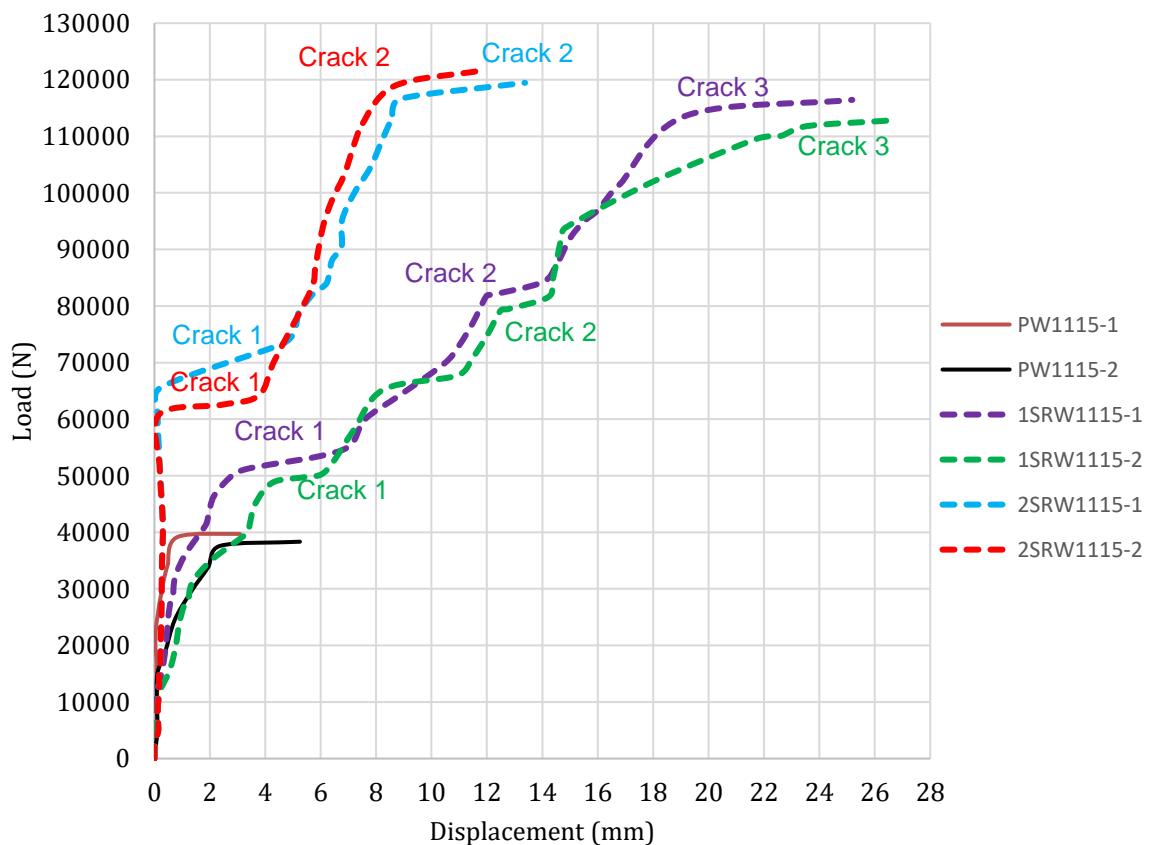


Figure 4.40. Load vs Displacement curve for specimens



1SRW1115-1



1SRW1115-2



2SRW1115-1



2SRW1115-2

Figure 4.41. Failure pattern of retrofitted masonry wall

4.3.5 Evaluation of Performance of the Proposed Technique

Table 4.13 summarises the main results of the out-of-plane bending test in term of the first/initial cracking, failure load and their corresponding displacement. In addition, the increase in limiting and overall toughness because of the retrofit application was also presented. Then, comparison charts at the occurrence of first crack (Fig. 4.42) and failure (Fig 4.43) were developed for the performance evaluation of the proposed retrofit technique. The average load and displacement for each group of specimens (i.e. PW, 1SRW and 2SRW) were used to develop the charts.

The comparison in term of capacity at first crack (Fig. 4.42) shows that the load that caused the first crack in 1SRW is 1.4times the maximum load at the failure of PW. Also, the first crack on the 2SRW specimen occurred at a load that is 1.8times the failure load of PW. This shows that the 2SRW resist more load before the first crack, about 1.4times that of 1SRW. At the failure point, the maximum load capacity of masonry wall retrofitted with OSB panel is 2.9times and 3.1times that of PW for 1SRW and 2SRW respectively (Fig 4.43). Unlike the load at the first crack, the load capacity of 2SRW is only 1.04times that of 1SRW.

The analysis of the test results also shows a significant increase in the out-of-plane displacement of retrofitted walls. This is due to the application of the OSB timber panel that has offered the masonry wall a significant lateral resistance, once the mortar interfaced cracked. As such, the retrofitted specimens were able to take more loads and absorbed more energy by displacing more without sudden failure. The increment in the out-of-plane displacement of the retrofitted walls is 6times and 3.1times that of PW for 1SRW and 2SRW respectively.

Similar to the observation in the small-scale test, the overall toughness gained due to the retrofit application when taken up to the failure of the OSB is enormous. An improvement of 16times and 10times that of the plain wall is estimated for application on single and both sides respectively (Fig. 4.43d). However, the performance of the technique at the limiting displacement is quite otherwise with the double-sided showing more toughness gained than one-sided application (2.4xPW and 1.6xPw for double and single-sided respectively). The analysis shows that the double-sided application offers the most improvement

in the toughness at the limiting displacement. Thus, the double-sided is the best option when higher energy absorption is required in a real situation.

Table 4.13: Summary of out-of-plane bending test results

Specimen Label	First crack		Failure		Toughness (Nmm)	
	Load (N)	Disp. (mm)	Load (N)	Disp. (mm)	Limiting	Overall
PW1115-1			39720	3.40	112000	115000
PW1115-2	The first crack is the failure point		38330	5.25	118000	122500
Average			39025	4.33	115000	118750
1SRW1115-1	54600	7.00	116444	25.20	186000	1920000
1SRW1115-2	50900	6.20	112800	26.55	178000	1965000
Average	52750	6.60	114622	25.88	182000	1942500
2SRW1115-1	70200	4.58	119460	13.38	260000	1205000
2SRW1115-2	67228	3.78	121657	11.84	280000	1190000
Average	68714	4.18	120559	12.61	270000	1197500

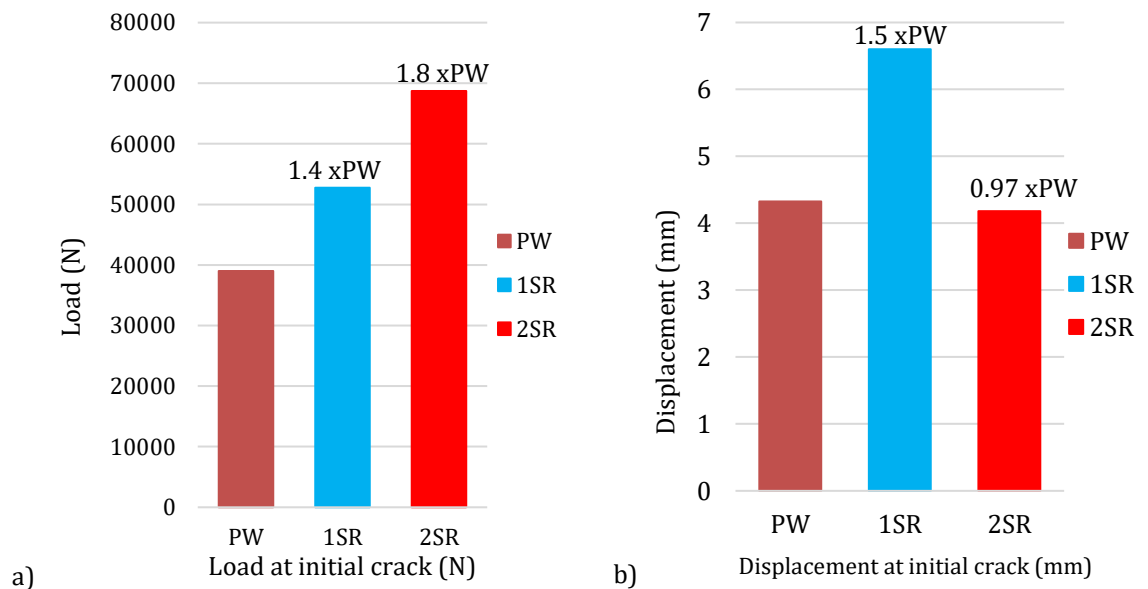


Figure 4.42. Performance at the occurrence of the first crack; (a) Load capacity (b) Displacement

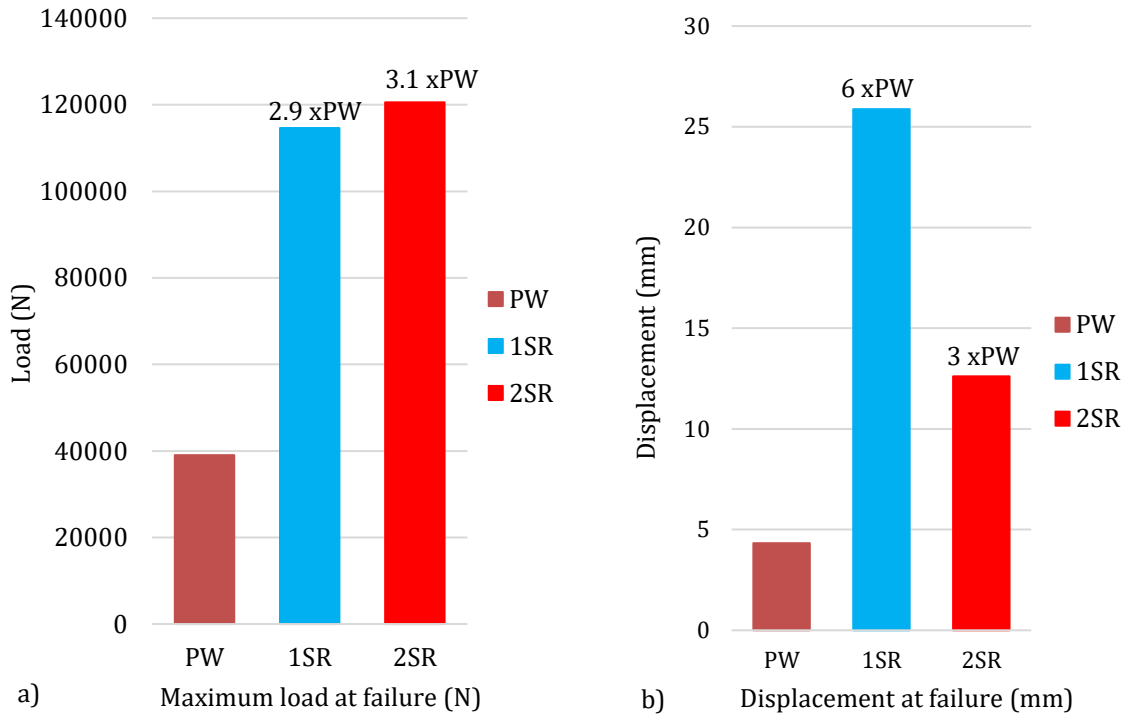


Figure 4.43. Performance at the failure; (a) Load capacity (b) Displacement

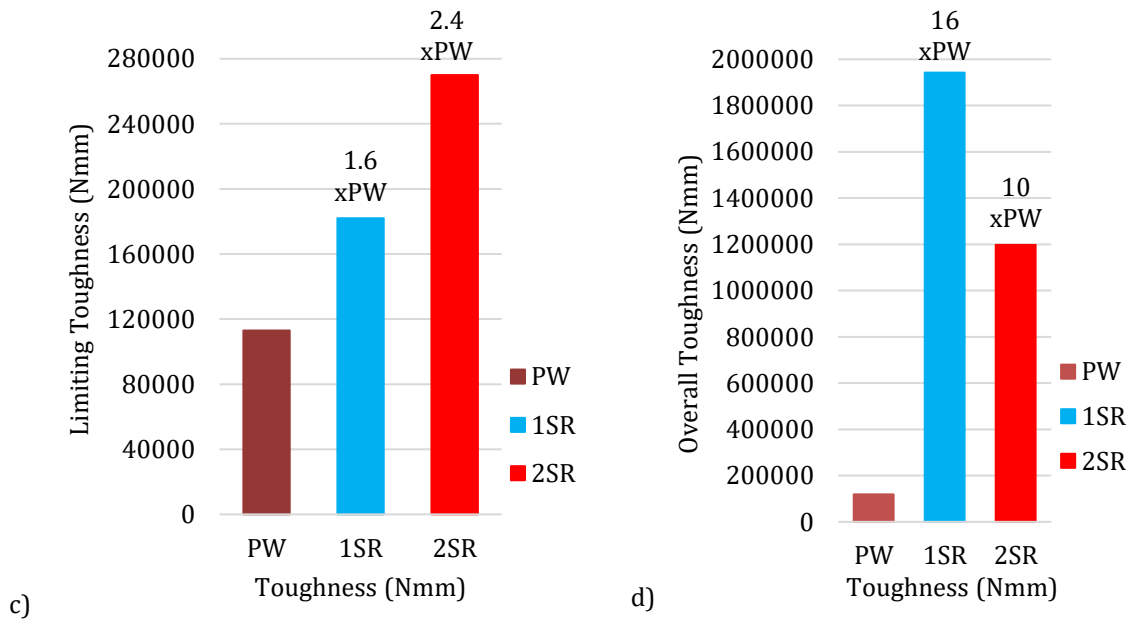


Figure 4.43. Performance at the failure; (c) Limiting Toughness (d) Overall Toughness

4.4 Summary of Findings

The first section of this chapter (section 4.1) presents the experimental tests to characterise the brick units and mortar that was used to study the efficiency of a proposed timber retrofit technique for masonry walls. Apart from testing each

component individually, an unconventional test has also been carried out to study the behaviour of a masonry cubic specimen under compression loading.

Clearly, the strength obtained for the brick units and mortar shows that the brick is a strong unit while the mortar is a weak joint, which makes the combination a strong unit-weak mortar joint, a typical characteristic of old masonry structures. Hence, the material source remained unchanged throughout the experimental campaign that is discussed in detail in subsequent section 4.2 and 4.3.

Also, the obtained mechanical properties of brick units and mortar were used in developing detailed numerical studies on masonry elements that are discussed in chapter five.

Secondly, a small-scale experimental campaign has been presented in section 4.2 to investigate the use of timber panels in retrofitting URM wall. Precisely, the experiment evaluates the out-of-plane performance of OSB panel in retrofitting URM prisms by comparing the toughness, flexural strength, out-of-plane load capacity, and displacement of both plain and OSB-retrofitted masonry prisms. In this experiment, flexural strength test in the form of four-point bending test was performed on nine MPs, three of which were tested as plain to establish a baseline for comparison. Two groups of three specimens each retrofitted with 18mm type 3, OSB panel using two different connection typologies (C1, adhesive anchor: threaded dry rod with an injectable chemical adhesive) and (C2, mechanical connection: threaded dry rod with a plastic anchor). The focus of this small-scale test is to generate knowledge and understanding of whether OSB panel can improve URM walls capacity against excessive out-of-plane loading.

Based on the test results, the application of the OSB panel at the back of MP greatly influenced its out-of-plane behaviour. In plain specimen (MP00), the collapse was sudden with the evolution of crack opening in single mortar bed joint within the inner bearing of the specimens. The failure (cracking) was abruptly occurred between the interface of the mortar joint and brick unit. While, in the retrofitted specimens (MPOSB), the OSB panel improved the flexural response of the specimens such that the failure was much more ductile. For the failure to occur, there are occurrences of crack openings in the interface of mortar and brick units on multiple bed joints within the inner bearing. This

proposed retrofit technique increased the initial crack load on the retrofitted specimens. Compared to the plain one, the OSB retrofitted MP not only demonstrated higher load capacity but also improved ductility and integrity of the MP. This is to the extent that even after the cracking of OSB panel, the damaged specimens remained as a unit, which prevents the sudden collapse of the specimens, unlike plain MP. An inference from this is that timber panel might not prevent the ultimate failure of the URM wall, but it improved the performance to at least collapse prevention. This is evident in the increased flexural resistance and energy absorption of the retrofitted specimens before collapsing. This will ensure that sudden failure is avoided and thus minimised the high risk of mortality and substantial damages that comes with the sudden collapse of the URM wall.

Indeed, the retrofitted MP is able to offer flexural strength to resist out-of-plane load almost 7.5times higher than plain MP in case of adhesive anchor and 5.0times greater when a mechanical connection was used. Adhesive anchors performed much better for the envisaged application. Consequently, the out-of-plane displacement showed in retrofitted MP is almost 2.0times higher than that of plain MP. This is because there is limited tensile strength in plain MP and the failure (collapse) is sudden. But the addition of OSB panel offered additional tensile strength and ductility in retrofitted specimens, and thus they were able to displace gradually before the timber failed.

Decisively, the performance of adhesive anchor (C1) is better than the mechanical connection (C2). C2 is not totally effective due to weak bonding between the OSB panel and MP. The reason for this weak bonding was observed to be the inability of plastic anchor to expand in the high dense brick unit. Although the results presented herein were based on initial tests on small specimens, the inferences from the results were promising. Although, the performance of the proposed retrofit technique recorded might have been amplified due to the fragility of the plain specimen, which is likely not to be truly representative of the real working condition of URM walls, in which case some confinement is present at the borders. As such, a larger-scale experimental campaign on 1115 x 1115 x 215mm single leaf, double wythe solid URM walls to study the proposed technique in detail is presented in subsequent section 4.3.

In conclusion, section 4.3 presents a larger-scale experimental study to propose the application of oriented stranded board (OSB) type 3 to retrofit masonry wall. In particular, it focused on the effectiveness of the proposed timber-based retrofit technique against out-of-plane failure. Here, six tests have been performed on 1115 x 1115 x 215mm single leaf, double wythe solid masonry walls. Two of the walls were tested as plain wall (PW), two as single-sided retrofitted masonry wall (1SRW), and the last two as double-sided retrofitted masonry wall (2SRW).

Out-of-plane bending test in the form of four-point loading test was performed on all the six specimens. The aim was to obtain the response of both the plain and retrofitted masonry walls against out-of-plane loading to evaluate the performance of the proposed technique. The aim was achieved by assessing the load-carrying capacities, energy absorption and displacement capacities of both plain and retrofitted walls.

The analysis of the experimental results revealed that the retrofitted masonry wall specimens were able to resist out-of-plane loading which is 1.4 times and 1.8 times higher than that of plain walls for both 1SRW and 2SRW before the initial crack occurred. Overall, the retrofitted walls were able to resist out-of-plane loading almost 3 times higher than that of plain walls for both 1SRW and 2SRW and can also resist an out-of-plane deflection that is 6 times and 3.1 times that of PW for 1SRW and 2SRW respectively. A key observation here is that the application of the retrofit on both faces of the wall does not increase the failure load when compared to one side application. However, the load at which the initial crack occurred in 2SRW is 1.4 times higher than the load at which the 1SRW first cracked. Also, the deflection resistance of the double-sided application is higher than the one-sided application.

Moreover, the application of the retrofit technique on both sides does affect the toughness of the composite system. The 1SRW absorbed more energy than the 2SRW. This is evident in the ability of the 1SRW to displace more than the 2SRW. Quantitatively, the one-side retrofitted walls were able to absorb more energy almost 16times higher than that of plain walls. Meanwhile, the 2SRW can absorb energy, which is 10times higher than that of PW. However, the double-sided application has advantages in term of the limiting toughness and stiffness,

showing a more excellent resistant against out-of-plane displacement. The 2SRW also absorbed more energy than 1SRW in the range where the displacement is within the allowable practical limit.

In term of the observed failure pattern, it emerged that the failure of the PW was sudden with the evolution of crack opening in mortar bed joint almost at the specimens' mid-height. The failure (cracking) was abruptly occurred between the interface of the mortar joint and brick unit, which then cut across the whole specimen thickness. Whereas, the application of the OSB type 3 to retrofit the wall shows that the walls were able to take more loads after the first crack which subsequently led to the formation of other horizontal cracks in the bed joint within the middle thirds of the walls. The failure/collapse of the retrofitted specimens occurred when the applied OSB timber reaches their ultimate strain and broken.

As previously highlighted in the small-scale test, the timber panel might not prevent the ultimate failure of the retrofitted wall, but it improved the performance to at least collapse prevention. The application ensured that sudden failure was avoided and thus minimised the high risk of mortality and substantial damages that comes with the sudden collapse of the unreinforced masonry wall.

Although, the results and observations made were based on specimens with free boundary conditions that replicate masonry wall without returning walls at the corner, which is a rarity. Pieces of evidence from the previous experimental works have shown that tests on panels without corners are a good indication in assessing the out-of-plane capacity of URM wall. Hence, the main conclusion from this study is that oriented strand board (OSB) type 3 can considerably increase the flexural capacity and toughness of the retrofitted masonry wall when subjected to out-of-plane loading.

CHAPTER FIVE – RETROFIT OF URM WALL WITH TIMBER PANEL: NUMERICAL STUDY

5.0 Introduction

This chapter presents the full numerical analysis performed to expand the experimental study in order to evaluate the efficiency of the proposed timber-based retrofit for URM walls. Foremost, this chapter presents the numerical simulations of the three stages of experimental works discussed in chapter four. The first section is the numerical simulation of the compression test on the masonry cubic specimen presented in section 4.1. Secondly, the numerical simulation of the flexural bond strength test on small-scale masonry prism described in section 4.2 is presented. Then, the numerical simulation of the out-of-plane loading test on the larger-scale masonry wall presented in section 4.3 is presented.

At each stage of the simulation, the developed models are validated using the experimental data. Finally, a parametric study to assess the model capability to simulate URM walls retrofitted with different OSB panel thickness and connection layout is presented.

5.1 Adopted Numerical Modelling Techniques

In this study, the detailed micro-modelling technique was adopted to perform the numerical simulation of the compression test on masonry cubic specimen. This is selected because the masonry cubic specimen is small, and a thorough description of the material is possible. This approach enables the combined action of unit, mortar and interface to be studied under a magnifying glass. Meanwhile, the simplified micro modelling technique was chosen for the simulation of both flexural bond strength test (small-scale test) and out-of-plane loading test (larger-scale). The detailed micro analysis consumed too much time and computer resource for a relatively well-detailed model such as the one presented for both the small and larger-scale models. So, the simplified micro modelling approach was used. This also helped to avoid convergence problems usually encounter after the peak load due to the inclusion of material damage

and too many contacts between the unit and mortar (unit/mortar interface). After that, the calibration and validation of the FE model were done using the experimental results and observed failure modes.

5.2 Numerical Simulation of Compression Test on MC Specimen

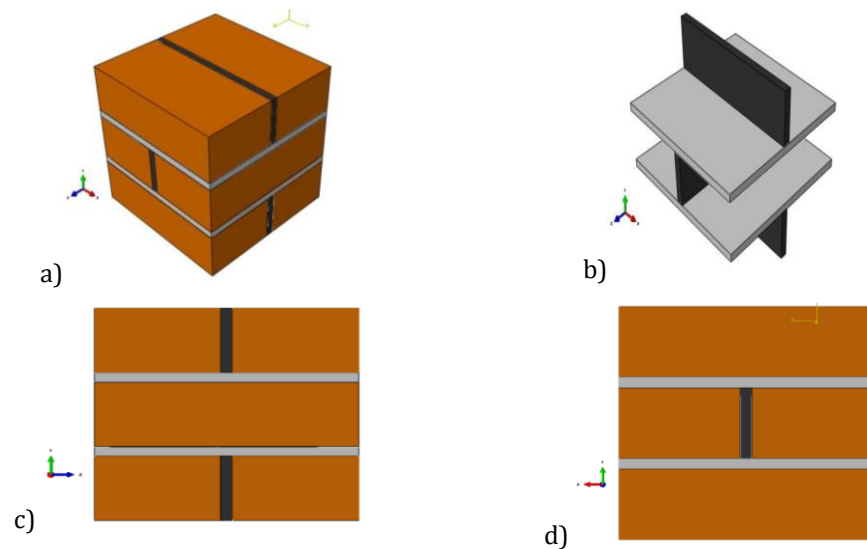
Section 4.1.3 discusses the experiment to determine the compressive strength of masonry cubic (MC) specimen. Here, the MC experiment is simulated by FE analysis through the ABAQUS FEA software (Simulia, 2014) to support the interpretation of the obtained compression tests results. This section focuses on achieving the accurate mechanical properties of the unit, mortar and the interfacial properties of the unit-mortar joint that is necessary to produce a detailed numerical analysis of the masonry wall. In order to achieve this, a complete description of each component was done based on the experimental results of compression tests on bricks, mortar and the masonry cubic specimen (Dauda et al., 2019). For the post-peak behaviour of the compressed brick and mortar, the concrete damaged plasticity (CDP) model in ABAQUS was used to characterise the non-linearity of the units and mortar in both tensile and compression regimes. The CDP approach was used because it can be used to effectively model the two desired typical failure mechanisms in quasi-brittle materials, which are the tensile fracture and compressive crushing. An additional parameter to control the dilatancy in the quasi-brittle material response was also applied to define the plastic strain rate using a non-associative flow rule generated by a Drucker-Prager type plastic potential. The details of this are given in section 5.2.3. The developed model was calibrated to create a well fitted numerical model that represents the complex behaviour of brick units and mortar working together as masonry.

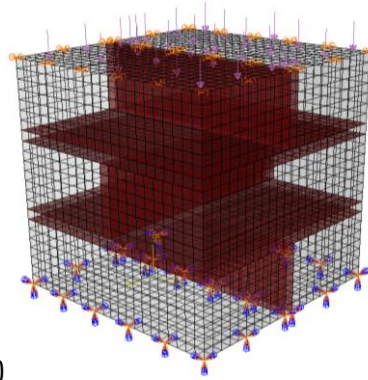
5.2.1 Description of FE model

A numerical model of a masonry cube (MC) was created using a three-dimensional solid (or continuum) elements in ABAQUS. In particular, hexahedral 8-node linear brick, reduced integration, hourglass control (C3D8R) which is cost-effective and has improved convergence compared to the full integration was selected to generate the mesh that represents the brick and mortar joint. The size of the unit is 215 x 102.5 x 65mm, and the thickness of the joint is 10mm.

The unit and joint (bed and perpend) were defined using their respective mechanical properties. The nonlinear behaviour of the brick unit and mortar, both in compression and tension regime, have been accounted for in the FEs model using the CDP constitutive model. The brick-mortar bond failure behaviours have also been considered using the nonlinear cohesive interfaces. Also, the contact penalty approach was enforced for the interaction between the brick and mortar interface. This means that the contact between the mortar interface and the unit interface is enforced by contact constraints in the normal direction. Simulia (2014) iterated that the penalty method typically does not generate additional degrees of freedom, unlike the contact constraint options, which would always generate Lagrange multiplier degrees of freedom. The penalty method for enforcing contact is available in ABAQUS/Standard and can provide more efficient solutions in many cases.

For the boundary condition, the nodes at the top of the cubes were restrained in x and z-direction. In addition, the bottom nodes were restrained in all the three directions (x, y, z) to replicate the friction in the test condition of the specimen (Fig. 5.2). The Static General step in ABAQUS standard/explicit was selected for the analysis. Figure 5.2 below shows the general assemblage of the masonry cubic model, FE mesh and the boundary condition.





e)

Figure 5.2: Micro modelling of masonry cube: a) Overall 3D geometry (b) mortar joints (c) front elevation (d) side elevation (e) FE mesh, boundary condition and surface interaction

5.2.2 Properties of Brick unit and Mortar

Obtaining exhaustive experimental data required for detailed micro-modelling of masonry structure have sometimes proved tedious. Compression tests are the most available and most reliable test on materials, particularly when the post-peak regime is captured. Compression tests allow to fully characterise the material behaviour in the form of a stress-strain curve, which is a requirement to perform nonlinear finite element analysis accurately.

The CDP constitutive model, available in ABAQUS and described by (Guo, 2014) was used to simulate the tensile and compressive non-linear behaviour of unit and mortar. The CDP model assumes a non-associated potential plastic flow, which is an adoption of Drucker-Prager hyperbolic function for flow potential. The failures recognised by the CDP model are cracking in tension and crushing in compression.

For the brick unit, the tensile and compressive plastic-damage nonlinear properties were estimated from the typical stress-strain response of brittle material under uniaxial loading. Figure 5.3 shows the behaviour in the compression regime. The curve has three different regions, the formulations for each region derived from Sinha et al. (1964), Guo (2014) and Santos et al. (2017) are shown from equations 5.1 to 5.7. The units' compressive strength ($f_{c,b}$) and elastic modulus (E) obtained experimentally were used in these equations.

Having obtained $f_{c,b}$, the stress-strain relationship in the compression regime is assumed to be consistent with the compressive fracture energy ($G_{f,c}$), which is equal to the area under the curve in figure 5.3a. $G_{f,c}$ is given by parabolic best-fit equations ($G_{f,c} = 15 + 0.43f_{c,b} - 0.0036f_{c,b}^2$) obtained from the Model Code 90

by Lourenco and Milani (2014) when the compressive strength of the brick unit is between 12 - 80N/mm². This is then useful in obtaining the ductility index which helps in defining the detail response of brick and mortar in the post-peak behaviour. Extensive information on how to obtain this $G_{f,c}$ in N/mm is presented by Angelillo (2014) and Lourenco and Milani (2014). However, for brick units with a compressive strength lower than 12N/mm² and higher than 80N/mm², an average ductility index in compression which is the ratio between the compressive fracture energy and the compressive strength is used to obtain the approximate fracture energy. The limit of this ductility index (1.6mm for strength lower than 12N/mm² and 0.33mm for strength higher than 80N/mm²) was specified in Model code 90 (Angelillo, 2014; Lourenco and Milani, 2014).

For the present study, an average ductility index in compression ($d_{u,c} = 0.33mm$) is used to obtain the approximate fracture energy because the compressive strength of the unit is 88N/mm². So, once the compressive strength of the brick unit ($f_{c,b}$) and the peak strain obtained directly from the experiment has been fixed, then the brittleness parameter is chosen to ensure that the area under the curve is equal to ($G_{f,c}$).

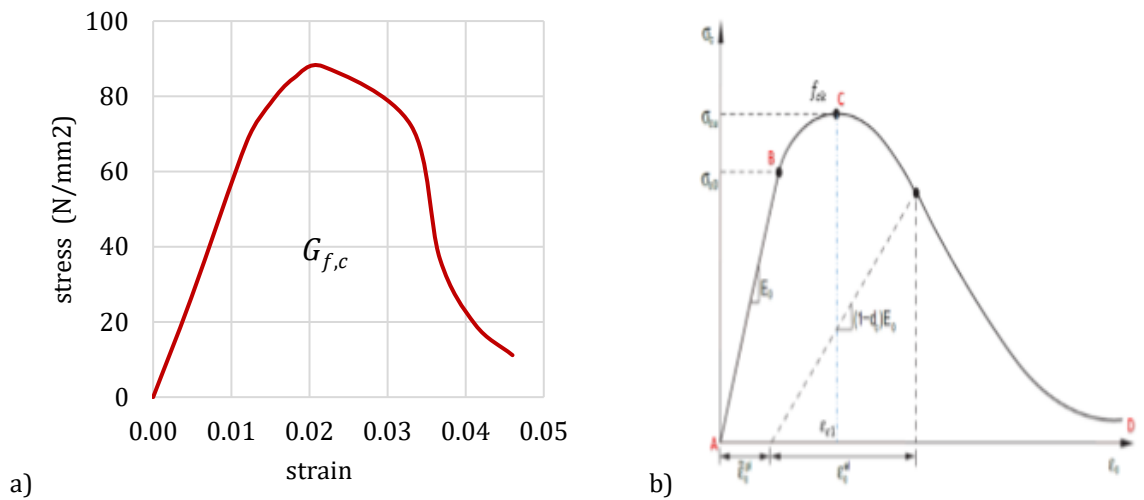


Figure 5.3: Masonry unit behaviour under uniaxial compression (a) numerical model (b) typical response in ABAQUS (Simulia, 2014).

The formulation for the damage plasticity of the brick unit under uniaxial compression shown in figure 5.3a above is given below;

- i) The First Region: Elastic Region (A to B)

$$\sigma_c = E_{i,b} * \varepsilon_c \tag{5.1}$$

ii) The Second Region: Inelastic Region (B to C i.e. $x \leq 1$)

$$\sigma_c = (\alpha_a x + (3-2 \alpha_a)x^2 + (\alpha_a -2)x^3) * f_{c,b} \quad (5.2)$$

iii) The third region: inelastic region (C to D, i.e. $x \geq 1$)

$$\sigma_c = f_{c,b}/(\alpha_d x(x - 1)^2) \quad (5.3)$$

Where;

$$x = \varepsilon_c/\varepsilon_{c1} \quad (5.4)$$

$$\alpha_a = E_{i,b}/E_b \quad (5.5)$$

$$1.5 \leq \alpha_a \leq 3 \quad (5.6)$$

$$0 \leq \alpha_d \leq \infty \quad (5.7)$$

Correspondingly, figure 5.4 shows the behaviour of the brick unit in the tensile region obtained from equations 5.8 to 5.10. The ductility index in tension ($d_{u,t} = 0.018mm$) which is a ratio between the fracture energy ($G_{f,t}$) and the tensile strength ($f_{t,b}$) was used to obtain the fracture energy (Pluijim, 1992; Lourenco, 1996; Lourenco & Milani, 2014; Angelillo, 2014).

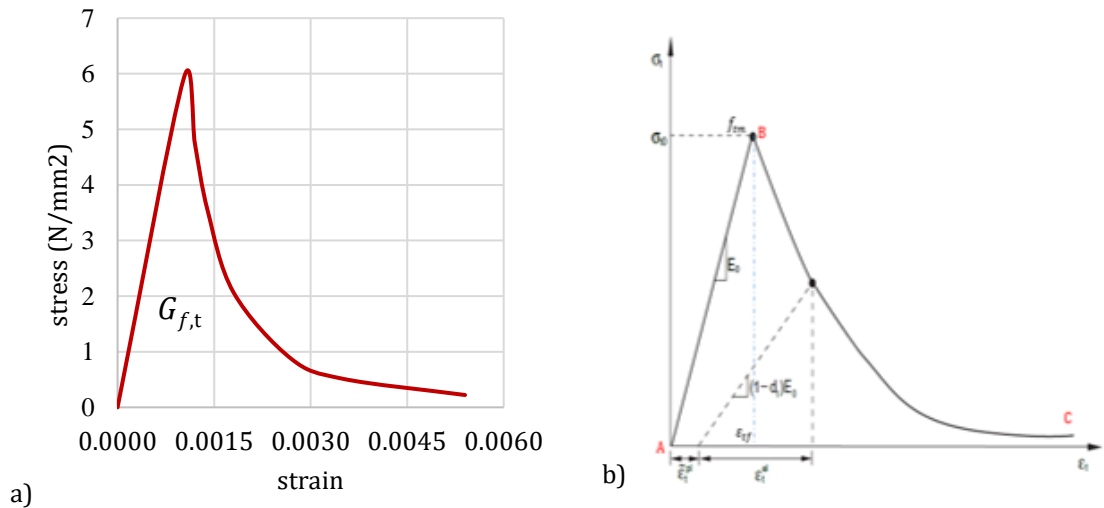


Figure 5.4: Masonry unit behaviour under uniaxial tension (a) numerical model (b) typical response in ABAQUS (Simulia, 2014).

Referring to figure 5.4 above, the formulation for damage plasticity of the brick unit under uniaxial tension are as follows;

i) The first region: elastic region (A to B)

$$f_{t,b} = E_{i,b} * \varepsilon_{cr} \quad (5.8)$$

$$f_{t,b} = 0.3 * (f_{c,b})^{2/3} \quad (5.9)$$

ii) The second region: inelastic region (B to C)

$$\sigma_t = (f_{t,b} * x) / (\alpha_t (x - 1)^{1.7} + x) \quad (5.10)$$

$$x = \varepsilon_t / \varepsilon_{cr} \quad (5.11)$$

$$\alpha_t = 0.312 f_{t,b} \quad (5.12)$$

Where; E_b : modulus of elasticity of masonry unit

$E_{i,b}$: initial modulus of elasticity of masonry unit

$f_{c,b}$: compressive strength of masonry unit

$f_{t,b}$: tensile strength of masonry unit

α_a : parameter for ascending branch of the compression curve

α_d : parameter for descending branch of the compression curve

ε_c : compressive strain

ε_{c1} : compressive strain at the peak stress

σ_c : compressive stress

Similarly, to put the plastic-damage nonlinear behaviour of the mortar in context as did for the brick unit, an average ductility index in compression ($d_{u,c} = 1.6mm$) is used to obtain the approximate compression fracture energy. Consistently, using the available information provided by (Pluijim, 1992; Lourenco, 1996; Lourenco & Milani, 2014; Silva et al., 2018), the ductility index in tension ($d_{u,t} = 0.065mm$) was used to obtain the approximate tensile fracture energy. To plot the strain-strain relationship to simulate the behaviour of the mortar, the procedures highlighted in BSI (2004) and Wang & Hsu (2011) were followed. The only available direct measurement from the tests is the mortar compressive strength ($f_{c,m}$). Other quantities such as longitudinal modulus of elasticity ($E_{c,m}$) and strain were calculated from equations 5.13 to 5.17. Thereafter, the plot of data obtained was compared to the standard chart given in BS EN 1992-1-2:2004 as shown in figure 5.5 below.

$$\sigma_c = f_{c,m} (k\eta - \eta^2) / (1 + (k - 2)\eta) \quad (5.13)$$

$$k = 1.05 E_{c,m} * (\varepsilon_{c1} / f_{c,m}) \quad (5.14)$$

$$\eta = \varepsilon_c / \varepsilon_{c1} \quad (5.15)$$

$$E_{c,m} = 22 * (f_{c,m} / 10)^{0.3} \text{ in GPa} \quad (5.16)$$

$$\varepsilon_{c1} = 0.7 * (f_{c,m})^{0.31} \quad (5.17)$$

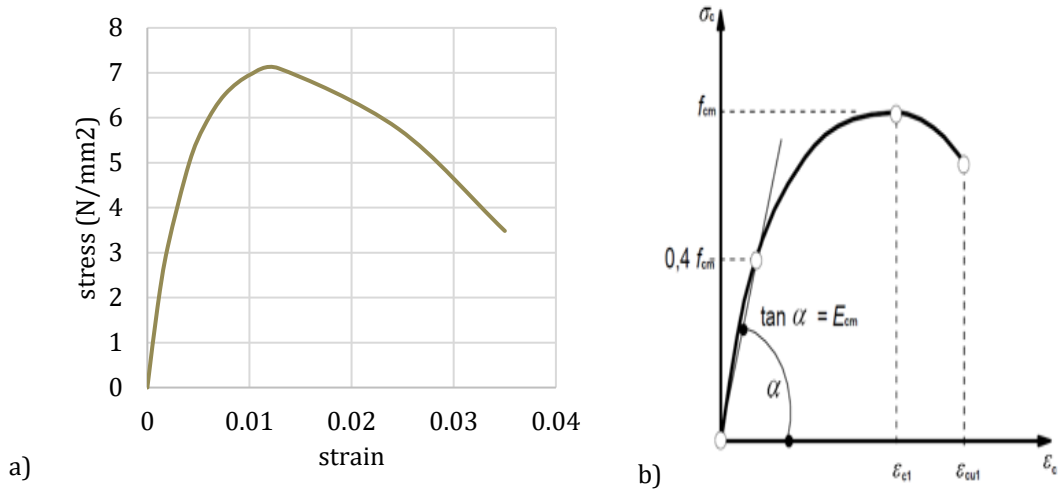


Figure 5.5: Mortar behaviour under uniaxial compression (a) numerical model (b) typical response in BS EN 1992-1-2:2004.

Meanwhile, the tensile strength of the mortar was not determined experimentally, but through equation 5.18 by BSI (2004). Moreso, equations 5.19 and 5.20 were used to simulate the tensile behaviour of mortar. As described in Simulia (2014), the tensile stress of mortar can be linearly reduced to zero, starting from the moment of reaching the tensile strength. This was done, and the resulting stress-strain curve was compared to the description in (Simulia, 2014 & BSI 2004) as shown in figure 5.6.

$$f_{t,m} = 0.3 * (f_{c,m})^{2/3} \quad (5.18)$$

$$\sigma_t = E_{c,m} * \varepsilon_t \quad \text{if } \varepsilon_t \leq \varepsilon_{cr} \quad (5.19)$$

$$\sigma_t = f_{c,m} * (\varepsilon_{cr}/\varepsilon_t)^{0.4} \quad \text{if } \varepsilon_t > \varepsilon_{cr} \quad (5.20)$$

Where; $f_{t,m}$: tensile strength of mortar

$f_{c,m}$: compressive strength of mortar

$E_{c,m}$: modulus of elasticity of mortar

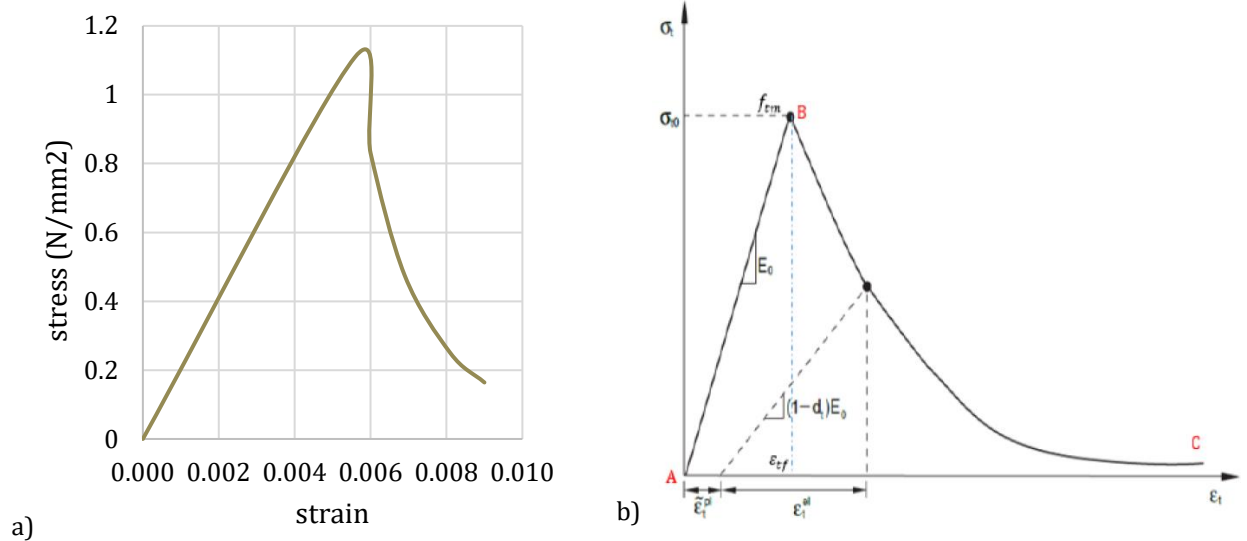


Figure 5.6: Mortar behaviour under uniaxial tension (a) numerical model (b) typical response in BS EN 1992-1-2:2004.

5.2.3 General Parameter for CDP of Brick and Mortar

Apart from the above-presented damage plasticity data, other parameters are needed for the application of CDP for quasi-brittle materials in ABAQUS. These parameters are defined as follows:

- Dilation angle (Ψ): this parameter is essential because it controls the amount of plastic volumetric strain developed during plastic shearing and is assumed constant during plastic yielding. The value of $\psi=34^\circ$ corresponds to concrete's angle of internal friction, which is in agreement with previous numerical study (Mohamad and Chen, 2016; Santos et al., 2017) was adopted in this study. This is also supported by earlier research by (Lubliner et al., 1989).
- Eccentricity parameter (e): this value ranges from 0-0.1 from the theory of Drucker-Prager. A value of $e = 0$ means the yield surface in the meridian planes is straight line while $e = 0.1$ means the yield surface takes shape in the form of a hyperbola. For this study, a moderate eccentricity ($e = 0.05$) was assumed.
- Bi and unidirectional compressive strength ratio (f_{bo}/f_{co}): this is the ratio between the bidirectional and unidirectional compressive strength of masonry. Here, a value equal to 1.16 (ABAQUS default) was used. This corresponds to the fact that a cube test (effectively biaxial stress) returns values 15% higher than a cylinder test (uniaxial stress).

- Stress ratio in tensile meridian (k): is the ratio of the second stress invariant on the tensile meridian. It is applied for viscoplastic regularisation of the constitutive equation. The maximum principal stress evolution of the model has minor dependence on this K ratio. As such, the computational response of the model is not too sensitive to this value but a key requirement in Abaqus is that the value must be between 0.5 and 1.0. In this model, 0.67 ABAQUS default value was used because makes it a lot easier to avoid convergence issue with the models.
- Viscosity parameter: the primary function of this parameter is to facilitate the numerical analysis convergence process in ABAQUS without affecting the result. Based on a preliminary study, a low value of 10^{-5} is chosen here.

5.2.4 Properties of Brick-Mortar Interface

In the present case, the response of the assemblage is controlled mostly by the mortar tensile strength and fracture energy, which mainly depends on the interaction of the unit-mortar interface. In this model, the interaction between the brick units and mortar is defined in the interaction module of ABAQUS. Surface-to-surface contact was implemented in the model using the three contact behaviours explained below:

- Normal behaviour: hard contact behaviour normal to the surfaces is selected. The purpose is to prevent interpenetration of surfaces and to allow a separation between them once a contact has been established.
- Tangential behaviour: When surfaces are in contact, they usually transmit shear and normal forces across their interface (Fig. 5.7). Thus, the analysis needs to take frictional forces, which resist the relative sliding of the surfaces, into account. Here, Coulomb friction was used to describe the interaction of contacting surfaces. This model characterises the frictional behaviour between the surfaces using a coefficient of friction (μ). The penalty friction formulation used is $\mu = 0.75$.
- Cohesive Behaviour: Cohesive elements that are used in modelling of bonded interfaces in ABAQUS was employed in this study to define an elasticity characterisation. This was used directly in terms of the normal and tangential stiffness. Mohamad and Chen (2016) summarised that three different methods could define the mechanical behaviour of a cohesive element to set this cohesive interaction performance for quasi-brittle materials. These are

uniaxial stress-based, continuum stress-based, and traction-separation constitutive model.

The traction-separation method is the most adopted, and it is highly compatible with ABAQUS. Therefore, it was adopted in this study. Zhang et al. (2017) state that traction separation law involves three criteria in ABAQUS: linear elastic behaviour (Eqn. 5.21), a damage initiation criterion and a damage evolution law.

$$\begin{bmatrix} t_n \\ t_s \\ t_t \end{bmatrix} = \begin{bmatrix} K_{nn} & & \\ & K_{ss} & \\ & & K_{tt} \end{bmatrix} \begin{bmatrix} \varepsilon_n \\ \varepsilon_s \\ \varepsilon_t \end{bmatrix} \quad (5.21)$$

To estimate this linear elastic behaviour which is stiffness interface expressed as K's in the matrix in equation 5.21, many guidelines have been proposed. The most widely adopted approach found in literature is by specifying a quite high penalty stiffness (D'Altri et al., 2018) to remove any penetration between elements. In this study, the ABAQUS default penalty stiffness was used. This contact leads to stiffness degradation, in which it is only necessary to specify the interface mode I fracture energy (G_f^I). The value specified in this model is ($f_t = 0.36 \text{ N/mm}^2$ and $G_f^I = 0.012 \text{ N/mm}$) which was derived from the tensile behaviour of the interface (purple line) in figure 5.8 and showed a good agreement with experimental results obtained in (Pluijim, 1992; Lourenco, 1996).

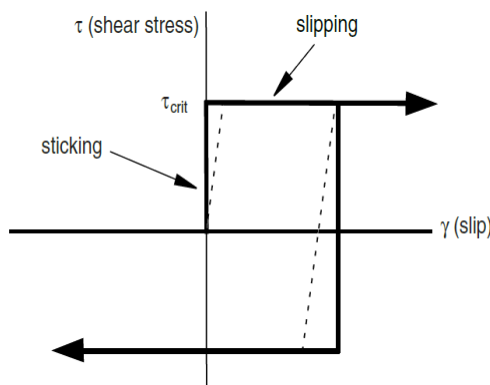


Figure 5.7: Friction behaviour (Simulia, 2014)

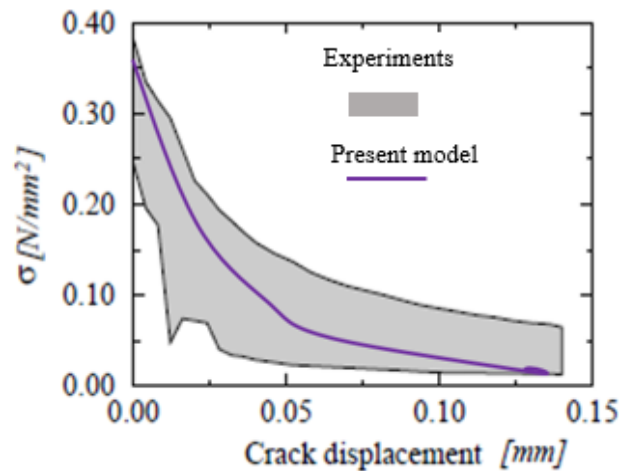


Figure 5.8: Tensile behaviour of present model vs experimental results from Pluijim (1992)

5.2.5 Input Parameter for Numerical Model

This section presents the mechanical properties of both the brick units and the mortar joint used in creating the models in table 5.1 and 5.2 respectively. The general parameter for damage-plasticity of the brick unit and mortar were also presented in table 5.3. After that, table 5.4 thus shows the contact behaviour (interfacial properties) of the mortar joints. In addition to all these parameters, the detail of the coefficient of both the compressive damage (d_c) and tensile damage (d_t) enforced in the ABAQUS was also given in appendix 5.1.

Table 5.1: Mechanical properties of the brick unit

<i>Elasticity parameters</i>			
Mass density (γ) in tonne/mm ³		2.2e ⁻⁹	
Young modulus (E) in N/mm ²		32470	
Poisson ratio (μ)		0.26	
<i>Plastic-damaging behaviour parameters</i>			
Compressive Behaviour		Tensile Behaviour	
Yield stress (N/mm ²)	Inelastic strain	Yield stress (N/mm ²)	Cracking strain
26.37	0.00000	5.93	0.00000
68.00	0.00713	4.76	0.00017
78.10	0.01013	3.54	0.00037
84.80	0.01313	2.07	0.00077
87.91	0.01688	0.87	0.00167
72.26	0.02813	0.51	0.00247
36.79	0.03183	0.22	0.00437
19.36	0.03633		
11.15	0.04113		

Table 5.2: Mechanical properties of mortar

<i>Elasticity parameters</i>			
Mass density (γ) in tonne/mm ³		2.17e-9	
Young modulus (E) in N/mm ²		19850	
Poisson ratio (μ)		0.2	
<i>Plastic-damaging behaviour parameters</i>			
Compressive Behaviour		Tensile Behaviour	
Yield stress (N/mm ²)	Inelastic strain	Yield stress (N/mm ²)	Cracking strain
1.79	0.00000	1.11	0.000000
3.13	0.00100	0.83	0.000418
5.00	0.00310	0.47	0.001318
5.82	0.00460	0.25	0.002518
6.52	0.00660	0.16	0.003418
6.97	0.00916		
7.10	0.01185		
5.75	0.02360		
3.48	0.03400		

Table 5.3: General parameter for damage-plasticity of brick unit and mortar

Dilation angle [degree]	34
Eccentricity parameter [\]	0.1
Bi and unidirectional compressive strength ratio [\]	1.16
Stress ratio in tensile meridian [\]	0.67
Viscosity parameter [\]	0.001

Table 5.4: Interfacial properties [contact behaviour of joints]

<i>Normal Behaviour</i>			<i>Tangential Behaviour</i>			
Hard contact			Coefficient of friction = 0.75			
<i>Cohesive Behaviour</i>						
Traction-separation stiffness coefficient			Damage Initiation (N/mm ²)			Evolution (Nmm)
K_{nn}	K_{ss}	K_{tt}	Normal	Shear I	Shear II	Energy
ABAQUS default			46.4	0.54	-	0.012

5.2.6 Calibration of the numerical model

The numerical model was calibrated through the following four steps:

- (i) First, reference material elastic properties were estimated based on the results of the compression test
- (ii) The Poisson’s ratio properties and coefficient of friction were further adjusted based on the comparison of the numerical results with those obtained in the experiments
- (iii) The CDP nonlinear material properties were adjusted based on the comparison of the stress-displacement envelope obtained with the one given in ABAQUS using the ductility index and fracture energy data available in many literatures (Pluijm,1992; Lourenco, 1996; Angelillo, 2014; Silva et al., 2018).
- (iv) Lastly, the influence of the mesh density i.e. the approximate global size of mesh was investigated (Fig. 5.9). The mesh sizes chosen were 2.5, 5, 7.5, 10 and 15mm. The loading and boundary conditions were kept the same throughout the mesh global seeds size variation.

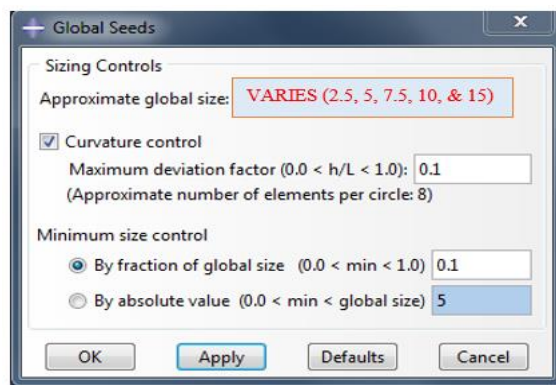


Figure 5.9: Mesh seed global size control (Simulia, 2014)

5.2.7 Results and discussion

Table 5.5 shows the result of the mesh sensitivity study. The analysis revealed that using a coarse mesh size (MS) of $\geq 15\text{mm}$ causes difficulty in obtaining convergence. The results were not acceptable due to a significant error and no convergence upon coarse mesh refinement. The results obtained from fine mesh sizes (2.5, 5, 7.5 and 10mm) converged well. The maximum stress obtained does not change significantly with a coefficient of variation (CoV) of 1.6% and agree with the experimental results. Since ABAQUS only allocates memory as needed during analysis, an increase in memory allocation was needed for computations when using smaller mesh sizes. For instances, when the mesh size was reduced from 10 to 5mm, the memory allocation was increased from 9.7GB to 15.9GB (64% increment). This increment implies that too dense mesh requires a large amount of computer memory and long run times, especially for nonlinear analysis of this type. Therefore, the most suitable mesh size considering the balance between accuracy, time and resources is MS10. The computational time with this mesh size is approximately 211secs with 98% accuracy to that of 5mm size mesh, which requires 738secs when using a computer equipped with a processor intel @ core™ i5-6400 CPU@ 2.70 GHz and 16 GB RAM.

Table 5.5: Mesh sensitivity results

Mesh size (mm)	Numerical	Experimental	Time (secs)	%Error (NM-EXP)/EXP
2.5	49.47	46.40	3435.00	6.61
5.0	48.91	46.40	1834.00	4.98
7.5	48.26	46.40	1043.00	4.01
10.0	47.75	46.40	211.00	2.91
15.0	42.81	46.40	143.00	-7.74

The influence of the mesh density was further investigated by comparing the stress vs strain plot for each mesh size, as shown in figure 5.10. Except for the case of MS15, decreasing the mesh size further produces only minor increases in peak stress and strain. For all the mesh sizes, the stress-strain curve has a good match up to 28N/mm^2 (60% of the maximum stress obtained experimentally).

This is the region where the model has a linear behaviour. However, for the non-linear region, the mesh sizes still produce comparable curves that predict the experimental value except for MS15. The obtained strength for MS15 is equal to 42.8 N/mm², which is lower than the experiment results. Therefore, a mesh size smaller than 15 is recommended. As such, MS10 was used in this study to save computational resources and time while still maintain the accuracy of the model.

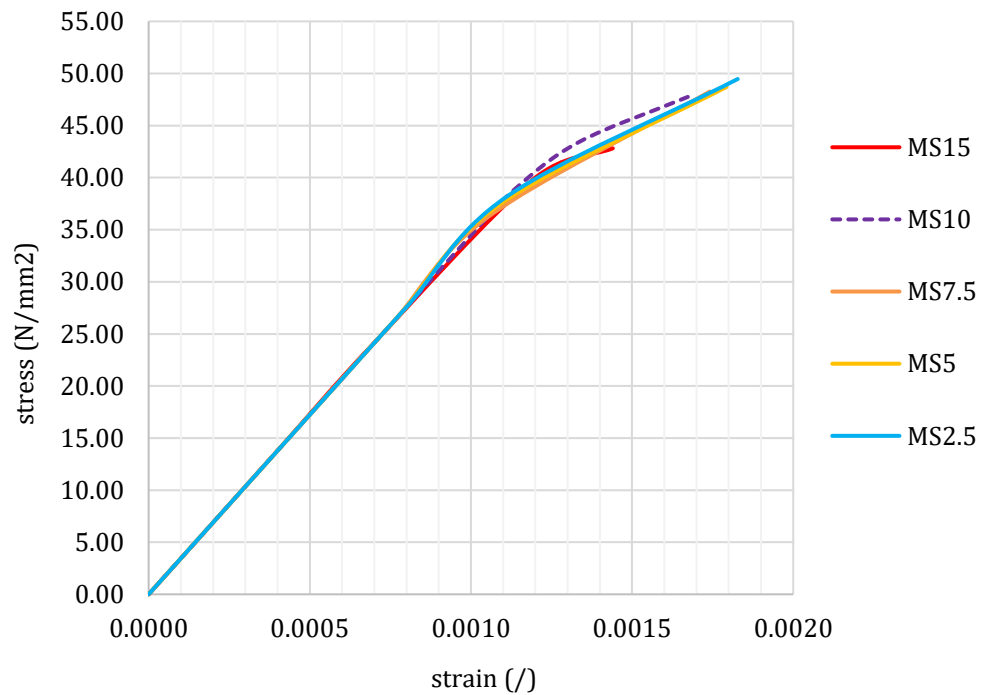


Figure 5.10: Influence of mesh density on the numerical model

Furthermore, the principal stress obtained from the analysis is compared to the average compressive strength of the specimens obtained experimentally. The maximum stress obtained from the numerical model is 48.7 N/mm². This value is only 5% different from the average compressive strength of masonry obtained from the experiment (46.4 N/mm²). Figures 5.11 below show the stresses contour and the damage contour plots obtained numerically for the masonry cubic specimen model.

Significantly, the failure mode observed in the model output (Fig. 5.11) is similar to what was observed experimentally with the maximum compressive stress occurring at the bottom edges of the cubic model. The stress diagrams in figure 5.11a & 5.11b also show that there is compressive stress in the bed joint and tensile stress in the perpendicular mortar joint. This tensile stress in the

perpendicular joint leads to lateral expansion of the mortar joint, which then induces high tensile stresses in the brick units.

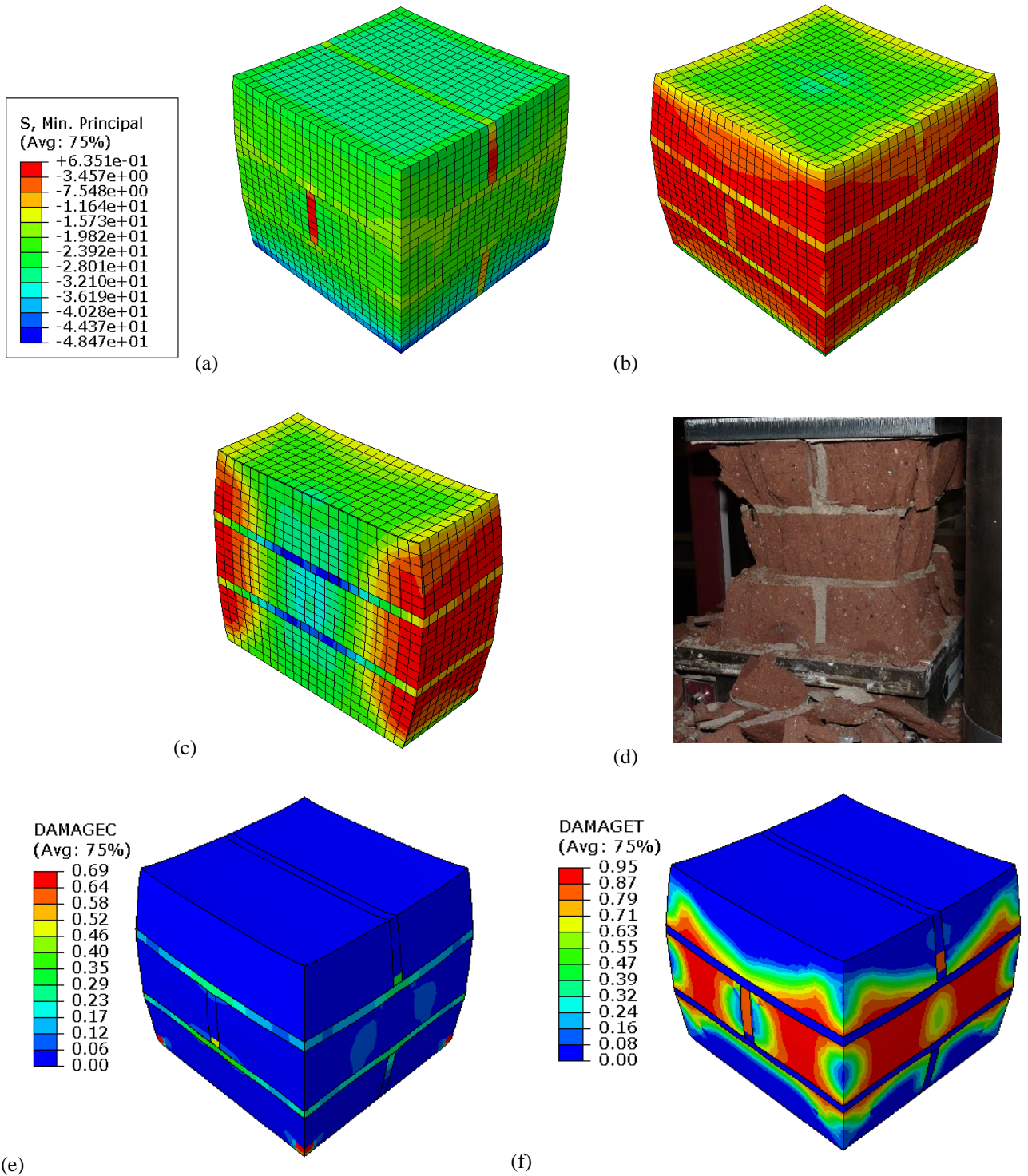


Figure 5.11: (a) minimum principal stress (b) maximum principal stress (c) view cut along y-plane to show stresses distribution in masonry cube (d) typical failure of specimen (e) compressive damage contour plot (f) tensile damage contour plot

Figure 5.11c shows a cut along y-plane of the cubic model to reveal the tensile stress distribution in the model. This figure shows areas of the cubic specimen where cracks are most likely to develop. The maximum principal stresses are an indication where cracks are expected to appear. The regions showing the highest values (colours tending towards red at edges of the model) can be associated with the development of cracks. In figure 5.11c, the areas with coral and red colour represent the region that split off during the experiment upon full crack formation as the load increases. The splitting off of these parts then leads to an *hourglass shape* specimen after the failure (Fig. 5.11d). Figure 5.11d can then be likened to the inner region of the obtained stress diagram shown in figure 5.11c. Despite the modelling limitation that prevents the part that split off during the test to break off from the model output, the portions of higher concentration of the stress are well consistent with the portion that split off in the experiment (Fig. 5.11c vs Fig.5.11d).

Additionally, to validate the agreement in the experimental failure with the numerical failure pattern, the damage pattern obtained by the developed numerical model is represented in term of compressive damage (DAMAGEC) and tensile damage (DAMAGET) contour plot (Fig. 5.11e & 5.11f). By comparing the numerical damage with the observed failure pattern, tensile damage and thus cracking of the brick unit is evidently visible in the central part of the cubic model (Fig. 5.11f). In particular, the tensile damage in the perpendicular mortar joint in the middle course identified in the experiment is clearly represented in the numerical output. Also, compressive damage plot (Fig. 5.11e) shows that the bed joints failed in compression. These observations are in good agreement with the ones observed in the experimental failure patterns.

In order to describe the full behaviour of the model under the continuous increase of load, stress-strain plot from static RIKS step (arc-length control) is shown in figure 5.12. The chart shows that the deformation (strain) increases as the stress increases until the peak stress is reached. After the peak stress is reached, softening, i.e. a gradual decrease of strength under a continuous increase in deformation is experienced. This is an ideal stress-strain relationship for a quasi-brittle material such as masonry cubic specimen under uniaxial compression. The stress-strain performances (Fig. 5.12) show a first linear

branch up to a stress of about 33N/mm^2 and strain of 0.006. The stress at this point compares with (31N/mm^2), the average stress obtained experimentally when the bricks start to split off) shows only 6% variation. To this effect, the stress-strain curve (Fig. 5.12) can be divided into two stages viz linear elastic branch (uncracked stage) and parabolic inelastic branch (crack formation stage). Each crack formation was associated with an increased strain until the peak load that causes the cubic specimen to fail by splitting is reached. The peak stress and strain obtained numerically are 49 N/mm^2 and 0.0018 respectively. The difference is within less than 5% of the average results obtained from the test.

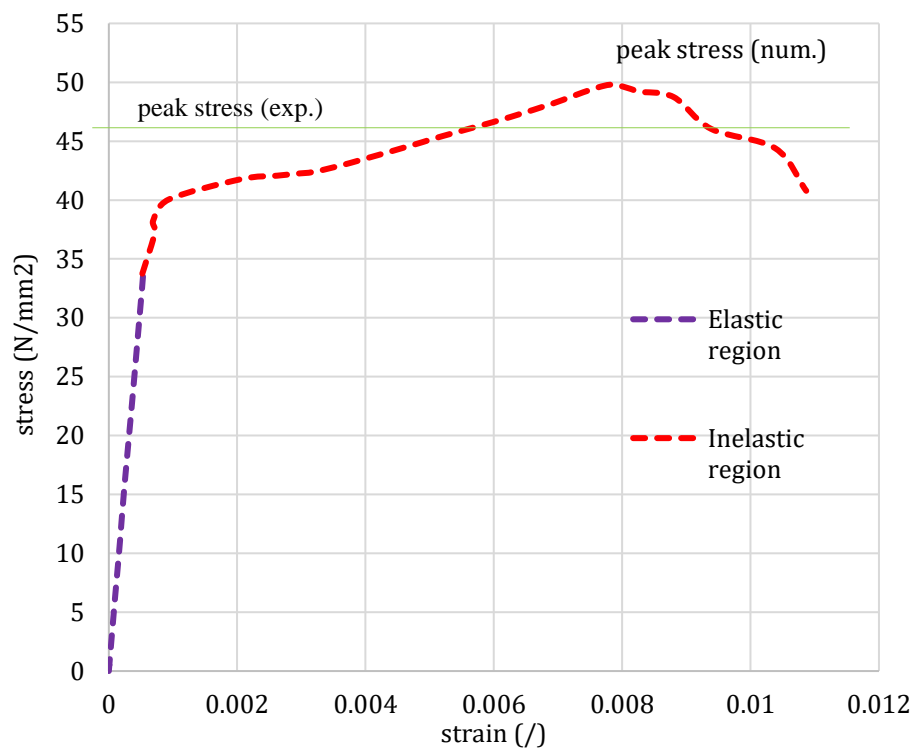


Figure 5.12: Stress-strain curve of masonry cubic model

5.3 Numerical Simulation of the Small-Scale Test: Flexural Bond Strength Test on Masonry Prism

An accurate finite element model and analysis of the four-point bending test was developed to corroborate the interpretation of the test results obtained from the flexural bond strength test on masonry prism (MP) provided in section 4.2. The main objective of this section is to develop a concise and efficient nonlinear 3-D finite element analysis to simulate the damage and failure pattern of the masonry prism tested in the laboratory. The adopted model was based on the simplified

micro-model technique described in figure 5b. The model was developed using commercial software ABAQUS FEA. The model was created with all the components in the four-point loading test properly modelled to obtain the best accurate results from the finite element analysis. The full description of the model, material properties and the interaction of the components considered in the model are as described in the subsequent sections.

5.3.1 Description of FE model

Two different models were created for the plain and retrofitted masonry prism, and the models were labelled as MP00-NM and MPOSB-NM respectively. The model identification follows the same style used in labelling the experimental specimens (i.e. MP00 for plain MP and MPOSB for OSB retrofitted MP). The addition of (NM) at the end is to indicate the reference to 'Numerical Model'.

5.3.1.1 Plain Masonry Prism Model (MP00-NM)

The plain MP model (MP00-NM) comprises of three components: brick unit, mortar and steel plate for load and support application. Each of these components was modelled as a separate part and assembled as shown in figure 5.13. The brick unit and mortar joint were model as 3-D deformable parts and meshed with a hexahedral 8-node linear brick, reduced integration, hourglass control (C3D8R) which has an improved convergence. The element has been identified in the ABAQUS library as a suitable type of element for nonlinear analysis including contact, deformation, plasticity and failure. The steel plate for load and support application was modelled using a 3-D discrete rigid element and discretised by rigid element R3D4 to represent a part that is so much stiffer (deformation negligible) than the masonry prism.

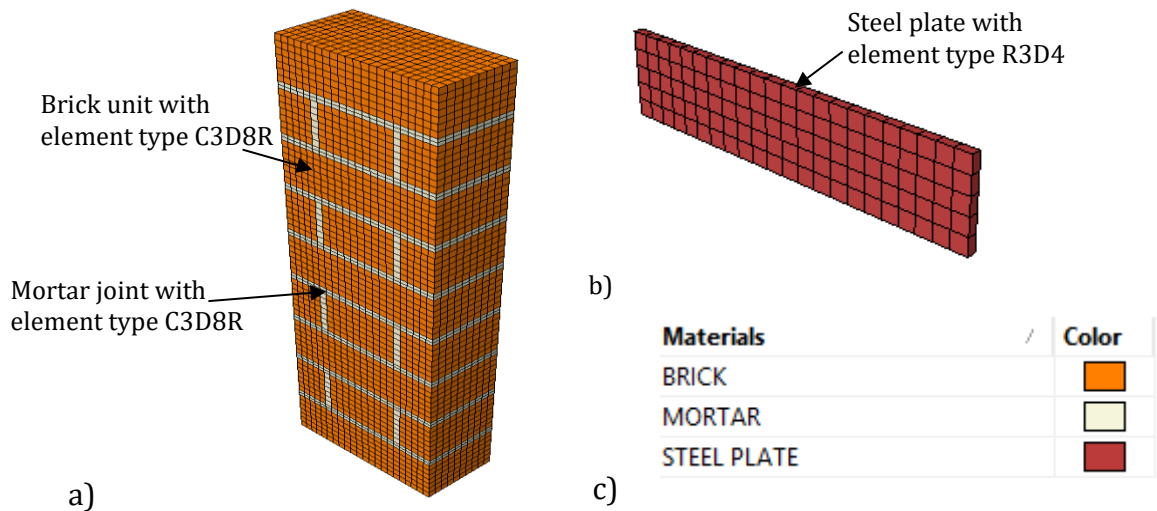


Figure 5.13: a) MP model comprising brick and mortar b) steel plate c) Material legend

5.3.1.2 Retrofitted Masonry Prism Model (MPOSB-NM)

For the retrofitted masonry prism model (MPOSB-NM), the bricks in the connection locations were partitioned and cut out at the region where the anchor rod will be placed before the assembly as done in the experiment. After that, two additional parts, which are the OSB timber panel and the anchor rod, were modelled as 3-D deformable parts and meshed with a hexahedral 8-node linear brick (C3D8R) (Fig. 5.14). The OSB timber panel was also cut out as done in the experiment. This represents a more rigorous model with comprehensive details to achieve accurate results.

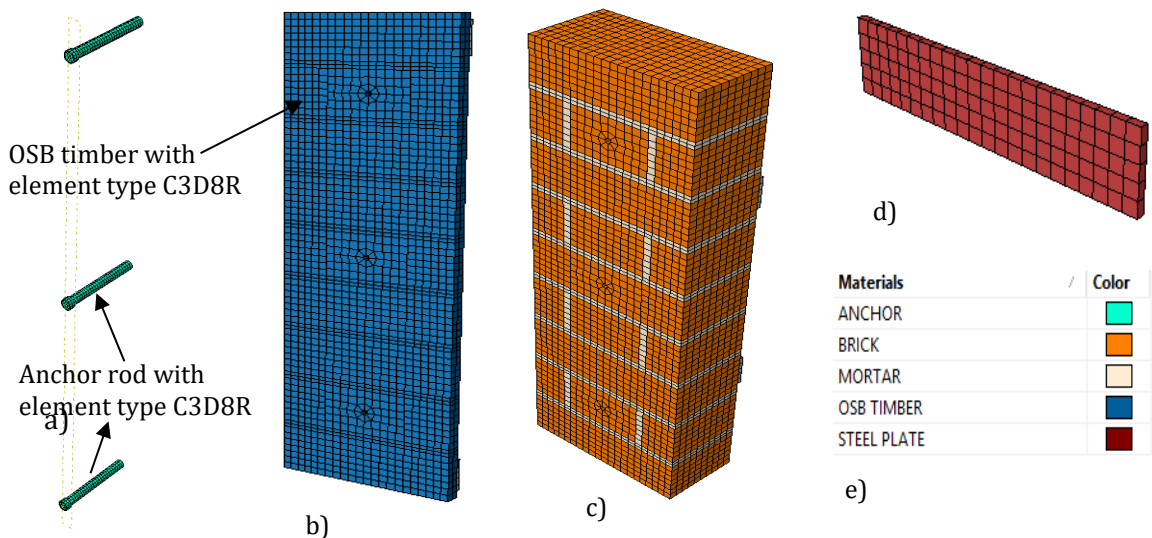


Figure 5.14: a) Anchor rod b) OSB timber c) MP model d) Steel plate e) Material legend

5.3.2 Interaction and Constraint Conditions in FE Model

The process to build the full model is such that an appropriate interaction and constraints between model components are implemented to represent the relationship between each component of the model. Since the simplified micro modelling strategy is employed here, the brick-mortar bond interface was not specified separately, so the brick continuum and mortar continuum were merged as shown in figure 5.15a. In order to place the loading at the front face of the model, the surface of the steel plate was tied to the surface of the brick at the 3rd and 7th course using tie constraints (Fig. 5.15b). Similarly, the steel plates were tied to the top and bottom brick at the back of the MP model as shown in figure 5.15c for the support application. The use of tie constraints ensured that the steel plate could not slip from the brick during analysis.

In the retrofitted model, the back-steel plates were tied to the back of the OSB (Fig. 5.15d). In addition to this, frictional, normal hard contact was specified between the surface of the OSB timber and MP model as shown in figure 5.15e. In this interaction, the friction coefficient was taken as 0.5, which is a typical coefficient of friction between timber and brick (Malhotra et.al, 2005).

For the anchor connection, the nodes on the surface of the brick around the connection holes were connected to the surface of the anchors using the default contact enforcement in ABAQUS (Fig. 5.15f). This connection ensures that there is a full adhesive bond between the anchor and the surface of the holes in MP. This kind of connection represents the retrofit system where the OSB timber panel is connected to the MP using adhesive anchor connection.

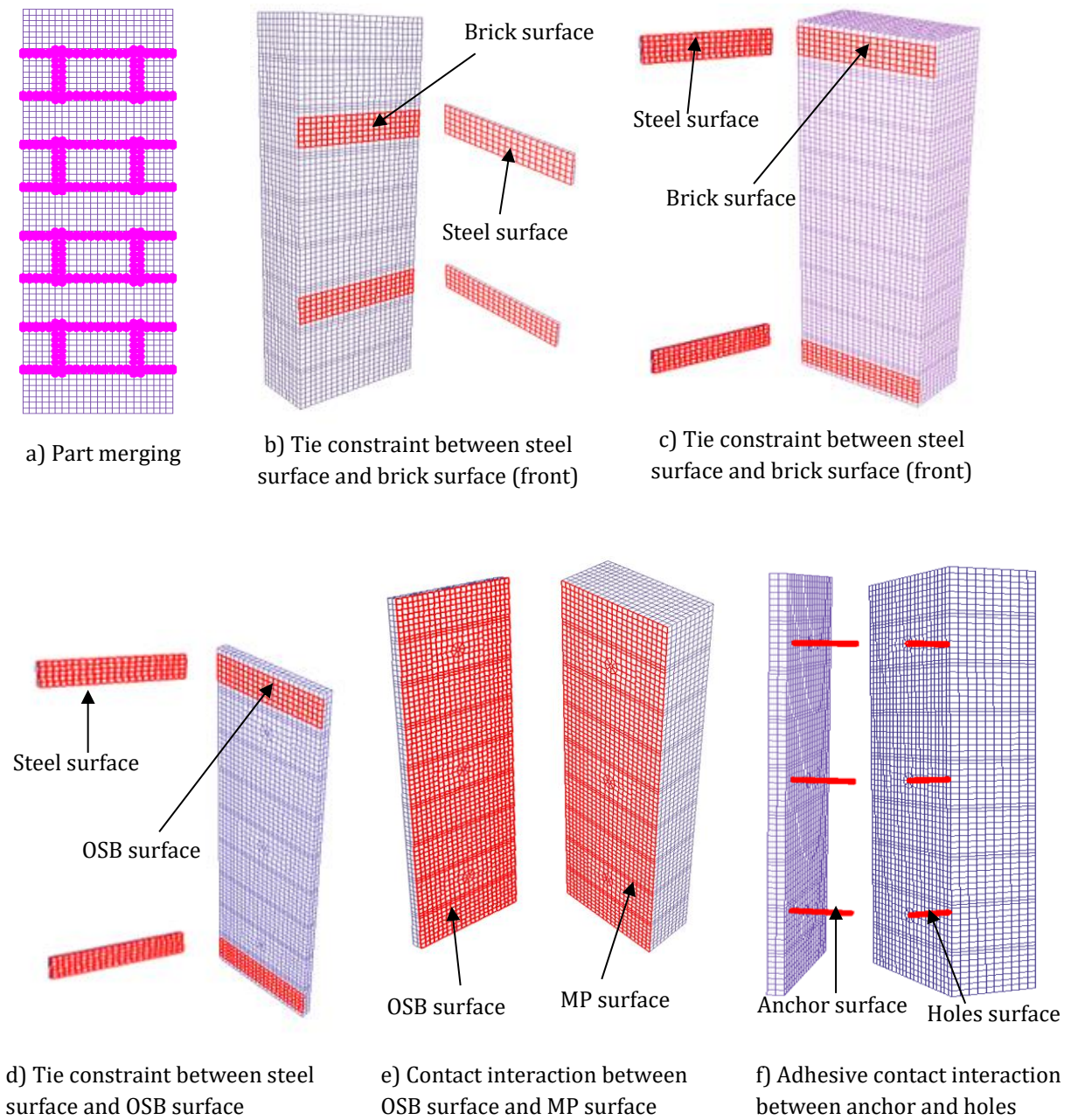


Figure. 5.15. Constraint and interaction surfaces in MP model

Finally, after all the interaction and the constraints have been applied to create the masonry prism model, the final assemblage of the plain and retrofitted model is shown in figure 5.16.

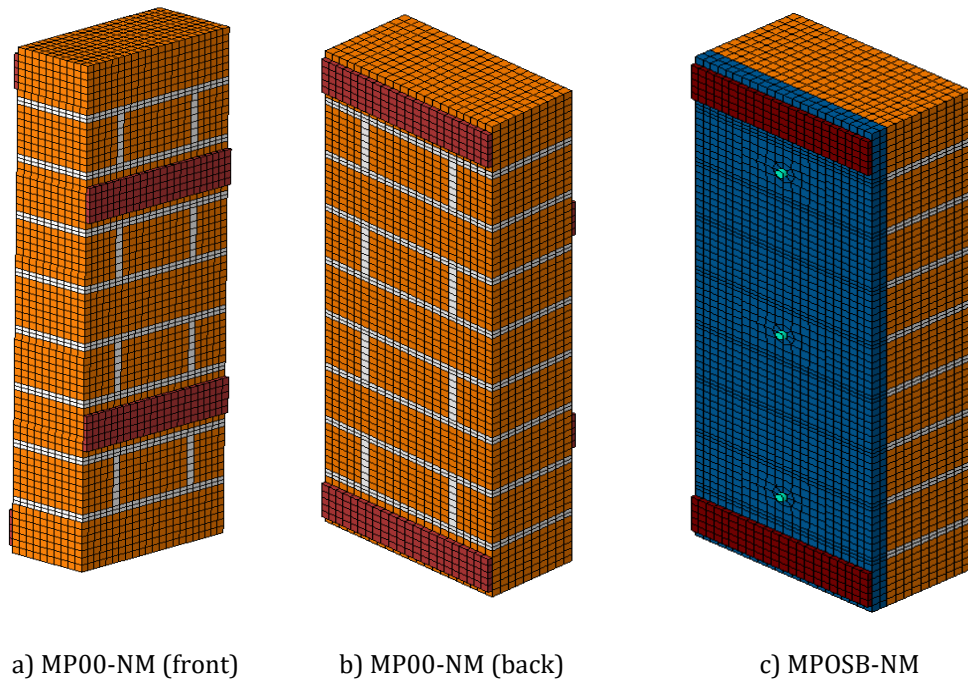


Figure. 5.16. General view of masonry prism model.

5.3.3 Boundary Condition and Loading

It is important to properly considerate wall boundary conditions in numerical simulation of the out-of-plane response of URM wall (Mendes et al., 2016). The models were constrained to replicate what was done experimentally to enable a sound basis for comparison of results. In the created models, the nodes at the middle of the back-steel plate at the top of the MP were restrained in x and z-direction. Also, the plate at the bottom was restrained in all the three directions (x, y, z) at the middle nodes to replicate the support condition of the tested specimen (Fig. 5.17a).

The loads considered in this analysis are self-weight and applied unit load in the out-of-plane direction at 3rd and 7th brick of the model. This loading and support arrangement is a replica of the four-point bending test carried out in the laboratory. The out-of-plane load is applied as a unit distributed load (UDL) on the steel plate tied to the front face of the model (Fig. 5.17b). The analysis is load control, similar to the test condition. The total load capacity of the model is measured as the load proportionately factor multiplied by the applied load in newton (N).

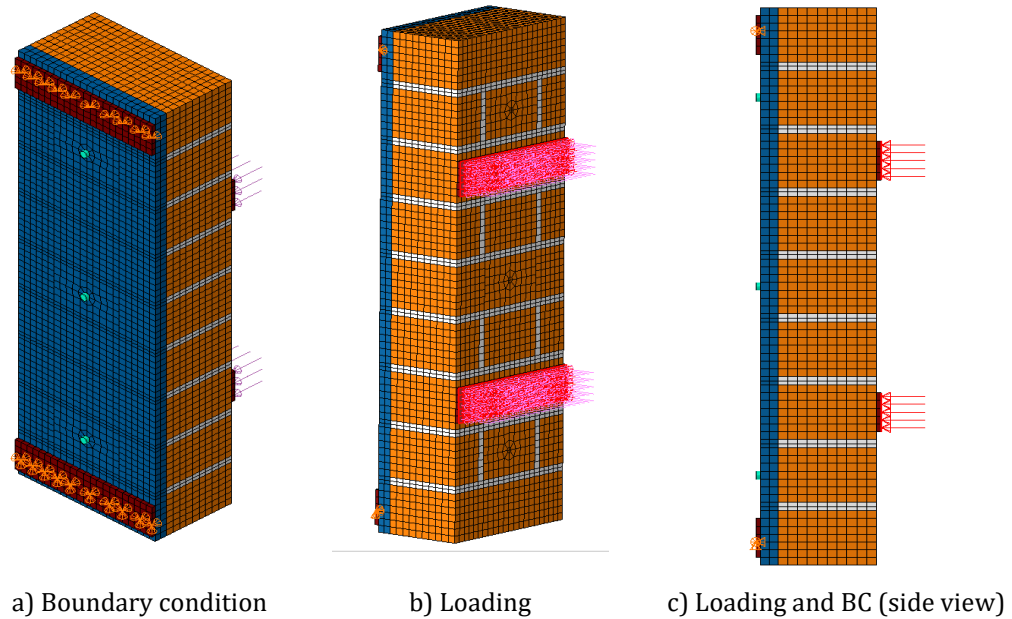


Figure. 5.17. Boundary condition and load application.

5.3.3 Analysis Method

In this study, the full behaviour of masonry prism model under a continuous increase of load in the form of load-displacement was obtained using the static RIKS method (arc-length control). The RIKS method was often used to investigate the behaviour of masonry wall under out-of-plane loading. RIKS method commonly referred to as the arc-length control method, and it is generally efficient in predicting the unstable and nonlinear collapse of structures. It is a load control analysis method. Since the test was also load controlled, it is thus an ideal analysis to validate the model with the obtained experimental data.

In the analysis using RIKS, the load is applied proportionally in several load steps. The equilibrium iteration is performed at each load increment, and the equilibrium path is tracked in the load-displacement space. This method is a robust method for nonlinear analysis, and it is capable of embedding the material damage property in the model. After performing the RIKS analysis, the damage pattern of the developed numerical model in term of compressive damage (DAMAGEC) and tensile damage (DAMAGET) were also obtained from the model.

5.3.4 Input Parameter for MP Model

The Concrete Damage Plasticity (CDP) constitutive model used to simulate the tensile and compressive non-linear behaviour of unit and mortar in numerical

simulation of the masonry cubic specimen (Section 5.2.2) was adopted here to create the MP model. However, the analysis consumed too much time and computer resource for a relatively well-detailed model such as the one presented here. This was due to the level of details presented in the model, which had all components modelled as separate parts and the need for the RIKS method to perform the equilibrium iteration. Also, convergence problems were encountered after the peak load due to the inclusion of material damage and too many contacts between the unit and mortar (unit/mortar interface). Therefore, the unit mortar interface interaction is then lumped into the properties of the mortar. This means that a new nonlinear property of mortar obtained through model calibration was used at this stage (Table 5.6). The input parameter for the brick units is the same as shown earlier in table 5.1.

Table 5.6: Mechanical properties of the mortar used for MP

<i>Elasticity parameters</i>			
Mass density (γ) in tonne/mm ³		2.17e ⁻⁹	
Young modulus (E) in N/mm ²		19850	
Poisson ratio (μ)		0.2	
<i>Plastic-damaging behaviour parameters</i>			
Compressive Behaviour		Tensile Behaviour	
Yield stress (N/mm ²)	Inelastic strain	Yield stress(N/mm ²)	Cracking strain
1.79	0.00000	0.319	0.00000
3.13	0.00100	0.296	0.01096
4.997	0.00310	0.258	0.02303
5.825	0.00460	0.220	0.03179
6.521	0.00660	0.198	0.04086
6.970	0.00916	0.099	0.05156
7.100	0.01185	0.049	0.06996
5.750	0.02360	0.025	0.09528
3.483	0.03400	0.012	0.11836
0.710	0.04800	0.006	0.34956

In addition to the properties of mortar and brick unit, the properties of the anchor connector and the OSB timber panel were also included for the creation of the retrofitted model (MPOSB-NM) were presented in table 5.7 and 5.8 respectively.

However, the failure of the retrofitted specimen during testing was mainly due to the failure of the mortar joint and subsequently the OSB timber, the anchor connector was then model as a pure linear elastic material. Table 5.7 below presents the elastic properties of the anchor connector used in the analysis.

Table 5.7: Mechanical properties of Anchor Connector used for MP

<i>Elasticity parameters</i>	
Mass density (γ) in tonne/mm ³	7.85E-09
Young modulus (E) in N/mm ²	210000
Poisson ratio (μ)	0.3

Table 5.8: Mechanical properties of OSB panel

<i>Elasticity parameters</i>			
Mass density (γ) in tonne/mm ³		6.5E-010	
Young modulus (E) in N/mm ²		3500	
Poisson ratio (μ)		0.24	
<i>Plastic-damaging behaviour parameters</i>			
Compressive Behaviour		Tensile Behaviour	
Yield stress (N/mm ²)	Inelastic strain	Yield stress (N/mm ²)	Cracking strain
1.98	0.0000	0.92	0.0000
6.60	0.0189	0.37	0.2957
5.28	0.0566	0.07	0.5027
4.22	0.1697	0.01	0.8545

In table 5.8, the nonlinear behaviour of the OSB timber panel is presented by an equivalent uniaxial stress-strain curve showing both the compressive and tensile stress behaviour. The elastic properties of the OSB type 3 used were obtained from the manufacturer specification. The nonlinear behaviour i.e. the stress-strain constitutive relation of the OSB was derived using guidelines from Chen & He (2017). After applying all the inputs mentioned above in the model, the developed FE model was calibrated against the experimental data. This allows the model to adequately capture the failure load and load-deflection response of the retrofitted MP, using the quasi-brittle constitutive law for the OSB.

For the calibration process, the properties of brick and mortar were not adjusted at this stage, because they were well-calibrated in the plain model (MP00-NM). Also, the material elastic properties obtained from manufacturer specification and the derived compressive crushing strength of OSB were kept constant. Only the tensile cracking, i.e. (yield stress (N/mm²) and cracking strain) were adjusted based on the comparison of the load-displacement envelope obtained in four-point bending test of MP with the obtained load-displacement curve from the performed RIKS analysis.

5.3.5 Results and Discussion

5.3.5.1 MP00-NM compared with MP00 Test Results

Figure 5.18 below shows the failure of the model alongside the actual damage specimen obtained from the test. The comparison shows that the failure occurred in the bed joints within the inner bearing (i.e loading span) of the specimen. In the actual test, the total failure occurred in one bed joint (Fig. 5.18a), but the numerical model shows the failure in two symmetrical bed joint (Fig. 5.18b). This is because of the numerical model created to have the same property for all joints, which is not possible in the test due to variation during specimen construction. Hence, the symmetrical joints in the model will experience the same load, and thus the failure will be simultaneous. Whereas, the failure occurred in the weakest joint during the experimental test.

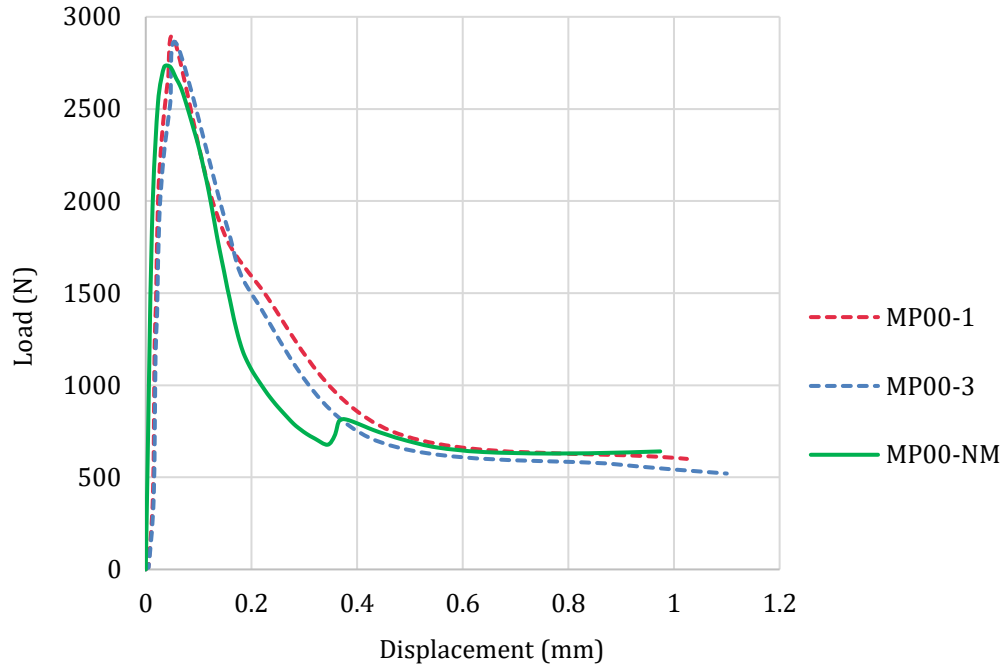


Figure. 5.19. Load displacement curve for plain MP (Experimental vs Numerical)

Table 5.9: Comparison of model and test average results

	Test average	Model	% Difference
Peak Load (N)	2857	2723	4.6
Corresponding Displacement (mm)	0.058	0.056	3.4
Toughness (Nmm)	1050	1020	2.9

5.3.5.2 MPOSB-NM compared with MPOSBC1 Test Results

In this section, the developed model for the retrofitted specimen (MPOSB-NM) is validated by the results of the tested masonry prism retrofitted with adhesive anchor connection (MPOSBC1). The comparison shows that the failure started in the bed joint of masonry prism within the inner bearing before propagating to the OSB timber. The failure plot (DAMAGET) at a load of 5340N which corresponds to the average load that the first crack failed completely in MPOSBC1 is presented in figure 5.20a. The damage plot shows that the mortar bed has failed but the OSB at the back of the model show resistant to this load with little deformation. The inference from the model behaviour shows that the application of the OSB timber panel at the back of the MP increased the resistance of the model. After the analysis has been completed, the final damage plot (Fig.

5.20b) and the corresponding load vs net out-of-plane displacement for the model were plotted and compared to the experimental results (Fig. 5.21).

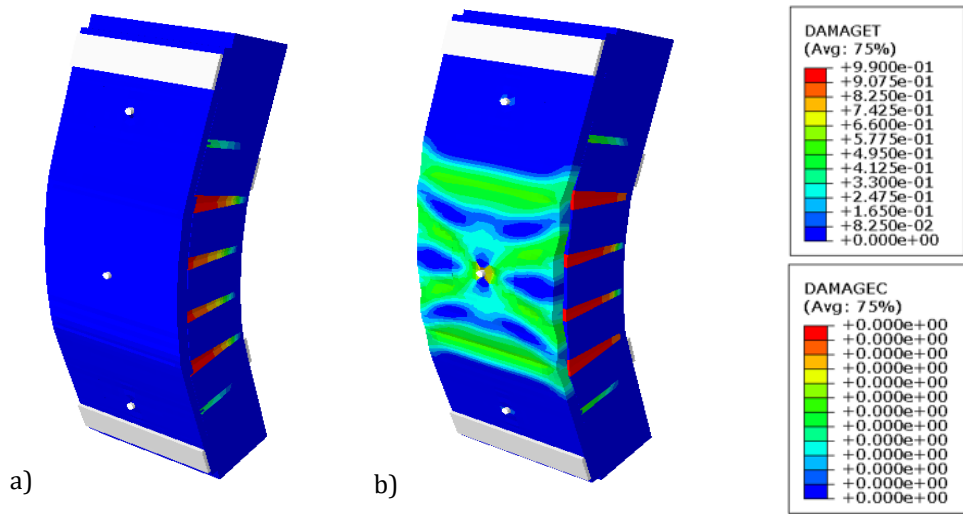


Figure. 5.20.a) Observed failure of MPOSB-NM

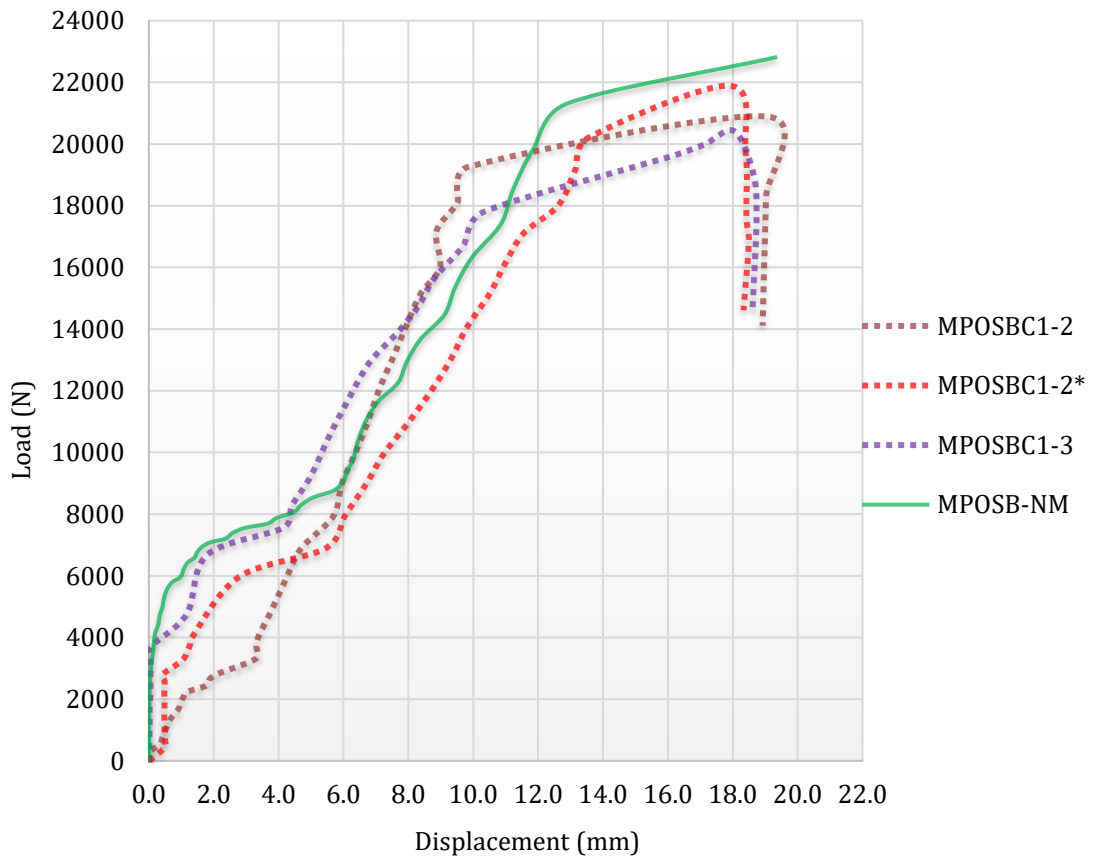


Figure. 5.21. Load displacement curve for retrofitted MP (Experimental vs Numerical)

On the load-displacement curve shown in figure 5.21, a similar numerical load-displacement profile was obtained for the model. The curve shows the behaviour of the specimen at the initial elastic phase where the OSB and the masonry are bonded together before the crack initiated at an average load of 3640N for tested

specimen and 3842N (5% variation) for the numerical model. This phase then followed by the complete failure of the joint in the masonry prism at an average load of 7982N and 8365N (4% variation) for the test and numerical specimen respectively. The final phase of the curve then presents a region where the masonry part has failed and the OSB is taking the load up to the failure of the OSB. The toughness, loads at different phases, maximum load and corresponding displacement at the failure of the model are within less than 5% of the average test results (Table 5.10).

Table 5.10: Comparison of model and test average results

	Test average	Model	% Difference
Peak Load (N)	21068	22120	5
Corresponding Displacement (mm)	18.74	19.37	3.3
Toughness (Nmm)	257333	271000	5

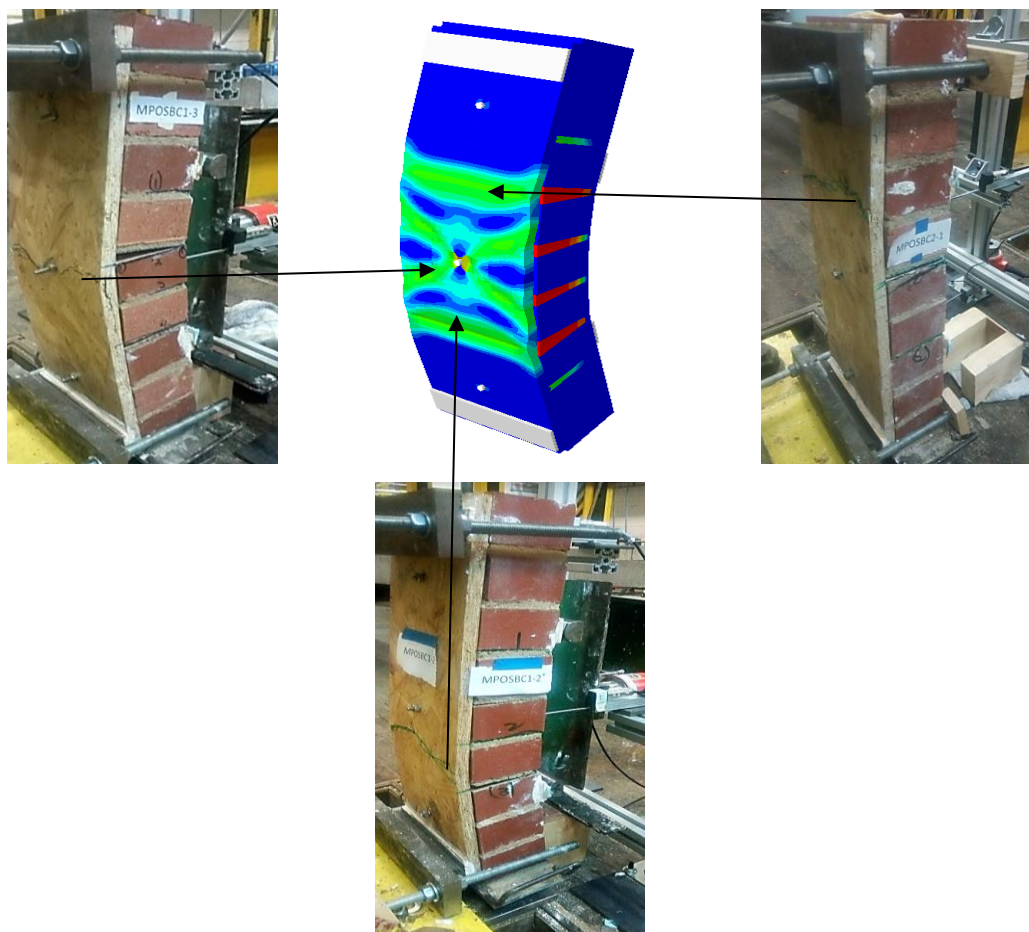


Figure. 5.22 Observed failure of MPOSB-NM vs MPOSB1

Finally, in figure 5.22 above, the damage pattern showing the failure pattern that was observed during the experiment, the location and type of failure observed in the model output were compared with the experimental observation as highlighted. In the model, the global damage pattern shows all the areas where crack and failure occurred in all 3 tested specimens. This indication and analysis show that the model is in good agreement with the experimental results. As such, the model is extended to the larger-scale test in section 5.4.

5.4 Numerical Simulation of Larger-Scale Test: Flexural Strength of Masonry Walls

In this section, the finite element analysis to simulate the larger-scale test is presented. Similar to the numerical simulation of the small-scale test performed in section 5.3, the model was created with all the components in the experimental setup included. Three different models were created, each for the plain wall (PW1115-NM), one side retrofitted masonry wall (1SRW1115-NM), and two sides retrofitted masonry wall (2SRW1115-NM) as shown in figure 5.23-5.25. The model creation follows the same process with the brick unit and mortar joint modelled as 3-D deformable parts and meshed with a hexahedral 8-node linear brick (C3D8R). The steel plate for load and support application was also modelled using 3-D discrete rigid element (R3D4). The interaction between components and boundary condition is the same as in the MP model (Fig. 5.15).

Figure 5.23-5.25 below shows the general arrangement, the boundary condition and the loads applied to the three models. Due to the symmetry of the wall specimen, only half of the four-point loading test arrangement was modelled. For this reason, another boundary condition (i.e. ZSYMM (U3=UR1=UR2=0)) was placed in the Z-axis to instruct the symmetry in the specimen. The analysis is load control, similar to the test condition, and the total load capacity of the model is measured as the load proportionately factor multiplied by the applied load.

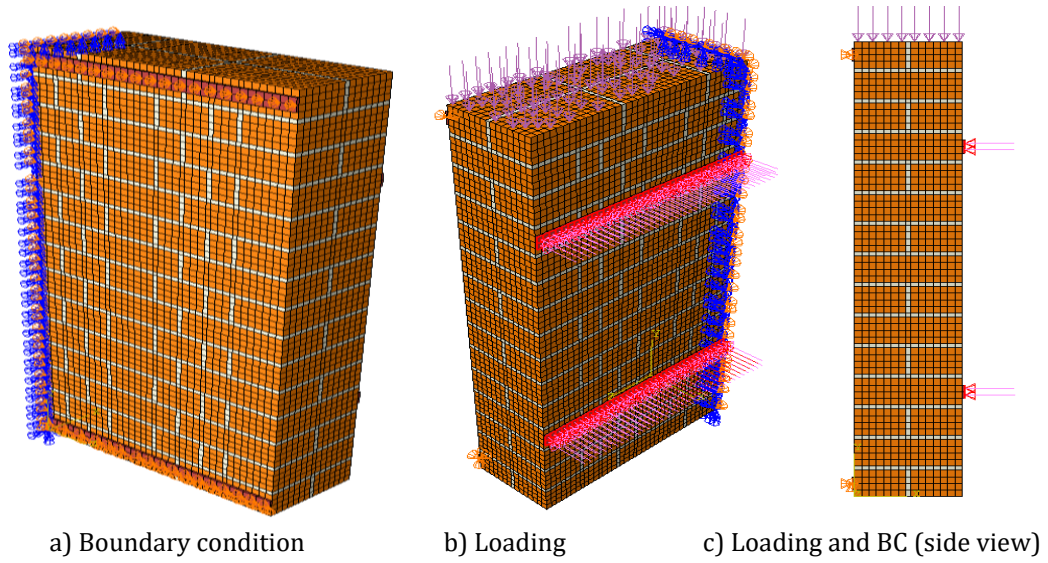


Figure. 5.23. Boundary condition and load application on PW1115-NM

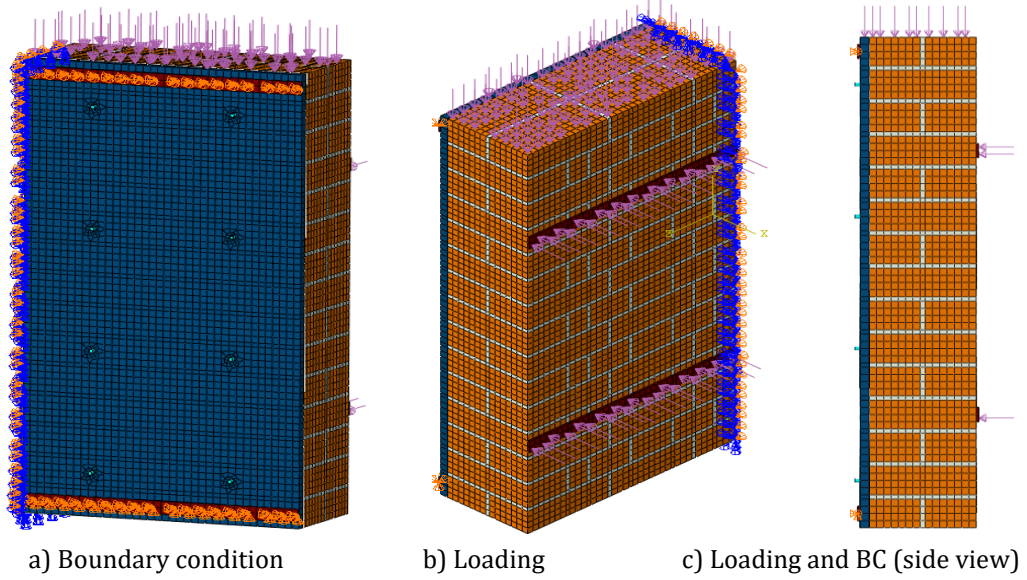


Figure. 5.24. Boundary condition and load application on 1SRW1115-NM

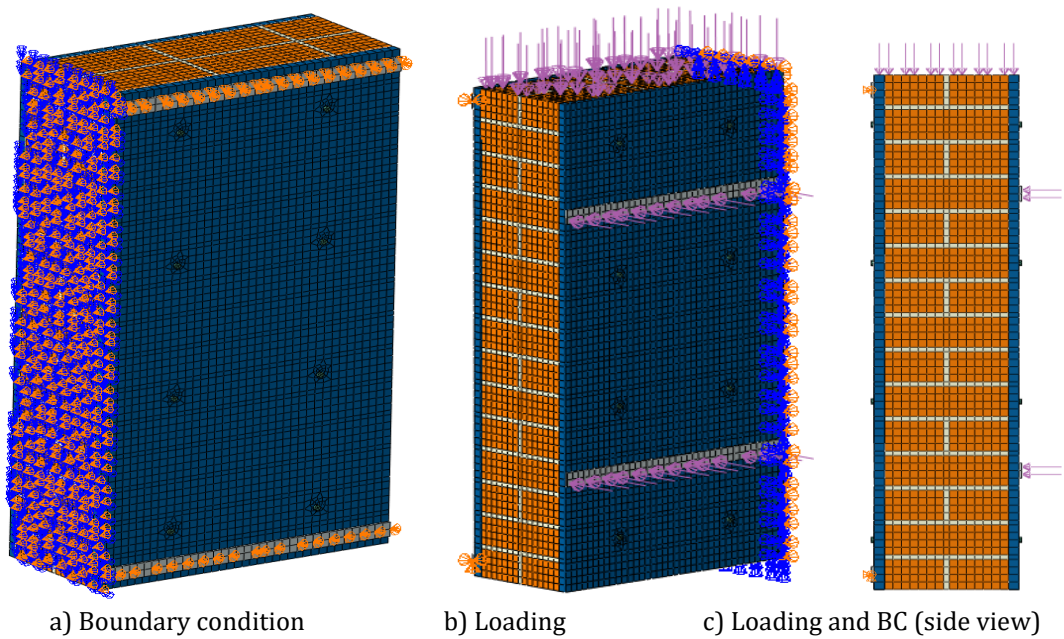


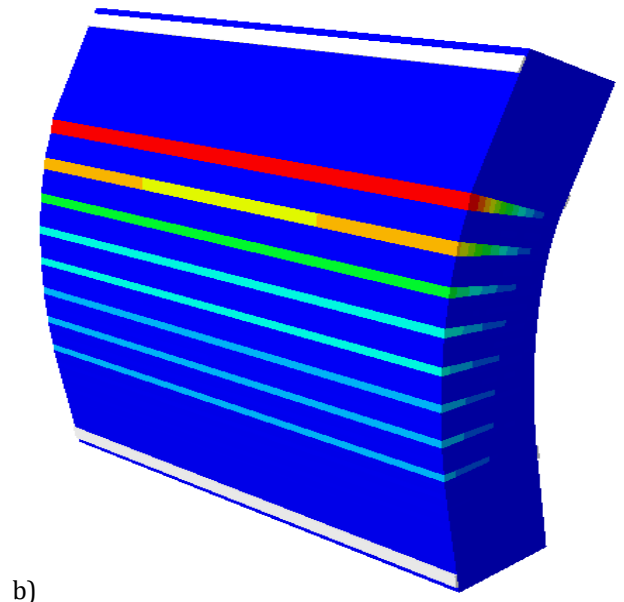
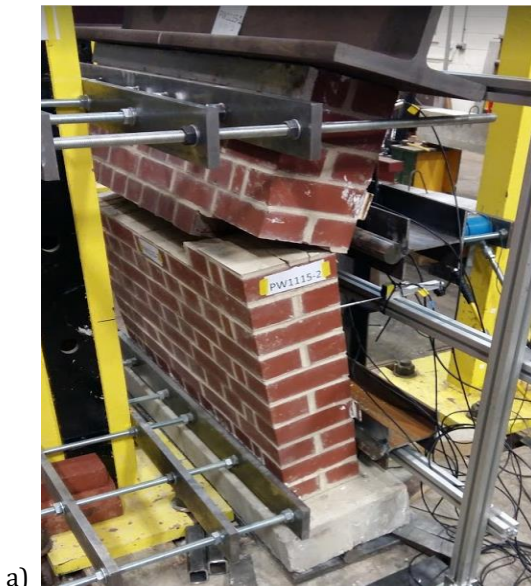
Figure. 5.25. Boundary condition and load application on 2SRW1115-NM

5.4.1 Results and Discussion

5.4.1.1 PW1115-NM compared with PW1115 Test Results

The result obtained from the numerical simulation of the plain wall was compared with the test results in term of both the capacity and failure mode. The comparison shows a relatively good agreement between the numerical and experimental results. Figure 5.26 below shows the failure of the model alongside the actual damage specimen obtained from the test. The comparison indicates that the specimen failure occurred in similar bed joints, which is in the 9th and 10th row of the experimental specimen.

Correspondingly, the tension damage in the model is maximum in the 10th row. The failure in the test specimen crossed the perpendicular joint due to the weaker zone in perpend joint. This weakness was not observed in the numerical model because the property of the mortar joint is the same for the bed joint and perpend joint. Indeed, the bed joint is the one in maximum tension during loading. The experimental failure was only due to variance in the specimen joint during construction which makes the joint in that zone weaker than the bed joint.



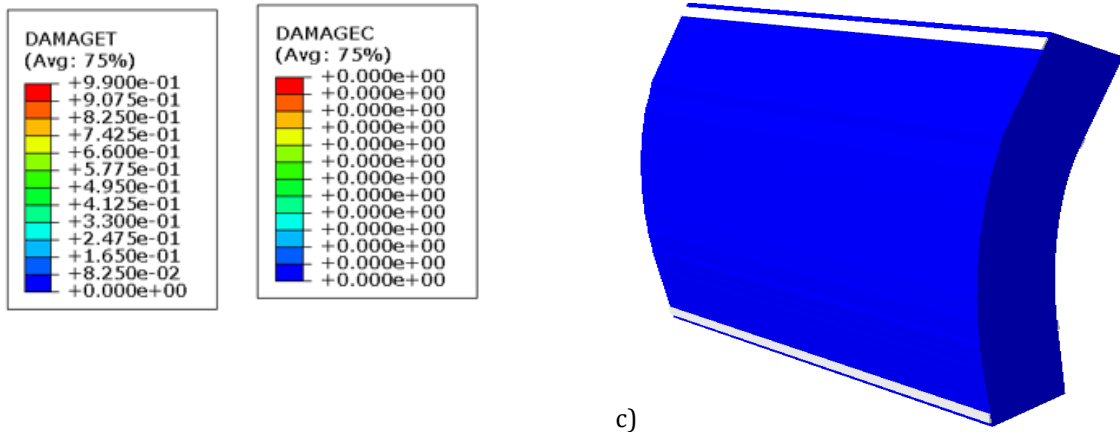


Figure. 5.26.a) Observed failure b) PW1115-NM (DAMAGET) c) PW1115-NM (DAMAGEC)

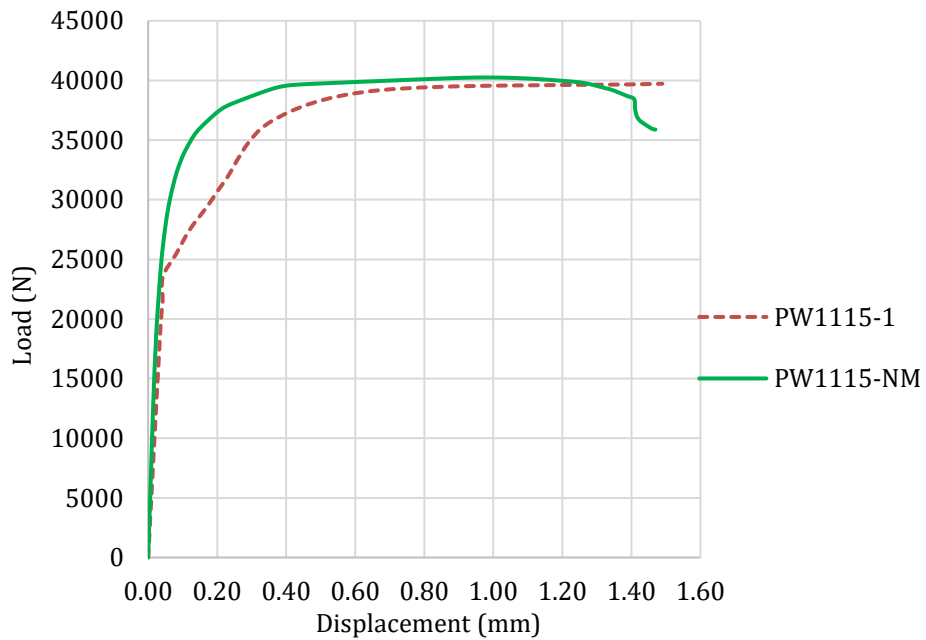


Figure. 5.27. Load displacement curve for Plain Wall (Experimental vs Numerical)

Furthermore, the load-displacement curve obtained from both numerical analysis and the experimental test is presented in figure 5.27. The toughness, maximum load and corresponding displacement at the failure of the model are within less than 5% of the average results obtained from the test (Table 5.11). This analysis means that the developed model is in good agreement with the experimental results. Although there is a little variance in the displacement from when the applied load is 24kN upward (Fig 5.27), this variation is due to the movement of the wall during testing at the initiation of the crack. This behaviour was noticed during the experiment, and it is not normal behaviour of the specimen but due to the test arrangement. However, since the numerical model assumed a perfect arrangement, the response is not captured and will be ignored.

Table 5.11: Comparison of model and test average results (PW)

	Test average	Model	% Difference
Peak Load (N)	39025	40150	2.8
Corresponding Displacement (mm)	1.50	1.45	3.3
Toughness (Nmm)	54750	56000	2.3

5.4.1.2 1SRW1115-NM compared with 1SRW1115 Test Results

The numerical failure of the 1SRW model was compared alongside with the damaged specimen from the test in figure 5.28. The damage pattern shows that the OSB panel at the back of the specimen failed after the mortar joint has failed. The location at which the OSB failed in the model is similar to what was observed in the test with the failure point been within two rows of connection.

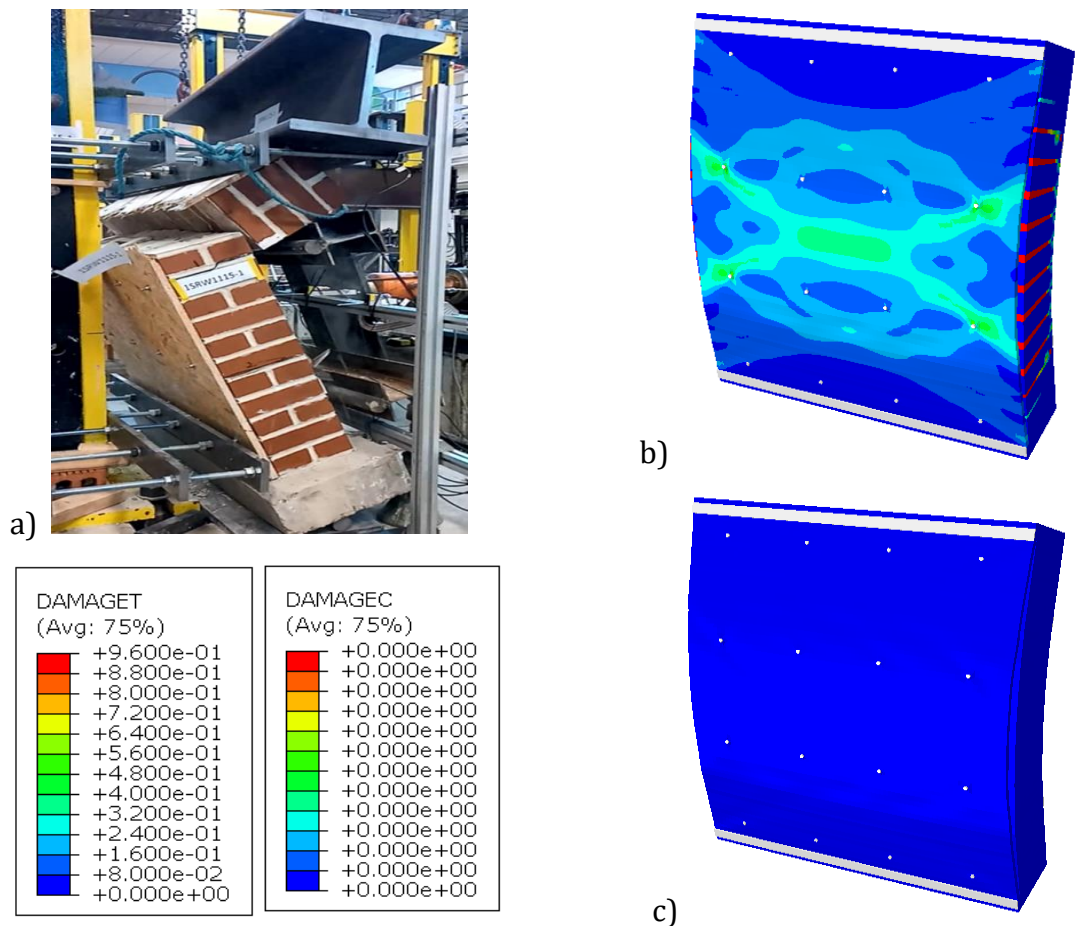


Figure. 5.28.a) Observed failure b) 1SRW1115-NM (DAMAGET) c) 1SRW1115-NM (DAMAGEC)

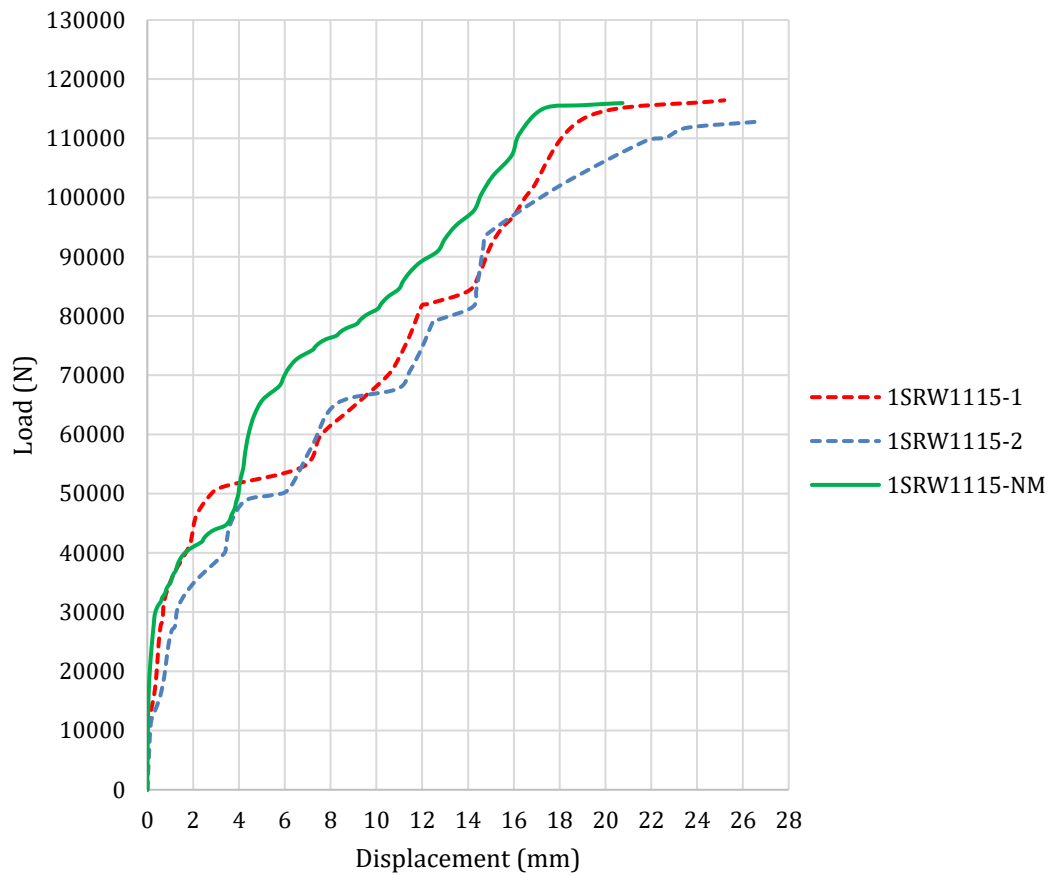


Figure. 5.29. Load displacement curve for 1SRW1115 (Experimental vs Numerical)

Similarly, load-displacement curves were compared in figure 5.29. The maximum load and the corresponding displacement of the numerical model compared well against the experimental results. The difference in the peak load is within less than 2% of the average test results as shown in table 5.12. However, the difference in the out-of-plane displacement from the test and model is about 8.3% which is still less than 10% and it is acceptable. The variation in the displacement of the numerical model from the test behaviour is obvious from the load-displacement curve in figure 5.29. This behaviour is attributed to the difficulty in the stability of the specimen during the experiment when the walls begin to damage. This can be ascertained from the fact that the curves compared well up to around 50000N load, which is where the specimen failure started.

However, another clear observation from the curve comparison is that the experimental curves have a clear set of steps, owing to the sequential failure of the bed joints and subsequent redistribution of the load to the OSB up to the failure of the OSB, which corresponds to the failure of the overall specimen. This is much less pronounced in the NM curve. This is because the failures of the bed

joints in the model are concurrent except for the joints in the 7th and 8th row which have failed at an average load of 52750N and 48551N (8% variation) for test and numerical model. For this reason, the load redistribution is not obvious in the model because of the smooth transition in the model which is not possible in the experiment due to the possible variation in the mortar joint during construction.

Table 5.12: Comparison of model and test average results (1SRW)

	Test average	Model	% Difference
Peak Load (N)	114622	115979	1.1
Corresponding Displacement (mm)	20.78	17.29	8.3
Toughness (Nmm)	1942500	1750000	9.9

5.4.1.3 2SRW1115-NM compared with 2SRW1115 Test Results

Similar to the previous two models, the observed failure pattern for both the numerical and experimental specimens were compared for the two-sided retrofitted specimens, as shown in figure 5.30. The failure pattern of the developed model is in good agreement with the experimental failure. The damage pattern indicates that the OSB panel at the back of the specimen failed after the mortar joint has failed. The location at which the OSB failed in the model is similar to what was observed in the test with the tensile stresses spreading across the middle of the panel. The OSB in the compression face does not fail as also seen in the experiment. The damage shown on the OSB on the compression side (i.e. loading face) was only occurred after the failure and as such, not replicated in the model.

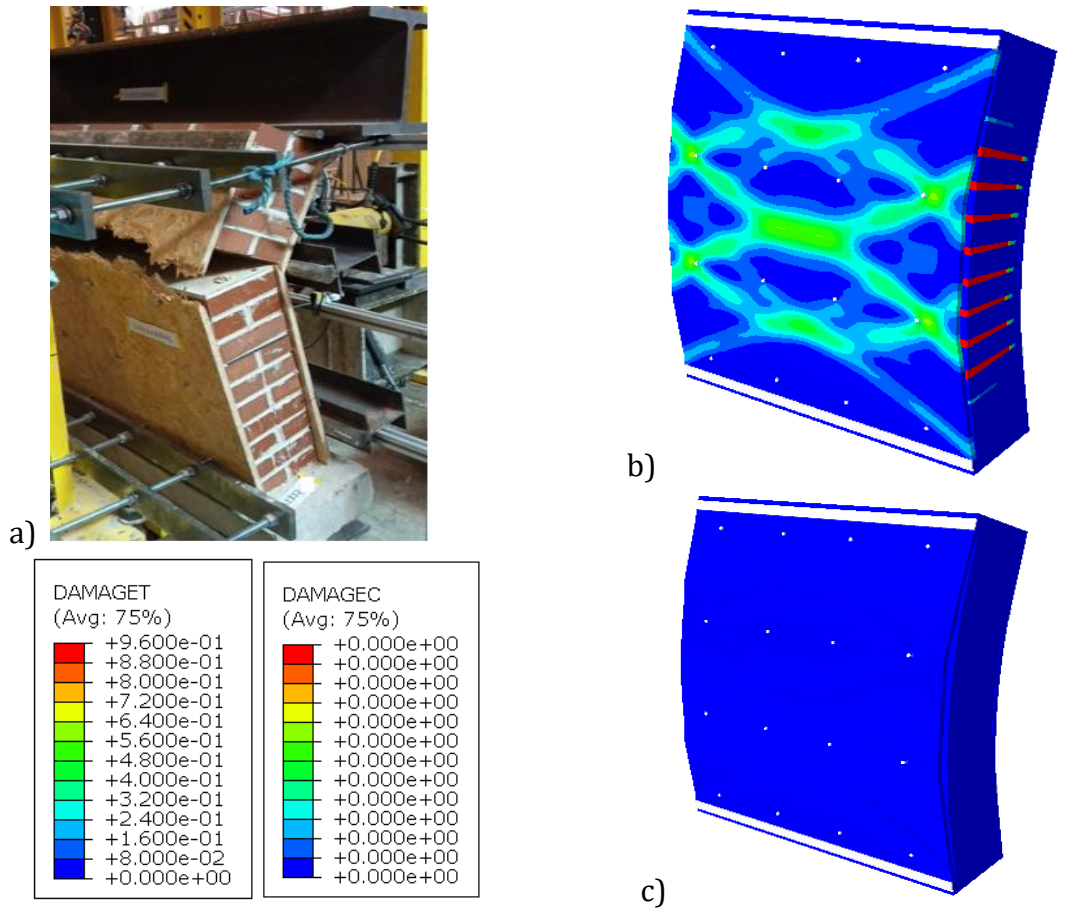


Figure. 5.30. a) Observed failure b) 2SRW1115-NM (DAMAGET) c) 2SRW1115-NM (DAMAGEC)

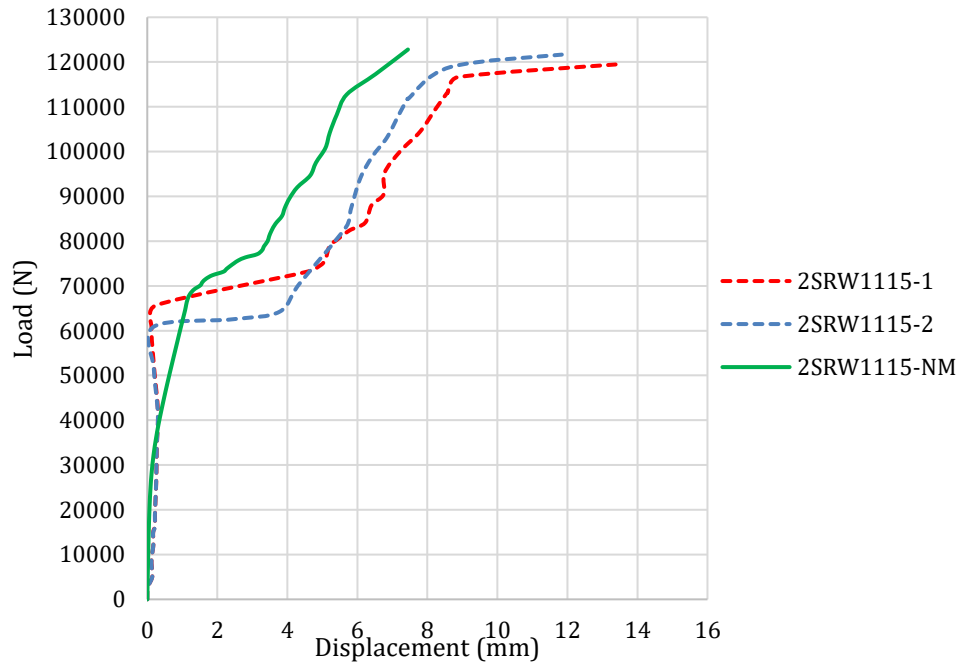


Figure. 5.31. Load displacement curve for 2SRW1115 (Experimental vs Numerical)

In addition to the comparison of the damage plots, the load-displacement curve for both the experimental and numerical model is presented in figure 5.31. Again, the difference between the NM and experimental curve, especially at the dilatant parts of the curve after 65000N and subsequent steps represent the jump in the

displacement of the specimen. This jump has been attributed to the stability issue in the specimen, which happened after the joint bed failed during testing. The inference from the load-displacement curves means that the developed model agrees with the experimental results. The difference in the maximum load and corresponding displacement of the numerical model and the experimental results is also within less than 10% of the average test results in table 5.13.

Table 5.13: Comparison of model and test average results (2SRW)

	Test average	Model	% Difference
Peak Load (N)	120559	122803	1.8
Corresponding Displacement (mm)	8.25	7.45	9.3

5.5 Parametric Study

This section presents the numerical parametric study on the developed model for the larger-scale retrofitted masonry wall described in previous section 5.4.

Table 5.14: Parametric study model identification

Group	Model Label	Variable	Constant
1	1SRW-18-T-16A	The side where OSB applied	18mm thick OSB used with 16 anchor connection
	1SRW-18-C-16A		
	2SRW-18-B-16A		
2	1SRW-10-T-16A	Thickness of OSB	All OSB applied on the tensile face with 16 anchors
	1SRW-18-T-16A		
	1SRW-25-T-16A		
3	1SRW-18-T-6A	Number of connections	18mm thick OSB applied on the tensile face
	1SRW-18-T-12A		
	1SRW-18-T-16A		

1SRW-18-T-16A means 18mm OSB applied on the tensile side using 16 anchors

C and T means application on the compression and tensile side respectively

B means application on both sides

The parametric study investigates 3 variables: (a) the OSB position, (b) the influence of the OSB thickness and (c) the number and spacing of connections. In total, nine models were created and compared as shown in table 5.14.

5.5.1 Influence of the application position of the retrofit

In order to have a better understanding of how the application of the proposed OSB timber retrofit technique influences the behaviour of the masonry wall, three applications have been investigated through the numerical model. The application with the OSB on the compression side (1SRW-18-C-16A) results in poorest performance showing no significant increase in the load capacity of the retrofitted wall. Although, the application on the compression side allows the wall to resist more out-of-plane displacement, unlike the plain model where the failure is brittle with negligible displacement before the collapse. The application on the tensile side (1SRW-18-T-16A) and both side (1SRW-18-B-16A) improved the out-of-plane capacity of the wall significantly. However, 1SRW-18-T-16A has reduced out-of-plane displacement resistance compared to 2SRW-18-B-16A.

In order to evaluate the efficiency of the application further, both limiting and overall toughnesses were obtained from the curve as done with the experimental results. The analysis reveals that the application on the compression side of the wall does not improve the load resistance capacity of the wall. Nevertheless, it shows a significant increase in the toughness of the retrofitted wall (15PW) when the allowable limit for the out-of-plane displacement of the wall is considered. Meanwhile, the application on the tensile sides shows an increment in the load capacity (2.9W), limiting toughness (18.6PW) and overall toughness (31.3PW) as shown in figure 5.33.

Although, in term of the load capacity, the 1SRW-T and 2SRW-B carried approximately equal load, but the 2SRW-B shows a better limiting toughness than the 1SRW-T (about 1.5 times that of 1SRW-T). This observation reveals that the double side application has more limiting toughness and lesser overall toughness than single-sided application (Fig. 5.33). Therefore, the double-sided application has more resilient in the allowable range and is thus recommended for improving the earthquake resilient of masonry walls. Figure 5.32 presents the damage plot. In addition, figure 5.33 shows the load-displacement curve for

the three models and the comparative chart comparing the effectiveness of each application.

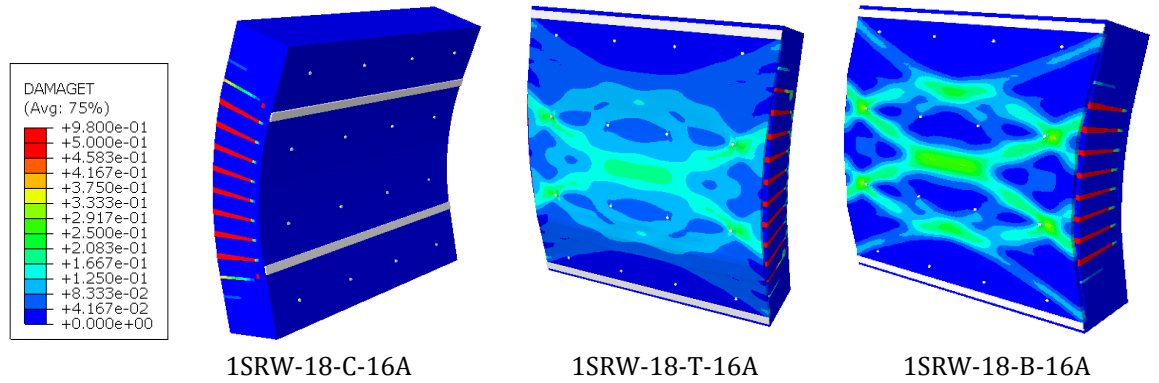


Figure. 5.32. Damage plot for different application of the proposed retrofit technique

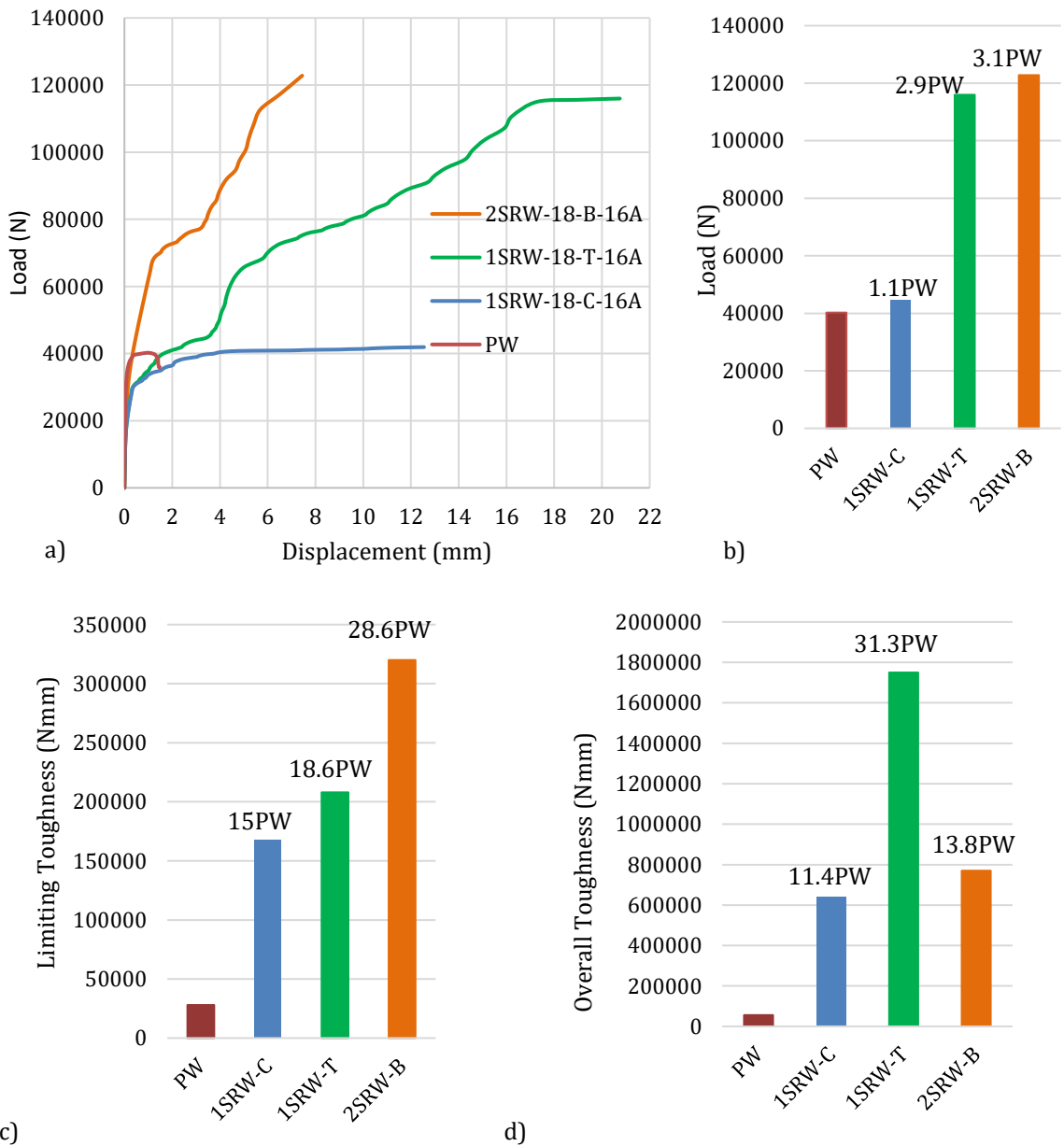


Figure. 5.33. a) Load vs Displacement curve b) Load capacity c) Limiting Toughness and d) Overall Toughness of the different application of the proposed retrofit technique

5.5.2 Influence of the thickness of OSB

For this study, three different OSB thicknesses, which are 10mm, 18mm and 25mm, were studied. From the analysis, a thickness of 18mm appears to be adequate for the retrofit application. In the model with 10mm thickness, the damage plot indicates some non-uniform thickness in the timber (warping) and also have a lesser increment in the load, twice that of the plain wall as against three and four times load capacity gained from 18 and 25mm OSB. The 10mm thickness might be considered thinner for load-bearing application because of the warping effect. Meanwhile, application with 25mm thickness shows the highest load increment (4.2 x PW), but damages appeared in the brick when the OSB is damaged (i.e red pattern in the brick edge above joints in model output). This might be too conservatives because damage in the brick will only occur after the wall has lost all its integrity. Figure 5.34 presents the damage plot and figure 5.35 presents the performance evaluation of each thickness of the OSB in term of load, limiting and overall toughness.

Furthermore, the energy absorption capacity of the different timber thicknesses was evaluated within the allowable limit and the overall performance. The analysis reveals that the thickness of the OSB does not have effects on the energy absorption capacity of the wall within the allowable limit. However, the overall energy capacity of the retrofitted system increases with the increase in the OSB thickness. Meanwhile, the overall toughness of the 18mm and 25mm OSB is relatively equal even though the 25mm OSB carried more load at the expense of excessive damage to the masonry part as highlighted earlier. An inference from this is that an 18mm thick OSB is recommended to provide an adequate increment in load capacity (2.9PW), limiting toughness (6.23PW) and overall toughness (31.3PW).

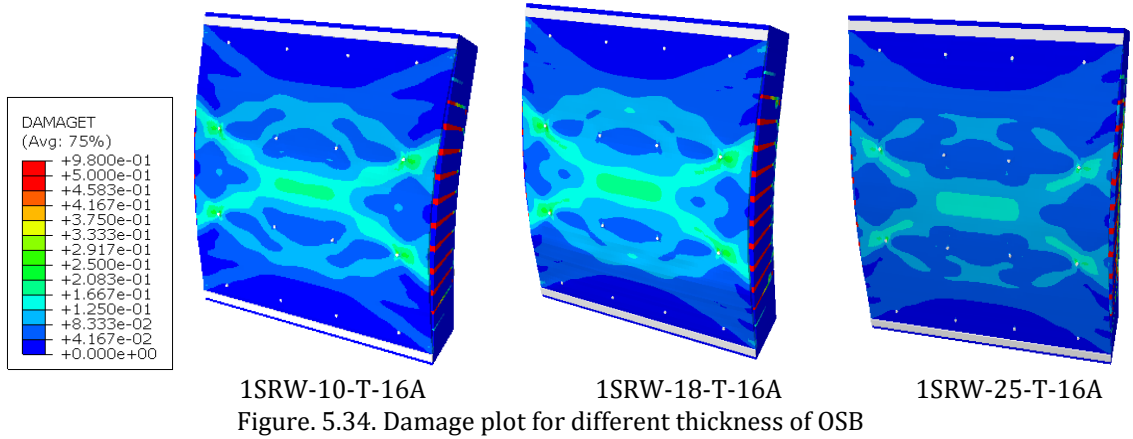


Figure. 5.34. Damage plot for different thickness of OSB

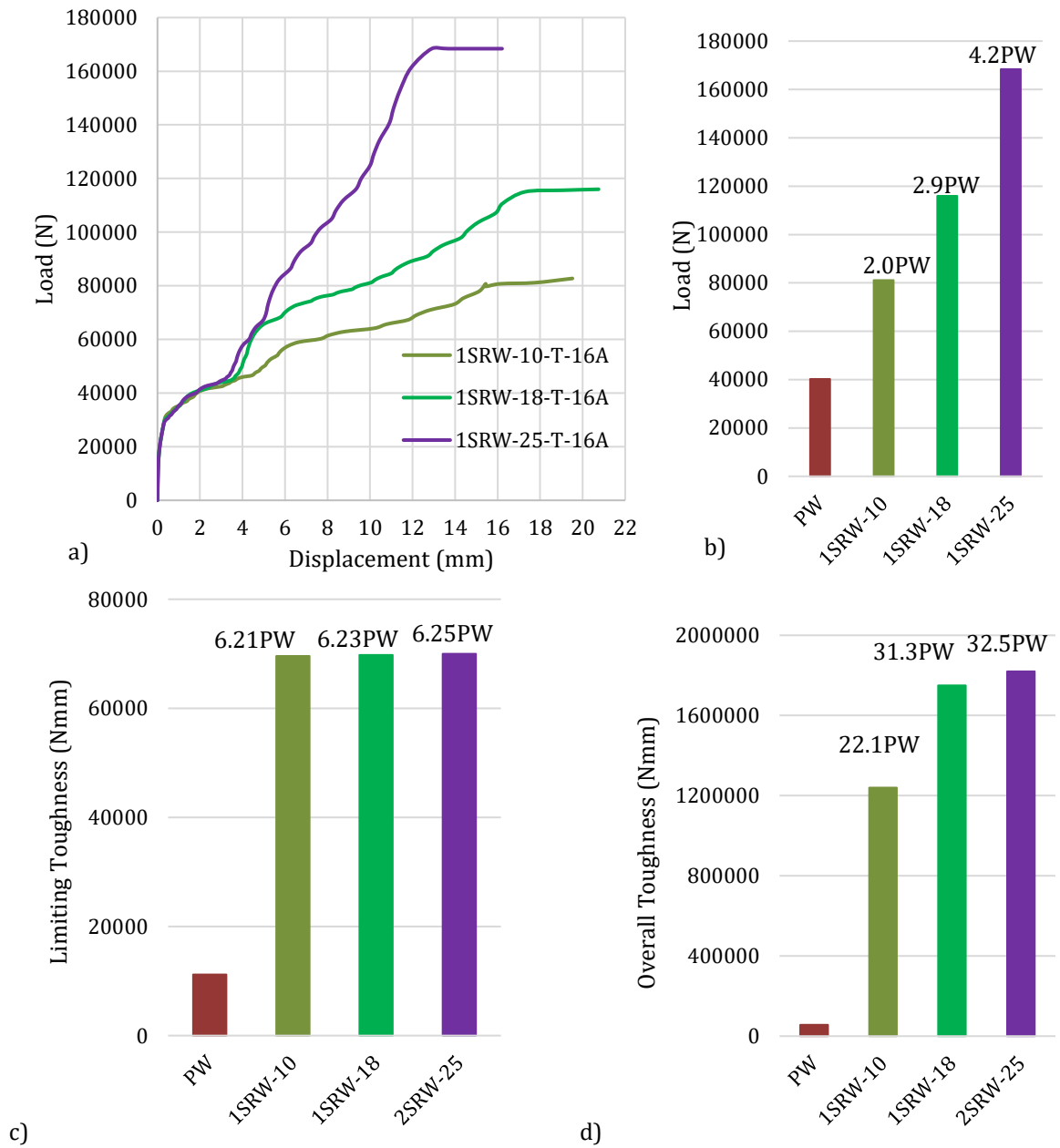


Figure. 5.35. a) Load vs Displacement b) Load capacity c) Limiting Toughness d) Overall Toughness of OSB thickness

5.5.3 Influence of number of connections

Keeping the correct edge distance and spacing between connections is key to the performance of this proposed retrofit technique. The parametric analysis performed involved studying the performance of 6, 12 and 16 number of anchors with a minimum of 250mm spacing. The analysis reveals that too much spacing (> 500mm) between the connections reduced the effectiveness of this technique. For the 1SRW-18-T-6A where only six anchors were used (i.e. spacing > 500mm), the behaviour shows that there is not enough composite action between the masonry and the OSB timber. Hence for this application, maximum spacing of 450mm is recommended as can be seen in the other two cases (12A and 16A) where the application increases the load by almost 3times. Also, it is important to keep the minimum spacing of 250mm to avoid close arrangement that reduces the cone of influence in which the anchor performance is affected.

Although the load increment gained from the application when 12 anchors and 16 anchors were used are almost the same (2.7PW and 2.9PW respectively), the overall toughness gained when 16 anchors were used is 1.5times the toughness gained when the system applied with 12 anchors. The additional toughness gained is due to the rigidity of the composite system because of the additional 4 anchors. However, the limiting toughness of both application (1SRW-18-T-12A and 1SRW-18-T-16A) is similar, about 2.2times that of the PW. Meanwhile, the 1SRW-18-T-6A show the least increment in the limiting and overall toughness of the system, which is because there is not enough composite action between the masonry and the OSB timber with 6 anchors. Figure 5.36 and 5.37 presents the damage plots and performance evaluation charts respectively.

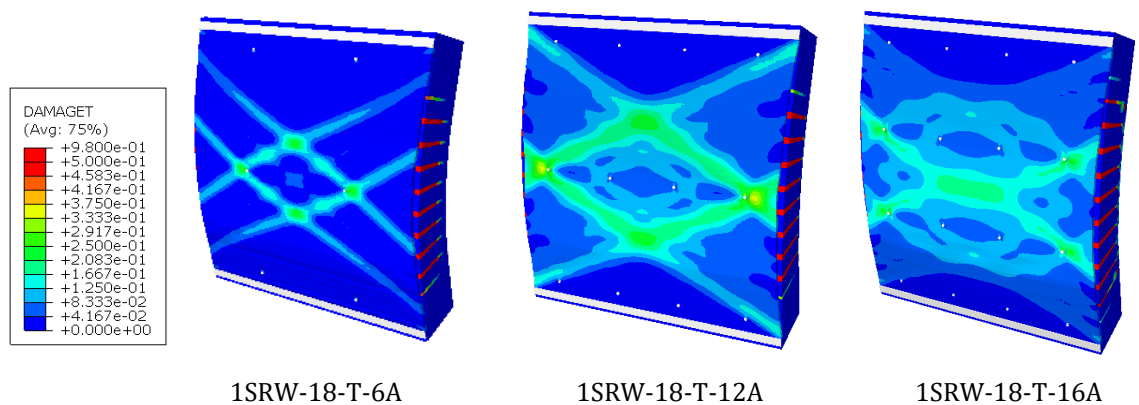


Figure. 5.36. Damage plot for different number of anchor connections

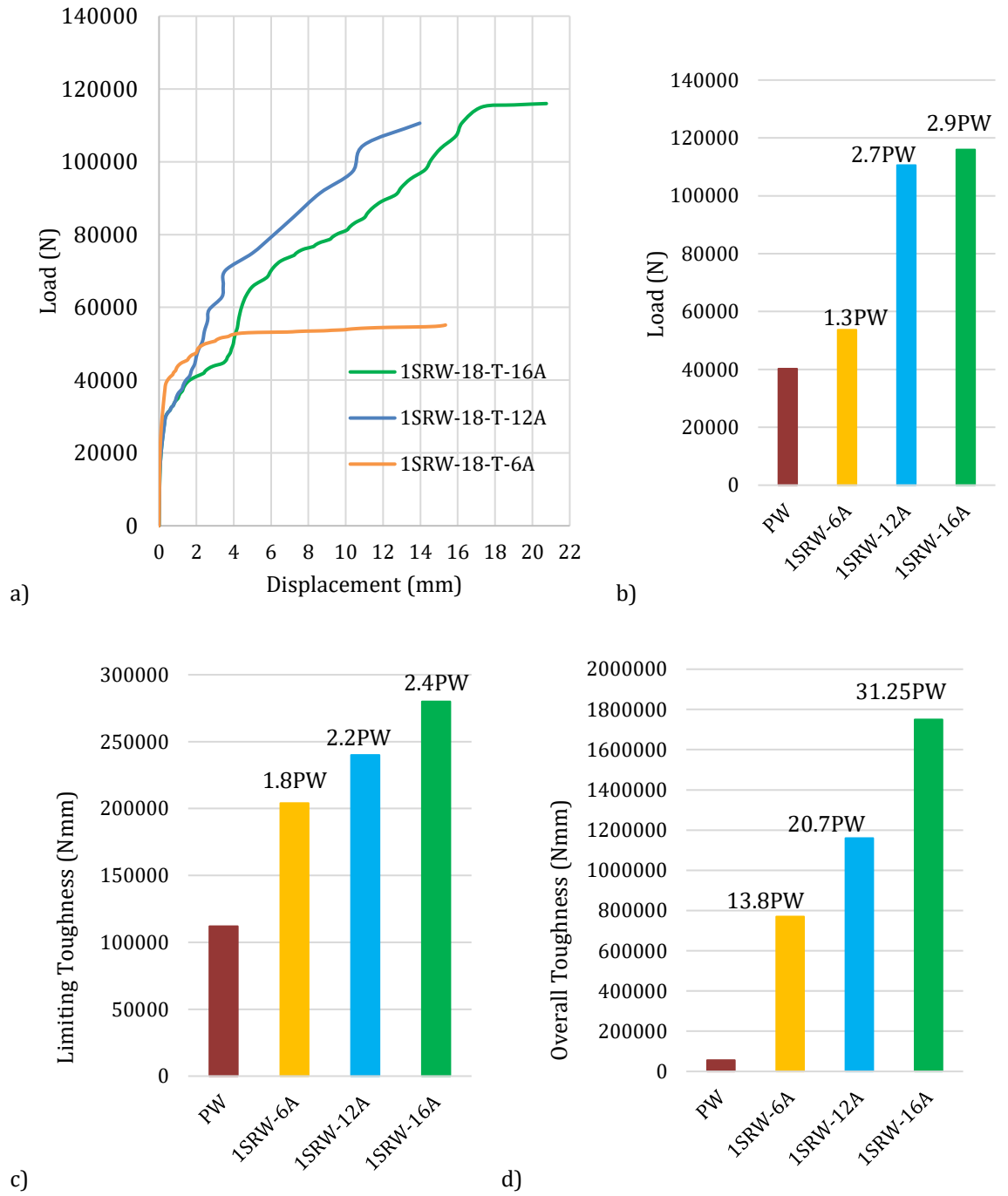


Figure. 5.37. a) Load vs Displacement curve b) Load capacity c) Limiting toughness d) Overall toughness of different number of anchors

5.6 Cost Evaluation of the Proposed Retrofit Technique

This section presents a brief cost analysis of the application. First, the total cost of applying the selected three thickness of the OSB was evaluated and compared against the overall toughness gained in table 5.15. After that, the cost implication based on the number of anchors used is also presented in table 5.16.

Table 5.15: Cost evaluation for different OSB thickness with 16 anchors

OSB thickness	Cost of OSB (£)	Cost of Anchor (£)	Total cost (£)	Overall Toughness gained x PW	Toughness gained/unit cost
10	6.84	35.36	42.20	22.1	0.52
18	11.75	35.36	47.11	31.3	0.71
25	16.81	35.36	52.17	32.5	0.62

Table 5.15 reveals that the overall toughness gained per unit cost of the application is at highest when 18mm thick OSB is used. This cost analysis further substantiated the claim that the 18mm thick OSB is the most suitable for this proposed application. This is the most cost-effective OSB for this application and it has a substantial gain in the load and toughness of the retrofitted wall.

Table 5.16: Cost evaluation for different number of anchors using 18mm OSB

Anchor quantity	Cost of OSB (£)	Cost of Anchor (£)	Total cost (£)	Overall Toughness gained x PW	Toughness gained/unit cost
6	11.75	13.26	25.01	13.8	0.55
12	11.75	26.52	38.27	20.7	0.54
16	11.75	35.36	47.11	31.25	0.71

Similarly, the cost analysis in table 5.16 reveals that the overall toughness gained per unit cost of the application with 16 anchors is the maximum of the three cases studied. This means that maximum spacing of 300mm is recommended to get the most out of the proposed retrofit application. This will ensure adequate composite action between the masonry and applied OSB panel. However, where huge toughness increment is not required, the connection spacing can be increased to save cost but, should not more than 500mm to ensure adequate composite action. Indeed, the cost of applying this proposed OSB technique on a square meter of a masonry wall is estimated to be £47. The costing (materials and labour) was evaluated referring to market prices in England.

5.7 Summary of Findings

The first section of the numerical analysis (section 5.2) presents a numerical study to characterise the masonry components. The section complements the experimental work on brick units, mortar and compression test on masonry cubic specimen. A detailed micro model of the masonry cubic specimen was developed and analysed in ABAQUS. Based on the results of the compression tests on the brick units and mortar, nonlinear behaviour of masonry unit and mortar both in compression and tension regime have been estimated and accounted for in the developed FE model using the constitutive damaged plasticity model. Properties of the interfacial behaviour of the brick unit-mortar interface were also included in the model. The calibration and validation of the FE model were done using the experimental results.

The developed FE model of masonry cubic specimen was able to predict the behaviour and failure of tested MC specimen. The result gives a difference of 5% between the numerical value and experimental value. This indicates that the model can predict the compressive strength of the masonry cubic specimen. Hence, the numerical simulation carried out here produced the strength material properties for the unit, mortar and interface. These properties were later used to analyse the out-of-plane response of plain and retrofitted masonry prism and wall in the subsequent section 5.3 and 5.4.

The numerical model to complement the results obtained from testing both the small-scale masonry prism (section 5.3) and larger-scale masonry wall (section 5.4) has been presented in this section. The simplified detailed micro model approach was employed in ABAQUS. Based on the results of the analysis of the numerical model, the developed FE model predict the behaviour and failure of tested specimens within less than 10% in all cases. This indicates that the model can be employed to carry out a parametric study to investigate the performance of the proposed retrofit technique further.

Hence, the parametric study to assess the model capability to simulate URM walls retrofitted with different OSB panel thickness and connection layout is presented in subsequent section 5.5. The parametric analysis reveals that the thickness of the OSB timber is directly proportional to the out-of-plane load and

displacement resistance of the system. The cost of application per a square meter of a masonry wall is estimated to be £47 using the market prices in England.

CHAPTER SIX – CONCLUSION AND RECOMMENDATION FOR FUTURE WORKS

6.0 Overview

This study has presented an experimental and numerical study investigating the effectiveness of a proposed timber-based retrofit technique for masonry walls. The research aims to examine the out-of-plane performance of URM wall retrofitted with the proposed timber-based technique by assessing the toughness, out-of-plane load and displacement capacity. For the proposed retrofit technique considered in this study, 18mm thick oriented stranded board (OSB) type 3 was connected to URM wall using $\varnothing 8\text{mm}/L50\text{mm}$ threaded anchor rods together with an option of plastic plug (mechanical connection) or injection mortar (adhesive anchor) to investigate how the out-of-plane behaviour of the retrofitted URM wall changes under out-of-plane loading.

The methodology adopted to deliver the overall aim and objectives of this study as identified in this thesis were experimental tests and numerical analyses. The study was grouped into three main phases listed below which also reflected the chronological order in which the research was done.

- ❖ Material Characterisation
- ❖ Small-Scale Test: flexural bond strength test on 665 x 225 x 102.5mm masonry prism
- ❖ Larger-Scale Test: flexural strength test on 1115 x 1115 x 215mm masonry wall

Although summarised concluding remarks were given at the end of each section, this chapter presents a comprehensive collection of the findings from both the experimental and numerical studies. These findings have then formed the basis for the subsequent sections highlighting the study contributions and recommendations for future works.

6.1 Experimental Study

The sequences of the experimental tests carried out in this study were first to characterise the brick units and mortar that were used to study the efficiency of the proposed timber retrofit technique for the masonry walls. The characterisation tests conducted (table 4.1) helped to determine the mechanical qualities and acceptability of the materials used for this study. The tests also helped to obtain the strength material properties for masonry unit, mortar, and the unit-mortar interface that were used to produce a detailed numerical analysis used to complements the experimental tests carried out in this study. The obtained material properties from the characterisation tests conformed to the manufacturer specification and met the specified requirements declared in various standards and codes. Hence, the analysis of the results from the characterisation test concluded that the selected materials are good, and their source remained unchanged throughout the experimental campaign. Most importantly, the strength obtained for the brick units and mortar shows that the brick is a strong unit while the mortar is a weak joint, which makes the combination a strong unit-weak mortar joint, a typical characteristic of old masonry structures. This is thus a suitable material selection for this study because the aim was to propose a new retrofit technique for old masonry walls. Here, it is noted that the most relevant property is the masonry bond strength, which depends on many factors, including the initial rate of absorption.

The second phase of the experimental studies involved small-scale experimental campaign on 665 x 215 x 102.5mm masonry prism to introduce the use of oriented strand board (OSB) timber panels in retrofitting URM wall. Here, nine masonry prism specimens were tested under four-point loading to evaluate the out-of-plane performance of the OSB panel in retrofitting URM prisms. The flexural strength, toughness, out-of-plane load capacity, and displacement of both plain and OSB-retrofitted masonry prisms were obtained and compared. In the small-scale experiment, two different connection typologies (C1, adhesive anchor: threaded dry rod with an injectable chemical adhesive) and (C2, mechanical connection: threaded dry rod with a plastic anchor) were studied. The focus of this small-scale test is first to understand whether the proposed

technique (i.e. OSB type 3 connected to the masonry wall) can improve URM walls capacity against excessive out-of-plane loading. Also, to identify which of the two connections is best to connect the timber to the wall. The main outcomes of the small-scale tests are given below:

- ❖ The failure (cracking) of plain specimens was abruptly occurred between the interface of the mortar joint and brick unit, causing the sudden collapse of the plain specimens.
- ❖ The application of OSB panel at the back of MP improved the flexural response and energy absorption (toughness) of the retrofitted specimens such that the failure was much more ductile.
- ❖ This proposed retrofit technique increased the initial crack load on the retrofitted specimens by 87% of the plain MP capacity.
- ❖ The retrofitted MPs have 400% and 638% increment in flexural strength to resist out-of-plane load when the adhesive anchor and mechanical connection was used respectively. Here, the performance of the proposed retrofit technique recorded might have been amplified due to the fragility of the plain specimen, which is likely not to be true representative of the real working condition of URM walls. As such, a larger-scale experimental campaign on 1115x 115 x215mm single leaf, double wythe solid URM walls to study the proposed technique in detail is presented.
- ❖ A 100% increment in the out-of-plane displacement capacity was achieved in retrofitted MP. This is because the addition of OSB panel offered additional tensile strength and ductility, which is lacking in plain MP to the retrofitted specimens, and thus they were able to displace gradually before the timber failed.
- ❖ Adhesive anchors (connection type 1:C1) performed much better for the envisaged application and thus selected for the larger-scale test.
- ❖ Mechanical connection (C2) is not totally effective due to the weak bonding between the OSB panel and MP. The reason for this weak bonding was observed to be the inability of the plastic anchor to expand in the high dense brick unit.
- ❖ Finally, the OSB retrofit application ensures that sudden failure is avoided and thus minimised the high risk of mortality and substantial damages that

comes with the sudden collapse of the URM wall. It thus improved the out-of-plane performance of masonry prism to at least collapse prevention.

The experimental study then completed by performing the larger-scale experimental test on 1115 x 1115 x 215 mm masonry wall to investigate the out-of-plane behaviour of OSB timber retrofitted masonry wall. Here, six masonry wall specimens, including retrofit application with the OSB on the flexural tension face only and on both surfaces were tested. Out-of-plane bending test in the form of four-point loading test was performed on all the six specimens. The experimental results of the larger-scale four-point bending tests evidenced significant improvements in the out-of-plane resistance, toughness and displacement capacities of the masonry wall retrofitted with the OSB panel. The key findings from the evaluation of the load-carrying and displacement capacities of both plain and retrofitted masonry walls are given below:

- ❖ The application of the OSB timber panel retrofit technique increased the out-of-plane load capacity of the retrofitted wall at the occurrence of the first crack by 35% and 76% for application on only the flexural tension face and both surfaces of the wall respectively.
- ❖ The displacement at the occurrence of the first crack in the one-sided retrofitted wall is 52% more than that of the plain wall, while is approximately the same thing for double-sided application.
- ❖ Overall, the retrofitted walls were able to resist out-of-plane loading with an increment of 194% and 209% for application on only the flexural tension face and both surfaces of the wall respectively.
- ❖ The application of the retrofit on both faces of the wall does not increase the failure load significantly when compared to the one-sided application (only 5% increment in load capacity). However, the load at which the initial crack occurred in the double-sided application is 30% higher than the load at which the one-sided application first cracked.
- ❖ Also, the deflection resistance of the double-sided application is higher than the one-sided application.
- ❖ The one-side retrofitted walls were able to absorb more energy almost 16 times higher than that of plain walls. Meanwhile, the 2SRW can absorb energy which is 10 times higher than that of PW. However, the double-

sided application has advantages in term of the stiffness and limiting toughness showing a more resilient against out-of-plane displacement.

- ❖ Hence, the main conclusion from this study is that oriented strand board (OSB) type 3 considerably increased the load and flexural capacity by (1.4 & 1.8 times), limiting toughness by (1.6 & 2.4 times) and overall toughness by (16 & 10 times) that of plain wall subjected to out-of-plane loading for (single & double-sided) application respectively. The proposed application in comparison with the other existing retrofit techniques performed well. The application of glass fibre reinforced polymer by Boem (2017) showed load increment of 1.8 times that of the unreinforced wall. Also, the application of fibre reinforced cement mortar (FRCM) and near-surface mount with cementitious additive (NSM) by Al-Jaberi (2018) shows 1.6 and 1.2 times that of plain wall respectively. Kashyap (2014) also reported a load increment of 2.3 times that of unstrengthened walls when FRP was used to retrofit masonry wall. Even though some of the previous application shows a slightly higher load increment than the proposed technique but the cost of FRP and fibre products is relatively higher than the cost of the OSB application. The cost of applying this proposed OSB technique on a square meter of a masonry wall is estimated to be £47 as against £152 estimated for fibre polymer applications on the 1m² masonry wall.

6.2 Numerical Analyses

The development of 3D finite element computational model to complement the experimental works was presented in the sequence in which the tests were done and validated with the results obtained from the experiments. After that, the study performed parametric analysis verifying how the application, variations in the thickness of the OSB timber panel, the spacing of anchor connection may affect the out-of-plane bending performances of the introduced timber-based retrofit technique. All the numerical analyses were performed using the software, ABAQUS FEA.

This first section of the numerical study fully characterised the masonry components by estimating the nonlinear behaviour of masonry unit and mortar

both in compression and tension regime using the constitutive damaged plasticity model. This section achieved the full mechanical properties of the unit, mortar and the interfacial properties of the unit-mortar joint. The obtained parameters were then used to produce a detailed micro-model of masonry cubic specimen simulating the behaviour and failure of tested masonry cubic specimen. The developed FE model was validated and predicted the behaviour and failure of tested masonry cubic specimen. The result gives a difference of 5% between the numerical value and experimental value. Hence, the main finding from this phase is that calibrated material properties for the unit, mortar and interface used in the numerical simulation of the compression tests represent the approximate properties of the materials. After that, the properties were later used to analyse the out-of-plane response of plain and retrofitted masonry wall in the subsequent phases.

The numerical simulation of the four-point bending test for both the small-scale and larger-scale test were also carried out. A concise and efficient nonlinear 3-D finite element analysis was developed to simulate the damage and failure pattern of the masonry prism and wall tested in the laboratory. As highlighted in section 5.3.4, the adopted model strategy for both masonry prism and wall were based on the simplified micro-model technique to avoid ABAQUS convergence issue as a result of too many contacts between the unit and mortar (unit/mortar interface). Thus, the interface properties were lumped into the properties of the mortar, and new non-linear properties of mortar were obtained and calibrated. The properties of the brick units calibrated in the previous step were used. Also, the damage constitutive model available in ABAQUS was used to define the non-linear behaviour of OSB timber. The OSB properties were incorporated together with the pure elastic properties of the anchor connection in the model for the creation of the retrofitted model. The analysis of the masonry prism/wall model under a continuous increase of load in the form of load-displacement was obtained using the static RIKS method (arc-length control). The comparative analysis of the numerical results with experimental data confirms that the developed FE models adequately captured the behaviour of both the plain and retrofitted model to the ultimate load. The models also show an excellent correlation of the compressive damage (DAMAGEC) and tensile damage

(DAMAGET) contour plot with the experimental failure pattern. Generally, the model predicted the peak load and the corresponding failure, toughness and resilience to within less than 10% of the average results obtained from the test.

The parametric analysis confirmed that the thickness of the OSB panel influences the performance of the retrofit technique. The thickness of the OSB timber is directly proportional to the out-of-plane load and displacement resistance of the system. Also, the connection spacing has little effect on the wall performance when the spacing is between 250-500mm. However, a connection spacing larger than 500mm reduces the rigidity of the composite system with the failure pattern showing an inadequate connection between the OSB panel and the masonry wall, leading to low load capacity and failure of OSB panel quickly.

6.3 Contribution

The main contributions of this study are highlighted as follows:

- ❖ A new timber-based retrofit technique for URM wall has been presented. The technique involved application of oriented stranded board (OSB/type 3) timber panel to the back of URM walls using adhesive anchor connection. This application improved the out-of-plane capacity of the retrofitted wall significantly. The possible uses of the proposed technique may be the application of the OSB panel on the internal surface of exterior URM walls so that external historic appearance of the building is preserved. And the application of the OSB panel on the external surfaces of exterior URM walls with the combination of plaster, brick-polymer based imitating finishings or clay tiles. The configuration with OSB on both sides is possible for seismic retrofit, and this would be applicable when less stringent heritage preservation is expected for the considered building. The application of the technique on the compression face is considered as a poorer performance as observed from the numerical study and thus considered less applicable.
- ❖ The system is best efficient with adhesive anchor connection. Anchoring system into masonry that requires plastic sleeve reduces the efficiency of the system due to poor bonding resulting from the inability of plastic anchor to expand in the high dense brick unit.

- ❖ Numerically, this study has contributed to the modelling of masonry wall retrofitted with OSB panels considering the mechanical properties of individual components i.e masonry unit, mortar and the retrofit materials (OSB timber and anchor connectors). Its application to simulate the behaviour of the retrofit system will facilitate laboratory experiments in studying further the efficiency of the proposed retrofit techniques.

6.4 Recommendation for future works.

The findings of this study have reinforced the vital role of good experimental testing and numerical investigation in finding an effective retrofit technique for masonry structures. As a result of this research work, new research lines can be defined, either for validation or extension of the main findings and also for assessing the behaviour of the proposed retrofit technique. Some recommendations are:

- ❖ An extension of experimental studies to investigate the effectiveness of the proposed OSB-timber retrofit system on similar URM walls with different slenderness ratios and dimensions, to increase the extent of acquired data and to check whether the observed improvement in the out-of-plane performances is similar to those presented in this work.
- ❖ The use of the results presented in this study is limited to the category of wall tested, which is a free-standing masonry wall panel without any party walls at the edges to generate restraint. Therefore, an investigation of the performance of the proposed technique on wall ideal for reproducing the in-situ condition of a portion of a typical load-bearing wall with corner walls is recommended.
- ❖ Another exciting research idea to develop is to extend the proposed retrofit application to a full-scale building (single or double-storey building). The full-scale building should be retrofitted with OSB panel connected at interior faces and both faces of the wall. These may be tested on shaking table facilities for evaluation of the seismic performance of the proposed retrofit technique.
- ❖ An extension of the numerical studies is also recommended to investigate the influence of openings on the performance of the retrofit technique. In

addition, other influential parameters such as different wall boundary conditions, loading scenario, size and location of openings should be further investigated.

- ❖ More researches should also be performed on not only the out-of-plane behaviour of the proposed retrofitted techniques but, also on the combined in-plane and out-of-plane behaviour since both actions act together in a real building.

References

- Abrams, D. (1998). *New Perspectives on Seismic Rehabilitation*. In: Proceedings of the Asia-Pacific Workshop on Seismic Design and Retrofit of Structures.
- Abrams, D., Alshawa, O., Lourenco, P. and Sorrentino, L. (2017). *Out-of-Plane Seismic Response of Unreinforced Masonry Walls: Conceptual Discussion, Research Needs, and Modelling Issues*. International Journal of Architectural Heritage, 11(1), pp.22-30.
- Al-Jaberi Z. (2018). *Strengthening of Reinforced Masonry Walls Subjected to Out-Of-Plane Pseudo-Static Cyclic Load using Advanced Composite*. PhD. Missouri University of Science and Technology.
- Alkhrdaji, T. (2013). *Strengthening: Adding or Restoring Structural Capacity*. [online]. Available: <https://www.structural.net/service/strengthening>. [Accessed 14 Dec. 2016].
- American Concrete Institute (2014). *Building Code Requirements for Structural Concrete (ACI 318-14)*. Texas, USA: ACI.
- Anon, A. (2009). *Brick Bonds: Heritage Directory Notes*. [online]. Available at: <http://www.theheritagedirectory.co.uk> [Accessed 23 Jul. 2017].
- Anon, A. (2018). *Technical Information Sheet for Oriented Strand Board*. [online] Available at: http://www.osb-info.org/Assets/file/EN/OSB_Technical [Accessed 23 Jul. 2018].
- Arash, S. (2012). *Mechanical Properties of Masonry Samples for Theoretical Modelling*. In Proceedings of 15th International Brick and Block Masonry Conference. Florianópolis, Brazil.
- Asteris, P., Chronopoulos, M., Chrysostomou, C., Varum, H., Plevris, V., Kyriakides, N. and Silva, V. (2014). *Seismic Vulnerability Assessment of Historical Masonry Structural Systems*. Engineering Structures, 62-63, pp.118-134.
- Asteris, P., Plevris, V., Sarhosis, V., Papaloizou, L., Mohebkhah, A., Komodromos, P. and Lemos, J. (2015). *Numerical Modeling of Historic Masonry Structures*. In: P. Asteris and V. Plevris, ed., Handbook of Research on Seismic Assessment and Rehabilitation of Historic Structures. IGI Global, pp.213-256.
- ASTM E518 -15 (2015). *Standard Test Methods for Flexural Bond Strength of Masonry*. West Conshohocken, PA: ASTM International.

- ASTM E72 - 15 (2015). *Standard Test Methods of Conducting Strength Tests of Panels for Building Construction*. West Conshohocken, PA: ASTM International.
- Babaeidarabad, S., Arboleda, D., Loreto, G. and Nanni, A. (2014). *Shear Strengthening of Unreinforced Concrete Masonry Walls with Fabric-Reinforced-Cementitious-Matrix*. *Construction and Building Materials*, 65, pp.243-253.
- Bailey, S., Dizhur, D., Trowsdale, J., Griffith, M. and Ingham, J. (2015). *Performance of Posttensioned Seismic Retrofit of Two Stone Masonry Buildings during the Canterbury Earthquakes*. *Journal of Performance of Constructed Facilities*, 29(4), p.04014111.
- Banfill, P. and Foster, A. (2000). *A Relationship between Hydraulicity and Permeability of Hydraulic Lime*. In: P. Bartos, C. Groot and J. Hughes, ed., *International RILEM workshop on historic mortars: Characteristics and tests*. Paisley, Scotland: Cachan: RILEM, pp.173-183.
- Berset, T., Schwegler, G., Stempfle, H. and Herter, R. (2011). *Seismic Resistance Analysis and innovative Earthquake Refit*. [online] Stresshead.ch. Available at: <http://www.stresshead.ch/assets/2014-report>. [Accessed 17 Dec. 2016].
- Beyer, K., Petry, S., Tondelli, M. and Paparo, A. (2014). *Towards Displacement-Based Seismic Design of Modern Unreinforced Masonry Structures*. In: A. Ansal, ed., *Perspectives on European Earthquake Engineering and Seismology*, 1st ed. Springer, pp.401-428.
- Biggs, D. (2003). *Masonry Magazine: Post-tension masonry*. [online] Available at: <http://www.masonrymagazine.com/10-03/post.html> [Accessed 20 Dec. 2006].
- Binda, L. and Cardani, G. (2015). *Seismic Vulnerability of Historic Centres: A Methodology to Study the Vulnerability Assessment of Masonry Building Typologies in the Seismic Area*. In: P. Asteris and V. Plevris, ed., *Handbook of Research on Seismic Assessment and Rehabilitation of Historic Structures*. IGI Global, pp.213-256.
- Boem, I. (2017). *Enhancement of the Seismic Performances of Historic Masonry Buildings through Glass Fiber-Reinforced Mortar*. PhD. Università Degli Studi di Trieste.

- Borri, A. Sisti, R., and Corradi M. (2020). *Seismic Retrofit of Stone Walls with Timber Panels and Steel Wire Ropes*. Proceedings of the ICE - Structures and Buildings. <https://doi.org/10.1680/jstbu.19.00100>.
- Borri, A., Castor, G., Corradi, M. and Speranzini, E. (2014). *Durability Analysis for FRP and SRG Composites in Civil Applications*. In Proceedings of Int. Conf. Mechanics of Masonry Structures Strengthened with Composite Materials Modelling, Testing, Design, Control. Italy: Trans Tech Publication.
- Borri, A., Corradi, M., Speranzini E. & Giannantoni, A. (2008). *Consolidation and reinforcement of stone walls using a reinforced repointing grid*. In Proceedings of the 6 ICSAHC, (2008), Bath, UK.
- Branco, M. and Guerreiro, L. (2011). *Seismic Rehabilitation of Historical Masonry Buildings*. Engineering Structures, 33(5), pp.1626-1634.
- British Standard Institution (1996). *BS EN 1996-1-1:2005: Eurocode 6 -Design of Masonry Structures - Part 1-1: General Rules for Reinforced and Unreinforced Masonry Structures*. London: British Standards Institution.
- British Standard Institution (1999). *BS EN 1015-11:1999: Methods of Test for Mortar for Masonry. Determination of Flexural and Compressive Strength of Hardened Mortar*. London: British Standards Institution.
- British Standard Institution (1999). *BS EN 1015-3:1999: Methods of Test for Mortar for Masonry - Determination of Consistence of Fresh Mortar (by Flow Table)*. London: British Standards Institution.
- British Standard Institution (1999). *BS EN 1052-1:1999: Methods of Test for Masonry-Part1- Determination of Compressive Strength*. London: British Standards Institution.
- British Standard Institution (2000). *BS EN 772-13:2000: Methods of Test for Masonry Units - Determination of Net and Gross Dry Density of Masonry Units (Except for Natural Stone)*. London: British Standards Institution.
- British Standard Institution (2004). *BS EN 1992-1-2:2004: Eurocode 2 - Design of Concrete Structures - General Rules Structural Fire Design*. London: British Standards Institution.
- British Standard Institution (2005). *BS 4551:2005: Methods of Test for Mortar and Screed- Chemical Analysis and Physical Testing*. London: British Standards Institution.

- British Standard Institution (2011). *BS EN 772-21:2011: Methods of Test for Masonry Units - Determination of Water Absorption of Clay and Calcium Silicate Masonry Units by Cold Water Absorption*. London: British Standards Institution.
- British Standard Institution (2011a). *BS EN 772-1:2011: Methods of Test for Masonry Units - Determination of Compressive Strength*. London: British Standards Institution.
- Brunner, J. And Shing, P. (1996). *Shear Strength of Reinforced Masonry Walls*. TMS Journal of Composite Materials, 14(1), pp.65-77.
- Brzev, S. (2014). *Confined Masonry Buildings: Key Components and Performance in Past Earthquake*. [Online] slideshare.net. Available At: [Http://www.slideshare.net/eerislides/th1-confined-masonry-svetlana](http://www.slideshare.net/eerislides/th1-confined-masonry-svetlana) [Accessed 15 Jan. 2018].
- Bui, T., Limam, A., Bertrand, D., Ferrier, E. And Brun, M. (2010). *Masonry Walls Submitted to Out-Of-Plane Loading: Experimental and Numerical Study*. In Proceedings of 8th International Masonry Conference. IMC Society.
- Castori, G., Borri, A. And Corradi, M. (2016). *Behavior of Thin Masonry Arches Repaired Using Composite Materials*. Composites Part B: Engineering, 87, pp.311-321.
- Chen, G. And He, B. (2017). *Stress-Strain Constitutive Relation of OSB under Axial Loading: An Experimental Investigation*. Bioresources, 12(3).
- Chiozzi, A., Simoni, M. And Tralli, A. (2015). *Base Isolation of Heavy Non-Structural Monolithic Objects at the Top of a Masonry Monumental Construction*. Materials and Structures, 49(6), Pp.2113-2130.
- Chrysostomou, C., Kyriakides, N., Roussis, P. And Asteris, P. (2015). *Emerging Technologies and Materials for the Seismic Protection of Cultural Heritage*. Handbook of Research on Seismic Assessment and Rehabilitation Of Historic Structures, Pp.576-606.
- Chrysostomou, C., Stassis, A., Demetriou, T. and Hamdaoui, K. (2008). *Application of Shape Memory Alloy Prestressing Devices on an Ancient Aqueduct*. Smart Structures and Systems, 4(2), pp.261-278.
- Chuang, S. and Zhuge, Y. (2005). *Seismic Retrofitting of Unreinforced Masonry Buildings - A Literature Review*. Australian Journal of Structural Engineering, 6(1), pp.25-36.

- Chuxian, S., Guiqiu, L. and Wenchao, W. (1997). *The Design of Brick Masonry Structure with Concrete Column*. In: 11th IB2MaC.
- Corradi, M., Osofero, A., Borri, A. and Castori, G. (2015). *Strengthening of Historic Masonry Structures with Composite Materials*. Handbook of Research on Seismic Assessment and Rehabilitation of Historic Structures, pp.257-292.
- Costa, A., Arêde, A., Costa, A. and Oliveira, C. (2011). *Out-of-Plane Behaviour of Existing Stone Masonry Buildings: Experimental Evaluation*. Bulletin of Earthquake Engineering, 10(1), pp.93-111.
- Costa, A., Arêde, A., Ferreira, T., Gomes, A. and Varum, H. (2014). *Experimental Study of the Out-of-Plane Behaviour of Unreinforced Sacco Stone Masonry Walls: Comparative Analysis of two Different Test Setups*. In: 9th International Masonry Conference.
- Csikai, B., Ramos, L., Basto, P., Moreira, S. and Lourenço, P. (2019). *Flexural Out-of-Plane Retrofitting Technique for Masonry Walls in Historical Constructions*. In: 9th International Conference on Structural Analysis of Historical Constructions. Mexico City, Mexico.
- D'Ayala, D. and Speranza, E. (2002). *An Integrated Procedure for the Assessment of Seismic Vulnerability of Historic Buildings*. In: 12th European Conference on Earthquake Engineering. Elsevier Science Ltd.
- D'Ayala, D. and Speranza, E. (2003). *Definition of Collapse Mechanisms and Seismic Vulnerability of Historic Masonry Buildings*. Earthquake Spectra, 19(3), pp.479-509.
- Da Porto, F., Valluzzi, M., Munari, M., Modena, C., Arêde, A. and Costa, A. (2018). *Strengthening of Stone and Brick Masonry Buildings*. In: A. Costal, A. Arêde and H. Varum, ed., Strengthening and Retrofitting of Existing Structures, 9th ed. Springer: Porto, pp.59-75.
- Dally, A. and Witarnawan, W. (1997). *Strengthening of Bridges using External Posttensioning*. [online] Pdfs.semanticscholar.org. Available at: <https://pdfs.semanticscholar.org/fd7d/9d41fe934af54dc2573106a110c9cf75be33.pdf> [Accessed 7 Apr. 2018].
- Dassault Systemes (2014). *Abaqus/CAE*. USA: Dassault Systemes Simulia Corp.
- Davidson, B. and Brammer, D. (1996). *Cyclic Performance of Nominally Reinforced Masonry Wall*. In: NZNSEE Conference. pp.144-151.

- Dawson, S. (2015). *Windpost*. [online] En.wikipedia.org. Available at: <https://en.wikipedia.org/wiki/Windpost> [Accessed 10 Apr. 2017].
- De Santis, S., Casadei, P., De Canio, G., de Felice, G., Malena, M., Mongelli, M. and Roselli, I. (2015). *Seismic Performance of Masonry Walls Retrofitted with Steel Reinforced Grout*. *Earthquake Engineering & Structural Dynamics*, 45(2), pp.229-251.
- Decanini, L., De Sortis, A., Goretti, A., Langenbach, R., Mollaioli, F. and Rasulo, A. (2004). *Performance of Masonry Buildings During the 2002 Molise, Italy, Earthquake*. *Earthquake Spectra*, 20(S1), pp. S191-S220.
- Derakhshan, H., Ingham, J. and Griffith, M. (2009). *Tri-Linear Force-Displacement Models Representative of Out-of-Plane Unreinforced Masonry Wall Behaviour*. [online] Hdl.handle.net. Available at: <http://hdl.handle.net/2292/22826> [Accessed 28 Jun. 2017].
- Dolce, M., Nigro, D., Ponzio, F. and Marnetto, R. (2001). *The CAM System for the Retrofit of Masonry Structures*. In: 7th International Seminar on Seismic Isolation, Passive Energy Dissipation and Active Control of Vibrations of Structures.
- Drysdale, R., Hamid, A. and Baker, L. (1993). *Masonry Structures: Behaviour and Design*. 1st ed. Englewood, Cliffs, NJ, Prentice Hall Inc.
- Durisol (2014). *British-Made Sustainable, ECO-Friendly Woodcrete ICF | Durisol*. [online] Durisol UK. Available at: <https://www.durisoluk.com/> [Accessed 23 Dec. 2019].
- ElGawady, M., Lestuzzi, P. and Badoux, M. (2004). *A Review of Conventional Seismic Retrofitting Techniques for URM*. In: Proceedings of 13th International Brick and Block Masonry Conference. [online] Amsterdam: International Brick and Block Masonry Conference, pp.1-10.
- Erdogmus, E. (2015). *Use of Fiber-Reinforced Cements in Masonry Construction and Structural Rehabilitation*. *Fibers*, 3(4), pp.41-63.
- European Organisation for Technical Approvals (2010). *Guideline for European technical approval of Metal Injection Anchors for Use in Masonry "ETAG 029"*. Brussel.
- Ferraioli, M., Costanzo, R. and Lavino, A. (2011). *Base Isolation Seismic Retrofit of a Hospital Building in Italy: Performance under Earthquake Strong Ground Motions*. In: Final Conference on COST Action C26: Urban Habitat

- Constructions under Catastrophic Events. Leiden: CRC Press/Balkema, pp.841-846.
- Ferraioli, M. and Mandara, A. (2016). *Base Isolation for Seismic Retrofitting of a Multiple Building Structure: Evaluation of Equivalent Linearization Method*. *Mathematical Problems in Engineering*, 2016, pp.1-17.
- Formisano, A., Candela, M., Borri, A., Barthel, R. and Fonti, R. (2017). *Rubble Masonry Response under Cyclic Actions: Experimental Tests and Theoretical Models*. *International Journal of Masonry Research and Innovation*, 2(1), p.30.
- Gattesco, N. and Boem, I. (2017). *Out-of-Plane Behavior of Reinforced Masonry Walls: Experimental and Numerical Study*. *Composites Part B: Engineering*, 128, pp.39-52.
- Gigla, B. and Wenzel, F. (1997). *The Repair of Historic Masonry Structures by Injection Anchors*. In: 11th International Brick/Block Masonry Conference.
- Gilda, F. (2010). *Vulnerability of Historical Masonry Buildings under Exceptional Actions*. PhD. Università Degli Studi di Napoli Federico II.
- Giongo, I., Schiro, G. and Piazza, M. (2017). *On the Use of Timber-Based Panels for the Seismic Retrofit of Masonry Structures*. In: 3rd International Conference on Protection of Historical Constructions.
- Guerrini G., Damiani, N., Miglietta, M. and Graziotti, F. (2020). *Cyclic Response of Masonry Piers Retrofitted with Timber Frames and Boards*. *ICE - Structures and Buildings*. <https://doi.org/10.1680/jstbu.19.00134>.
- Haach, V., Vasconcelos, G., Lourenço, P. and Mohamad, G. (2007). *Composition Study of a Mortar Appropriate for Masonry Cavities and Joints*. In: North American Masonry Conference. USA: The Masonry Society, pp.530-541.
- Hamid, A., El-Sayed, T. and Salama, A. (1994). *Seismic Retrofit of Historic Multiwythe Stone Masonry Walls*. In: 8th North America Masonry Conference, Austin, Texas, USA.
- Hamoush, S., McGinley, M., Mlakar, P., Scott, D. and Murray, K. (2001). *Out-of-Plane Strengthening of Masonry Walls with Reinforced Composite*. *Composites for Construction*, 5(3), pp.139-145.
- Hendry A.W. (1998). *The Strength of Masonry Compression Elements*. In: *Structural Masonry*. Palgrave, London.

- Indirli, M., Castellano, M., Clemente, P. and Martelli, A. (2001). *Demo-Application of Shape Memory Alloy Devices: The Rehabilitation of the S. Giorgio Church Bell-Tower*. In: Proceedings of SPIE, Smart Structures and Materials.
- Ingham, J. and Griffith, M. (2011). *The Performance of Unreinforced Masonry Buildings in the 2010/2011 Canterbury Earthquake Swarm August 2011*. Report number: ENG.ACA.0001FAffiliation: Canterbury Earthquakes Royal Commission.
- Ismail, N. and Ingham, J. (2016). *In-Plane and Out-of-Plane Testing of Unreinforced Masonry Walls Strengthened using Polymer Textile Reinforced Mortar*. Engineering Structures, 118, pp.167-177.
- Ismail, N. and Khattak, N. (2019). *Observed Failure Modes of Unreinforced Masonry Buildings During the 2015 Hindu Kush Earthquake*. Earthquake Engineering and Engineering Vibration, 18(2), pp.301-314.
- Izmir, C. and Erberik, M. (2015). *A Case Study for Seismic Assessment and Restoration of Historic Buildings: The Arditi Residence*. Handbook of Research on Seismic Assessment And Rehabilitation Of Historic Structures, ch013.
- Jansen, P. and Tilly, G. (1999). *Wall Repair & Strengthening (Paratec)*. [online] Available at: <http://cintec.com/anchoring-reinforcement/civil-engineering/wall-repair-strengthening-paratec/> [Accessed 12 Dec. 2016].
- Jorgustin, K. (2011). *Earthquake Fatality Trends – Increasing?* [online] Modern Survival Blog. Available at: <http://modernsurvivalblog.com/earthquakes/earthquake-fatality-trends-increasing/> [Accessed 14 Dec. 2016].
- Karantoni, F. and Fardis, M. (1992). *Effectiveness of Seismic Strengthening Techniques for Masonry Buildings*. Journal of Structural Engineering, 118(7), pp.1884-1902.
- Langenbach, R. (2007). *From “Opus Craticium” to the “Chicago Frame”:* *Earthquake-Resistant Traditional Construction*. International Journal of Architectural Heritage, 1(1), pp.29-59.
- Lantz, L., Maynez, J., Cook, W. and Wilson, C. (2016). *Blast Protection of Unreinforced Masonry Walls: A State-of-the-Art Review*. Advances in Civil Engineering, 2016, pp.1-11.

- Lin, Y., Lawley, D., Wotherspoon, L. and Ingham, J. (2016). *Out-of-Plane Testing of Unreinforced Masonry Walls Strengthened Using ECC Shotcrete*. Structures, 7(2016), pp. 33-42.
- Lourenco, P. (1996). *Computational Strategies for Masonry Structures*. PhD. Delft University of Technology.
- Lourenco, P. (1998). *Experimental and Numerical Issues in the Modelling of the Mechanical Behaviour of Masonry*. Structural Analysis of Historical Constructions, II.
- Lourenço, P., Mendes, N., Costa, A. and Campos-Costa, A. (2017). *Methods and Challenges on the Out-Of-Plane Assessment of Existing Masonry Buildings*. International Journal of Architectural Heritage, 11(1), pp.1-1.
- Lublinter, J., Oliver, J., Oller, S. and Onate, E. (1989). *Plastic-Damage Model for Concrete*. International Journal of Rock Mechanics and Mining Sciences & Geomechanics Abstracts, 26(5), p.252.
- Maccarini, H., Vasconcelos, G., Rodrigues, H., Ortega, J. and Lourenço, P. (2018). *Out-of-Plane Behavior of Stone Masonry Walls: Experimental and Numerical Analysis*. Construction and Building Materials, 179, pp.430-452.
- Magenes, G. and Calvi, G. (1994). *Experimental Results on Unreinforced Masonry Shear Walls Damaged And Repaired*. In: 10th IB2MaC. pp.509-518.
- Magenes, G. and Calvi, G. (1997). *In-Plane Seismic Response of Brick Masonry Walls*. Earthquake Engineering & Structural Dynamics, 26(11), pp.1091-1112.
- Maheri, M., Najafgholipour, M. and Rajabi, A. (2008). *The Influence of Mortar Head Joints on the In-Plane and Out-of-Plane Seismic Strenght of Brick Masonry Walls*. Iranian Journal of Science and Technology, 35(1), pp.63-79.
- Malhotra, M., Subramanian, R., Gahlot, P. and Rathore, B. (2005). *Textbook in Applied Mechanics*. New Delhi: Wiley Eastern.
- Manzouri, T., Schuller, M., Shing, P. and Amadei, B. (1996). *Repair and Retrofit of Unreinforced Masonry Structures*. Earthquake Spectra, 12(4), pp.903-922.
- Martelli, A. (2008). *Recent Progress of Application of Modern Anti-Seismic Systems in Europe – Part 2: Energy Dissipation Systems, Shape Memory Alloy Devices and Shock Transmitters*. In: Proceedings of the 14th World Conference on Earthquake Engineering, Beijing.

- Martins, A., Vasconcelos, G., Fangueiro, R. and Cunha, F. (2015). *Experimental Assessment of an Innovative Strengthening Material for Brick Masonry Infills*. Composites Part B: Engineering, 80, pp.328-342.
- Matsagar, V. and Jangid, R. (2008). *Base Isolation for Seismic Retrofitting of Structures*. Practice Periodical on Structural Design and Construction, 13(4), pp.175-185.
- Melkumyan, M., Mihul, V. and Gevorgyan, E. (2011). *Retrofitting by Base Isolation of Existing Buildings in Armenia and in Romania and Comparative Analysis of Innovative vs Conventional Retrofitting*. In: Conference on Computational Methods in Structural Dynamics and Earthquake Engineering. Corfu, Greece.
- Mendes, N., Costa, A., Paulo B. Lourenço, P., Rita Bento, R., Modena, C., Oliveira, D., Penna, A. and Sorrentino, L. (2016). *Methods and Approaches for Blind Test Predictions of Out-of-Plane Behavior of Masonry Walls: A Numerical Comparative Study*. International Journal of Architectural Heritage.
- Menon, A. and Magenes, G. (2008). *Out-of-Plane Seismic Response of Unreinforced Masonry: Definition of Seismic Input. Research Report*. Pavia, Italy: IUSS Press/European School for Advanced Studies in Reduction of Seismic Risk.
- Minaie, E. (2009). *Behavior and Vulnerability of Reinforced Masonry Shear Walls*. PhD. Drexel University.
- Mohamad, A. and Chen, Z. (2016). *Experimental and Numerical Analysis of the Compressive and Shear Behavior for a New Type of Self-Insulating Concrete Masonry System*. Applied Sciences, 6(9), p.245.
- Mohd Jani, J., Leary, M., Subic, A. and Gibson, M. (2014). *A Review of Shape Memory Alloy Research, Applications and Opportunities*. Materials & Design (1980-2015), 56, pp.1078-1113.
- Nanni, A. and Tumialan, J. (2003). *Fiber-Reinforced Composites for the Strengthening of Masonry Structures*. Structural Engineering International, 13(4), pp.271-278.
- Nazir, S. (2015). *Studies on the Failure of Unreinforced Masonry Shear Walls*. PhD. Queensland University of Technology, Australia.
- NBRI (2016). *National Building Research Institute (NBRI) – Civil and Environmental Engineering*. [online] Cee.technion.ac.il. Available at:

<https://cee.technion.ac.il/vision-and-goals/about/research-centers-and-labs/national-building-research-institute-nbri/> [Accessed 10 Aug. 2018].

- NCMA TEK 18-1B (2011). *Evaluating the Compressive Strength of Concrete Masonry: Quality Assurance & Testing*. National Concrete Masonry Association. Virginia.
- Nelson, S. (2014). *Earthquakes Seismic Activity*. [online] Earthsci.org. Available at: <http://earthsci.org/processes/geopro/seismic/seismic.html> [Accessed 2 Jan. 2017].
- Oliveira, D., Silva, R., Garbin, E. and Lourenço, P. (2012). *Strengthening of Three-Leaf Stone Masonry Walls: An Experimental Research*. *Materials and Structures*, 45(8), pp.1259-1276.
- Pan, Y., Xie, D., Yuan, S. and Wang, X. (2016). *Seismic Damages of Nepalese Cultural Heritage Buildings and Strengthening Measures: Case Studies on three Durbar Squares in Ms 8.1 Gorkha Earthquake*. *Harbin Gongye Daxue Xuebao/Journal of Harbin Institute of Technology*, 48(12), pp.172-182.
- Paret, T., Freeman, S., Searer, G., Hachem, M. and Gilmartin, U. (2008). *Using Traditional and Innovative Approaches in the Seismic Evaluation and Strengthening of a Historic Unreinforced Masonry Synagogue*. *Engineering Structures*, 30(8), pp.2114-2126.
- Pelenur, M. (2013). *Retrofitting the Domestic Built Environment: Investigating Household Perspectives Towards Energy Efficiency Technologies and Behaviour*. PhD. University of Cambridge, Queens' College.
- Peña, F., Lourenço, P., Mendes, N. and Oliveira, D. (2010). *Numerical Models for the Seismic Assessment of an Old Masonry Tower*. *Engineering Structures*, 32(5), pp.1466-1478.
- Phipps, M., Mirza, S., Bell, A., Pettit, G., Ormesher, M. and Lewis, N. (2001). *Characteristic Compressive Strength of Concrete Block Masonry*. [online] Istructe.org. Available at: <https://www.istructe.org/webtest/files/13/13fe8f4c-1319-4314-99e4-43c9adbcec0d.pdf> [Accessed 24 Dec. 2019].
- Pierre, P., Pleau, R. and Pigeon, M. (1999). *Mechanical Properties of Steel Microfiber Reinforced Cement Pastes and Mortars*. *Journal of Materials in Civil Engineering*, 11(4), pp.317-324.

- Portioli F. and Cascini L. (2017). *Large Displacement Analysis of Dry-Jointed Masonry Structures Subjected to Settlements using Rigid Block Modelling*. Engineering Structures, 148, pp. 485-496, ISSN: 0141-0296, doi: 10.1016/j.engstruct.2017.06.073.
- Portioli F.P.A. (2020). *Rigid Block Modelling of Historic Masonry Structures using Mathematical Programming: A Unified Formulation for Non-Linear Time History, Static Pushover and Limit Equilibrium Analysis*. Bulletin Of Earthquake Engineering, 18 (1), pp. 211-239. doi: 10.1007/s10518-019-00722-0.
- Post-Tensioning Institute (2006). *Post-Tensioning Manual*. Post-Tensioning Institute in Phoenix, AZ.
- Prabaharan, A. (2008). *Seismic Strengthening of Masonry Buildings*. PhD. Anna University Chennai 600 025.
- Priestley, M. (1985). *Seismic Behaviour of Unreinforced Masonry Walls*. Bulletin of the New Zealand National Society for Earthquake, 18(2), pp.191. [online] Available:[http://www.nzsee.org.nz/db/Bulletin/Archive/18\(2\)0191.pdf](http://www.nzsee.org.nz/db/Bulletin/Archive/18(2)0191.pdf) [Accessed 17 Jun. 2017].
- Ramos, L. and Lourenço, P. (2004). *Modeling and Vulnerability of Historical City Centers in Seismic Areas: A Case Study in Lisbon*. Engineering Structures, 26(9), pp.1295-1310.
- Reinhorn, A. and Madan, A. (1995). *Evaluation of Tyfo-S Fibre Wrap System for Out-of-Plane Strengthening of Masonry Walls*. [online] Available at: [http://civil.eng.buffalo.edu/~reinhorn/PUBLICATIONS/Reinhorn%20\(1995\)%20Report..%20EVAL.%20TYFO-S%20FIBER%20WRAP.pdf](http://civil.eng.buffalo.edu/~reinhorn/PUBLICATIONS/Reinhorn%20(1995)%20Report..%20EVAL.%20TYFO-S%20FIBER%20WRAP.pdf) [Accessed 3 Mar. 2017].
- Riccadonna D., Giongo, I., Schiro, G., Rizzi, E., and Parisi, M. (2019). *Experimental Shear Testing of Timber-Masonry Dry Connections for the Seismic Retrofit of Unreinforced Masonry Shear Walls*, Constr. and Building Materials, (211), pp.52-72, <https://doi.org/10.1016/j.conbuildmat.2019.03.145>.
- Saadatmanesh, H. (2014). *Bridge Retrofit using Fiber Reinforced Polymer - C+S Engineer*. [online] Available at: <http://csengineermag.com/article/bridge-retrofit-using-fiber-reinforced-polymer/> [Accessed 6 Jun. 2017].

- Sandoval C. and Roca P. (2012). *Study of the influence of different parameters on the buckling behaviour of masonry walls*. Constr. and Building Materials, 35, pp 888-899, <https://doi.org/10.1016/j.conbuildmat.2012.04.053>.
- Santos, C., Alvarenga, R., Ribeiro, J., Castro, L., Silva, R., Santos, A. and Nalon, G. (2017). *Numerical and Experimental Evaluation of Masonry Prisms by Finite Element Method*. IBRACON Structures and material journal, 10(2), pp.477-508.
- Seible, F., Priestley, M., Hegemier, G. and Innamorato, D. (1997). *Seismic Retrofit of RC Columns with Continuous Carbon Fiber Jackets*. Journal of Composites for Construction, 1(2), pp.52-62.
- Shing, P., Noland, J., Klamerus, E. and Spaeh, H. (1991). *Inelastic Behavior of Concrete Masonry Shear Walls*. Journal of Structural Engineering, 117(9), pp.2807-2808.
- Shrestha, K. (2011). *Development of Seismic Retrofitting Techniques for Historical Masonry Structures with Application of High-Performance Materials*. PhD. Kyoto University.
- Shrestha, K., Pareek, S. and Araki Y., Y. (2011). *Use of Polymer-Cement Pastes as Bonding Agents for Pinning Retrofitting of Masonry Construction*. In: Proceedings of JCI. pp.1661-1666.
- Silva, L., Lourenço, P. and Milani, G. (2018). *Derivation of the Out-of-Plane Behaviour of Masonry through Homogenization Strategies: Micro-Scale Level*. Computers & Structures, 209, pp.30-43.
- Silva, R., Jaquin, P., Oliveira, D., Miranda, T., Schueremans, L. and Cristelo, N. (2013). *Conservation and New Construction Solutions in Rammed Earth*. Structural Rehabilitation of Old Buildings, pp.77-108.
- Sinha, B., Gerstle, K. and Tulin, L. (1964). *Stress-Strain Relations for Concrete Under Cyclic Loading*. ACI Journal Proceedings, 61(2), pp.195-211.
- Solarino, F., Oliveira, D. and Giresini, L. (2019). *Wall-to-Horizontal Diaphragm Connections in Historical Buildings: A State-of-the-Art Review*. Engineering Structures, 199, p.109.
- Staalesson, E. (2014). *Energy Dissipation Devices – Earthquake Resistant Design Technique*. [online] <http://21stcenturybuilder.org/energy-dissipation-devices-earthquake-resistant-design-technique>. Available at:

<http://21stcenturybuilder.org/energy-dissipation-devices-earthquake-resistant-design-technique> [Accessed 2 Jan. 2017].

- Sustersic, I. and Dujic, B. (2014). *Seismic Strengthening of Existing Concrete and Masonry Buildings with Crosslam Timber Panels*. Materials and Joints in Timber Structures, pp.713-723.
- UMINHO (2006). *Review on the Experimental In-Plane and Out-of-Plane Testing: Developing Innovative Systems for Reinforced Masonry Walls*. [online] Italy: Università di Padova (Italy). Available at: http://diswall.dic.unipd.it/Results/D5.1_FINAL.pdf [Accessed 14 Mar. 2017].
- Valluzzi, M., Cardani, G., Binda, L. and Modena, C. (2004). *Seismic Vulnerability Methods for Masonry Buildings in Historical Centres: Validation and Application for Prediction Analyses and Intervention Proposals*. In: 13th World Conference on Earthquake Engineering. [online] Available at: http://www.iitk.ac.in/nicee/wcee/article/13_2765.pdf [Accessed 24 Dec. 2017].
- Varum, H., Tarque, N., Silveira, D., Camata, G., Lobo, B., Blondet, M., Figueiredo, A., Rafi, M., Oliveira, C. and Costa, A. (2013). *Structural Behaviour and Retrofitting of Adobe Masonry Buildings*. Structural Rehabilitation of Old Buildings, pp.37-75.
- Vasconcelos, G. and Lourenço, P. (2009). *Experimental Characterization of Stone Masonry in Shear and Compression*. Construction and Building Materials, 23(11), pp.3337-3345.
- Wang, C., Forth, J., Nikitas, N. and Sarhosis, V. (2017). *Retrofitting of Masonry Walls by Using a Mortar Joint Technique: Experiments and Numerical Validation*. Engineering Structures, 117, p.58-70.
- Wang, C., Sarhosis, V. and Nikitas, N. (2018). *Strengthening/Retrofitting Techniques on Unreinforced Masonry Structure/Element Subjected to Seismic Loads: A Literature Review*. The Open Construction and Building Technology Journal, 12(1), pp.251-268.
- Ward, S. (2004). *Retrofitting Existing Masonry Buildings to Resist Explosions*. Journal of Performance of Constructed Facilities, 18(2), pp.95-99.

- Willis, C., Seracino, R. and Griffith, M. (2010). *Out-of-Plane Strength of Brick Masonry Retrofitted with Horizontal NSM CFRP Strips*. *Engineering Structures*, 32(2), pp.547-555.
- Zeiny, A. and Larralde, J. (2010). *Seismic Evaluation of the Performance of Retrofitted and Repaired Brick Walls by Means of Expansive Epoxy Injection*. [online] Zeiny.net. Available at: <http://zeiny.net/FundedProjects/FoamReport/FoamReport.htm> [Accessed 13 Mar. 2017].
- Zezhen, N., Qi, D., Jianyou, C. and Runtao, Y. (1984). *Study of a Seismic Strengthening for Multi-Story Brick Building by Additional R/C Columns*. In: 8th WCEE. pp.591-598.
- Zhang, S., Yang, D., Sheng, Y., Garrity, S. and Xu, L. (2017). *Numerical Modelling of FRP-Reinforced Masonry Walls under In-Plane Seismic Loading*. *Construction and Building Materials*, 134, pp.649-663.

Appendix

Appendix 4.1a: Properties of fresh mortar for all sample preparation

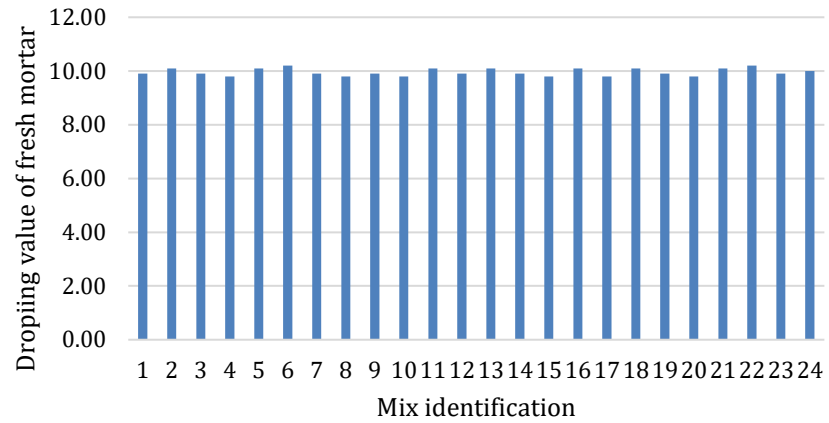
Consistency of Fresh Mortar (dropping and flow value)					
Specimen Label	Number of mixes	Dropping value (mm)			Flow (mm)
		Trial 1	Trial 2	Average	
MC 1, 2 & 3	1	10.00	9.80	9.90	170.00
MC 4, 5 & 6	2	10.20	10.00	10.10	168.00
MP00-1, 2 & 3	3	9.80	10.00	9.90	170.00
MPOSBC1-1, 2 & 3	4	9.80	9.80	9.80	172.00
MPOSBC1-2*	5	10.20	10.00	10.10	170.00
MPOSBC2-1, 2 & 3	6	10.20	10.20	10.20	168.00
PW1115-1	7	9.80	10.00	9.90	172.00
	8	9.80	9.80	9.80	170.00
	9	9.80	10.00	9.90	168.00
PW1115-2	10	9.80	9.80	9.80	170.00
	11	10.20	10.00	10.10	168.00
	12	9.80	10.00	9.90	172.00
1SRW1115-1	13	10.20	10.00	10.10	170.00
	14	9.80	10.00	9.90	168.00
	15	9.80	9.80	9.80	170.00
1SRW1115-2	16	10.20	10.00	10.10	169.00
	17	9.80	9.80	9.80	167.00
	18	10.20	10.00	10.10	171.00
2SRW1115-1	19	9.80	10.00	9.90	170.00
	20	9.80	9.80	9.80	168.00
	21	10.20	10.00	10.10	171.00
2SRW1115-2	22	10.20	10.20	10.20	172.00
	23	9.80	10.00	9.90	170.00
	24	10.20	9.80	10.00	168.00

Appendix 4.1b: Properties of hardened mortar for all sample preparation

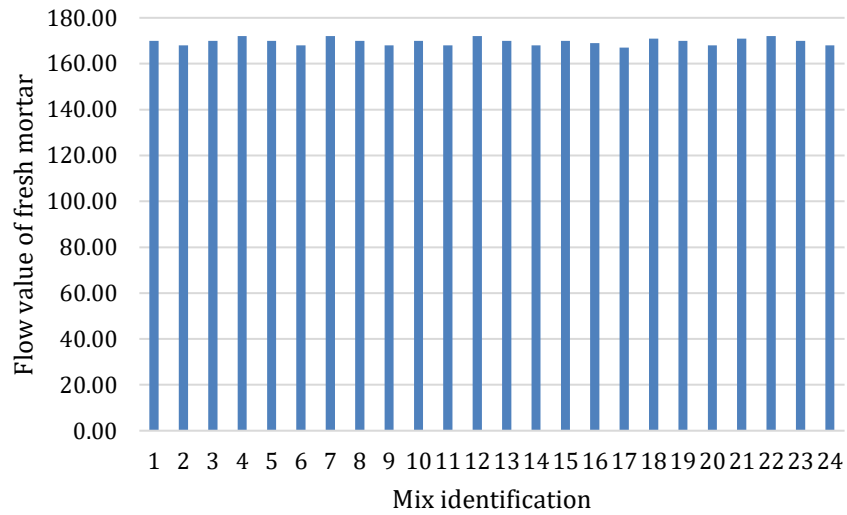
Compressive Strength of hardened mortar cube					
Specimen Label	Number of mixes	Compressive strength (N/mm ²)			
		M1	M2	M3	Average
MC 1, 2 & 3	1	7.20	6.80	7.00	7.00
MC 4, 5 & 6	2	7.40	7.10	7.20	7.23
MP00-1, 2 & 3	3	6.90	7.10	7.10	7.03
MPOSBC1-1, 2 & 3	4	7.40	7.20	7.10	7.23
MPOSBC1-2*	5	7.20	7.10	7.00	7.10
MPOSBC2-1, 2 & 3	6	6.90	7.00	6.80	6.90
PW1115-1	7	7.00	7.05	7.03	7.03
	8	7.23	7.20	6.80	7.08
	9	7.03	7.40	7.10	7.18
PW1115-2	10	7.23	6.90	7.10	7.08
	11	7.10	7.40	7.20	7.23
	12	6.90	7.20	7.10	7.07
1SRW1115-1	13	6.93	6.90	7.00	6.94
	14	7.18	7.04	7.03	7.08
	15	7.08	7.03	7.08	7.06
1SRW1115-2	16	7.18	7.23	7.18	7.19
	17	7.07	7.03	7.08	7.06
	18	7.08	7.28	7.23	7.20
2SRW1115-1	19	7.06	7.12	7.07	7.08
	20	7.19	6.95	6.94	7.03
	21	7.06	7.18	6.90	7.04
2SRW1115-2	22	7.14	7.07	7.40	7.20
	23	7.14	7.08	7.20	7.14
	24	7.15	7.06	6.90	7.04

Appendix 4.1c: Properties of mortar for all sample preparation

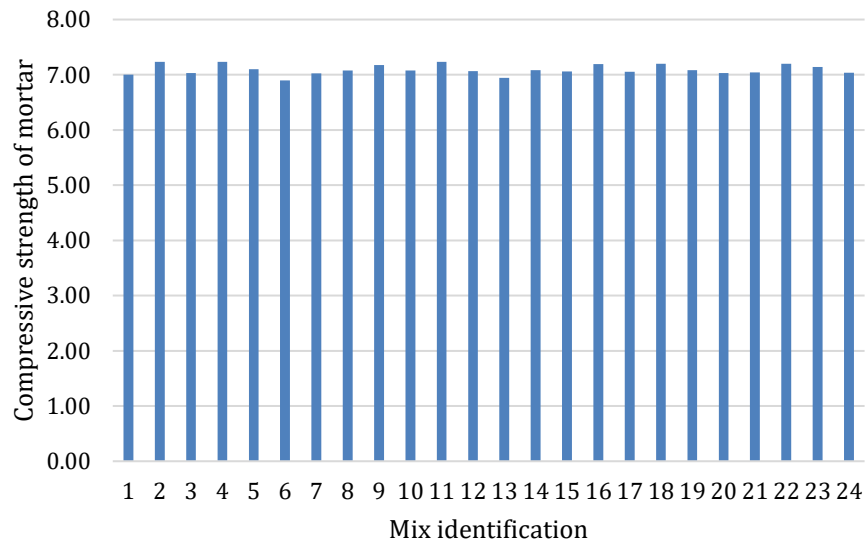
Dropping value of Mortar (mm)



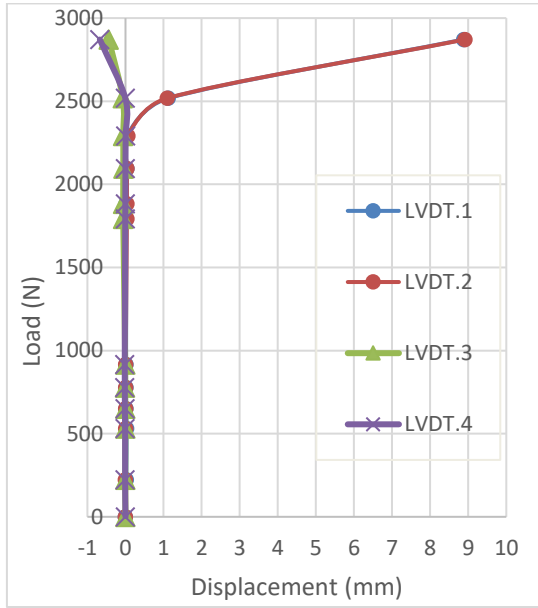
Flow value of Mortar (mm)



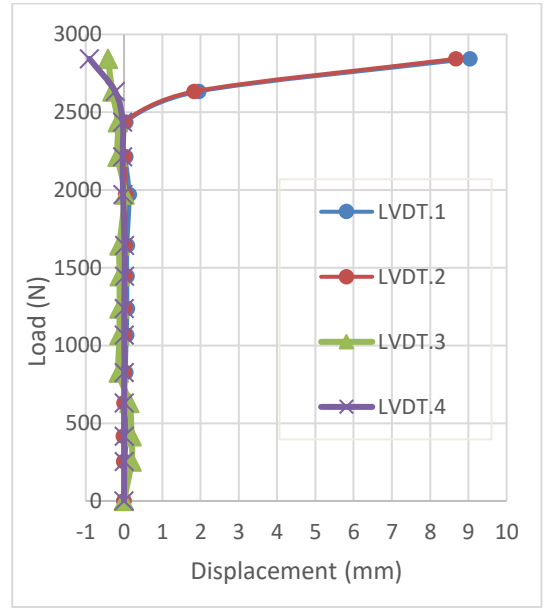
Compressive strength of hardened Mortar (N/mm²)



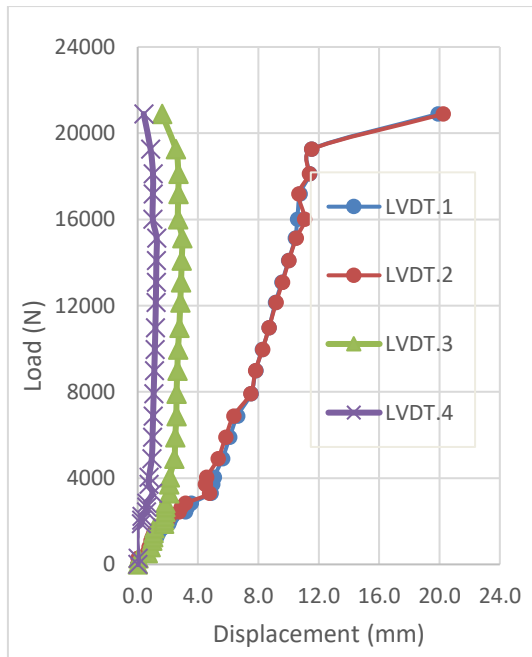
Appendix 4.2: Load vs displacement of all four LVDTs for all MP specimens



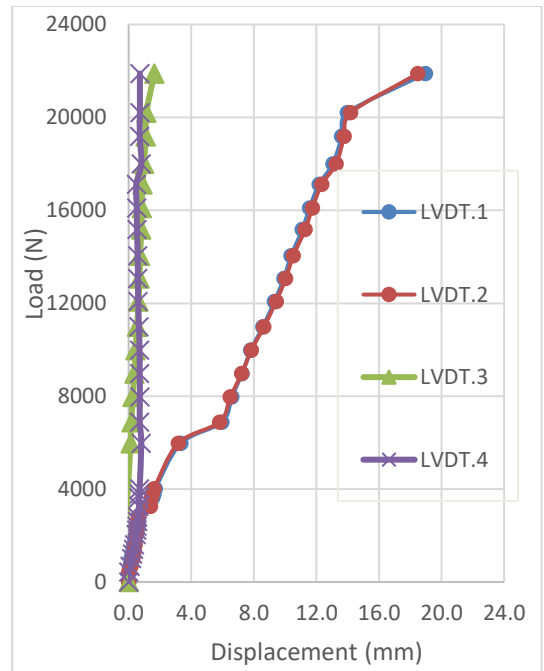
MP00-1



MP00-2

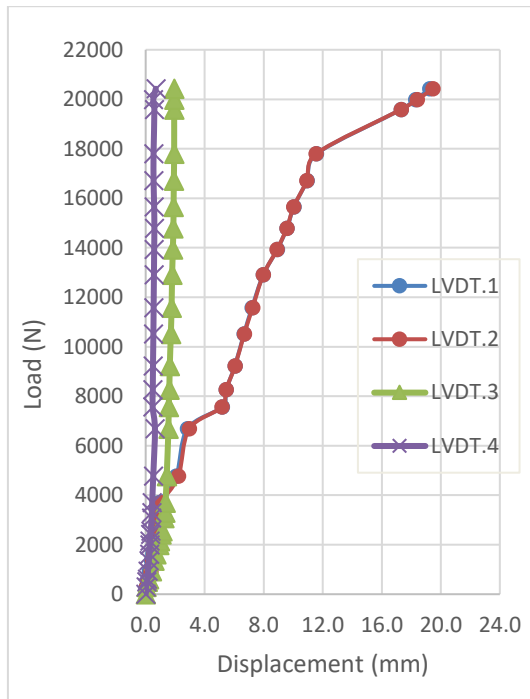


MPOSBC1-2

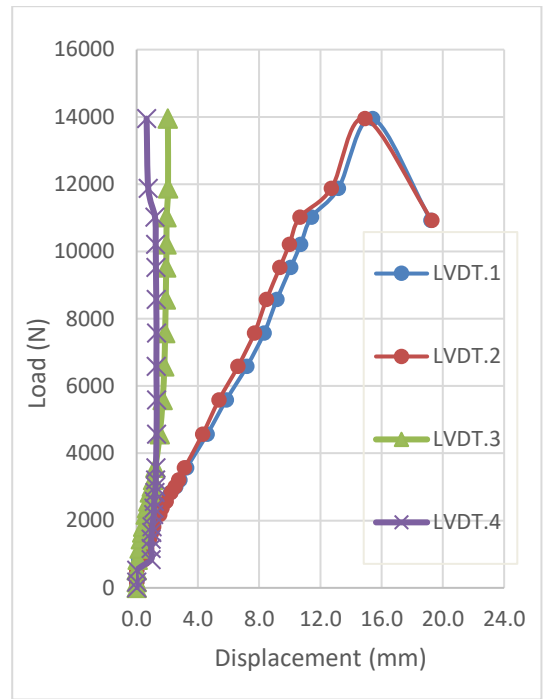


MPOSBC1-2*

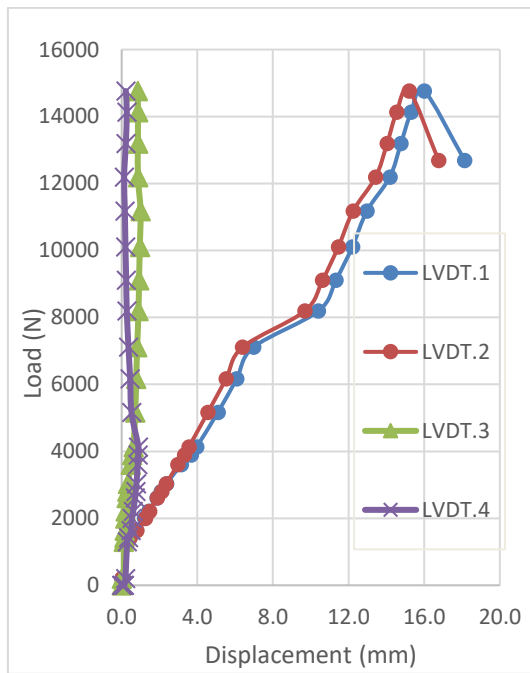
Appendix 4.2: Load vs displacement of all four LVDTs for all MPs (contd.)



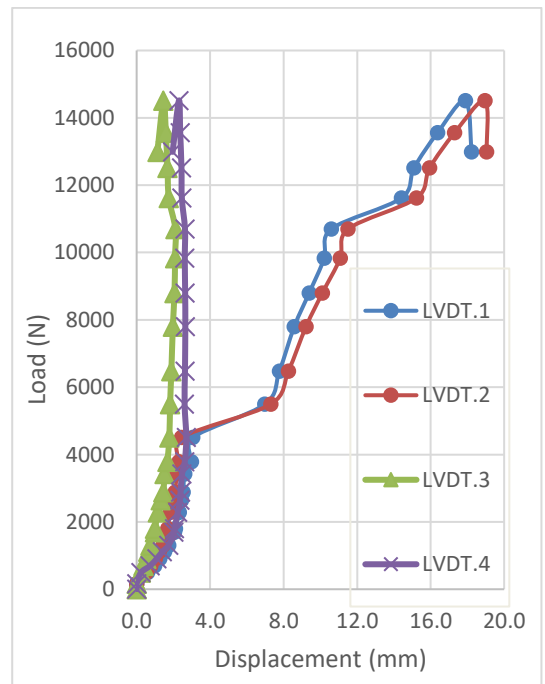
MPOSBC1-3



MPOSBC2-1



MPOSBC2-2



MPOSBC2-3

Appendix 5.1a: ABAQUS CDP input parameter for brick unit

Compressive		Tensile		Damage Parameter			
Yield stress	Inelastic strain	Yield stress	Inelastic strain	dc	Inelastic strain	dt	Inelastic strain
26.37	0.00000	5.93	0.00000	0.00	0.00000	0.00	0.00000
68.00	0.00713	4.76	0.00017	0.00	0.00713	0.20	0.00017
78.10	0.01013	3.54	0.00037	0.00	0.01013	0.40	0.00037
84.80	0.01313	2.07	0.00077	0.00	0.01313	0.65	0.00077
87.91	0.01688	0.87	0.00167	0.00	0.01688	0.85	0.00167
72.26	0.02813	0.51	0.00247	0.18	0.02813	0.91	0.00247
36.79	0.03183	0.22	0.00437	0.58	0.03183	0.96	0.00437
19.36	0.03633			0.78	0.03633		
11.15	0.04113			0.87	0.04113		

Appendix 5.1b: ABAQUS CDP input parameter for mortar

Compressive		Tensile		Damage Parameter			
Yield stress	Inelastic strain	Yield stress	Inelastic strain	dc	Inelastic strain	dt	Inelastic strain
1.794	0.00000	0.319	0.00000	0.00	0.00000	0.00	0.00000
3.133	0.00100	0.296	0.01096	0.00	0.00100	0.07	0.01096
4.997	0.00310	0.258	0.02303	0.00	0.00310	0.19	0.02303
5.825	0.00460	0.220	0.03179	0.00	0.00460	0.31	0.03179
6.521	0.00660	0.198	0.04086	0.00	0.00660	0.38	0.04086
6.970	0.00916	0.099	0.05156	0.00	0.00916	0.69	0.05156
7.100	0.01185	0.049	0.06996	0.00	0.01185	0.84	0.06996
5.750	0.02360	0.025	0.09528	0.19	0.02360	0.92	0.09528
3.483	0.03400	0.012	0.31836	0.51	0.03400	0.96	0.31836
0.710	0.04800	0.006	0.64956	0.90	0.04800	0.98	0.64956

Appendix 5.1c: ABAQUS CDP input parameter for 10mm OSB

Compression		Tensile		Damage Parameter			
Yield stress	Inelastic strain	Yield stress	Inelastic strain	dc	Inelastic strain	dt	Inelastic strain
2.18	0.0000	1.02	0.0000	0.00	0.0000	0.00	0.0000
7.26	0.0207	0.41	0.3252	0.00	0.0207	0.60	0.3252
5.81	0.0622	0.08	0.5529	0.20	0.0622	0.92	0.5529
4.65	0.1867	0.02	0.9400	0.36	0.1867	0.98	0.9400

Appendix 5.1d: ABAQUS CDP input parameter for 18mm OSB

Compression		Tensile		Damage Parameter			
Yield stress	Inelastic strain	Yield stress	Inelastic strain	dc	Inelastic strain	dt	Inelastic strain
1.98	0.0000	1.85	0.0000	0.00	0.0000	0.09	0.0000
6.60	0.0189	0.74	0.2957	0.00	0.0189	0.64	0.2957
5.28	0.0566	0.15	0.5027	0.20	0.0566	0.93	0.5027
4.22	0.1697	0.03	0.8545	0.36	0.1697	0.99	0.8545

Appendix 5.1e: ABAQUS CDP input parameter for 25mm OSB

Compression		Tensile		Damage Parameter			
Yield stress	Inelastic strain	Yield stress	Inelastic strain	dc	Inelastic strain	dt	Inelastic strain
1.78	0.0000	0.83	0.0000	0.00	0.0000	0.00	0.0000
5.94	0.0170	0.33	0.2661	0.00	0.0170	0.60	0.2661
4.75	0.0509	0.07	0.4524	0.20	0.0509	0.92	0.4524
3.80	0.1527	0.01	0.7691	0.36	0.1527	0.98	0.7691